9th International Conference on Advanced COmputational Methods in ENgineering and Applied Mathematics

ACOMEN2025

September 15–19, 2025

Zebrastraat, Ghent, Belgium

Book of Abstracts

GHENT UNIVERSITY

ANALYSIS PDE CENTER

GHENT ANALYSIS PDE CENTER

Plenary speakers

Peter Bastian
Universität Heidelberg

Jerome Droniou
University of Montpellier

Jan S. Hesthaven
Karlsruhe Institute of Technology (KIT)

Barbara Kaltenbacher
Alpen-Adria-Universität Klagenfurt

Michael Klibanov
University of North Carolina at Charlotte

Matti Lassas
University of Helsinki

Barbara Wohlmuth
Technical University of Munich

Contents

Plenary Talks

Book of abstracts of the 9th International Conference on
Advanced Computational Methods in ENgineering and Applied Mathematics
September, 15–19, 2025.

Coupled shallow surface and subsurface flow with application to high mountain catchments

Peter Bastian[1]

[1] *Interdisciplinary Center for Scientific Computing, Heidelberg University*

e-mails: peter.bastian@iwr.uni-heidelberg.de

Abstract

High mountain catchments convert glacier melt, snowmelt and liquid precipitation into surface runoff. Part of the surface runoff recharges the groundwater aquifer, while the remaining part appears as surface discharge at the valley outlet. Being considered unimportant initially, it is now established that groundwater, and not just surface water, plays a critical role in mountain hydrogeology by supplying baseflow in rivers. In this contribution we will present a mathematical model to describe coupled surface-subsurface flow in mountain catchments, consider its numerical solution and discuss a case study of a glacierised catchment in the cold-arid region of Ladakh, Trans-Himalaya.

Key words: 76-10, 35K65, 65M08, 65M55

1 Introduction

High mountain catchments convert glacier melt, snowmelt and liquid precipitation into surface runoff. Part of the surface runoff recharges the groundwater aquifer, while the remaining part appears as surface discharge at the valley outlet. Being considered unimportant initially, it is now established that groundwater, and not just surface water, plays a critical role in mountain hydrogeology by supplying baseflow in rivers [1, 3]. In this contribution we will present a mathematical model to describe coupled surface-subsurface flow in mountain catchments, consider its numerical solution and discuss a case study of a glacierised catchment in the cold-arid region of Ladakh, Trans-Himalaya.

2 Mathematical Model

Figure 1 illustrates relevant processes for water flow in high mountain catchments [1]. Glacier melt, snow melt and precipitation will be provided by data (see case study below) and act as source terms while surface flow and subsurface flow are modelled as shallow flows. Exchange between surface and subsurface is modelled by a source sink/term. Sublimation, evaporation and permafrost regions are neglegted in our model.

The shallow flow assumption states that i) the vertical velocity component is zero, ii) the horizontal velocity components do not deviate much from their vertical average and iii) there exists a unique vertical position of the water surface at every horizontal position. These assumptions allow one to rigorously derive the shallow water equations (also dynamic wave

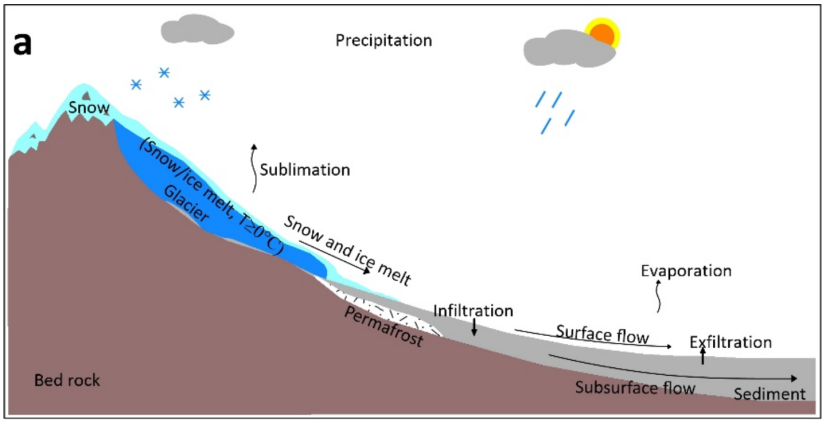

Figure 1: Relevant processes in mountain hydrology.

equation) for the vertically averaged horizontal velocity components and water depth from the three-dimensional Navier-Stokes equations with a free surface. Assuming further that gravitational and bottom friction terms are dominant, the shallow water equations can be simplified to the diffusive wave approximation equation [2] for the position of the surface water table $w_s(x,t)$:

$$\partial_t w_s - \nabla \cdot \left(\frac{1}{n(x)} \frac{(w_s - b_s(x))^\alpha}{\|\nabla w_s\|^{1-\gamma}} \nabla w_s \right) = f_s(x,t) - q(x, w_s, w_a), \tag{1}$$

where $n(x)$ is mannings coefficient, $b_s(x)$ is the bathymmetry (position of the earth surface), $1 \leq \alpha \leq 2$, $0 < \gamma \leq 1$ are empirical constants related to the surface type, $f_s(x,t)$ is the source term and q models the exchange with the subsurface. Note that $h_s(x,t) = w_s(x,t) - b_s(x) \geq 0$ is the height of the surface water column at (x,t) and a flat water surface $\nabla w_s = 0$ results in a well-defined no flow situation since $\gamma > 0$ (lake at rest).

For groundwater, the starting point is the groundwater flow equation consisting of mass conservation and Darcy's law. Vertical averaging based on the shallow flow assumption replaces Darcy's law with the Dupuit-Forchheimer equation for the position of the groundwater table $w_a(x,t)$:

$$\phi \partial_t (\min(w_a, b_s) - b_a) - \nabla \cdot (k(x)(w_a - b_a)\nabla w_a) = f_a(x,t) + q(x, w_s, w_a), \tag{2}$$

where ϕ is porosity, $b_a(x)$ is the bathymmetry of the subsurface, $k(x)$ is hydraulic conductivity and $f_a(x,t)$ is the groundwater source/sink term (e.g. groundwater pumping).

The exchange between surface and subsurface water is modelled as follows:

$$q(x, w_s, w_a) = L_i \max(w_s - b_s(x), 0) \frac{\max(w_s - w_a, 0)}{C + \max(w_s - w_a, 0)} - L_e \max(w_a - w_s, 0), \tag{3}$$

with the infiltration parameter L_i, exfiltration parameter L_e and the parameter C.

Equations (1)–(3) form a nonlinear parabolic - elliptic system of partial differential equations. Note that $w_a(x,t) > b_s(x)$ is possible. In this case the aquifer becomes confined, equation (2) is (locally) elliptic and exfiltration from subsurface water to surface water may occur.

3 Numerical Methods

The system (1)–(3) is solved numerically using a fully-coupled approach using a finite volume discretization in space and the implicit Euler method in time. Two finite volume methods have been implemented: the cell-centered approach on structured, axiparallel grids and the vertex-centered method on Voronoi cells. In these approaches the bathymmetry functions b_s, b_a are approximated as piece-wise constant functions. Handling of wetting and drying is of paramount importance in practical applications and is achieved by the following two-point flux function for the the flux $Q_{e,e'}$ from cell e to e':

$$Q_{e,e'} = (\max(\max(W_e, W_{e'}) - \max(B_{e'}, B_e), 0))^{\alpha} \frac{W_e - W_{e'}}{\|x_e - x_{e'}\|}$$

where we have set $\gamma = 1$. Here $W_e, W_{e'}$ are the water tables in the two cells and $B_e, B_{e'}$ are the bathymmetry values in the two cells. For this flux one can show non-negativity of the water heights $W_e - B_e$. If time permits, we will present results for a discontinuous Galerkin discretization of the system offering the possibility to use more general meshes as well as a piecewise linear bathymmetry approximation.

The arising nonlinear algebraic systems per system are solved with Newton's method and the resulting sparse linear systems are solved with the GMRES method preconditioned by an overlapping domain decomposition method.

4 Case Study

The model above has been applied to Stok catchment located near the city of Ladakh on northern India [4]. Glacier and snow melt has been modelled with a temperature index model based on satellite and weather data while precipitation data is extrapolated from a near-by weather station. Selected parameters of the system have been calibrated from discharge measurements at the outlet of the catchment obtained in 2019. Surface bathymmetry is taken from the HydroSHEDS data base (`https://www.hydrosheds.org/`) while subsurface bathymmetry has been estimated from accumulation and surface elevation. The calibrated model has been used to reconstruct surface and subsurface discharge for the years 2003–2018.

References

[1] M. Hayashi, *Alpine Hydrogeology: The Critical Role of Groundwater in Sourcing the Headwaters of the World*, Groundwater, 58, 498–510, https://doi.org/10.1111/gwat.12965, 2020.

[2] V. M. Ponce and D. B. Simons, *Shallow wave propagation in open channel flow*, Journal of the Hydraulics Division. 1977 Dec;103(12):1461-76.

[3] L. D. Somers and J. M. McKenzie, *A review of groundwater in high mountain environments*, WIREs Water, 7, e1475, https://doi.org/10.1002/wat2.1475, 2020.

[4] M. Soheb, P. Bastian, S. Schmidt, S. Singh, H. Kaushik, A. Ramanathan and M. Nüsser, *Surface and subsurface flow of a glacierised catchment in the cold-arid region of Ladakh, Trans-Himalaya*, J. Hydrol., 635, 131063, https://doi.org/10.1016/j.jhydrol.2024.131063, 2024.

Book of abstracts of the 9th International Conference on
Advanced Computational Methods in ENgineering and Applied Mathematics
September, 15–19, 2025.

The Discrete De Rham method for electromagnetic models: from Maxwell to Yang–Mills to manifolds

Jérôme Droniou[1,2]

[1] *Institut of Mathematics Alexander Grothendieck, CNRS & University of Montpellier, France*

[2] *School of Mathematics, Monash University, Australia*

e-mails: jerome.droniou@umontpellier.fr

Abstract

Electromagnetic models are systems of partial differential equations involving evolution equations and (stationary) constraint equations, the latter being preserved through the evolution thanks to the relative properties of the differential operators in these models (curl, divergence). These properties are encoded in the de Rham complex, and designing a scheme that preserve the constraints at the discrete level requires an approximation of this complex. We will present one of these approximations, the Discrete De Rham (DDR) method, which has two important features: it is applicable on meshes made of generic polyhedra, and has an arbitrary degree of accuracy, enabling the design of high-order schemes. We will consider the application of DDR to electromagnetic models, from the simple Maxwell equations on an open domain of $\mathbb{R}^3$, to the geometric non-linear Yang–Mills equations, to the Maxwell equations on a manifold.

Key words: constraint preservation, de Rham complex, Maxwell equations, polytopal complex, Yang–Mills equations.

1 Introduction

Electromagnetic processes are modelled by systems of partial differential equations (PDE) that involve *evolution* equations and *constraint* equations (structural conditions on the fields). For the Maxwell equations, without sources and dropping the physical parameters for simplicity, these are:

$$\underbrace{\partial_t E - \mathbf{curl}\, B = 0\,,\ \partial_t B + \mathbf{curl}\, E = 0}_{\text{Evolutions}} \quad \text{and} \quad \underbrace{\operatorname{div} E = 0\,,\ \operatorname{div} B = 0}_{\text{Constraints}}\,.$$

The constraints are preserved by the evolution equations: if the initial conditions satisfy them, then so do the evolved fields at each time. The proof of constraints preservation relies on the well-known calculus formulas

$$\operatorname{div} \mathbf{curl} = 0\,, \qquad \mathbf{curl}\, \mathbf{grad} = 0. \tag{1}$$

To preserve the constraints in numerical approximations, one has to design methods that exactly reproduce (1) at the discrete level.

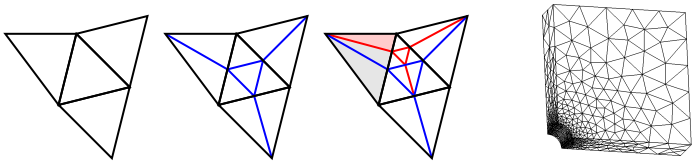

Figure 1: Local refinements using triangular/tetrahedral meshes.

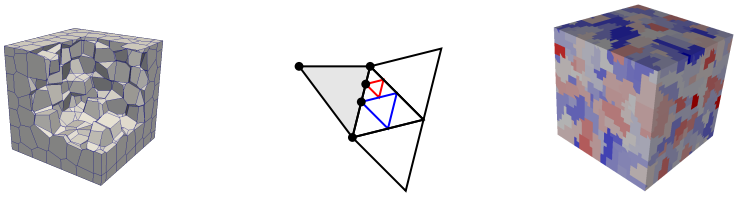

Figure 2: Polytopal meshes: Voronoi tessellation, locally refined mesh, agglomerated mesh.

2 The Discrete De Rham method

The de Rham complex is the following sequence of spaces connected by differential operators:

$$H^1(\Omega) \xrightarrow{\text{grad}} \boldsymbol{H}(\mathbf{curl};\Omega) \xrightarrow{\text{curl}} \boldsymbol{H}(\text{div};\Omega) \xrightarrow{\text{div}} L^2(\Omega) \xrightarrow{0} \{0\}. \tag{2}$$

The complex property means that $\operatorname{Im}\mathbf{grad} \subset \ker\mathbf{curl}$ and $\operatorname{Im}\mathbf{curl} \subset \ker\text{div}$, which is just another way of writing the key formulas (1).

Constraint-preserving schemes require to design discrete versions of this de Rham complex. In the Finite Element approach [1], these discrete complexes consists in replacing the continuous spaces by piecewise polynomial subspaces:

$$\begin{array}{ccccccccc} V_h^1 & \xrightarrow{\text{grad}} & V_h^2 & \xrightarrow{\text{curl}} & V_h^3 & \xrightarrow{\text{div}} & V_h^4 & \xrightarrow{0} & \{0\}. \\ \cap & & \cap & & \cap & & \cap & & \\ H^1(\Omega) & & \boldsymbol{H}(\mathbf{curl};\Omega) & & \boldsymbol{H}(\text{div};\Omega) & & L^2(\Omega) & & \end{array}$$

Designing such subspaces essentially restricts the construction to tetrahedral or hexahedral meshes, and may require a large number of degrees of freedom (DOF) to enforce suitable inter-element continuity conditions. The restrictions on the elements geometry also severely limits possibilities of mesh agglomeration (as used in multi-grid solvers), and forces the use of intermediate layers to preserve mesh regularity in local refinement procedures (see Fig. 1).

In the last couple of decades, a trend in numerical analysis of PDEs has been to design numerical methods that are applicable on generic polyhedral meshes. Such meshes have several desirable features (see Fig. 2): seamless local mesh refinement and coarsening (by agglomeration), better capture of complicated geometries, etc.

In the context of discrete complexes, this has led to Virtual Element Methods (VEM) [3, 2] and to Discrete De Rham (DDR) methods [7, 6]. Besides being applicable to generic meshes, these methods also have an arbitrary degree of polynomial accuracy, and can thus be used to design high-order schemes on such meshes. The "high level" approach used in the design

	Tetrahedra			Hexahedra		
Discrete space	$k=0$	$k=1$	$k=2$	$k=0$	$k=1$	$k=2$
$H^1(T)$	4 (4)	10 (10)	20 (20)	8 (8)	20 (27)	32 (64)
$\boldsymbol{H}(\mathbf{curl};T)$	6 (6)	23 (20)	53 (45)	12 (12)	39 (54)	77 (144)
$\boldsymbol{H}(\mathrm{div};T)$	4 (4)	18 (15)	44 (36)	6 (6)	24 (36)	56 (108)
$L^2(T)$	1 (1)	4 (4)	10 (10)	1 (1)	4 (8)	10 (27)

Table 1: Number of DOFs on an element T of the (serendipity) DDR complex. In brackets: number of DOFs for the Raviart-Thomas–Nédélec FE complex.

of polytopal complexes, which do not require global conforming piecewise-polynomial shape functions, also leads to numerical methods that, even on standard meshes, may have (much) fewer DOFs than finite element complexes – see Table 1.

In this presentation, we will focus on the DDR method and its application to various models of electromagnetism.

3 Maxwell and Yang–Mills equations

A DDR scheme is obtained by replacing, in the weak formulations of the Maxwell equations, $\boldsymbol{H}(\mathbf{curl};\Omega)$ and $\boldsymbol{H}(\mathrm{div};\Omega)$ by the corresponding DDR spaces and the continuous L^2-inner products by discrete ones. This scheme preserves the constraints (one in strong form, the other in weak form, as with the usual finite element approach). Some generalised electromagnetic models however lead to non-linear geometric PDEs which present additional challenges regarding constraint preservations.

For example, under the temporal gauge the Yang–Mills system is written on Lie algebra-valued fields A, E under the following form:

$$\partial_t E - \mathbf{curl}\, B = \star[A,B]\,,\ \partial_t A = -E, \quad \mathrm{div}\, E + \star[A,\star E] = 0, \quad \text{with} \quad B = \mathbf{curl}\, A + \frac{1}{2}\star[A,A].$$

Here, $[\cdot,\cdot]$ is the Lie bracket and $\star$ the Hodge-star operator (the operators $\star[\cdot,\cdot]$ and $\star[\cdot,\star\cdot]$ generalise the cross and dot products). Even in the finite element setting, this preservation cannot be established using a discrete version of (1) and a scheme based on the weak formulation; instead, a modified formulation must be considered [5].

For polytopal methods, the situation is even more complicated. Their inherent non-conformity means that a discrete form of Lie bracket must first be designed. We will present the solution found in [9, 10] for the DDR method, which is to our knowledge the first polytopal method ever used on the Yang–Mills equations.

4 Polytopal Exterior Calculus, applications to manifolds

The de Rham complex (2) can be written in the framework of differential forms, that is, with spaces of multilinear alternating forms: $H^1(\Omega)$ corresponds to 0-forms (scalar-valued functions), $\boldsymbol{H}(\mathbf{curl};\Omega)$ to 1-forms (linear maps), $\boldsymbol{H}(\mathrm{div};\Omega)$ to 2-forms (antisymmetric bilinear maps) and $L^2(\Omega)$ to 3-forms (alternating trilinear maps). The operators gradient, curl and divergence are replaced by the exterior derivative. This framework has the benefit of providing a unified treatment of all spaces and differential operators, and simplifies the design and

analysis of discrete complexes (see the Finite Element Exterior Calculus theory [1] for finite elements).

We will discuss the recent Polytopal Exterior Calculus framework of [4], which expresses the VEM and DDR in the framework of differential forms. This framework made it possible to design polytopal complexes on manifolds, and design arbitrary-order schemes for the Maxwell equations on the torus and the sphere [8].

Acknowledgements This work was partially funded by the European Union (ERC Synergy NEMESIS, project N° 101115663). Views and opinions expressed are those of the authors only and do not necessarily reflect those of the European Union or the European Research Council Executive Agency. Neither the European Union nor the granting authority can be held responsible for them.

References

[1] Arnold, D. (2018). *Finite Element Exterior Calculus*. SIAM.

[2] Beirão da Veiga, L., Brezzi, F., Dassi, F., Marini, L. D., and Russo, A. (2018). A family of three-dimensional virtual elements with applications to magnetostatics. *SIAM J. Numer. Anal.*, 56(5):2940–2962.

[3] Beirão da Veiga, L., Brezzi, F., Marini, L. D., and Russo, A. (2016). $H(\mathrm{div})$ and $H(\mathrm{curl})$-conforming VEM. *Numer. Math.*, 133:303–332.

[4] Bonaldi, F., Di Pietro, D. A., Droniou, J., and Hu, K. (2024). An exterior calculus framework for polytopal methods. *Journal of the European Mathematical Society*, page 55p.

[5] Christiansen, S. H. and Winther, R. (2006). On constraint preservation in numerical simulations of Yang-Mills equations. *SIAM J. Sci. Comput.*, 28(1):75–101.

[6] Di Pietro, D. A. and Droniou, J. (2023). An arbitrary-order discrete de Rham complex on polyhedral meshes: Exactness, Poincaré inequalities, and consistency. *Found. Comput. Math.*, 23:85–164.

[7] Di Pietro, D. A., Droniou, J., and Rapetti, F. (2020). Fully discrete polynomial de Rham sequences of arbitrary degree on polygons and polyhedra. *Math. Models Methods Appl. Sci.*, 30(9):1809–1855.

[8] Droniou, J., Hanot, M., and Oliynyk, T. (2024). A polytopal discrete de Rham complex on manifolds, with application to the Maxwell equations. page 33p.

[9] Droniou, J., Oliynyk, T. A., and Qian, J. J. (2023). A polyhedral discrete de Rham numerical scheme for the Yang–Mills equations. *J. Comput. Phys.*, 478:Paper no. 111955, 26p.

[10] Droniou, J. and Qian, J. J. (2024). Two arbitrary-order constraint-preserving schemes for the Yang–Mills equations on polyhedral meshes. *Mathematics in Engineering*, 6(3):468–493.

Book of abstracts of the 9th International Conference on
Advanced Computational Methods in ENgineering and Applied Mathematics
September, 15–19, 2025.

Time-domain reduced order models through the Laplace transform

Jan S. Hesthaven[1]

[1] *Faculty of Informatics, Karlsruhe Institute of Technology (KIT)*

e-mails: jan.hesthaven@kit.edu

Abstract

During the last few decades, reduced basis methods have proven themselves to be an effective way to develop fast and accurate models of reduced computational complexity for very general classes of problems described by parameterized partial differential equations. However, this success has primarily been limited to time-independent problems and the extension to time-dependent problems has proven to be more challenging, due primarily to stability problems associated with the reduced models, developed primarily with a focus on accuracy.

In this talk, in which we begin with a brief introduction to the reduced basis method, we discuss the use of the Laplace transform to address this challenge. In the first part we use both the forward and the inverse transform to recast the initial value problem to a parametrized harmonic problems for which we can then apply the reduced basis method. This avoids the need to advance the reduced model and, thus, eliminates the challenges associated with stability. While the approximation of the inverse Laplace transform is known to be challenging, in particular for problems originating in wave dominated problems, we demonstrate the success of this approach in the context of structural health monitoring.

We also highlight the challenges of using the inverse Laplace transform for more complex problems as the efficiency of the inverse transform relies on details of the underlying problem which is often not available.

To address this challenge we propose in the second part a different approach in which only the forward Laplace transform is applied to recast the problem as a parametrized problem for which a reduced basis can be computed. Using this basis in a Galerkin approach on the original problem we then recover a reduced dynamical system which can be advanced using standard techniques. While this is demonstrated to work well and not suffer from stability problems, it is, however, counter intuitive that this basis would be accurate. We shall discuss the analysis that confirms the accuracy of the basis and demonstrate the application of this new method.

References

[1] J. S. Hesthaven, G. Rozza, and B. Stamm, *Certified Reduced Basis Methods for Springer Brief in Mathematics*, Springer Verlag, Berlin, Germany, 2016.

[2] C. Bigoni and J. S. Hesthaven, *Simulation-Based Anomaly Detection and Damage Localization: an Application to Structural Health Monitoring*, Comput. Methods Appl. Mech. Engin. **363** (2020) 112896.

[3] J. S. Hesthaven, C. Pagliantini, and G. Rozza, *Reduced Basis Methods for Time-Dependent Problems*, Acta Numerica **31** (2022) 265–345.

[4] F. Henriquez and J. S. Hesthaven, *Fast numerical approximation of parabolic problems using model order reduction and the Laplace transform*, submitted (2025).

[5] F. Henriquez and J. S. Hesthaven, *Fast Numerical Approximation of Linear, Second-Order Hyperbolic Problems Using Model Order Reduction and the Laplace Transform*, submitted (2025).

Book of abstracts of the 9th International Conference on
Advanced Computational Methods in ENgineering and Applied Mathematics
September, 15–19, 2025.

Forward and Inverse Problems in Nonlinear Acoustics

Barbara Kaltenbacher[1]

[1] *Department of Mathematics, University of Klagenfurt*

e-mails: barbara.kaltenbacher@aau.at

Abstract

The importance of ultrasound is well established in the imaging of human tissue. In order to enhance image quality by exploiting nonlinear effects, recently techniques such as harmonic imaging and nonlinearity parameter tomography have been put forward. As soon as the pressure amplitude exceeds a certain bound, the classical linear wave equation loses its validity and more general nonlinear versions have to be used. Another characteristic property of ultrasound propagating in human tissue is frequency power law attenuation leading to fractional derivative damping models in time domain.

This talk we will first of all provide some background on modeling of nonlinearity on one hand and of fractional damping on the other hand, also giving an idea on the challenges in the analysis of the resulting PDEs. In the practically relevant case of periodic excitations with a source operating at a single or a few frequencies, it is useful to formulate the problem in frequency domain by means of a multiharmonic expansion. In order to justify this, existence of periodic solutions needs to be proven and we will report on recent joint work with Teresa Rauscher (University of Klagenfurt) and Benjamin Rainer (Austrian Institute of Technology) on this.

In the second part of the talk, we address some relevant inverse problems in this context, in particular the above mentioned task of nonlinearity parameter imaging, which leads to a coefficient identification problem for a quasilinear wave equation. In particular, we investigate the recovery of the nonlinearity coefficient commonly labeled as B/A in the literature, which is part of a space dependent coefficient κ in the Westervelt equation governing nonlinear acoustics. Corresponding to the typical measurement setup, the overposed data consists of time trace measurements on some manifold Σ representing the receiving transducer array. We will show some recent results pertaining to the formulation of this inverse problem in frequency domain and numerical reconstruction of piecewise constant coefficients in two space dimensions. The latter is joint work with Bill Rundell (Texas A&M University).

Key words: nonlinear acoustics, multiharmonic expansion, nonlinearity parameter imaging.

1 Models of nonlinear acoustics

The main physical quantities involved in the description of sound propagation are

- the acoustic particle velocity $\mathbf{v}$;
- the acoustic pressure p;
- the mass density ϱ;
- the absolute temperature ϑ;
- the heat flux $\mathbf{q}$;
- the entropy η;

that can be decomposed into their constant mean and a fluctuating part

$$\mathbf{v} = \mathbf{v}_0 + \mathbf{v}_\sim\,, \quad p = p_0 + p_\sim\,, \quad \varrho = \varrho_0 + \varrho_\sim, \quad \text{etc.}$$

where $\mathbf{v}_0 = 0$ in the absence of a flow.

These quantities are interrelated by the following physical balance and material laws:

- the Navier Stokes equation (balance of linear momentum) which under the assumption $\nabla \times \mathbf{v} = 0$ reads
$$\varrho\Big(\mathbf{v}_t + \nabla|\mathbf{v}|^2\Big) + \nabla p = \Big(\frac{4\mu_V}{3} + \zeta_V\Big)\triangle\mathbf{v}\,, \tag{1}$$
where ζ_V is the bulk viscosity and μ_V the shear viscosity;
- the equation of continuity (balance of mass)
$$\nabla\cdot(\varrho\mathbf{v}) = -\varrho_t\,; \tag{2}$$
- the entropy equation: $\varrho\vartheta(\eta_t + \mathbf{v}\cdot\nabla\eta) = -\nabla\cdot\boldsymbol{q}$
- the Gibbs equation (a thermodynamic axiom) $\vartheta d\eta = c_v d\vartheta - p\frac{1}{\varrho^2}d\varrho$
- the equation of state relating the acoustic pressure and density fluctuations $p_\sim$ and $\varrho_\sim$:
$$\varrho_\sim = \frac{p_\sim}{c^2} - \frac{1}{\varrho_0 c^4}\frac{B}{2A}p_\sim^2 - \frac{\varkappa}{\varrho_0 c^4}\Big(\frac{1}{c_V} - \frac{1}{c_p}\Big)p_{\sim t}\,, \tag{3}$$
where B/A is the parameter of nonlinearity, $\varkappa$ the adiabatic exponent, and c_p, c_V the specific heat capacitance at constant pressure and constant volume, respectively.

Analogously to the derivation of the linear wave equation from the linearized versions of these equations, we proceed by subtracting the divergence of (1) from the time derivative of (2) to eliminate the linear velocity term, and inserting the state equation to eliminate the mass density. In the resulting second order in time PDE, we may neglect higher order terms, according to a certain hierarchy, which in nonlinear acoustics is known as Blackstock's scheme, but can alternatively be derived by a non-dimensionalization and asymptotic expansion.

This yields the classical second order in time models of nonlinear acoustics:
The more general of these is Kuznetsov's equation

$$p_{\sim tt} - c^2\triangle p_\sim - b\triangle p_{\sim t} = \left(\frac{1}{\varrho_0 c^2}\frac{B}{2A}p_\sim^2 + \varrho_0|\mathbf{v}|^2\right)_{tt} \tag{4}$$

where b is the diffusivity of sound, $b = \frac{1}{\varrho_0}\Big(\frac{4\mu_V}{3} + \zeta_V\Big) + \frac{\varkappa}{\varrho_0}\Big(\frac{1}{c_V} - \frac{1}{c_p}\Big)$ and the velocity is related to the pressure via the linearization of (1) $\varrho_0\mathbf{v}_t = -\nabla p_\sim$.
If we ignore local nonlinear effects modeled by the quadratic velocity term, thus approximating $\rho_0|\mathbf{v}|^2_{tt} \approx \frac{1}{\rho_0^2 c^2}p^2_{tt}$, we arrive at the Westervelt equation

$$p_{\sim tt} - c^2\triangle p_\sim - b\triangle p_{\sim t} = \frac{\beta_a}{\varrho_0 c^2}p^2_{\sim tt} \tag{5}$$

with $\beta_a = 1 + B/(2A)$.

Taking into account advanced models for interdependence of the quantities above, we arrive at higher order models of nonlinear acoustics, such as the Blackstock-Crighton equation

$$(\partial_t - a\Delta)\left(\psi_{tt} - c^2\Delta\psi - b\Delta\psi_t\right) - r\Delta\psi_t = -\left(\frac{B}{2Ac^2}(\psi_t^2) + |\nabla\psi|^2\right)_{tt} \tag{6}$$

where $a = \frac{\nu}{\mathrm{Pr}}$ is the thermal conductivity or the Jordan-Moore-Gibson-Thompson JMGT equation

$$\tau\psi_{ttt} + \psi_{tt} - c^2\Delta\psi - b\Delta\psi_t = -\left(\frac{B}{2Ac^2}(\psi_t)^2 + |\nabla\psi|^2\right)_t \tag{7}$$

where τ is the relaxation time, that allows to counteract the infinite speed of propagation paradoxon arising in (4) and (5). Also replacement of the strong damping term $b\Delta\psi_t$ by fractional order derivatives leads to refinements of the model, such as, e.g., the fractional JMGT equation

$$\tau^\alpha D_t^{2+\alpha}\psi + \psi_{tt} - c^2\Delta\psi - (\delta + \tau^\alpha c^2)\Delta D_t^\alpha\psi = \left(\frac{B}{2Ac^2}(\psi_t)^2 + |\nabla\psi|^2\right)_t, \tag{8}$$

taking into account power law frequency dependence of the attenuation, cf. [4] and the references therein.

Challenges in the analysis of these models arise from the fact that they exhibit potential degeneracy or equivalently nonlinear state dependence of the wave speed.

2 Multiharmonic Expansion

Motivated by the appearance of so-called higher harmonics in nonlinear acoustics, we aim at formulations in frequency (rather than time) domain in the practically relevant case of sinosoidal type excitations. To this end, recall that for the linear wave equation using a harmonic excitation $r(x,t) = \Re(\hat{r}(x)e^{\imath\omega t})$ and a harmonic ansatz $u(x,t) = \Re\left(\hat{u}(x)e^{\imath\omega t}\right)$ leads to the Helmholtz equation. In case of the Westervelt equation

$$u_{tt} - c^2\Delta u - b\Delta u_t = \kappa(x)(u^2)_{tt} + r$$

a harmonic excitation $r(x,t) = \Re(\hat{r}(x)e^{\imath\omega t})$ and a multiharmonic expansion of u

$$u(x,t) = \Re\left(\sum_{k=1}^{\infty}\hat{u}_k(x)e^{\imath k\omega t}\right)$$

lead to the coupled system

$$-\omega^2 m^2\hat{u}_m - (c^2 + \imath\omega mb)\Delta\hat{u}_m = -\frac{\kappa}{4}\omega^2 m^2\sum_{\ell=1}^{m-1}\hat{u}_\ell\hat{u}_{m-\ell} - \frac{\kappa}{2}\omega^2 m^2\sum_{k=m+2:2}^{\infty}\overline{\hat{u}_{\frac{k-m}{2}}}\hat{u}_{\frac{k+m}{2}} \quad m\in\mathbb{N}.$$

To justify such an expansion, existence of time periodic solutions is essential, which has been done for the Westervelt equation in [1] and for the JMGT equation in [3].

3 Imaging with Nonlinear Ultrasound

Nonlinearity parameter imaging (cf. [2, 5, 6, 7] and the references therein) leads to the inverse problem of identifying the space-dependent coefficient $\kappa(x)$ in Westervelt model

$$\begin{aligned}&\left(u - 2\kappa(x)u^2\right)_{tt} - c_0^2\Delta u - \delta\Delta D_t^\alpha u = r \text{ in } \Omega \times (0,T)\\ &\partial_\nu u + \beta u_t + \gamma u = 0 \text{ on } \partial\Omega \times (0,T), \quad u(0) = 0, \quad u_t(0) = 0 \quad \text{in } \Omega\end{aligned}$$

(with excitation r) from boundary observations

$$g = u \quad \text{on } \Sigma \times (0,T),$$

where $\Sigma \subset \overline{\Omega}$ represents the receiving transducer array. Challenges in this problem result from the fact that the model equation is nonlinear, with the nonlinearity occuring in the highest order term. The unknown coefficient $\kappa(x)$ actually appears in this nonlinear term. Moreover, $\kappa(x)$ is spatially varying whereas the data $g(t)$ is in the "orthogonal" time direction. This is well known to lead to severe ill-conditioning of the inverse problem.
However, multiplication of information in the nonlinear situation due to the appearance of higher harmonics helps the reconstruction and can be seen to even enhance identification of linear parameters in the PDE such as the speed of sound, as needed in ultrasound tomography.

Acknowledgements This work was funded in part by the Austrian Science Fund (FWF) [10.55776/P36318].

References

[1] Barbara Kaltenbacher. Periodic solutions and multiharmonic expansions for the Westervelt equation. *Evolution Equations and Control Theory EECT*, 10:229–247, 2021.

[2] Barbara Kaltenbacher. Identifiability of some space dependent coefficients in a wave equation of nonlinear acoustics. *Evolution Equations and Control Theory*, 2023. see also arXiv:2305.04110 [math.AP].

[3] Barbara Kaltenbacher. Well-posedness of the time-periodic Jordan-Moore-Gibson-Thompson equation. 2024. submitted; see also arXiv:2409.05355 [math.AP].

[4] Barbara Kaltenbacher and Vanja Nikolić. Time-fractional Moore-Gibson-Thompson equations. *Mathematical Models and Methods in the Applied Sciences M3AS*, 32:965–1013, 2022. see also arXiv:2104.13967 [math.AP].

[5] Barbara Kaltenbacher and William Rundell. On the identification of the nonlinearity parameter in the Westervelt equation from boundary measurements. *Inverse Problems & Imaging*, 15:865–891, 2021.

[6] Barbara Kaltenbacher and William Rundell. On an inverse problem of nonlinear imaging with fractional damping. *Mathematics of Computation*, 91:245–276, 2022. see also arXiv:2103.08965 [math.AP].

[7] Barbara Kaltenbacher and William Rundell. Nonlinearity parameter imaging in the frequency domain. *Inverse Problems and Imaging*, 18:388–405, 2023. see also arXiv:2303.09796 [math.NA].

Book of abstracts of the 9th International Conference on
Advanced Computational Methods in ENgineering and Applied Mathematics
September, 15–19, 2025.

Convexification Method in Inverse Problems

Michael V. Klibanov[1]

[1] *Department of Mathematics and Statistics, University of North Carolina at Charlotte*

e-mails: mklibanv@charlotte.edu

Abstract

Coefficient Inverse Problems for PDEs are nonlinear. Therefore, their numerical solution via the least squares minimization method faces the phenomenon of multiple local minima of corresponding cost functionals. The convexification method of the presenter provides a radically different approach which avoids this phenomenon. Carleman estimates form the foundation of the convexification method.

Key words: Carleman estimates, Convexification, Global convergence, Numerical studies

1 Introduction

It is well known that Coefficient Inverse Problems (CIPs) for PDEs are highly nonlinear. Therefore, conventional least squares cost functionals for CIPs suffer the phenomenon of multiple local minima and ravines. Hence, convergence of any gradient-like method of the minimization of such a functional can be rigorously guaranteed only if the starting point of its iterations is located in a sufficiently small neighborhood of the true solution. In other words, this is local convergence, which is close to the small perturbations approach. However, that neighborhood is rarely known in applications.

To avoid the above drawback, the presenter has been developing for many years, starting from works in 1995 and 1997 [7, 8] a radically different the so-called "convexification method". First two papers [7, 8] were purely theoretical ones. However, starting from the paper [1], publications are flourishing, where the theory is combined with numerical studies, see, e.g. [2, 3], [9]-[11] and references cited therein. The book [12] contains a summary of results as of 2021.

The main idea of the convexification comes from the work of Bukhgeim and Klibanov [4] of 1981, in which the tool of Carleman estimates was introduced in the field of Inverse Problems for the first time. The initial goal of [4] was to prove global uniqueness theorems for multidimensional Coefficient Inverse Problems, since such theorems did not exist at that time. However, it was discovered later in [7, 8] that the idea of [4] can be extended to address the above mentioned problem of multiple local minima and ravines of conventional least squares cost functionals for CIPs.

The convexification consists of two steps. On the first step the original CIP is transformed via a nonlinear transformation to a boundary value problem for an integral differential equation, in which the unknown coefficient is not present. On the second step this problem is solved. To do this, a weighted Tikhonov-like functional is constructed. The key element of

that functional is the presence in it of a Carleman Weight Function. This is the function, which is involved as the weight in the Carleman estimate for the corresponding Partial Differential Operator. That functional is minimized on a bounded set $B \subset H$, where H is an appropriate Hilbert space. The diameter $d > 0$ of the set B is an arbitrary fixed number. An important point is that a smallness condition is not imposed on d.

The key theorem is the one which claims the strong convexity of that functional on the set $\overline{B}$ as well as the existence and uniqueness of the minimizer. Furthermore, an estimate of the distance between that minimizer and the true solution is explicitly written. The final theorem claims the convergence of the gradient descent method to the true solution if starting from an arbitrary point of B. Thus, since smallness conditions are not imposed on d, then this is the *global* convergence. At the time being, the convexification is the only numerical method for CIPs with the global convergence property.

References

[1] A. B. Bakushinskii, M. V. Klibanov, and N. A. Koshev, *Carleman weight functions for a globally convergent numerical method for ill-posed Cauchy problems for some quasilinear PDEs*, Nonlinear Analysis: Real World Applications, **34** (2017), 201-224.ield games, *ESAIM Control Optim. Calc. Var.,* 25, paper number 44, 2019.

[2] L. Baudouin, M. de Buhan, and S. Ervedoza, *Global Carleman estimates for waves and applications*, Communications in Partial Differential Equations, **38** (2013), 823–859.

[3] L. Baudouin, M. de Buhan, S. Ervedoza, and A. Osses, *Carleman-based reconstruction algorithm for waves*, SIAM J. Numer. Anal. **59** (2021), 998-1039.

[4] A. L. Bukhgeim and M. V. Klibanov, *Uniqueness in the large of a class of multidimensional inverse problems*, Soviet Math. Doklady, **17** (1981) 244–247.

[5] M. V. Klibanov, *Inverse problems and Carleman estimates*, Inverse Problems, **8** (1992), 575-596.

[6] M. V. Klibanov, *Carleman estimates for global uniqueness, stability and numerical methods for coefficient inverse problems*, J. Inverse and Ill-Posed Problems, **21** (2013), 477–510.

[7] M. V. Klibanov and O. V. Ioussoupouva, *Uniform strict convexity of a cost functional for 3-D inverse scattering problem*, SIAM J. Mathematical Analysis, **26** (1995), 147–179.

[8] M. V. Klibanov, *Global convexity in a three-dimensional inverse acoustic problem*, SIAM J. Mathematical Analysis, **28** (1997) 1371–1388.

[9] M.V. Klibanov, J. Li and W. Zhang, *Convexification for an inverse parabolic problem*, Inverse Problems **36** (2020), 085008.

[10] M.V. Klibanov, J. Li and Z. Yang, *Convexification for the viscocity solution for a coefficient inverse problem for the radiative transfer equation*, Inverse Problems **39** (2023) 125002.

[11] M. V. Klibanov, J. Li and Z. Yang, *Convexification numerical method for the retrospective problem of mean field games*, Applied Mathematics and Optimization, **90**:**6** (2024).

[12] M.V. Klibanov and J. Li, *Inverse Problems and Carleman Estimates: Global Uniqueness, Global Convergence and Experimental Data*, De Gruyter, 2021.

Book of abstracts of the 9th International Conference on
Advanced Computational Methods in ENgineering and Applied Mathematics
September, 15–19, 2025.

Neural networks and inverse problems

Matti Lassas[1]

[1] *Department of Mathematics and Statistics, University of Helsinki*

e-mails: Matti.Lassas@helsinki.fi

Abstract

The goal in inverse problems is to recover information from indirect, incomplete or noisy observations. The problems arise in medical and seismic imaging where measurements made on the exterior of a body are used to deduce the properties of the inaccessible interior. Solution algorithms for these problems can be obtained by combining the classical analytical techniques for inverse problems with neural networks and neural operators which are infinite dimensional generalisations of neural networks.

Key words: Inverse problems, Neural networks, Neural operators

1 Introduction

In [3], we designed neural networks with the essential feature that as the input they take a matrix that is considered as a linear operator. In inverse problems the typical data is a Neumann-to-Dirichlet operator, or a source-to-solution operator, that map an external source to the measured signal. In a finite dimensional case, these data correspond to a matrix.

Naturally, the input matrix $X \in \mathbb{R}^{n\times n}$ can be regarded as a vector in $\mathbb{R}^{n^2}$, but in doing so one does not use the property that the data have the structure of a linear operator. Whereas the standard neural networks, such as the convolutional neural networks, can consider 2-dimensional (tensorial) inputs X in $\mathbb{R}^{n\times n}$ so that they take the neighborhood structure into account, the operator recurrent networks respect the property that the inputs are linear maps.

In [3] we introduced the recurrent operator networks to solve the inverse problem for the wave equation in a 1-dimensional space, that is, to reconstruct a wave speed $c(x)$ from the Neumann-to-Dirichlet map on the boundary. These networks were based on the boundary control method, pioneered in [1], which is an analytic solution method solving the inverse problem for a wave equation. This solution method contains several compact linear operators. When this algorithm is written as a neural network, these compact operators correspond to the weight matrices of a neural network. Instead of assuming that these matrices are fixed, one considers them as 'parameters' of the algorithm that are trained using preferable input-output pairs. In the study of iterative numerical methods using standard neural networks, this approach is called unrolling an algorithm. As the design of the architecture of the network is based on an analytic algorithm, the trained neural network produces at least as good solution to the problem as the analytic algorithm. Thus the training produces a rigorously justified neural network. Moreover, the appropriate bounds for the weight matrices significantly reduce the size of the training data needed to obtain given accuracy with a specified probability. The results in [3] indicate that the operator recurrent networks have the potential to be applied for several traditional solution methods of inverse problems and produce improved algorithms that are rigorously justified.

2 Neural networks and inverse problems for wave equations

In this section we recall a method used to solve an inverse problems for the wave equation in 1-dimensional case, and describe how to transform the method to a neural network.

Let $u(x,t) = u^f(x,t)$ solve the wave equation

$$(\partial_t^2 - c(x)^2\Delta)u(x,t) = 0 \quad \text{on } (x,t) \in M \times \mathbb{R}_+,$$
$$\partial_\nu u(x,t)|_{\partial M\times\mathbb{R}_+} = f(x,t), \quad u|_{t=0} = 0, \quad \partial_t u|_{t=0} = 0,$$

where h is boundary source, $M \subset \mathbb{R}^d$ is a smooth bounded domain. The Neumann-to-Dirichlet map for the wave speed function $c(x)$ is

$$Y_c f = u^f(x,t)\big|_{(x,t)\in\partial M\times\mathbb{R}_+}.$$

In the inverse problem we aim to find the unknown wave speeds $c(x)$ from boundary measurements Y_c.

Next we consider this problem in the 1-dimensional case. Let $u(x,t)$ be the solution of the wave equation

$$(\frac{\partial^2}{\partial t^2} - c(x)^2\frac{\partial^2}{\partial x^2})u(x,t) = 0, \quad x \in \mathbb{R}_+,\ t \in \mathbb{R}_+$$
$$\frac{\partial}{\partial x}u|_{x=0} = f(t), \quad u|_{t=0} = 0, \quad \frac{\partial}{\partial t}u|_{t=0} = 0,$$

where the wave speed $c(x)$ is unknown. Again, we denote $u(x,t) = u^f(x,t)$.

Let $T > 0$. Suppose we are given the Neumann-to-Dirichlet map, $Y = Y_c$, given by

$$Y_c(f) = u^f(x,t)|_{x=0}, \quad t \in (0,2T).$$

The map Y_c is a linear operator, that can be approximated by a matrix. Physically, Y_c maps the boundary source f to the boundary value of the wave $u^f|_{x=0}$.

The travel time of the wave from the boundary point 0 to the point x is

$$\tau(x) = \int_0^x \frac{1}{c(x')}\,dx'.$$

The travel time $\tau(x)$ is equal to the distance of the point x to the boundary point 0 in the Riemannian metric $g = c(x)^{-2}dx^2$. As we discuss below, the wave speed $c(x)$ can be computed using the function $\tau(x)$. Due to this, we study below the inverse problem of finding the inverse travel time function τ^{-1} when Y_c is given.

The solution of the inverse problem, discussed in detail in [3, 6, 7], is based on a blind control problem for a wave equation on the half-axis $\mathbb{R}_4$ with a unknown wave speed $c(x)$. Our aim is to find a boundary source f that produces a wave $u^f(t,x)$ solving the wave equation with unknown wave speed $c(x)$ such that at time $t = T$ the value of the wave, $u^f(T,x)$, is as close as possible to the constant function having the value 1. When the wave speed (or the corresponding metric g) is known, this is a traditional control problem. We consider a blind control problem when the wave speed $c(x)$ is unknown and we only know the map Y_c. We consider the following mimimization problem:

Let $z \in \mathbb{R}_+$ be so large that $\tau(z) > T$. For the depth parameter $0 \le s \le T$, let $h_{\beta,s} \in L^2(\mathbb{R}_+)$ solve

$$\min_h \|u^h(T) - 1\|^2_{L^2(0,z)} + \beta\|Ah\|_{\ell^1} \tag{1}$$

where $supp(h) \subset [T-s, T]$ and $\beta > 0$ is a regularization parameter.

Above, $A : L^2(0, 2T) \to \ell^2$ is an isometry. We define the map $F_{wave,\beta,s} : Y \to h_{\beta,s}$, where $h_{\beta,s}$ is the solution of the minimization problem (1). As the boundary sources h are supported on the time interval $[T-s, T]$, and $\tau(z) > T$, it is not possible to find a boundary source h for which the wave $u^h(\cdot, T)$ would be equal to 1 on the whole interval $[0, z]$. However, it is possible to find sources which are close to 1 on the interval $[0, \tau^{-1}(s)]$. Indeed, it holds that

$$\lim_{\beta \to 0} u^{h_{\beta,s}}(x, T) = \begin{cases} 1, & \text{if } \tau(x) \leq s \\ 0, & \text{otherwise.} \end{cases}$$

We call $h_{\beta,s}(t)$ the optimized sources. Using the optimized sources $h_{\beta,s}$, we compute

$$V(s) = \lim_{\beta \to 0} \langle u^{h_{\beta,s}}(T), 1 \rangle_{L^2(\mathbb{R}_+, c^{-2}dx)} = \mathrm{vol}_c([0, \tau^{-1}(s)]) = \int_0^{\tau^{-1}(s)} \frac{1}{c(x)^2}\, dx.$$

In geometric terms $V(s)$ is the volume of the set $[0, \tau^{-1}(s)]$ in the measure $c(x)^{-1}dV_g$, where $dV_g = c(x)^{-1}dx$ is the Riemannian volume form corresponding to the metric $g = c(x)^{-2}dx$. Furhter, using the function $w(t) = \frac{\partial}{\partial t} V(t)$ one can compute

$$\tau^{-1}(s) = \int_0^s \frac{1}{w(t)}\, dt \quad \text{and} \quad c(\tau^{-1}(s)) = \frac{1}{w(s)}. \tag{2}$$

This means that the wave speed $c(x)$ can be reconstructed in the travel-time coordinates using the Neumann-to-Dirichlet map Y_c.

Next consider how the above algorithm can be implemented using neural networks. To this end, we define a family of neural networks (operator recurrent networks) than can approximate functions $f : \mathbb{R}^{n \times n} \to \mathbb{R}^n$. Before this, we recall the definition of the more standard neural networks, whose input is a vector $x \in \mathbb{R}^n$. Afterwards, we define the operator recurrent networks which input is a matrix $Y \in \mathbb{R}^{n \times n}$.

Definition 1 *A standard neural network is a function $f_\theta : \mathbb{R}^{d_0} \to \mathbb{R}^{d_L}$ defined by*

$$\begin{aligned} h_0 &= x, \\ h_{\ell+1} &= \phi\left(A_\theta^\ell h_\ell + b_\theta^\ell\right), \quad \ell = 0, \ldots, L-1, \\ f_\theta(x) &= h_L. \end{aligned}$$

*Above, $L+1$ is the depth of the neural network, $\ell = 0, 1, 2, \ldots, L$ is the index of a layer, and h_ℓ are intermediate output at layer ℓ. Moreover, $b_\theta^\ell \in \mathbb{R}^{d_{\ell+1}}$ and $A_\theta^\ell \in \mathbb{R}^{d_{\ell+1} \times d_\ell}$ are the bias vectors and the weight matrixes that depend on the parameters $\theta = (\theta_1, \theta_2, \ldots, \theta_m)$ respectively. Moreover, ϕ is the activation function, the Rectified Linear Unit (*relu*), given by*

$$\phi : \mathbb{R}^d \to \mathbb{R}^d, \quad \phi(x_1, \ldots, x_d) = (\max(0, x_1), \ldots, \max(0, x_d))$$

Definition 2 *An* operator recurrent network *with depth $L+1$, width n, and parameters θ is a function $f_\theta : \mathbb{R}^{n \times n} \to \mathbb{R}^n$ given by*

$$\begin{aligned} h_0 &= b_\theta^{0,1}, \\ h_\ell &= \phi\left(A_\theta^{\ell,1} h_{\ell-1} + A_\theta^{\ell,2} Y h_{\ell-1} + b_\theta^\ell\right), \\ f_\theta(Y) &= h_L, \end{aligned}$$

where the initial vector $h_0 = b_\theta^{0,1} \in \mathbb{R}^n$ is independent of the input $Y \in \mathbb{R}^{n \times n}$ and $A_\theta^{\ell,i} \in \mathbb{R}^{n \times n}$, $b_\theta^{\ell,i} \in \mathbb{R}^n$. The activation functions ϕ are the relu functions.

By applying the iterated soft-thresholding algorithm (ISTA) of Daubechies, Defrise and de Mol, developed in [2], it turns out that there are recurrent neural networks that define functions $F_{j,\beta,s} : Y \to h_{\beta,s}$, $j \in \mathbb{Z}_+$ such that $F_{wave,\beta,s}(Y) = \lim_{j\to\infty} F_{j,\beta,s}(Y)$. Thus, the solution of the inverse problem for the wave equation can written as a limit of recurrent neural networks. This leads to the following result:

Theorem 1 *Let $T > 0$ and $x \in [0,T]$. Then, there are recurrent neural networks $f_{\theta(\beta,s,x)}$ and vectors $m_{\beta,s,x}$, having the depth $L = L(\beta,s)$, the width $D = D(\beta,s)$, and the weight matrixes and bias vectors $\theta^*(\beta,s,x) = (A^{\ell,1}_{\beta,s,x}, A^{\ell,2}_{\beta,s,x}, b^{\ell,2}_{\beta,s,x})_{\ell=1}^{L}$, depending on $\beta > 0$, $s > 0$, and x, such that the value of the wave speed function $c(\cdot)$ at the point x, that is, $c(x)$, can be reconstructed from the Neumann-to-Dirichlet map Y_c corresponding to $c = c(\cdot)$ by using the formulas (2) and the function*

$$w(s) = \lim_{\beta\to 0} f_{\theta^*(\beta,s,x)}(P_L(Y_c)) \cdot m_{\beta,s,x}, \tag{3}$$

where P_L maps an operator $Y : L^2([0,2T]) \to L^2([0,2T])$ to a matrix $M = (M_{j,k})_{j,k=1}^{D}$, $M_{j,k} = \langle Y(\chi_{j,D}), \chi_{k,L}\rangle_{L^2(0,2T)}$, where $\chi_{j,D}(t)$ are the indicator functions of the intervals $(2T(j-1)/D, 2Tj/D) \subset [0,2T]$.

In addition to the above results, in the talk we will consider the mapping properties, in particular the injectivity, of neural networks, considered in [4, 5].

Acknowledgements This work has been partially supported by the Advanced Grant project 101097198 of the European Research Council and Research Council of Finland, project 336786 and 359186.

References

[1] M. Belishev, *An approach to multidimensional inverse problems for the wave equation. (Russian)* Dokl. Akad. Nauk SSSR 297 (1987), 524–527.

[2] I. Daubechies, M. Defrise, Michel, C. De Mol, *An iterative thresholding algorithm for linear inverse problems with a sparsity constraint.* Comm. Pure Appl. Math. 57 (2004), 1413-1457.

[3] M. de Hoop, M. Lassas, C. Wong. *Deep learning architectures for nonlinear operator functions and nonlinear inverse problems.* Math. Statistics and Learning, 4 (2021), 1-86.

[4] T. Furuya, M. Puthawala, M. Lassas, M. de Hoop, *Globally injective and bijective neural operators.* Advances in Neural Information Processing Systems 36 (NeurIPS) 2023, 57713.

[5] T. T. Furuya, M. Puthawala, M. Lassas, M. de Hoop, *Can neural operators always be continuously discretized?* Advances in Neural Information Processing Systems (NeurIPS) 2024.

[6] A. Katchalov, Y. Kurylev, M. Lassas, *Inverse boundary spectral problems.* Chapman-Hall/CRC, Boca Raton, FL, 2001. xx+290 p.

[7] J. Korpela, M. Lassas, L. Oksanen, *Discrete regularization and convergence of the inverse problem for 1+1 dimensional wave equation.* Inverse Problems and Imaging 13 (2019), 575-596.

Book of abstracts of the 9th International Conference on
Advanced Computational Methods in ENgineering and Applied Mathematics
September, 15–19, 2025.

Hybrid pde models for bio-medical applications

Barbara Wohlmuth[1]

[1] *TUM School of Computation, Information and Technology, Technical University of Munich (TUM)*

e-mails: wohlmuth@cit.tum.de

Abstract

In this talk, we consider the mathematical modelling and numerical simulation of different bio-medical applications ranging from cerebral aneurysmen to vascular tumor growth and drug response. We combine numerical schemes on different spatial scales and illustrate the mathematical and numerical challenges of the coupling of 0D-1D-3D models as well as of agent-based dynamics. Firstly, we consider an abstract framework for mixed dimensional approaches. While nonlinear hyperbolic 1D PDE models can effectively be used to describe the flow and transport in the vascular tree, homogenized 3D porous media models can be considered to simulate flow and transport in capillaries and tissue. We introduce a calibrated generic arterial network to generate inflow data for patient specific vasculature and tissue data sets. Secondly, we comment on the interaction of micro- and macro-scales effects. While agent-based simulation approaches can effectively model cell-cycle effects, the extensions to tissue-scale mechanical interactions is not straightforward. To overcome these limitations, agent based cell dynamics is coupled to a FEM based poro-elastic formulation of the surrounding tissue. This enables us to study the interplay between cellular processes and macroscopic mechanical forces, such as interstitial fluid flow and pressure-induced cell responses. Thirdly, we consider different aspects and mathematical challenges in case of cerebral aneurysmen. From non-Newtonian 3D blood flow by Lattice Boltzmann methods in patient specific geometries to the endovascular coil embolization by an extended discrete elastic rod model taking into account bending, twisting and self-contact to the formation of clots by a system of reaction-advetion-diffusion equations coupled to the Navier–Stokes system.

Minisymposia

MS1: Numerical and computational methods for wave equations

Organiser: Kristof Cools and Le Van Chien (Ghent University)

Description: The rapidly rising variety of acoustic and electromagnetic applications has demanded the high-precision computing capacity of wave equations in complicated scenarios, for instance, modelling and analyzing systems in the presence of wide bandwidth data, large-scale, multi-scale and multi-physics geometries with complex material properties. This demand has accelerated the critical need for studies of robust, stable and highly efficient computational methods, necessitating more and more efforts from both mathematicians, physicists, computer scientists, and engineers. Within this mini symposium, we aim to bring together international experts in the field of numerical and computational methods for acoustic and electromagnetic wave equations to discuss the latest research and knowledge, explore challenges and new directions, as well as to foster interaction and collaboration between communities. The topics of this mini symposium cover both frequency-domain and time-domain challenges, with a particular focus on finite and boundary element methods.

Book of abstracts of the 9th International Conference on
Advanced Computational Methods in ENgineering and Applied Mathematics
September, 15–19, 2025.

On a New Class of Fast Direct Solvers for High-Frequency Problems Based on Operator Filtering

Viviana Giunzioni[1], Johann Bourhis[2], Clément Henry[2], Adrien Merlini[2] and Francesco P. Andriulli[1]

[1] *Department of Electronics and Telecommunications, Politecnico di Torino, Turin, Italy*

[2] *Microwave Department, IMT Atlantique, Brest, France*

Abstract

We present a new family of fast direct solvers for high-frequency scattering and radiation problems, readily applicable within inverse-problem workflows. By exploiting the spectral structure of properly regularized integral operators, we obtain low-rank representations through compression and application of newly introduced filtering techniques, which allow for compensation of spectral pollution and enable fast and efficient direct inversion.

Key words: Integral equations, High-frequency, Fast direct solver, Filtering techniques

1 Introduction

A wide range of inverse methods, particularly those targeting source inversion, require repeatedly solving forward problems to converge to a solution. In such cases, direct solvers are especially advantageous over iterative ones due to their efficiency in handling multiple right-hand sides. Among the different forward solution techniques, the boundary element method (BEM) is particularly effective for modeling time-harmonic electromagnetic scattering from objects of arbitrary shape. A commonly used formulation in this setting is the Electric Field Integral Equation (EFIE), which, although widely employed, presents notable computational difficulties, yielding dense, ill-conditioned linear systems [1]. Furthermore, LU factorization of these dense matrices typically costs $O(N^3)$, with the problem size N growing at least as $(ka)^{d-1}$—where ka is the electrical size and d the dimensionality—making high-frequency simulations prohibitively expensive. Fast algorithms, such as the Fast Multipole Method, reduce the cost of matrix-vector products to quasi-linear levels, while ill-conditioning is often addressed through techniques like Calderón preconditioning [2], multilevel strategies, and algebraic corrections. However, acceleration and preconditioning have traditionally been treated as distinct challenges and addressed independently, yielding frameworks suited to iterative but not direct solvers.

This work removes that separation by introducing a new class of methods that integrate acceleration and regularization into a unified framework. Leveraging structural features of fast solvers and preconditioners for boundary integral operators, we introduce a regularization process that yields formulations naturally compatible with fast direct inversion. However, accomplishing this is challenging due to the spectral pollution and BEM discretization error of standard integral operators. A key idea enabling this synthesis is the recently introduced Operator Filtering [3], which allows correction of spectral deficiencies and enables efficient direct inversion.

2 New Fast Direct Solution Strategies

We study the time-harmonic electromagnetic scattering by a perfectly electrically conducting (PEC) object whose boundary is a smooth, closed curve $\Gamma \subset \mathbb{R}^2$, under either transverse-electric (TE) or transverse-magnetic (TM) polarization. The problem is modeled by the electric or by the magnetic field integral equation (EFIE or MFIE), which, after Galerkin discretization, lead to the matrix systems $\mathbf{Z}\mathbf{j} = \mathbf{v}_e$ and $(\mathbf{I}/2 + \mathbf{D})\mathbf{j} = \mathbf{v}_h$. Calderón preconditioning naturally extends to a combined-field formulation, but naively combining the preconditioned EFIE with the MFIE reintroduces interior resonances, since the two operators share part of their nullspace. To suppress these spurious modes, the wavenumber of the preconditioner must be complex. While the Yukawa potential—using a purely imaginary wavenumber—is a common choice, dynamic applications benefit more from a fully complex wavenumber with a tunable negative imaginary part. This lossy component can be optimized to enhance stability and performance across a wide range of geometries. The resulting preconditioned system is $\left(\frac{1+2\alpha}{4}\mathbf{I} + \mathbf{C}\right)\mathbf{j} = \mathbf{v}_{e,\text{prec.}} + \alpha\mathbf{v}_h$, where matrices $\mathbf{I}$ and $\mathbf{C}$ denote matrices with spectrum clustering to 1 and 0, respectively. Hence, (2) represents the discretization of the sum of a scaled identity and a compact operator, i.e., a second-kind Fredholm operator.

During the talk, we will show how to leverage the spectral structure of the preconditioned operator to isolate its principal part contribution and compress its reminder. Filtering and compression techniques will be applied to extract the relevant degrees of freedom of the compact part, to retain only those modes needed to meet a prescribed accuracy. Consequently, the compact part will admit a rank-deficient skeleton representation, characterized by a slowly increasing rank, typically $O\left((ka)^{1/3}\right)$. Substituting this decomposition into the Woodbury inversion formula will yield an efficient algorithm for applying the inverse operator to any vector. Numerical experiments will validate the theory and demonstrate the practical impact of the proposed techniques. Results on both convex and trapping geometries will be presented to assess the performance of the proposed schemes over a diverse set of scatterers.

Acknowledgements This work was supported by the European Innovation Council (EIC) through the European Union's Horizon Europe research Programme under Grant 101046748 (Project CEREBRO).

References

[1] S. B. Adrian, A. Dély, D. Consoli, A. Merlini, F. P. Andriulli, *Electromagnetic integral equations: Insights in conditioning and preconditioning*, IEEE Open Journal of Antennas and Propagation, vol. 2, pp. 1143–1174, 2021.

[2] F. P. Andriulli, K. Cools, I. Bogaert, E. Michielssen, *On a well-conditioned electric field integral operator for multiply connected geometries*, IEEE Transactions on Antennas and Propagation, vol. 61, no. 4, pp. 2077–2087, 2013.

[3] A. Merlini, C. Henry, D. Consoli, L. Rahmouni, A. Dély, F. P. Andriulli, *Laplacian filtered loop-star decompositions and quasi-Helmholtz filters: Definitions, analysis, and efficient algorithms*, IEEE Transactions on Antennas and Propagation, vol. 71, no. 12, pp. 9289–9302, 2023.

Book of abstracts of the 9th International Conference on
Advanced Computational Methods in ENgineering and Applied Mathematics
September, 15–19, 2025.

An arbitrary order finite-volume scheme for two-dimensional elliptic Helmholtz equation with interfaces

Nicolas Bourdineaud[1,2], Guillaume Duchateau[1] and Rodolphe Turpault[2]

[1] *CEA-CESTA, 15 Avenue des Sablières, CS60001, 33116 Le Barp Cedex, France,*

[2] *Univ. Bordeaux, CNRS, Bordeaux INP, IMB, UMR 5251, F-33400, Talence, France,*

e-mails: nicolas.bourdineaud@u-bordeaux.fr, Guillaume.DUCHATEAU@cea.fr, rodolphe.turpault@u-bordeaux.fr

Abstract

A numerical method is implemented to evaluate the propagation of a laser electric field, described by the Helmholtz equation, into a porous medium. It consists of a high-order finite volume scheme to solve the Helmholtz equation with interfaces where the optical properties are discontinuous. Both the reliability and efficiency of the numerical scheme are presented. Results for multiple scattering are also shown.

Key words: Finit volume, Helmholtz, High order, Interfaces

1 Introduction

Wave propagation in heterogeneous media, and in particular porous media leading to multiple scattering, is a subject of interest leading to numerous applications. Examples include the attenuation of acoustic waves or the scatterring of electromagnetic waves by porous media. The propagation of these waves is described by the Helmholtz elliptic equation. In particular, we are interested in electromagnetic waves here described with its electric fields. Solving this equation is computationally expensive, since large computational domains (hundreds of wavelengths) have to be considered, and porosities have to be properly meshed. Increasing the order of the scheme leads to a more efficient method in terms of calculation time. To our knowledge, there is no high-order finite volume schemes for solving the Helmoltz equation, which is the purpose of the present work. A particular work has been carried out to preserve the order of convergence of the method at interfaces between two media (at the porosity interface here). Results are presented to demonstrate the efficiency of the method.

2 Arbitrary order finite-volume schemes for two-dimensional Helmholtz equation

The complex Hemholtz equation describes the propagation of a monochromatic electromagnetic wave in a medium :

$$\Delta E + k_0^2 \varepsilon E = 0, \tag{1}$$

with $E \in \mathbb{C}$ the laser electric field, $k_0 = 2\pi/\lambda$ the wave number (λ the wavelength) and $\varepsilon \in \mathbb{C}$ the permittivity accounting for the optical response of the medium. Note that the permittivity ε is discontinuous at the interface between two media.

The Helmholtz equation is solved with a high-order finite-volume scheme using polynomial reconstruction of degree d on an unstructured triangular mesh. A special treatment, at the interface between two media where the permittivity is discontinuous, which is inspired from [2], is proposed to preserve the high order. The scheme denoted M1 corresponds to the method without taking discontinuity into account, while M2 indicates the scheme that uses flux adaptation at interfaces.

Figure 1 shows convergence results for a test case of plane wave scattering through a circular pore. Figure 1(a) shows a convergence calculation in space. It can be seen that the discontinuity at the interface decreases the order of convergence of the M1 scheme (order 2), while the M2 scheme maintains the high order. Thus, for the M2 scheme, polynomials of degree d yields to a scheme converging to order d. Note that the M2 method with $d = 7$ method saturates due to various numerical errors. Figure 1(b) shows the relative error of the scheme as a function of machine computation time. It can be seen that increasing the order and taking into account the interfaces in the M2 method results in a more efficient scheme in terms of computation time. These results demonstrate the efficiency of our approach, and in particular how properly the interfaces are handled. In the presentation, calculations of multiple scattering within a porous medium will be shown.

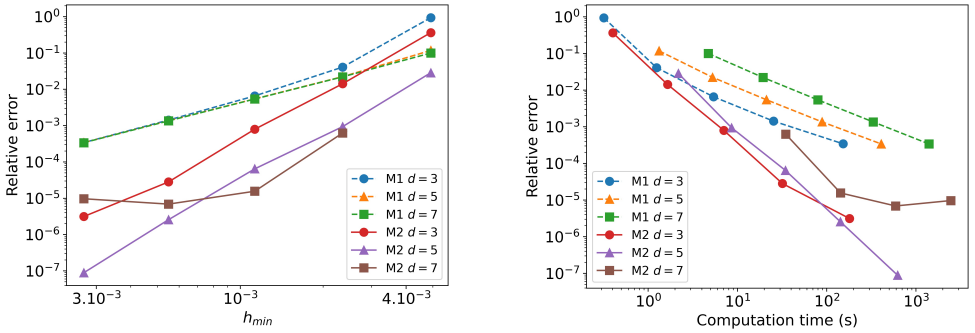

(a) Convergence curves in space

(b) Relative error as a function of computation time

Figure 1: (a) Convergence in space and (b) computation time for different polynomial degrees. Without interface adaptation: M1 method. With interface adaptation: M2 method.

References

[1] M. Born, E. Wolf, A. B. Bhatia, P. C. Clemmow, D. Gabor, A. R. Stokes, A. M. Taylor, P. A. Wayman, and W. L. Wilcock, *Principles of Optics: Electromagnetic Theory of Propagation, Interference and Diffraction of Light,* 7th ed. (Cambridge University Press, 1999).

[2] R. Costa, J. M. Nóbrega, S. Clain, and G. J. Machado, *Very high-order accurate polygonal mesh finite volume scheme for conjugate heat transfer problems with curved interfaces and imperfect contacts*, Computer Methods in Applied Mechanics and Engineering 357, 112560 (2019).

Book of abstracts of the 9th International Conference on
Advanced Computational Methods in ENgineering and Applied Mathematics
September, 15–19, 2025.

Multi-domain/multi-method preconditioners for an efficient solution of EFIE

T. Galtier[1] and D. Levadoux[1]

[1] *Information Processing and Modeling Department, ONERA*

e-mails: timothee.galtier@onera.fr, david.levadoux@onera.fr

Abstract

Wave diffraction problems can be formulated in integral form and then solved by the Boundary Element Method (BEM). However, BEM requires the resolution of full, large, and ill-conditioned linear systems. Various preconditioning techniques exist, but each is limited to the treatment of very specific geometries. However, the applications we are targeting (typically a weapon aircraft with all its surface details) are made up of very different parts (landing gear, air inlet, etc.) each requiring specific treatment. To deal with this difficulty, we develop a **multi-domain** and **multi-method** preconditioner using a technique called BDM (Body Decomposition Method).

Key words: Finite Elements Methods, High Performance Computing, Integral equation, Preconditionner, Wave diffraction

The Electric Field Integral Equation (EFIE) operator is physically interpreted as an impedance operator $\mathrm{Z} : \mathbf{n} \times \mathbf{H} \mapsto \mathbf{E}_{|\tan}$, linking a surface electric current injection to the voltage created in response. We note Y the inverse of Z and $\widetilde{\mathrm{Y}}$ its approximation. In order to construct a $\widetilde{\mathrm{Y}}$ capable of fully exploiting the geometric characteristics of the diffracting object, we construct a piecewise preconditioner. We draw inspiration from a method that has proven its effectiveness in designing new well-conditioned equations [1].

The method begins by using a quadratic partition of unity which allows us to split the diffracting object into different components (called *bodies*), on each of which a suitable $\widetilde{\mathrm{Y}}$ approximation technique is implemented. In practice, the object is covered by several subsurfaces, on which a parametrix of Z is accessible by analytical or numerical means. The initial surface Γ is therefore decomposed into N bodies Γ_n ($n \in [\![1, N]\!]$) and a neighbourhood Γ_s of $\bigcup_n \partial\Gamma_n$ called the skeleton of Γ to which are associated a quadratic partition of the unity $\{(\Gamma_n, \chi_n)\}_{1\leq n\leq N} \cup \{(\Gamma_s, \chi_s)\}$. For a given body Γ_n, we use a map $\psi_n : \Gamma_n \to \widetilde{\Gamma}_n$ associating Γ_n to a simpler geometry $\widetilde{\Gamma}_n$ on which Y is more easy to approximate. The map ψ_n canonically induces a linear operator, still denoted ψ_n, mapping surface currents from Γ_n to $\widetilde{\Gamma}_n$. We propose to approximate Y as

$$\widetilde{\mathrm{Y}} = \chi_s \mathrm{Y}_s \chi_s + \sum_n \chi_n \psi_n^{-1} \widetilde{\mathrm{Y}}_n \psi_n \chi_n \,, \tag{1}$$

where Y_s, $\widetilde{\mathrm{Y}}_n$ are resp. some approximations the admittance of Γ_s, $\widetilde{\Gamma}_n$ playing the role of local precondioners of various kinds :

- $\sigma^{-1}(Z)$ denotes a family of preconditioners whose underlying operators have a principal symbol equal to that of Y [1][2].
- FFT is a kind of preconditioner given by the convolution of elementary solutions ("elementary currents") compressed with a fast Fourier transform [3] .
- $\mathcal{H}$-LU is the preconditioner based on the inverse of Z obtained with a LU decomposition in the $\mathcal{H}$-matrix format [4].

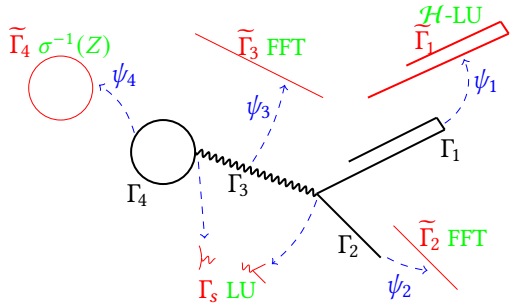

Figure 1: Example of body decomposition performed by the BDM preconditioner. Local preconditioners are shown in green.

We emphasize that the role of the skeleton Γ_s and its cut-off function χ_s is crucial because it allows to build a global preconditioner whose underlying operator has the "good" principal symbol (i.e., that of the admittance Y of the object).

The talk will present the treatment of various application cases (cavity, plates exfoliation, etc.) of this approach. We will discuss the different possible decompositions for each case and the local preconditioners used for bodies.

References

[1] D. Levadoux, *Stable integral equations for the iterative solution of electromagnetic scattering problems*, Comptes Rendus Physique, vol. 7, 2006.

[2] D. Levadoux, F. Millot, S. Pernet, *New Trends in the Preconditioning of Integral Equations of Electromagnetism*, Scientific Computing in Electrical Engineering SCEE, 2008.

[3] M. Baray, *Approche tensorielle pour la résolution des équations intégrales en acoustique et en électromagnétisme*, Thèse de doctorat, Université de Toulouse , 2023.

[4] B. Lizé, *Résolution directe rapide pour les éléments finis de frontière en électromagnétisme et acoustique : H-matrices. Parallélisme et applications industrielles*, Thèse de doctorat, Université Paris-Nord- Paris XIII , 2014.

Book of abstracts of the 9th International Conference on
Advanced Computational Methods in ENgineering and Applied Mathematics
September, 15–19, 2025.

BEACHpack: a BEM software package for frequency sweeping calculations

Kobe Bruyninckx[1], Simon Dirckx[2], Daan Huybrechs[1] and Karl Meerbergen[1]

[1] *Department of Computer Science, KU Leuven*

[2] *Oden Institute for Computational Engineering & Sciences, University of Texas at Austin*

e-mails: kobe.bruyninckx@kuleuven.be, simon.dirckx@austin.utexas.edu, daan.huybrechs@kuleuven.be, karl.meerbergen@kuleuven.be

Abstract

Boundary Element Methods (BEM) are a popular approach to simulate wave scattering and propagation problem in the frequency domain. BEM discretizations typically give rise to dense systems, but fast solvers and memory-efficient representations have been thoroughly investigated. However, these are typically used to solve a system at a particular frequency. The BEACHpack software package, developed at KU Leuven by the authors, optimizes for the discretization and solution of scattering problems for a range of frequencies. We refer to this as the frequency sweeping problem. The software includes a memory-compact format for the representation of frequency dependent integral operators. The format is based on tensor extensions of Hierarchical Matrices and of Uniform Hierarchical Matrices. In addition, the code aims to enable linearization techniques for the efficient representation of frequency-dependent solutions. BEACHpack is written in C++ and is publicly available.

Key words: integral equations, boundary element method, hierarchical matrices, frequency sweeping

1 Introduction

BEACHpack centers on scattering problems as described by the 3D Helmholtz equation

$$\Delta u + k^2 u = 0, \qquad x \in \mathbb{R}^3 \setminus \Omega,$$

formulated as an integral equation. The parameter k in this equation is called the wavenumber. Boundary conditions should be provided along the boundary of a domain Ω, which is assumed given in the form of a mesh. Several common integral equation formulations are supported, including the single layer, double layer and hypersingular operator. For technical definitions of the standard mathematical formulations in this context, we refer to [1].

The software is written in C++ and is publicly available in a git repository: https://gitlab.kuleuven.be/numa/software/beachpack/. The principles of the software are explained in a number of publications, which we will now review.

2 Algebraic data-compact representation

A popular approach for the representation of an integral operator after discretization is through hierarchical matrices or H-matrices. Although the matrix at hand is dense, large subblocks may be well approximated by matrices of low rank. This can be used to reduce the storage requirements, as well as to expedite a matrix-vector product. Such low-rank approximations can be constructed using Adaptive Cross Approximation techniques.

This approach is extended in [2] to represent a wavenumber-dependent discretization of the operator. This gives rise to a tensor format, in which the third mode – the direction of the wavenumber – is continuous. A variant of adaptive cross approximation is described and rational approximation is used to compress the continuous direction to a discrete dimension with a very modest number of degrees of freedom.

This results in a very compact representation which is valid for a continuous range of frequencies, rather than a single frequency. The amount of memory needed for such representations is only a small multiple of that needed for the H-matrix representation at a single frequency.

3 Uniform H-matrix compression

Compression results are further improved in [3]. Here, the H-matrix representation is substituted for a so-called uniform H-matrix representation, in which data of the low-rank approximations is efficiently shared across several subblocks of the system. However, the recursive complexity of $\mathcal{H}^2$-matrices is avoided. It is shown in [3] that this leads to a constant reduction both in memory usage and in matrix-vector timings. The format and the computations remain amenable to straightforward parallellization, in contrast to more advanced $\mathcal{H}^2$-matrix formats or Fast Multipole Method formulations.

4 Ongoing research

The current topics of research relate to exploiting the data-compact representation in order to develop fast frequency-sweeping solvers. We will give an overview of the main ideas and some promising initial numerical results.

Acknowledgements This work has been supported by FWO-Flanders project G088622N.

References

[1] D. Colton, R. Kress, *Integral equation methods in scattering theory*, Wiley, 1993.

[2] S. Dirckx, D. Huybrechs, K. Meerbergen, *Frequency Extraction for BEM Matrices Arising From the 3D Scalar Helmholtz Equation*, SIAM J. Sci. Comput. **44** (2022) B1282–B1311.

[3] K. Bruyninckx, D. Huybrechs, K. Meerbergen, *Uniform H-Matrix Compression with Applications to Boundary Integral Equations*, SIAM J. Sci. Comput. **44** (2025) B618–B644.

Book of abstracts of the 9th International Conference on
Advanced Computational Methods in ENgineering and Applied Mathematics
September, 15–19, 2025.

Local Multiple Traces Formulation for Heterogeneous Electromagnetic Scattering

Paul Escapil-Inchauspé[1] **and Carlos Jerez-Hanckes**[1]

[1] *Fundación INRIA Chile, Santiago, Chile*

e-mails: paul.escapil@inria.cl, carlos.jerez@inria.cl

Abstract

We consider the three-dimensional time-harmonic electromagnetic (EM) wave scattering transmission problem involving heterogeneous scatterers using the local multiple traces formulation (MTF). This scheme assigns independent boundary unknowns to each subdomain and weakly enforces Calderón identities along with interface transmission conditions. As a result, the MTF effectively handles shared points or edges among multiple subdomains, while supporting various preconditioning and parallelization strategies. Nevertheless, implementing standard solvers presents significant challenges. To address these difficulties, we propose a novel framework that suitably defines approximation spaces and enables the efficient exchange of normal vectors across subdomain boundaries. This framework leverages the skeleton mesh, representing the union of all interfaces, as the computational backbone, and constitutes the first scalable implementation of the EM MTF. Furthermore, we explore the effects of increasing subdomains and block On- Surface-Raditation-Condition (OSRC) preconditioning, to validate our approach and provide insights for future developments.

Keywords: Maxwell scattering, multiple traces formulation, boundary element methods, operator preconditioning

1 Problem Statement

We address the solution of electromagnetic (EM) wave transmission problems involving heterogeneous, open, and bounded scatterers $\Omega_S \in \mathbb{R}^3$ such that, for $M \in \mathbb{N}$, one can write $\overline{\Omega}_S := \bigcup_{i=1}^{M} \overline{\Omega}_i$, $\Omega_0 := \mathbb{R}^3 \setminus \overline{\Omega}_S$, $\Gamma_i := \partial\Omega_i$, with interfaces $\Gamma_{ij} := \Gamma_i \cap \Gamma_j$, defining

$$\Lambda_i := \left\{ j \in \{0, \dots, M\} : j \neq i \quad \text{and} \quad \Gamma_{ij} \neq \emptyset \right\}, \quad i \in \{0, \dots, M\},$$

and $\Sigma := \bigcup_i \Gamma_i$. For $i \in \{0, \dots, M\}$, we define the *Cauchy trace space* of electric and magnetic surface currents:

$$\mathbb{H}(\Gamma_i) := \boldsymbol{X}(\Gamma_i) \times \boldsymbol{X}(\Gamma_i), \quad \text{with} \quad \boldsymbol{X}(\Gamma_i) := \boldsymbol{H}_{\times}^{-1/2}(\mathrm{div}_{\Gamma_i}, \Gamma_i),$$

and the *multiple traces spaces* $\mathbb{H}(\Sigma) := \mathbb{H}(\Gamma_0) \times \cdots \times \mathbb{H}(\Gamma_M)$, with clear extensions to $\widetilde{\boldsymbol{H}}_{\times}^{-1/2}(\mathrm{div}_{\Gamma_i}, \Gamma_i)$. For $\mathbf{u}^{\mathrm{inc}} \in \mathbb{H}(\Sigma)$, seek $\mathbf{u} \in \mathbb{H}(\Sigma)$ such that the variational form:

$$\langle \mathbf{M}\mathbf{u}, \mathbf{v} \rangle_{\times} = \langle \mathbf{u}^{\mathrm{inc}}, \mathbf{v} \rangle_{\times}, \quad \forall \mathbf{v} \in \widetilde{\mathbb{H}}(\Sigma), \tag{1}$$

is satisfied with

$$\mathbf{M} := 2\boldsymbol{\mathcal{A}} + \boldsymbol{\mathcal{X}} = \begin{bmatrix} 2\boldsymbol{\mathcal{A}}_0 & \boldsymbol{\mathcal{I}}_{10} & \dots & \boldsymbol{\mathcal{I}}_{M0} \\ \boldsymbol{\mathcal{I}}_{01} & 2\boldsymbol{\mathcal{A}}_1 & \dots & \boldsymbol{\mathcal{I}}_{M1} \\ \vdots & \vdots & \ddots & \vdots \\ \boldsymbol{\mathcal{I}}_{0M} & \boldsymbol{\mathcal{I}}_{1M} & \dots & 2\boldsymbol{\mathcal{A}}_M \end{bmatrix}. \tag{2}$$

wherein the scaled Calderón operators in $\boldsymbol{\mathcal{A}} := \mathrm{diag}(\boldsymbol{\mathcal{A}}_i)$ contain the electric and magnetic field boundary integral operators $\mathcal{K}_k^i$, $\mathcal{T}_k^i$, and the transmission operators across interfaces $\boldsymbol{\mathcal{I}}_{ij}$ are restriction-orientation-and-extension-by-zero operators per interface, following [1, 3].

2 Implementation and Preconditioning

We implement the EM-MTF in Bempp-cl [2] on the skeleton mesh Σ^h of Σ. We assemble operators on the triangles associated with the given subdomains and set the corresponding normal vector. For each element $\tau \in \Sigma_h$, we attach a normal orientation multiplier `swap` $\in \{-1, 1\}$ and its degrees of freedom `dofs`. The normal multipliers allows to swap the normal vector orientation in assembly routines. By observing that $\Gamma_i = \bigcup_{j\in\Lambda_i} \Gamma_{ij}$, one can infer that the set Λ_i can be represented as a connectivity graph. Each subdomain Γ_i for $i \in \{0, \dots, M\}$ is defined as a node, and an edge is added between nodes i and j if $j \in \Lambda_i$. Since the normal vector is defined from $\min(i, j)$ to $\max(i, j)$, no action is needed when $\min(i, j) = i$ (i.e., `swap` $= 1$), while the normal is swapped when $\min(i, j) = j$ (i.e., `swap` $= -1$). Additionally, the normal swapping vector can be easily integrated into the core assembly routines. For any $\boldsymbol{\phi}_n \in \mathrm{RWG}_i$, $n \in \{1, \dots, N_i\}$ and $\boldsymbol{\psi}_m \in \mathrm{RWG}_j$, $m \in \{1, \dots, N_j\}$, the matrix for the transmission operator reads as

$$\widetilde{\mathbf{I}}_{mn}^{ij} = \langle \widetilde{\mathcal{I}}^{ij} \boldsymbol{\phi}_n, \boldsymbol{\psi}_m \rangle_\times = \sum_{\tau \in \Gamma_{ij}^h} \boldsymbol{\phi}_n \cdot (\mathbf{n}_{ij} \times \boldsymbol{\psi}_m) = \langle \mathcal{I}^i \boldsymbol{\phi}_n, \boldsymbol{\psi}_m \rangle_\times, \tag{3}$$

To avoid the computational cost of barycentric refinement for standard multiplicative Calderón preconditioning an OSRC version was employed following [4]. Our numerical experiments explore the effects of increasing subdomains and block OSRC preconditioning.

Acknowledgements This work has been partially supported by Fondecyt Regular 1231112 and ECOS ANID C23E10.

References

[1] R. Hiptmair and C. Jerez-Hanckes, *Multiple traces boundary integral formulation for Helmholtz transmission problems*, Adv. Comput. Math. **37** (2012), 39–91.

[2] T. Betcke and M. Scroggs, *Bempp-cl: A fast Python based just-in-time compiling boundary element library*, J. Open Source Softw. **6** (2021), 2879–2879.

[3] P. Escapil-Inchauspé and C. Jerez-Hanckes, *Local Multiple Traces Formulation for Heterogeneous Electromagnetic Scattering: Implementation and Preconditioning*, arXiv preprint `https://arxiv.org/abs/2502.10907`.

[4] I. Fierro-Piccardo and T. Betcke, *An OSRC Preconditioner for the EFIE*, IEEE Trans. Antennas Propag. **71**(4) (2023), 3408–3417.

Book of abstracts of the 9th International Conference on
Advanced COmputational Methods in ENgineering and Applied Mathematics
September, 15–19, 2025.

Electromagnetic scattering by composite objects: A coupled FEM-BEM approach

Kristof Cools[1], **Van Chien Le**[1] **and Quang Huy Nguyen**[1]

[1] *IDLab, Department of Information Technology, Ghent University—imec*

e-mails: kristof.cools@ugent.be, vanchien.le@ugent.be, quanghuy.nguyen@ugent.be

Abstract

We investigate the scattering of electromagnetic waves by a penetrable composite object. Building upon Costabel's framework and the multi-trace formulation, we develop a coupling strategy that integrates a variational formulation of Maxwell's equations within a heterogeneous subdomain with boundary integral equations corresponding to surrounding homogeneous subdomains. Numerical experiments are provided to validate the accuracy and effectiveness of the proposed coupling approach.

Key words: electromagnetic scattering, FEM-BEM coupling, multi-trace formulation.

1 Introduction

Consider the domain decomposition of $\mathbb{R}^3$ given by $\mathbb{R}^3 = \cup_{i=0}^{n} \overline{\Omega}_i \cup \overline{\Omega}_\Sigma$, where each subdomain is Lipschitz-regular and connected. Among these, only Ω_0 is unbounded, while all other subdomains are bounded. The transmission problem for the time-harmonic Maxwell's equations can be reformulated into the following system:

$$\begin{cases} \mu_\Sigma \mathbf{curl}\mu_\Sigma^{-1}\mathbf{curle} - \kappa_\Sigma^2 \mathbf{e} = \mu_\Sigma \mu_0^{-1}\mathbf{f} & \text{in} \quad \Omega_\Sigma, \\ \mathbf{curlcurle} - \kappa_i^2 \mathbf{e} = \mathbf{0} & \text{in} \quad \Omega_i, \\ \mathbf{e} \times \mathbf{n}_j + \mathbf{e} \times \mathbf{n}_k = \mathbf{0} & \text{on} \quad \partial\Omega_j \cap \partial\Omega_k, \\ \mu_j^{-1}\mathbf{curle} \times \mathbf{n}_j + \mu_k^{-1}\mathbf{curle} \times \mathbf{n}_k = \mathbf{0} & \text{on} \quad \partial\Omega_j \cap \partial\Omega_k, \\ \mathbf{e} \times \mathbf{n}_j + \mathbf{e} \times \mathbf{n}_\Sigma = \mathbf{0} & \text{on} \quad \partial\Omega_i \cap \partial\Omega_\Sigma, \\ \mu_j^{-1}\mathbf{curle} \times \mathbf{n}_j + \mu_\Sigma^{-1}\mathbf{curle} \times \mathbf{n}_\Sigma = \mathbf{0} & \text{on} \quad \partial\Omega_i \cap \partial\Omega_\Sigma, \\ \mathbf{e} - \mathbf{e}_0 \text{ is } \kappa_0\text{-outgoing radiating}, \end{cases}$$

for $i, j, k = 0, \ldots, n$. Here, $\mathbf{n}_i$ with $i = 0, \ldots, n$ (or $\mathbf{n}_\Sigma$) denotes the unit normal vector on $\partial\Omega_i$ (or $\partial\Omega_\Sigma$), oriented outward from Ω_i (or Ω_Σ). Moreover, the wave number κ is assumed to be a spatially varying function $\kappa : \mathbb{R}^3 \to \mathbb{R}^+$:

$$\kappa(\mathbf{x}) = \begin{cases} \kappa_\Sigma(\mathbf{x}) > 0 & \text{for all} \quad \mathbf{x} \in \Omega_\Sigma, \\ \kappa_i > 0 & \text{for all} \quad \mathbf{x} \in \Omega_i. \end{cases}$$

Boundary element methods (BEMs) provide a highly flexible framework for addressing the homogeneous scattering problem in the unbounded exterior subdomain Ω_0. Moreover,

these methods typically involve solving a relatively small number of unknowns while offering high accuracy, particularly away from the boundary, and remain robust even at high frequencies. In the context of multi-subdomain scattering problems, various BEM approaches have been developed, including those based on the Poggio-Miller-Chew-Harrington-Wu-Tsai (PMCHWT) formulation [1], the multi-trace formulation [2], and related techniques such as the boundary element tearing and interconnecting (BETI) method [3].

On the other hand, due to the spatial variability of material parameters within Ω_Σ, the interior field problem is not suitable for treatment via BEMs. Instead, finite element methods (FEMs) can be employed to discretize a variational formulation of the wave equation in this heterogeneous subdomain.

To solve the above problem, which involves a composite scattering object consisting of an arbitrarily heterogeneous subdomain and multiple piecewise homogeneous subdomains, we propose a coupling approach that integrates the FEM with a multi-trace BEM. Leveraging the favorable properties of BEMs, our approach aims to exploit their advantages wherever feasible, specifically, across all homogeneous subdomains of the scattering object. Based on the multi-trace formulation, we seek two pairs of Cauchy traces on each interface between homogeneous subdomains. To marry with the FEM, we utilize the exterior Calderón projector acting on the transmission data of the total field at the boundary of Ω_Σ. The resulting FEM-BEM formulation is a natural extension of the schemes introduced in [4, 5]. Numerical experiments are presented to demonstrate the efficiency and accuracy of the proposed formulation.

Acknowledgements This work has been supported by the European Research Council (ERC) under the European Union's Horizon 2020 research and innovation programme (Grant agreement No. 101001847).

References

[1] Y. Chang, R. Harrington, *A surface formulation for characteristic modes of material bodies*, IEEE Trans. Antennas Propag. **25** (1977) 789–795.

[2] X. Claeys, R. Hiptmair, *Electromagnetic scattering at composite objects: a novel multi-trace boundary integral formulation*, ESAIM Math. Model. Numer. Anal. **46** (2012) 1421–1445.

[3] M. Windisch, *Boundary element tearing and interconnecting methods for acoustic and electromagnetic scattering*, Ph.D. thesis, Graz University of Technology, 2010.

[4] R. Hiptmair, *Coupling of finite elements and boundary elements in electromagnetic scattering*, SIAM J. Numer. Anal. **41** (2003) 919–944.

[5] M. Bonazzoli, X. Claeys, *Multidomain FEM-BEM coupling for acoustic scattering*, J. Integral Equations Appl. **36** (2024) 129–167.

Book of abstracts of the 9th International Conference on
Advanced Computational Methods in ENgineering and Applied Mathematics
September, 15–19, 2025.

Higher Order Conforming Impedance Boundary Condition

Jay Prakash[1] **and Kristof Cools**[1]

[1] *Department of Information Technology, Ghent University*

e-mails: jprakash.jayprakash@ugent.be, krcools@ugent.be

Abstract

Impedance boundary condition can be used to solve the electromagnetic problem by perfect conductors with thin coatings or certain lossy penetrable media. However, the widely used Leontovich Impedance Boundary Condition[1] can be conformingly discretized. In this work, we present a higher order equivalent for a conforming Impedance Boundary Condition proposed by Dely et al. [2]. We solve the formulation using the Boundary Element Method and report the accuracy results of the presented formulation via numerical experiments on a cuboidal object.

Key words: Boundary Element Method, Impedance Boundary Condition

Acknowledgements This project has received funding from the European Research Council (ERC) under the European Union's Horizon 2020 research and innovation program (Grant Agreement No. 101001847).

References

[1] D. J. Hoppe, Impedance Boundary Conditions In Electromagnetics. London, England: CRC Press, Mar. 1995.

[2] A. Dély, F. P. Andriulli, and K. Cools, "On a conforming impedance boundary condition efie," in 2018 IEEE International Symposium on Antennas and Propagation & USNC/URSI National Radio Science Meeting, pp. 2349–2350, 2018

Book of abstracts of the 9th International Conference on
Advanced Computational Methods in ENgineering and Applied Mathematics
September, 15–19, 2025.

Convergence of Calderón Residuals

Anouk Wisse[1], Ralf Hiptmair[2] and Carolina Urzúa-Torres[1]

[1] *Delft Institute of Applied Mathematics, TU Delft*

[2] *Seminar of Applied Mathematics, ETH Zürich*

e-mails: A.C.Wisse@tudelft.nl, hiptmair@sam.math.ethz.ch,
C.A.Urzuatorres@tudelft.nl

Abstract

We present a tool to validate the implementation of boundary integral operators by computing expected convergence rates for residuals based on the Calderón identities for general differential operators. These rates can be used to validate the implementation of boundary integral operators. Our estimates are in standard infinity and Euclidean vector norms, thus avoiding the use of hard-to-compute norms. We illustrate this with two examples: the Laplacian and time-harmonic Maxwell's equations. For implementation, we use the software package Bempp (https://bempp.com/).

Key words: Boundary element method, Calderón identity, convergence rate

1 Introduction

Convergence rates for Galerkin discretizations of boundary integral equations are usually available in fractional and sometimes even negative order spaces. Because of this, when one wishes to debug a BEM code, one chooses a reference solution and typically uses some of the Galerkin matrices to measure the error. In other words, one exploits the norm equivalence between the solution space of the boundary integral equation and the energy norm of the operator. However, this method only works if the implementation of the Galerkin matrices is done correctly, which can be hard to verify.

We describe a framework to compute expected convergence rates for residuals based on the Calderón identities for general second order differential operators for which fundamental solutions are known. The idea is that these rates could be used to validate implementations of boundary integral operators and allow to test operators separately by choosing solutions where parts of the Calderón identities vanish. Our estimates rely on simple vector norms, and thus avoid the use of hard-to-compute norms and the residual computation can be easily implemented in existing boundary element codes.

2 General idea

Let $\Omega \subset \mathbb{R}^d$ for $d = 2, 3$ be a bounded domain with Lipschitz boundary $\Gamma = \partial\Omega$. We consider a second order partial differential equation of the type

$$\begin{cases} \mathcal{L}u = 0 \quad \text{in } \mathbb{R}^d \setminus \overline{\Omega}, \\ + \text{ b.c. on } \Gamma \text{ and r.c. at } \infty, \end{cases} \tag{1}$$

which we want to solve using boundary integral equations. Based on the corresponding Calderón identity $\mathsf{C}\,\boldsymbol{\gamma} = \boldsymbol{\gamma}$, where

$$\mathsf{C} := \begin{pmatrix} \mathsf{A}_1 + \frac{1}{2}\,\mathsf{Id} & \mathsf{A}_2 \\ \mathsf{A}_3 & \mathsf{A}_4 + \frac{1}{2}\,\mathsf{Id} \end{pmatrix}, \quad \boldsymbol{\gamma} = \begin{pmatrix} \gamma_0 u \\ \gamma_1 u \end{pmatrix},$$

$A_1, \ldots, A_4$ are the boundary integral operators (BIOs) and γ_0 and γ_1 are the traces, we define the *Calderón residuals* as

$$r_0(\psi) := \int_\Gamma [(\mathsf{A}_1 - \tfrac{1}{2}\,\mathsf{Id})\mathcal{I}_0\gamma_0 u + \mathsf{A}_2\,\mathcal{I}_1\gamma_1 u]\psi \,\mathrm{d}\Gamma \tag{2a}$$

$$= \int_\Gamma [(\mathsf{A}_1 - \tfrac{1}{2}\,\mathsf{Id})(\mathcal{I}_0 - \mathsf{Id})\gamma_0 u + \mathsf{A}_2(\mathcal{I}_1 - \mathsf{Id})\gamma_1 u]\psi \,\mathrm{d}\Gamma, \quad \psi \in X_1, \tag{2b}$$

$$r_1(\phi) := \int_\Gamma [\mathsf{A}_3\,\mathcal{I}_0\gamma_0 u + (\mathsf{A}_4 - \tfrac{1}{2}\,\mathsf{Id})\mathcal{I}_1\gamma_1 u]\phi \tag{2c}$$

$$= \int_\Gamma [\mathsf{A}_3(\mathcal{I}_0 - \mathsf{Id})\gamma_0 u + (\mathsf{A}_4 - \tfrac{1}{2}\,\mathsf{Id})(\mathcal{I}_1 - \mathsf{Id})\gamma_1 u]\phi \,\mathrm{d}\Gamma\,\mathrm{d}\Gamma, \quad \phi \in X_0. \tag{2d}$$

Here $\mathcal{I}_0$ and $\mathcal{I}_1$ are operators that map the traces $\gamma_0 u$ and $\gamma_1 u$ to suitable finite dimensional subspaces defined on a mesh $\mathcal{G}_h$, where the $(\mathcal{G}_h)_{h\in\mathbb{H}}$ is a family of dyadically refined meshes of Γ. They can be interpolators or projections. We expect these residuals to become small when $h \to 0$. In other words, we bound the residuals by

$$\begin{aligned} |r_0(\psi)| &\leq \Big[\left\|\mathsf{A}_1 - \tfrac{1}{2}\,\mathsf{Id}\right\|_{X_0 \to X_0} \|(\mathcal{I}_0 - \mathsf{Id})\gamma_0 u\|_{X_0} \\ &\qquad + \|\mathsf{A}_2\|_{X_1 \to X_0} \|(\mathcal{I}_1 - \mathsf{Id})\gamma_1 u\|_{X_1} \Big] \|\psi\|_{X_0'}, \\ |r_1(\phi)| &\leq \Big[\|\mathsf{A}_3\|_{X_0 \to X_1} \|(\mathcal{I}_0 - \mathsf{Id})\gamma_0 u\|_{X_0} \\ &\qquad + \left\|\mathsf{A}_4 - \tfrac{1}{2}\,\mathsf{Id}\right\|_{X_1 \to X_1} \|(\mathcal{I}_1 - \mathsf{Id})\gamma_1 u\|_{X_1} \Big] \|\phi\|_{X_1'}. \end{aligned} \tag{3}$$

Since estimates of the type $\|(\mathcal{I}_i - \mathsf{Id})w\|_{X_i} \leq h^{\alpha_i} \|w\|_{X_i}$, $i = 0, 1$, are usually available and we choose the spaces X_0 and X_1 such that the BIOs are continuous, it only remains to estimate the test functions when these are taken in the finite-dimensional subspaces as mentioned above. For this, let $\{\beta_i, i = 1, \ldots, N_0\}$ and $\{b_j, j = 1, \ldots, N_1\}$ be bases of the finite dimensional subspaces. With this, we define the *residual vectors*

$$\boldsymbol{\rho}_0 := [r_0(\beta_i)]_{i=1}^{N_0}, \quad \boldsymbol{\rho}_1 := [r_1(b_j)]_{j=1}^{N_1}.$$

Hence, we need to bound $\|\beta_i\|_{X_0}$ and $\left\|b_j\right\|_{X_1}$ and by combining this with (3) we know how the residual vectors will change with h. Consequently, one can use these convergence rates to deduce if the Galerkin matrices for the different BIOs are implemented correctly by employing a manufactured solution to the exterior BVP (1); calculating the traces exactly, and finally letting the code compute the residuals and checking whether the observed rate agrees with the expected one. In the talk, we look into how this works for the Laplacian and time-harmonic Maxwell's equations, and calculate the convergence rates for these equations with use of the software package Bempp.

MS2: Advancements in Neural Network Solvers for PDEs: Applications and Challenges

Organiser: Minseok Choi (Pohang University of Science and Technology) and Jooyoung Hahn (Czech Technical University in Prague)

Description: This symposium addresses recent developments and persistent challenges in using neural network solvers for partial differential equations (PDEs), with a particular focus on the limitations and potential of physics-informed neural networks (PINNs). Despite their innovative approach, PINNs often face significant hurdles such as poor convergence, dependency on large data sets, and difficulties in generalizing across different types of PDEs. The session will examine how integrating classical mathematical concepts and numerical methods has begun to overcome these issues, enhancing the robustness and accuracy of neural network approaches. The discussion will highlight the latest adaptations in neural networks that incorporate advanced sampling strategies, optimization of network architectures, and novel training techniques that reduce the computational burden. Additionally, the symposium will present specific applications where modified PINNs have shown improved performance in solving complex, nonlinear PDEs in real-time scenarios, and in sensor placement strategies that optimize data acquisition in sparse environments. By bringing together diverse perspectives from applied mathematics and engineering, the session aims to provide a comprehensive understanding of how traditional numerical methods can be seamlessly integrated with modern machine learning techniques to address some of the most challenging problems in scientific computing.

Book of abstracts of the 9th International Conference on
Advanced Computational Methods in ENgineering and Applied Mathematics
September, 15–19, 2025.

COMMET. A performant and scalable architecture for finite elements with neural network based constitutive models

Benjamin Alheit[1,2], Mathias Peirlinck[1] and Siddhant Kumar[2]

[1] *Department of BioMechanical Engineering, Delft University of Technology*

[2] *Department of Material Science, Delft University of Technology*

e-mails: B.H.Alheit@tudelft.nl, mplab-me@tudelft.nl, Sid.Kumar@tudelft.nl

Abstract

Neural network-based constitutive models (NCMs) offer a highly expressive and flexible framework for modeling complex material behavior in solid mechanics. However, their practical adoption in large-scale finite element simulations remains limited due to significant computational costs, especially in evaluating stress and stiffness. In this work, we introduce COMMET, an open-source finite element solver designed for performant integration of NCMs. Our approach features a novel assembly algorithm that supports batched and vectorized constitutive updates, optimized implementation of hand-derived derivatives to replace automatic differentiation, and distributed-memory parallelism using MPI. We demonstrate that these design choices lead to substantial reductions in runtime, achieving speed-ups of more than three orders of magnitude compared to traditional scalar AD-based implementations. This framework enables scalable and performant solid mechanics simulations with NCMs, thus unlocking their potential for broad applications in science and engineering.

Key words: automatic differentiation, data-driven modeling, high-performance computing, neural network-based constitutive models, vectorization

1 Introduction

Neural network-based constitutive models (NCMs) offer a powerful framework for learning complex material behaviour from data, outperforming traditional constitutive equations in expressiveness and flexibility [1]. As such, NCMs are particularly well suited for modelling the complex behaviour exhibited by soft biological tissues [2]. Despite their promise, practical integration of NCMs into large-scale finite element (FE) simulations remains limited due to their high computational cost. To overcome this challenge, we present a performant and scalable FE solver purpose-built for NCMs, enabling their routine use in large-scale solid mechanics applications.

2 Methods

Key to our FE architecture is a novel assembly algorithm that allows for vectorized and batched evaluation of the constitutive update. Compute performance is further enhanced by replacing automatic differentiation with hand-derived stress and stiffness derivatives. Additionally, we implement distributed-memory parallelization using MPI, allowing for scalable simulations across multiple compute nodes.

3 Results

Benchmark experiments demonstrate that vectorization and batching reduce cache misses and wall time by up to two orders of magnitude (Fig. 1 (a)). Further speed-ups of up to are achieved through compute graph optimization (CGO), resulting in a combined speed-up exceeding three orders of magnitude compared to scalar AD-based implementations. We provide a demonstrative application of passive myocardial inflation in Fig. 1 (b). Figure 1: Using NCMs in a simulation of passive inflation of myocardium: The simulation was repeated for three different implementations of the same NCM: scalar AD, batch vectorized AD (with a batch size of 1024), and batch vectorized CGO (with a batch size of 1024). The associated wall times were 1554 s, 10.1 s, and 5.63 s, respectively, with identical solutions.

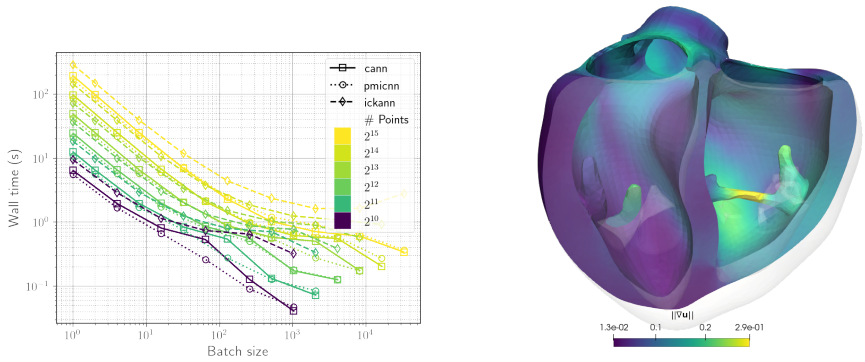

(a) (b)

Figure 1: **Selective results:** (a) Wall time vs. batch size for constitutive update of material points with different NCM architectures and (b) an exemplary simulation of myocardium using the developed FE solver with NCMs.

4 Discussion and Conclusions

Our work demonstrates that targeted algorithmic and implementation strategies – specifically batching, vectorization, and CGO – can drastically reduce the computational bottlenecks of NCMs in FE simulations. These enhancements make large-scale simulations with NCMs feasible, enabling broader adoption of data-driven constitutive modelling. The presented FE solver is freely available as part of the open-source computational mechanics and machine learning toolkit (COMMET)[1].

References

[1] P. Thakolkaran, A. Joshi, Y. Zheng, M. Flashel, L. De Lorenzis, S. Kumar, *NN-EUCLID: Deep-learning hyperelasticity without stress data*, JMPS **169** (2022) 105076.

[2] M. Peirlinck, J.A. Hurtado, M.K. Rausch, A. Tepole, E. Kuhl, *A universal material model subroutine for soft matter systems*, Eng. Comput. **9** (2024).

[1]The software is available at `https://commet-code.github.io/`.

Book of abstracts of the 9th International Conference on
Advanced Computational Methods in ENgineering and Applied Mathematics
September, 15–19, 2025.

CEENs: Causality-enforced evolutional networks for solving time-dependent partial differential equations

Jeahan Jung[1], Heechang Kim[1], Hyomin Shin[1] and Minseok Choi[1]

[1] *Department of Mathematics, Pohang University of Science and Technology (POSTECH)*

e-mails: obok13@postech.ac.kr, heechangkim@postech.ac.kr,
zhainl@postech.ac.kr, mchoi@postech.ac.kr

Abstract

Despite the growing popularity of physics-informed neural networks (PINNs), their applicability in the long-time integration of partial differential equations (PDEs) remains constrained. We argue that this problem stems from the lack of consideration of temporal causality in the original PINN formulation, resulting in a bias towards satisfying governing equations at later times before learning the initial condition and hence leading to erroneous solutions. To this end, we propose a novel method that seamlessly integrates temporal causality into the training process. Drawing inspiration from classical numerical methods where the temporal causality is reflected, we divide the time domain into nonoverlapping subintervals, assign a unique neural network to each subinterval, and construct a loss function founded on the integral form of PDEs within these subintervals. The proposed networks undergo sequential training, beginning with the initial time step. Our method demonstrates significant improvement in accuracy for long-time simulations of various PDE problems where the original PINN method fails while it requires less computational cost and memory compared to the PINN method. A parallelization algorithm is provided to further enhance the computational efficiency, showing a significant speedup for solving time-dependent PDEs.

Key words: Physics-informed neural network, Long-time integration, Partial differential equation, Predictive modeling, Nonlinear dynamics

Book of abstracts of the 9th International Conference on
Advanced Computational Methods in ENgineering and Applied Mathematics
September, 15–19, 2025.

Acceleration of Multi-Scale Finite-Element Superconducting Magnet Simulations with Neural Network Surrogate Models

Louis Denis[1], Julien Dular[2], Vincent Nuttens[3], Mariusz Wozniak[2], Benoît Vanderheyden[1] and Christophe Geuzaine[1]

[1] *Montefiore Institute, University of Liège, Belgium*

[2] *CERN, Geneva, Switzerland*

[3] *Ion Beam Applications S.A., Louvain-la-Neuve, Belgium*

e-mails: louis.denis@uliege.be, julien.dular@cern.ch, vincent.nuttens@iba-group.com, mariusz.wozniak@cern.ch, b.vanderheyden@uliege.be, cgeuzaine@uliege.be

Abstract

A multi-scale Finite-Element (FE) framework for low-temperature superconducting (LTS) magnets is accelerated by replacing costly mesoscopic-scale simulations with a neural network surrogate. Trained on high-fidelity simulation data, the surrogate enables a 600-fold speed-up of the 3D multi-scale model. The accelerated multi-scale FE model is found to produce reliable predictions for practical magnet ramp-up procedures.

Key words: Finite-element, Multi-scale, Neural networks, Superconducting magnets

Motivation, Modelling and Verification

Efficient and accurate prediction of AC losses in LTS magnets is crucial for their design. In previous work [1], we developed a magneto-thermal multi-scale approach that couples a homogenized 3D FE model of the LTS magnet for averaged magnetic field and temperature predictions with a single-filament FE model for accurate mesoscopic loss estimation. In this work, we generalize this method by replacing the single-filament model with a more detailed wire-in-channel (WIC) model at the mesoscopic scale. The WIC conductor is efficiently simulated using the CATI method [2], which allows faster phenomena to be described. However, one WIC-based multi-scale simulation requires 15h on 100 CPUs (1500 CPU-hours).

Acceleration is achieved by replacing the mesoscopic WIC model with a neural network (NN) surrogate, as successfully applied in multi-scale nonlinear mechanics [3]. The NN, which relies on Gated Recurrent Units (GRUs) [4], takes local macroscopic fields as input to predict the mesoscopic loss to be upscaled. The training dataset is generated from 10000 offline mesoscopic simulations. To ensure good generalization, the dataset is built using randomized current ramps that comprehensively explore the input space relevant to magnet ramp-ups.

When applied to the IBA S2C2 magnet for proton therapy [1], offline dataset generation requires 150 000 CPU-hours, while training is completed in less than 1 hour on a single GPU. Once trained, the GRU-based multi-scale simulation runs in 2.5h on a single CPU, achieving a

600-fold speed-up. As shown in Fig. 1, the proposed method reproduces WIC-based multi-scale loss predictions when tested on practical engineering ramp-ups of different durations, including the current IBA S2C2 ramp-up profile [1]. Notably, loss contributions of different physical nature and spanning several orders of magnitude can be accurately captured.

The full paper will discuss the coupling between FE models, the training procedure and the design of the surrogate, as well as the performance of the GRU-based multi-scale model, which allows for real-time simulation and iterative design of LTS magnets.

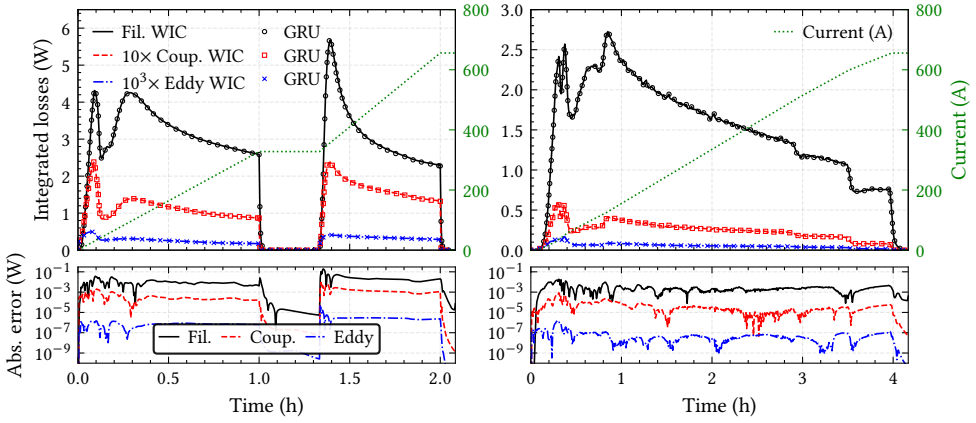

Figure 1: Top: volume-integrated AC losses during ramp-up of the IBA S2C2 magnet, including filament hysteresis, coupling, and eddy losses, for two testing current ramps (not in the training set). Bottom: corresponding absolute error between GRU-based multi-scale and WIC-based multi-scale. Left: Artificial ramp-up consisting of two linear ramps with an intermediate pause. Right: Current IBA S2C2 ramp-up profile [1].

Acknowledgements The work of L. Denis is supported by the F.R.S.-FNRS. The work of J. Dular and M. Wozniak is partially supported by the CERN HFM program. The present research benefited from computational resources made available on Lucia, the Tier-1 supercomputer of the Walloon Region, infrastructure funded by the Walloon Region under the grant agreement n°1910247.

References

[1] L. Denis *et al.*, *AC Loss Computation in Large-Scale Low-Temperature Superconducting Magnets: Multiscale and Semianalytical Procedures*, IEEE TASC **35** (2025) 1–19.

[2] J. Dular *et al.*, *Coupled axial and transverse currents method for finite element modelling of periodic superconductors*, SUST **37** (2024) 095002.

[3] L. Wu *et al.*, *A recurrent neural network-accelerated multi-scale model for elasto-plastic heterogeneous materials subjected to random cyclic and non-proportional loading paths*, Comput. Meth. Appl. Mech. Eng. **369** (2020) 113234.

[4] K. Cho *et al.*, *Learning phrase representations using RNN encoder-decoder for statistical machine translation*, arXiv:1406.1078 (2014).

Book of abstracts of the 9th International Conference on
Advanced Computational Methods in ENgineering and Applied Mathematics
September, 15–19, 2025.

Deep Learning with Viscosity-Reduction Variational Approach for Anisotropic Eikonal Equations

Yesom Park[1] and Jooyoung Hahn[2]

[1] *Department of Mathematics, University of California, Los Angeles*

[2] *Department of Software Engineering, Czech Technical University in Prague*

e-mails: yeisom@math.ucla.edu, jooyoung.hahn@fjfi.cvut.cz

Abstract

We propose a mesh-free deep learning method for solving the anisotropic eikonal equation via a variational approach with vanishing viscosity. This method addresses two key challenges: the nonlinearity of the gradient norm and the numerical instability when the viscosity parameter approaches zero. To handle the nonlinearity, we use a variable-splitting technique and enforce a normalized output for the neural network, effectively imposing the unit-gradient (anisotropic) constraint during training. To handle instability, we exploit the mesh-free nature of deep learning, allowing the network to represent the solution continuously without a fixed grid. Numerical tests show that the viscosity-reduction variational approach successfully recovers accurate solutions despite steep gradients and vanishing diffusion. We also demonstrate examples of surface reconstruction from 3D point clouds.

1 Introduction

The eikonal equation is a first-order nonlinear partial differential equation frequently arising in wave propagation, geometrical optics, and related fields [1]. In a spatially varying, direction-dependent medium, the *anisotropic eikonal equation* takes the form in the domain Ω

$$\|\nabla u\|_M = 1 \ \text{ in } \Omega \setminus \Gamma, \quad u|_\Gamma = g,$$

where $\|\cdot\|_M$ is a Riemannian metric norm and Γ is a compact subset in Ω. In practice, $u(x)$ represents the minimal travel time or geodesic distance from a source set Γ under anisotropic speeds. The physically relevant solution is defined in the viscosity sense, which ensures uniqueness: for zero boundary data, the viscosity solution is exactly the distance from the boundary set. Computing this solution is challenging, since the equation is highly nonlinear and can have discontinuous gradient.

Traditional numerical methods (e.g. fast marching or sweeping) rely on mesh-based discretizations to propagate the solution from the boundary. These methods have been successful in many settings, but can struggle with complex geometries or high anisotropy on polyhedral meshes [2]. Recently, deep neural networks have been applied to solve PDEs in a mesh-free way. In particular, physics-informed neural networks (PINNs) can embed differential operators in the loss function. However, naively minimizing the PDE residual does not guarantee

convergence to the correct viscosity solution, and can easily fail in the presence of singularities or steep gradients.

In this work, we take a variational perspective using vanishing viscosity method. By adding a small diffusion term $\epsilon\Delta u$, one can derive a variational problem whose minimizer converges to the viscosity solution of the original anisotropic eikonal equation as $\epsilon \to 0$. This functional explicitly reveals two main computational challenges of the vanishing-viscosity approach: (i) *nonlinearity* due to the gradient norm $\|\nabla u\|_M$, and (ii) *instability* due to the singularly perturbed term, $e^{-\frac{2u}{\epsilon}}$, as $\epsilon \to 0$.

To overcome the nonlinearity, we employ a variable-splitting strategy together with a *normalized output representation*. Concretely, our neural network predicts both u and an auxiliary vector field $\mathbf{p}$, with a hard constraint $\|\mathbf{p}\|_M = 1$ enforced via normalization. This removes the need to directly handle the $\|\nabla u\|_M$ term in the loss. Apart from this effect, the constraint also contributes to the delocalization of the functional. The hard constraint ensures that the auxiliary variable properly remains scaled, independent of the exponential decay of singularly perturbed term. Meanwhile, to address instability from the singularly perturbed term, we rely on the mesh-free nature of neural networks: training random points can be sampled eventually near regions of Γ, and there is no fixed stencil that breaks down as $\epsilon \to 0$. In effect, the neural network learns the limiting viscosity solution directly.

The above strategy yields a novel deep learning/variational solver. We formulate a loss based on the viscosity-regularized functional (whose Euler–Lagrange equation matches the vanishing-viscosity PDE) and train the network to minimize it:

$$\min_{u,\mathbf{p}} \int_\Omega e^{-\frac{2u}{\epsilon}} + \frac{\lambda}{2} \int_\Omega \|\nabla u - \mathbf{p}\|^2 \quad \text{s.t. } u = g \text{ on } \Gamma,\ \|\mathbf{p}\|_M = 1 \text{ in } \Omega.$$

Importantly, the normalized neural output ensures a strong enforcement of the gradient norm constraint, while the mesh-free sampling resolves the steep features. In computational examples, including surface reconstruction from point clouds, our method accurately recovers the viscosity solution of the anisotropic eikonal equation, even in highly anisotropic settings. Thus, the proposed viscosity-reduction variational approach provides a stable and accurate framework for solving anisotropic eikonal problems in geometry and mechanics.

References

[1] P.L. Lions., *Generalized Solutions of Hamilton-Jacobi Equations*, Chapman & Hall/CRC research notes in mathematics series. Pitman, 1982.

[2] J. Hahn, K. Mikula, P. Frolkovič, *Laplacian regularized eikonal equation with soner boundary condition on polyhedral meshes*, Comput. Math. Appl. **156** (2024) 74–86.

Book of abstracts of the 9th International Conference on
Advanced Computational Methods in ENgineering and Applied Mathematics
September, 15–19, 2025.

Adaptive sampling for physics-informed neural networks

Bianca Giovanardi[1], Alexander Heinlein[2] and Coen Visser[1]

[1] *Department of Aerospace Structures and Materials, Delft University of Technology*

[2] *Delft Institute of Applied Mathematics, Delft University of Technology*

e-mails: b.giovanardi@tudelft.nl, a.heinlein@tudelft.nl,
c.l.visser@student.tudelft.nl

Abstract

Physics-informed neural networks (PINNs) approximate solutions to partial differential equations (PDEs) by minimizing a loss function evaluated at collocation points. The placement of these points is crucial for accuracy, but many sampling strategies, including adaptive ones, struggle with challenging or high-dimensional problems. We introduce the Point Adaptive Collocation Method for Artificial Neural Networks (PACMANN), which efficiently shifts collocation points toward regions of high residuals using gradient-based optimization. PACMANN achieves state-of-the-art accuracy and efficiency in low dimensions and outperforms existing methods in high-dimensional settings, while remaining easy to integrate into existing PINN frameworks.

Key words: differential equations, physics-informed neural networks (PINNs), adaptive sampling, residual gradient

1 Introduction

Physics-informed neural network (PINNs) [2] use neural networks to approximate solutions to partial differential equations (PDEs) by minimizing a composite loss function. This loss combines the PDE residual and the initial/boundary conditions, all evaluated at collocation points. The placement of these points is crucial for accuracy, and adaptive sampling strategies—such as residual-based refinement and probability density function (PDF)-based methods [3]—have been developed to address this, though they often become costly in high dimensions.

Given a PDE of the form

$$\boldsymbol{u}_t + \mathcal{N}[\boldsymbol{u}] = 0,$$

defined on a spatio-temporal computational domain $\Omega \times [0, T]$ with initial and boundary conditions. A PINN model $\hat{\boldsymbol{u}}(\boldsymbol{x}, t, \boldsymbol{\theta})$ is defined via the minimization problem

$$\boldsymbol{\theta}^* = \arg\min_{\boldsymbol{\theta}} \left[\lambda_{ic}\mathcal{L}_{ic} + \lambda_{bc}\mathcal{L}_{bc} + \lambda_r\mathcal{L}_r\right], \tag{1}$$

where the physics-informed loss term is given by the squared residual

$$\mathcal{L}_r = \frac{1}{N_r}\sum_{i=1}^{N_r}\left(\hat{\boldsymbol{u}}_t(\boldsymbol{x}_r^i, t_r^i) + \mathcal{N}[\hat{\boldsymbol{u}}](\boldsymbol{x}_r^i, t_r^i)\right)^2$$

sampled in collocation points $X \coloneqq \{(x_r^i, t_r^i)\}_{i=1}^{N_r}$. Furthermore, $\mathcal{L}_{ic}$ and $\mathcal{L}_{bc}$ are the loss terms for the initial and boundary conditions, respectively, each sampled at corresponding sets of data points. The weights λ_r, λ_{ic}, and λ_{bc} balance the loss terms.

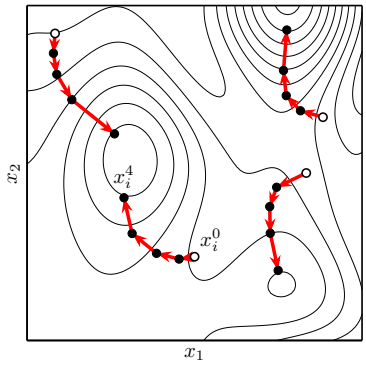

Figure 1: Schematic of PACMANN with four gradient ascent steps on a contour plot of the squared residual.

sampling method	L_2 rel. error (mean ± SD)		mean runtime [s]
uniform	17.89%	± 0.94%	742
Hammersley	82.08%	± 3.23%	**734**
random	11.03%	± 0.69%	772
RAR	56.84%	± 4.46%	753
RAD	10.07%	± 0.75%	851
RAR-D	88.30%	± 1.53%	774
PACMANN	**5.93%**	± **0.46%**	778

Table 1: Mean and standard deviation of test error and mean runtime for various sampling methods on a 5D Poisson equation; cf. [1].

2 Point Adaptive Collocation Method for Artificial Neural Networks

To overcome the limitations of adaptive sampling in high-dimensional settings, we introduce the Point Adaptive Collocation Method for Artificial Neural Networks (PACMANN) [1]. PACMANN adaptively relocates collocation points toward regions with high residuals by leveraging gradient-based optimization, thereby enhancing accuracy and scalability.

The core idea of PACMANN is to use the gradient of the squared residual to iteratively move collocation points toward areas of largest error, effectively transforming the resampling process into a maximization problem. Unlike the standard PINN formulation in (1), training with PACMANN involves a min-max optimization:

$$\boldsymbol{\theta}^* = \arg\min_{\boldsymbol{\theta}} \left[\lambda_{ic}\mathcal{L}_{ic}(\boldsymbol{\theta}) + \lambda_{bc}\mathcal{L}_{bc}(\boldsymbol{\theta}) + \max_{\boldsymbol{X}_r \subset \mathcal{D}} \lambda_r \mathcal{L}_r(\boldsymbol{X}_r, \boldsymbol{\theta}) \right].$$

Here, only the collocation points $\boldsymbol{X}_r$ are updated adaptively, while the points for boundary and initial conditions remain fixed. Table 1 presents results for a five-dimensional Poisson equation, demonstrating that PACMANN achieves comparable or superior accuracy and efficiency relative to existing adaptive sampling methods [3].

References

[1] C. Visser, A. Heinlein, B. Giovanardi, *PACMANN: Point Adaptive Collocation Method for Artificial Neural Networks*, arXiv preprint arXiv:2411.19632, 2024.

[2] M. Raissi, P. Perdikaris, G. E. Karniadakis, *Physics-informed neural networks: a deep learning framework for solving forward and inverse problems involving nonlinear partial differential equations*, Journal of Computational Physics, 378 (2019), pp. 686–707.

[3] C. Wu, M. Zhu, Q. Tan, Y. Kartha, L. Lu, *A comprehensive study of non-adaptive and residual-based adaptive sampling for physics-informed neural networks*, Computer Methods in Applied Mechanics and Engineering, 403 (2023), 115671.

Book of abstracts of the 9th International Conference on
Advanced Computational Methods in ENgineering and Applied Mathematics
September, 15–19, 2025.

Data-Efficient Operator Networks with Asymptotic Bases for Singularly Perturbed PDEs

Jinsil Lee[1], Jaeyong Lee[2], Seungchan Ko[3] and Youngjoon Hong[1]

[1] *Department of Mathematical Sciences, Seoul National Universit*

[2] *Department of AI, Chung-Ang University*

[3] *Department of Mathematics, Inha University*

e-mails: jl74942@snu.ac.kr, jaeyong@cau.ac.kr, scko@inha.ac.kr, hongyj@snu.ac.kr

Abstract

Recent advancements in machine learning (ML) have shown promise in solving partial differential equations (PDEs), but significant challenges remain, particularly in handling complex scenarios. Singularly perturbed differential equations present unique computational difficulties due to rapid transitions within thin boundary or interior layers, where ML methods often struggle. Moreover, these problems require massive adaptive mesh refinement, making dataset generation computationally expensive. In this paper, we introduce eFEONet, an enriched Finite Element Operator Network designed to overcome these challenges. By leveraging singular perturbation analysis from PDE theory, eFEONet incorporates special basis functions that capture the asymptotic behavior of solutions, enabling accurate modeling of sharp transitions. Our approach is highly data-efficient, requiring minimal training data or even functioning without a dataset. Furthermore, we provide a rigorous convergence analysis and empirically validate eFEONet across various boundary and interior layer problems.

Key words: scientific machine learning, finite element methods, physics-informed operator learning, boundary layer
MSC 2020: 65M60, 65N30, 68T20, 68U07

Boundary and interior layer phenomena are of paramount importance in many scientific and engineering disciplines, including fluid dynamics, biology, and chemical reactions [1, 2].

$$\begin{aligned} -\varepsilon \operatorname{div}(a(x)\nabla u_\varepsilon) + b(x)\cdot\nabla u_\varepsilon &= f \quad \text{in } D. \\ u_\varepsilon &= 0 \quad \text{on } \partial D. \end{aligned} \tag{1}$$

These problems are characterized by sharp changes in solution profiles within thin layers, making them notoriously difficult to handle with advanced numerical methods and machine learning-based approaches. The challenge arises from the small diffusive parameter $\varepsilon > 0$ in these equations, which leads to steep gradients over small spatial regions. See Figure 1 where the examples of interior layer phenomena are presented. Developing methods to accurately and efficiently solve such problems remains a challenging task in scientific computing [3, 4]. In this presentation, we introduce an enriched Finite Element Operator Network (eFEONet), specifically designed to address these challenges. eFEONet builds upon the FEONet framework [5], a highly data-efficient operator learning method that requires minimal training data

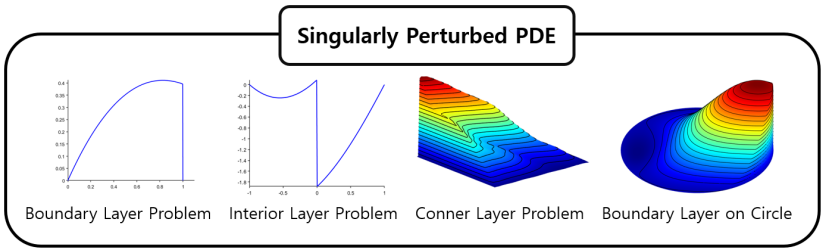

Figure 1: Representative solution profiles for singularly perturbed PDEs, illustrating the inherent stiffness of boundary and interior layers across various domains. The sharp gradients, localized structures, and rapid transitions depicted here highlight the intrinsic stiffness and associated computational challenges.

or no dataset at all. Unlike traditional operator networks, eFEONet leverages the structure of finite element methods (FEMs), where the solution is expressed as a linear combination of nodal coefficients and basis functions. This design not only eliminates the need for large datasets but also ensures the exact satisfaction of boundary conditions. We proposes eFEONet, a novel framework that incorporates singular perturbation analysis into the FEONet architecture, enabling accurate resolution of sharp gradients in both boundary and interior layers of singularly perturbed partial differential equations (PDEs). Traditional approaches typically require extremely fine meshes as the perturbation parameter $\varepsilon > 0$ becomes small, resulting in high computational costs for dataset generation. In contrast, eFEONet is highly data-efficient, capable of achieving high accuracy with minimal training data—or even without any training dataset at all.

The effectiveness of eFEONet is demonstrated through comprehensive experiments on challenging convection-diffusion problems in one- and two-dimensional domains, including cases with boundary and interior layers. The results show that eFEONet achieves up to two orders of magnitude reduction in error compared to existing methods, even in the absence of training data. Moreover, the proposed framework is supported by a rigorous theoretical foundation, combining finite element approximation with asymptotic analysis. This solid analytical basis allows for formal convergence analysis, ensuring the method's reliability, accuracy, and interpretability when solving singularly perturbed PDEs.

References

[1] H. Schlichting and K. Gersten, *Boundary-layer theory*, Springer, 2016.

[2] G. K. Batchelor, *An introduction to fluid dynamics*, Cambridge University Press, 2000.

[3] O. C. Zienkiewicz and R. L. Taylor, *The Finite Element Method: Its Basis and Fundamentals*, Butterworth-Heinemann, 2000.

[4] T. J. R. Hughes, *The Finite Element Method: Linear Static and Dynamic Finite Element Analysis*, Dover Publications, 2000.

[5] J. Y. Lee, S. Ko, and Y. Hong, *Finite Element Operator Network for Solving Elliptic-type parametric PDEs*, SIAM J. Sci. Comput., 2024.

Book of abstracts of the 9th International Conference on
Advanced Computational Methods in ENgineering and Applied Mathematics
September, 15–19, 2025.

Unconditionally gradient stable but explicit numerical method for solving gradient flows

Seunggyu Lee[1,2]

[1] *Department of Applied Mathematics, Korea University*

[2] *Biomedical Mathematics Group, Institute for Basic Science*

e-mails: sky509@korea.ac.kr

Abstract

We propose an explicit linear scheme to solve the Allen–Cahn equation that satisfies energy stability and maximum principle. Our approach is based on a finite-difference spatial discretization, and we prove the maximum principle and energy stability without any time-step restriction. The proposed method can be easily extended to the 2nd order accuracy in time. Numerical experiments demonstrate its accuracy, energy stability, and maximum principle.

Key words: Allen–Cahn equation, convex splitting method, energy stability, explicit scheme, maximum principle
MSC 2020: 65M12

1 Introduction

The Allen–Cahn (AC) equation was originally introduced to model a phase separation in binary alloys [1] and it is written as the following form:

$$\frac{\partial \phi}{\partial t}(\mathbf{x}, t) = -\frac{F'(\phi)}{\epsilon^2} + \Delta\phi, \quad \mathbf{x} \in \Omega, \ t \in (0, T), \tag{1}$$

with the periodic boundary condition, where $\phi(\mathbf{x}, t) \in [-1, 1]$ is an order parameter, $F(\phi) = 0.25(1-\phi^2)^2$ is a bulk free energy, and ϵ is a coefficient related to an interfacial energy.

It is an important research topic to propose an energy stable method for gradient flow type equations including the AC equation, so there have been developed the enumerous schemes preserving the energy dissapation law. However, in author's knowledge, there are only few literatures addressing the explicit-type energy stable schemes because it is well-known that an explicit scheme usually suffers a serious stability or consistency issue in spite of its efficiency.

In this talk, we present a linear, energy stable, and maximum principle preserving numerical method for solving the AC equation in an explicit manner based on a finite-difference spatial discretization. Without any time-step restriction, its maximum principle and energy stability are clearly proven. Moreover, the proposed scheme can be straightforwardly extended to the 2nd order accuracy in time using the concept of the CSRK (convex splitting Runge–Kutta) method [2].

2 Numerical method

Let $\Omega = (0,1)$ be a domain and $\mathcal{G} := \{x_i : (i-0.5)h, i = 1, \cdots, N\}$ be a set of cell-centered N-grid points with a uniform spatial step size h. Given an approximation $\phi_i^n = \phi(x_i, n\Delta t)$ defined on $\mathcal{G}$ with a time step Δt, we propose the 1st order discrete scheme (ES1) for solving (1) as follows:

$$\frac{\phi_i^{n+1} - \phi_i^n}{\Delta t} = -\frac{\left(\phi_i^n\right)^3 - (1+\alpha)\phi_i^n + \alpha\phi_i^{n+1}}{\epsilon^2} + \mathcal{D}_i^h\left(\boldsymbol{\phi}^{n+1}, \boldsymbol{\phi}^n\right), \quad i = 1, \cdots, N, \tag{2}$$

where $\alpha \geq 2$ is a stabilizing factor and $\mathcal{D}_i^h$ is the discrete Laplacian operator defined as:

$$\mathcal{D}_i^h\left(\boldsymbol{\phi}^{n+1}, \boldsymbol{\phi}^n\right) = \frac{\phi_{i+1}^n - 2\phi_i^{n+1} + \phi_{i-1}^n}{h^2}. \tag{3}$$

Remark *The scheme* (2) *can be solved explicitly, i.e., it can be rewritten as the form* $A\boldsymbol{\phi}^{n+1} = \boldsymbol{\phi}^n$ *where* A *is the diagonal matrix,* $\boldsymbol{\phi}^{n+1} = \left(\phi_1^{n+1}, \cdots, \phi_N^{n+1}\right)$, *and* $\boldsymbol{\phi}^n = \left(\phi_1^n, \cdots, \phi_N^n\right)$,

Theorem (Maximum principle) *If* $\alpha \geq 2$, *then* $\|\boldsymbol{\phi}^n\|_\infty \leq 1$ *imples* $\left\|\boldsymbol{\phi}^{n+1}\right\|_\infty \leq 1$, *for any* $\Delta t > 0$, $h > 0$, *and* $n \in \mathbb{N}_0$.

Theorem (Energy stability) *If* $\alpha \geq 2$, *then* $\mathcal{E}^h(\boldsymbol{\phi}^{n+1}) \leq \mathcal{E}^h(\boldsymbol{\phi}^n)$ *for any* $\Delta t > 0$, $h > 0$, *and* $n \in \mathbb{N}_0$.

The CSRK method was proposed as a framework to solve a gradient flow extending the classical CS method, which has the 1st order accuracy in time, to the higher order accuracy using the IMEX Runge–Kutta method [2].

Acknowledgements This work was supported by the National Research Foundation of Korea (NRF) grant funded by the Korea government (MSIP) (No. RS-2024-00342949).

References

[1] S. M. Allen, J. W. Cahn, A microscopic theory for antiphase boundary motion and its application to antiphase domain coarsening, Acta Metallurgica 27 (6) (1979) 1085–1095.

[2] J. Shin, H. G. Lee, J.-Y. Lee, Unconditionally stable methods for gradient flow using Convex Splitting Runge–Kutta scheme, Journal of Computational Physics 347 (2017) 367–381.

Book of abstracts of the 9th International Conference on
Advanced Computational Methods in ENgineering and Applied Mathematics
September, 15–19, 2025.

Understanding the Diffusion Process via ODE-based Sampling

Yeonju Lee[1]

[1] *Division of Applied Mathematical Sciences, Korea University*

e-mails: leeyeonju08@korea.ac.kr

Abstract

Diffusion-based generative models define a continuous-time process that transforms data distributions into a standard Gaussian prior by gradually injecting noise. This forward process is mathematically formulated as a stochastic differential equation (SDE), where the drift and diffusion terms specify the deterministic and stochastic components of the dynamics. The reverse-time process can be equivalently described by the probability flow ordinary differential equation (ODE), which produces the same marginal distributions and enables sample generation by solving an initial value problem from the prior toward the data distribution. Existing ODE-based samplers often rely on low-order polynomial interpolation to approximate the time-dependent score function, defined as the gradient of the log-density with respect to the input. In this work, we propose a higher-order ODE solver based on kernel interpolation. We also derive a sufficient condition on the kernel weights that ensures accuracy of the resulting numerical method in diffusion models.

Key words: diffusion, flow-ODE, kernel interpolation

1 Introduction

Diffusion-based generative models have become a leading framework for modeling high-dimensional data distributions through a continuous-time stochastic process [1]. The central idea is to define a *forward diffusion process* that incrementally corrupts data by injecting Gaussian noise and then to learn how to invert this transformation to synthesize new samples from pure noise. This paradigm achieves state-of-the-art results in image, audio, and 3-D generation.

The forward process is formulated as a stochastic differential equation (SDE) that maps data to a standard Gaussian prior. Sampling proceeds by solving the associated *reverse-time* dynamics. Two families of samplers are common: (i) stochastic simulation of the learned reverse SDE; (ii) deterministic integration of the *probability-flow ordinary differential equation (ODE)*, which shares the same marginals as the reverse SDE while eliminating randomness [2, 3]. ODE-based sampling permits the use of explicit numerical solvers and often attains comparable quality with far fewer steps than stochastic methods.

Recent work accelerates ODE sampling by designing high-order solvers that approximate the continuous-time dynamics with fewer score-network evaluations [4]. Most existing solvers rely on fixed low-degree polynomial interpolants of the time-dependent score, which can struggle to capture rapid or localized variations. To address this limitation, we introduce a kernel-based interpolation strategy that adapts to the local geometry of the score trajectory. We further derive a simple sufficient condition on the kernel weights that guarantees the desired integration accuracy.

2 Diffusion Process

Let $x_0 \sim p_0(x)$ be a data sample. Define latent variables $\{x_t\}_{t\in[0,T]}$ via the Itô SDE

$$\mathrm{d}x_t = f(t, x_t)\,\mathrm{d}t + g(t)\,\mathrm{d}w_t, \tag{1}$$

where w_t is standard Brownian motion, f the drift, and g the diffusion coefficient. In the variance-preserving (VP) formulation used by DDPM,

$$f(t, x) = -\tfrac{1}{2}\beta(t)\,x, \qquad g(t) = \sqrt{\beta(t)}, \tag{2}$$

with a *noise schedule* $\beta(\cdot)$ that is continuously differentiable and monotonically increasing and linear and cosine schedules are common choices.
Given a score network $s_\theta(t, x) \approx \nabla_x \log p_t(x)$ trained via denoising score matching, the reverse dynamics obey

$$\mathrm{d}x_t = \big[f(t, x_t) - g(t)^2\, s_\theta(t, x_t)\big]\mathrm{d}t + g(t)\,\mathrm{d}\bar{w}_t, \tag{3}$$

where $\bar{w}_t$ denotes Brownian motion under time reversal.
The same marginals are produced by the deterministic ODE [2]

$$\frac{\mathrm{d}x_t}{\mathrm{d}t} = f(t, x_t) - \tfrac{1}{2}g(t)^2\, s_\theta(t, x_t), \tag{4}$$

distinguished from (3) by the factor $1/2$ in front of $g(t)^2$. Integrating (4) from $t = T$ (where x_T is nearly Gaussian) back to $t = 0$ yields deterministic samples consistent with p_0. The DDIM sampler [3] can be interpreted as a discrete approximation of this ODE.

The accuracy and efficiency of ODE-based generation thus depend on the integration scheme applied to (4), motivating the adaptive, kernel-based method proposed in this work.

Acknowledgements This work has been partially supported by the Basic Science Research Program through the Na- tional Research Foundation of Korea (NRF) funded by the Ministry of Education of the Government of the Republic of Korea (2021R1A2C1008360).

References

[1] J. Ho, A. Jain, and P. Abbeel, *Denoising Diffusion Probabilistic Models*, NeurIPS **33** (2020), 6840–6851.

[2] Y. Song, J. Sohl-Dickstein, D. P. Kingma, A. Kumar, S. Ermon, and B. Poole, *Score-Based Generative Modeling through Stochastic Differential Equations*, ICLR (2021).

[3] J. Song, C. Meng, and S. Ermon, *Denoising Diffusion Implicit Models*, ICLR (2021).

[4] C. Lu, Y. Liu, D. He, J. Zhu, and S. Ermon, *DPM-Solver: A Fast ODE Solver for Diffusion Probabilistic Models*, NeurIPS **35** (2022), 21461–21473.

Book of abstracts of the 9th International Conference on
Advanced Computational Methods in ENgineering and Applied Mathematics
September, 15–19, 2025.

Causality-enhanced physics-informed simulators with sparse sensor measurements for real-time full-field estimation

Jae Hyuk Lim[1], Hong-Kyun Noh[2] and Jeong-Hoon Park[2]

[1] *Department of Mechanical Engineering, Kyung Hee University*

[2] *Department of Mechanical Engineering, Jeonbuk National University*

e-mails: jaehyuklim@khu.ac.kr, jjjrrr8@jbnu.ac.kr, jhpark1@jbnu.ac.kr

Abstract

This study proposes two surrogate modeling frameworks for real-time full-field inference of transient responses in time-dependent partial differential equations (PDEs) using sparse sensor measurements. The first approach, the causal PINN-based surrogate model (causal PBSM), incorporates temporal weighting to improve generalization across time. The second, the Fixed-time increment PINN-based surrogate model (FTI-PBSM), introduces numerical differentiation across fixed time steps, implicitly encoding partial temporal causality without requiring explicit time as an input. Both methods were evaluated on various benchmark PDEs—the Euler–Bernoulli beam, diffusion–reaction dynamics, Korteweg–de Vries (KdV) equation, and Kirchhoff–Love plate—under various levels of sensor sparsity, noise, and structural uncertainty. The results demonstrate that these frameworks provide accurate and efficient surrogate models capable of real-time prediction and generalization beyond the training range.

Key words: Fixed-time increment, Partial differential equations, Physics-informed neural network, Real-time simulation, Surrogate model, Temporal causality, Unmodeled effect

1 Introduction

Real-time prediction of time dependent PDEs is critical in structural health monitoring and dynamic system control, but conventional numerical solvers are often too slow for practical use. Recent advances in Physics-Informed Neural Networks (PINNs) [1] have enabled data efficient modeling by embedding governing equations into deep learning frameworks. However, standard PINNs struggle with long time integration due to a lack of temporal causality. This study explores two causality-enhanced physics-informed simulators: causal PBSM [2] and FTI-PBSM.

2 Causality-enhanced physics-informed simulators

The causal PINN-Based Surrogate Model (causal PBSM) [2] uses both spatio-temporal coordinates and sparse sensor data as inputs. To enhance temporal generalization, it incorporates a causal PINN framework, prioritizing accurate predictions at earlier time steps and gradually learning time evolution. The Fixed Time Increment PBSM (FTI-PBSM) removes the temporal coordinate from the input features and instead applies numerical differentiation with respect to time to compute the evolution of the solution across time steps.

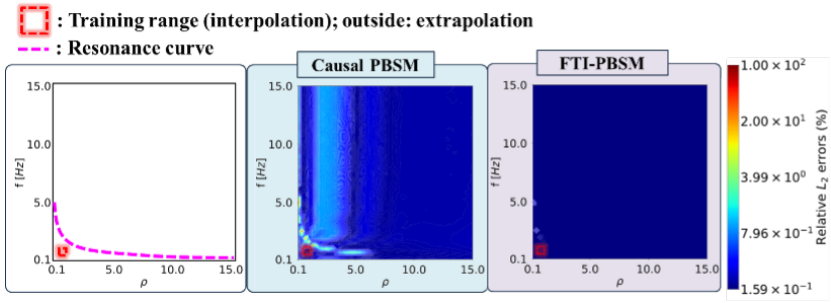

Figure 1: Contour plot comparison of relative L2 errors in predictions for unseen data across the causal PBSM and FTI-PBSM.

3 Results and Discussion

This chapter evaluates the performance of the proposed surrogate models using the Euler-Bernoulli beam example, focusing on interpolation and extrapolation. Interpolation refers to test cases within the training range of material density and excitation frequency, while extrapolation includes out-of-range cases and damped systems. Both causal PBSM and FTI-PBSM achieve accurate results under interpolation. However, FTI-PBSM shows clear advantages in extrapolation, demonstrating stronger generalization and robustness. This is particularly evident in damped cases, where FTI-PBSM accurately predicts full-field responses despite unmodeled damping effects, as shown in Figure 1.

4 Conclusion

This study examined two PINN based surrogate models, causal PBSM and FTI-PBSM, for real time full field prediction of time dependent PDEs using sparse sensor data. Evaluated on the Euler–Bernoulli beam example, both models performed well under interpolation, while FTI-PBSM showed superior generalization in extrapolation due to its use of temporal differentiation. These results suggest that FTI-PBSM is suitable for real time monitoring and predictive maintenance in dynamic systems.

Acknowledgements This work was supported by a grant from Kyung Hee University in 2025. (KHU-20251484)

References

[1] M. Raissi, P. Perdikaris, G.E. Karniadakis, *Physics-informed neural networks: a deep learning framework for solving forward and inverse problems involving nonlinear partial differential equations*, J. Comput. Phys. **378** (2019) 686–707.

[2] H. K. Noh, M. Choi, J. H. Lim, *Real-time full-field estimation of transient responses in time-dependent partial differential equations using causal physics-informed neural networks with sparse measurements*, Eng. Anal. Bound. Elem. 192 Part B (2025) 106363.

Book of abstracts of the 9th International Conference on
Advanced Computational Methods in ENgineering and Applied Mathematics
September, 15–19, 2025.

A Deep Learning-based Numerical Algorithm for a Tumor Growth Model with Moving Boundary Conditions

Sanchita Malla[1], Sitikantha Roy[2] and Dietmar Oelz[3]

[1] *UQ-IITD Research Academy, Indian Institute of Technology Delhi, New Delhi, India 110016*

[2] *Applied Mechanics Department, Indian Institute of Technology Delhi, New Delhi, India 110016*

[3] *School of Mathematics and Physics, The University of Queensland, Australia, QLD 4072*

e-mails: qiz218587@iitd.ac.in, sroy@iitd.ac.in, d.oelz@uq.edu.au

Abstract

In this work, we present a mesh-free, Physics-Informed Neural Network-based framework for simulating a reduced continuum tumor growth model. The formulation solves PDEs for the densities of living and dead tumor cells and nutrient concentration within the tumor region, while incorporating the influence of the external microenvironment through moving boundary conditions and capillaries concentration. A level set function, approximated by an additional PINN, is used to track moving tumor boundary evolution. The results highlight the potential of PINNs as a computationally efficient alternative for moving boundary problems in mathematical biology.

Key words: Computational Methods, Deep Learning, Mathematical Modeling, Moving Boundary Problem, Tumor Growth Model

1 Tumor Growth Model Formulations

In this work, we focus on developing a mesh-free method to solve a reduced model that restricts the computation to the tumor region [1]. In the formulation of the reduced model, only the PDEs for the density of living tumor cells (c_t), the density of dead tumor cells (c_d), and the concentration of nutrients (c_n) are solved with moving boundary conditions.

Let us consider a fixed computational domain $\mathcal{D} = [-8, 8] \times [-8, 8]$, within which the tumor region $\Omega(t) \subset \mathcal{D}$ with the moving boundary $\Gamma(t)$ grows over time. The governing PDEs of the model to be solved are as

$$\begin{aligned}
\frac{\partial c_t}{\partial t} &= w\nabla \cdot (c_t \nabla u) + c_t c_n \, H(c_n - \tilde{u} c_t) - \lambda_t H(\bar{u} c_t - c_n) c_t, \\
\frac{\partial c_d}{\partial t} &= \lambda_t H(\bar{u} c_t - c_n) c_t - \lambda_d c_d, \\
\frac{\partial c_n}{\partial t} &= \lambda_n \left[\nabla \cdot ((1 + k\hat{u}_c) \nabla c_n) - c_t c_n \right].
\end{aligned} \tag{1}$$

The values of the parameters are $w = 10$, $\tilde{u} = 0.9$, $\bar{u} = 0.8$, $\lambda_t = 5$, $\lambda_n = 10$, $\lambda_d = 0.001$ and $k = 0.2$. While we focus only on living tumor cell density and nutrient concentration, all the parameters preserve the biological meaning established in the original model. Here,

the overall cell density $u = c_t + c_d + \hat{u}_c$, and $\hat{u}_c(\mathbf{x})$ is the density of pre-existing capillaries, which is stationary and given. The boundary conditions at the tumor interface $\partial\Omega(t)$ are defined as $c_t = 1 - c_d - \hat{u}_c$, $c_d = 0$, $c_n = 1 + \beta(\hat{u}_c)$. The interface $\partial\Omega(t)$ evolves with a normal velocity given by $V = -w\nabla u \cdot \mathbf{n}$, where $\mathbf{n}$ is the unit outward normal vector to the moving boundary $\partial\Omega(t)$. The tumor boundary $\partial\Omega(t)$ is defined parametrically using the parameter $s \in [0, 1]$, and with $\theta = 2\pi s$, the radial profile of the initial tumor boundary is given by $r(\theta) = 4.8 - 0.4\cos(4\theta + \pi/4) - 0.4\sin(4\theta + \pi/4)$. The corresponding Cartesian coordinates of the boundary are $x = r(\alpha)\cos(\alpha), \quad y = r(\alpha)\sin(\alpha)$, which together define a noncircular initial tumor region. The initial conditions for c_t and c_n are taken to be 1 and for c_d to be 0 within the tumor domain $\Omega(t)$.

2 Deep Learning-based Method and Results

The proposed deep learning–based framework is conceptually straightforward and draws inspiration from the level set method [2]. In our formulation, three PINNs are employed to approximate the state variables u_t, u_d and u_n . To capture the evolution of the moving boundary, we introduce a continuous level set function φ such that $\varphi(\mathbf{x}) = 0$ corresponds to the moving boundary $\Gamma(t)$, $\varphi(\mathbf{x}) = -d(\mathbf{x})$ within the tumor region, and $\varphi(\mathbf{x}) = +d(\mathbf{x})$ in the exterior of the tumor region $\Omega^c(t)$. $d(\mathbf{x})$ denotes the signed Euclidean distance from the point $\mathbf{x}$ to the moving boundary. An additional PINN is dedicated to approximating φ . The governing equation for φ is derived from the moving boundary condition. For the governing equation of φ, the associated loss term is multiplied by a Gaussian smoothing function $\delta(\varphi) = \frac{1}{\sqrt{\pi\epsilon}} exp\left(-\frac{\varphi^2}{\epsilon^2}\right)$, which ensures the correct implementation of the moving boundary condition.

To evaluate the proposed PINN architecture, we compared its predictions against reference solutions obtained using the standard Level Set Method (LSM). Figure 1 provides a visual comparison of the results for the time point 0.03 s. Quantitative performance was assessed via relative L_2 errors. These results highlight the capability of PINNs to simulate continuum tumor growth models involving multiple coupled nonlinear PDEs with moving boundary conditions.

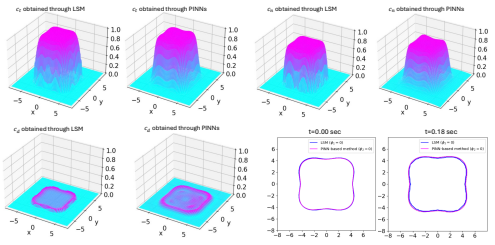

Figure 1: Comparison of the proposed algorithm and the LSM for $t = 0.03$ s.

References

[1] C. S. Hogea, B. T. Murray, J. A. Sethian, *Simulating complex tumor dynamics from avascular to vascular growth using a general level-set method*, J. Math. Biol. **53** (2006) 86–134.

[2] S. Chen, B. Merriman, S. Osher, P. Smereka, *A Simple Level Set Method for Solving Stefan Problems*, J. Comput. Phys. **135** (1997) 8–29.

[3] M. Raissi, P. Perdikaris, G. E. Karniadakis, *Physics-informed neural networks: A deep learning framework for solving forward and inverse problems involving nonlinear partial differential equations*, J. Comput. Phys. **378** (2019) 686–707.

Book of abstracts of the 9th International Conference on
Advanced Computational Methods in ENgineering and Applied Mathematics
September, 15–19, 2025.

Accounting for Hysteresis and Eddy Currents in FEM Simulations of Ferromagnetic Laminated Cores using a Recurrent Neural Network

Florent Purnode[1], Louis Denis[1], François Henrotte[1], Gilles Louppe[1] and Christophe Geuzaine[1]

[1] *Department of Electrical Engineering and Computer Science, University of Liège, Belgium*

e-mails: florent.purnode@uliege.be, louis.denis@uliege.be, francois.henrotte@uliege.be, g.louppe@uliege.be, cgeuzaine@uliege.be

Abstract

Accounting for hysteresis and eddy currents in finite element simulations of electrical machines with ferromagnetic laminated cores is expensive. These phenomena have however a significant impact on the machine performance. To account for them with a low computational cost, we propose to train a recurrent neural network to serve as material law in 2D finite element simulations.

Key words: FEM Simulation, Hysteresis, Laminated Core, Recurrent Neural Network

1 Introduction

Computing hysteresis and eddy current losses during the design phase of electrical machines remains an open challenge, as traditional multiscale Finite Element Model (FEM) simulations with integrated hysteresis modeling are computationally too demanding. In R&D, hysteresis is therefore often simply neglected during the simulation and losses are evaluated a posteriori. In this work, a Recurrent Neural Network (RNN) is trained to replicate a lamination model, and is integrated into a 2D FEM simulation in order to account for the effect of eddy currents and hystesresis at reasonable cost directly during the simulation.

2 RNN Architecture and Training

Since hysteresis intrinsically depends on the magnetic field history, an RNN, whose hidden state keeps memory of past field values, is a convenient architecture to deal with hysteresis. We use a single-layer gated recurrent unit [1] with a hidden size of 256. Embedding and decoding both use a two-layer feed-forward neural network with `ReLU` and `Linear` activation functions.

The training dataset is populated with magnetic field $\mathbf{H}$ sequences, generated artificially to mimic fields encountered in electrical machines. The corresponding magnetic flux density $\mathbf{B}$ sequences are obtained by solving a 1D magneto-dynamic problem with the energy-based model on a single lamination [2]. All in all, $5 \cdot 10^5$ $(\mathbf{H}, \mathbf{B})$ sequence pairs of 10^3 time steps are generated in about 3 hours on an `AMD EPYC 7763 CPU`. The training is then performed in about 6 hours on a `NVIDIA A100 40GB GPU`.

3 FEM simulation

The RNN is integrated into a magnetic-field-conforming FEM formulation, written in terms of the scalar potential ϕ, with $\mathbf{H} = -\nabla\phi$. At each iteration i of the Newton-Raphson iterative scheme, the following weak formulation is solved for $\mathbf{H}_i$:

$$\left(\mathbf{B}(\mathbf{H}_{i-1}) + \frac{\partial \mathbf{B}}{\partial \mathbf{H}}(\mathbf{H}_{i-1})(\mathbf{H}_i - \mathbf{H}_{i-1}), -\nabla\phi'\right)_\Omega = 0, \ \forall\, \phi', \tag{1}$$

where $\mathbf{B}(\mathbf{H}_{i-1})$ is computed in the RNN's forward pass and $\frac{\partial \mathbf{B}}{\partial \mathbf{H}}(\mathbf{H}_{i-1})$ is obtained by reverse-mode automatic differentiation through the RNN. Figure 1 shows **HB** curves obtained on a reference square mesh, with ramped-up sinusoidal source magnetic field. These curves perfectly match with the reference ones, obtained by directly coupling the FEM simulation with the 1D lamination model used to generate the training dataset.

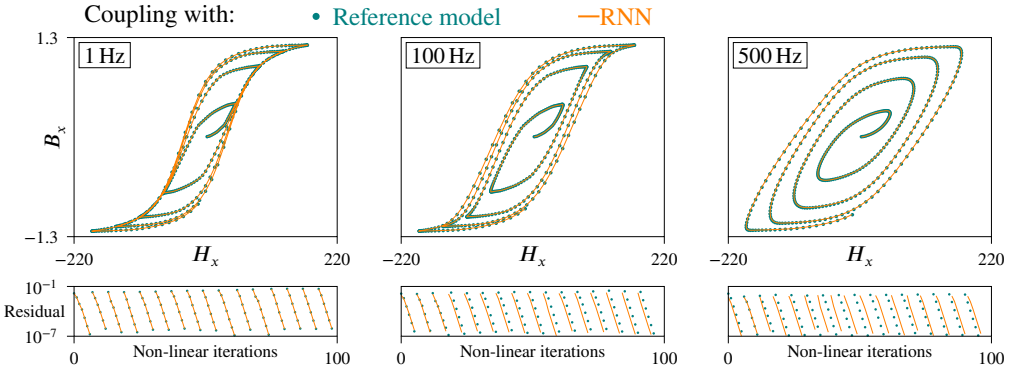

Figure 1: H_xB_x curves from the FEM simulation under loading condition at different frequencies. Coupling the FEM simulation with the RNN provides the same results as a direct coupling with the reference model, which has been used to generate the training dataset. In fact, the root mean squared error between RNN and reference **H** and **B** fields does not exceed 0.2 A/m and 4 mT respectively. In both cases, convergence is also quickly reached.

Acknowledgements The present research benefited from computational resources made available on Lucia, the Tier-1 supercomputer of the Walloon Region, infrastructure funded by the Walloon Region under the grant agreement n°1910247. The work of L. Denis was supported by the F.R.S-FNRS.

References

[1] K. Cho, B. Van Merriënboer, C. Gulcehre , D. Bahdanau, F. Bougares, H. Schwenk, Y. Bengio, *Learning phrase representations using RNN encoder-decoder for statistical machine translation*, Proceedings of the conference EMNLP, 2014

[2] F. Henrotte, S. Steentjes, K. Hameyer, C. Geuzaine, *Iron loss calculation in steel laminations at high frequencies*, IEEE transactions on magnetics, 2014

Book of abstracts of the 9th International Conference on
Advanced Computational Methods in ENgineering and Applied Mathematics
September, 15–19, 2025.

A Natural Deep Ritz Method for Essential Boundary Value Problems

Shuo Zhang[1,2]

[1] *Academy of Mathematics and System Sciences, Chinese Academy of Sciences*

[2] *School of Mathematical Sciences, University of Chinese Academy of Sciences*

e-mails: szhang@lsec.cc.ac.cn

Abstract

Deep neural network approaches for PDEs face challenges in enforcing boundary conditions, especially the essential problems. We propose a novel, intrinsic approach to impose essential boundary conditions through a framework inspired by intrinsic structures. The main essence of the approach is to transfer the original essential boundary value problem to a series of natural boundary value problems. We demonstrate the effectiveness of this approach using the deep Ritz method applied to Poisson problems, with the potential for extension to more general equations and other deep learning techniques. Numerical results are provided to substantiate the efficiency and robustness.

Key words: neural network, essential boundary value problem, deep Ritz method

1 Introduction

In the design and implementation of neural network-based methods, the imposition of boundary conditions is a critical challenge. As the DNNs are globally defined, enforcing boundary conditions becomes nontrivial. For the natural boundary conditions, the deep Ritz method reformulates the original problem into a variational form, which can reduce the smoothness requirements and potentially lower the training cost by allowing natural boundary conditions to be imposed without additional operations. However, imposing essential boundary conditions remains a challenging task. Approaches have been developed for addressing essential boundary conditions, however with issues on design, construction and implementations.

This talk presents a novel method for solving essential boundary value problems, transforming the original problem into a sequence of natural boundary value problems, which are then solved sequentially or concurrently using the deep Ritz method. We refer to this method as the **natural deep Ritz method**. As one major advantage, this approach elimites the need of tuning a boundary penalty parameter, thus simplifies the training process and avoids introducing additional errors associated with boundary condition enforcement.

2 The main approach

Take the Poisson equation with Dirichlet boundary condition (1) as example:

$$\begin{cases} -\Delta u &= f \quad \text{in } \Omega, \\ u &= g \quad \text{on } \Gamma = \partial\Omega. \end{cases} \tag{1}$$

Basically, we construct several boundary value problems as below:

Subproblem 1

$$\begin{cases} -\Delta\tilde{u} &= f & \text{in } \Omega, \\ \frac{\partial\tilde{u}}{\partial\mathbf{n}} &= -\frac{1}{|\Gamma|}\int_\Omega f, & \text{on } \partial\Omega. \end{cases} \tag{2}$$

Subproblem 2

$$\begin{cases} -\Delta\varphi &= 0 & \text{in } \Omega, \\ \operatorname{curl}\varphi\cdot\mathbf{t} &= \partial_{\mathbf{t}}g - \partial_{\mathbf{t}}\tilde{u}, & \text{on } \partial\Omega. \end{cases} \tag{3}$$

Subproblem 3

$$\begin{cases} -\Delta u_c &= f & \text{in } \Omega, \\ \frac{\partial u_c}{\partial\mathbf{n}} &= \partial_{\mathbf{n}}\tilde{u} - \partial_{\mathbf{t}}\varphi, & \text{on } \partial\Omega. \end{cases} \tag{4}$$

Then u_c is equal to u up to a constant which can be fixed by the boundary condition.

We illustrate the performance of the method for a simple test problem here. We use deep Ritz method to solve the natural boundary value problems one by one, and the results are illustrated in Figure 1. Detailed interpretations and further applications are given in the talk.

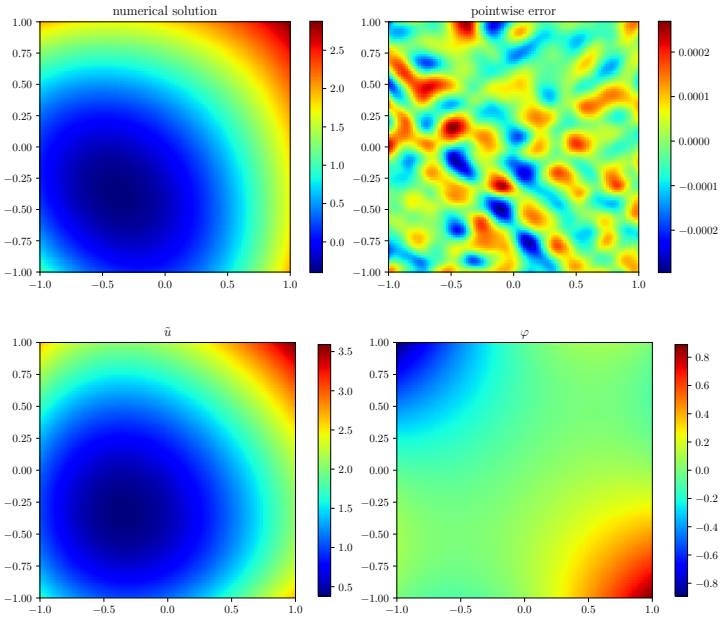

Figure 1: The learned numerical solution and $\tilde{u}$, φ functions for the example.

Acknowledgements This work is partially supported by NSFC (92370205, 12494543, 12271512, 12171467, 12161141017).

References

[1] H. Yu, S. Zhang, *A Natural Deep Ritz Method for Essential Boundary Value Problems*, J. Comput. Phy. **537**(2025), 114133.

MS3: Modelling, simulation and analysis of inertial particle dynamics

Organiser: Anna Klünker (Leuphana University Lüneburg) and Vamika Rathi (Hamburg University of Technology)

Description: Inertial particles exhibit distinct transport behaviors compared to passive or ideal fluid particles. Their study is critical for a wide range of applications, from industrial processes like chemical reactors to natural phenomena such as marine snow or the transport of micro- or macro plastics in the ocean. This mini-symposium will discuss recent advancements in the mathematical modelling, simulation, and analysis of inertial particle transport across various applications. Talks will present novel numerical approaches for solving the Maxey-Riley equation, a key model to describe the motion of small inertial particles. They will also present various Lagrangian analysis tools that have been developed in the last decades to investigate transport and mixing in fluid flows. These tools provide valuable insights into the dispersion patterns of inertial particles, offering a deeper understanding of their complex behaviors in fluid systems.

Book of abstracts of the 9th International Conference on
Advanced Computational Methods in ENgineering and Applied Mathematics
September, 15–19, 2025.

Mathematical Modelling for Gravity Waves Interactions Coupled with Localized Water Vapour and Ozone in the Atmosphere

Ahmed Saleh Almohaimeed[1]

[1] *Department of Mathematics, College of Science, Qassim University, Saudi Arabia*

e-mails: ahs.almohaimeed@qu.edu.sa

Abstract

In the atmosphere, the interrelationship between dynamics and chemistry results in mutual influence and interaction. The behavior of internal gravity waves is influenced by the thermal effects caused by chemical components present in the atmosphere. In this investigation, the equations determining gravity waves are coupled with those characterizing the behavior of ozone and water vapor. To investigate the coupled equations, numerical analyses are conducted, and the resulting numerical results are presented. Internal gravity waves have been observed to influence the distribution of ozone and water vapor within the Earth's atmosphere. It has been demonstrated, based on our findings, that wave fluctuations play a significant role in exerting a substantial effect. In addition, it has been observed that the influence of ozone and water vapor-induced heating on gravity waves is significant, particularly near the critical level where the mean flow induced by gravity waves plays a significant role.

1 Introduction

The decline in atmospheric density as one moves away from the Earth's surface results in the atmosphere being relatively stable and stratified. The combination of the buoyancy-restoring force resulting from stratification and the gravitational force gives rise to the formation of internal gravity waves.

The atmosphere consists of major chemical constituents such as nitrogen (N_2), oxygen (O_2), argon (Ar), water vapor (H_2O), as well as trace gases like carbon dioxide (CO_2), methane (CH_4), and ozone (O_3).

Previous studies focus was mostly on the photochemical effect on gravity waves. The wave-induced mean flow results from gravity-wave interactions, due to nonlinear terms in gravity waves, with the mean flow. This effect of the wave-induced mean flow on the distribution of chemical species was not studied as most previous studies considered linear representation of gravity waves.

Our focus in this work is to show the effect of the wave-induced mean flow as we study the full nonlinear system of internal gravity waves coupled with continuity equations for ozone and water vapor. We will investigate the impact of wave-induced mean flow on the distribution of chemical species in the atmosphere; and conversely we will study the effect of the chemical on the nonlinear gravity waves taken into account the presence of wave-induced mean flow.

2 More

As shown in [1], the full nondimensional model for equations modelling gravity waves coupled with ozone and water vapor takes the form

$$\zeta_t + \bar{u}\zeta_x - \bar{u}''\psi_x + \varepsilon(\psi_x\zeta_z - \psi_z\zeta_x) = -\frac{g}{\bar{\rho}}\rho_x, \tag{1}$$

$$\zeta = \nabla^2\psi\,, \tag{2}$$

$$\rho_t + \bar{u}\rho_x + \bar{\rho}'\psi_x + \varepsilon(\psi_x\rho_z - \psi_z\rho_x) = \gamma_{o_3}\frac{D\,C(O_3)}{Dt} + \gamma_{h_2o}\frac{D\,C(H_2O)}{Dt}\,, \tag{3}$$

$$u = -\psi_z \quad \text{and} \quad w = \psi_x. \tag{4}$$

$$\frac{D\,C(O_3)}{Dt} = \frac{\partial C(O_3)}{\partial t} + (\bar{u} + \varepsilon u)\frac{\partial C(O_3)}{\partial x} + \varepsilon w\frac{\partial C(O_3)}{\partial z} = -\sigma_{o_3}C(O_3) + \mathcal{D}\nabla^2 C(O_3), \tag{5}$$

$$\frac{D\,C(H_2O)}{Dt} = \frac{\partial C(H_2O)}{\partial t} + (\bar{u} + \varepsilon u)\frac{\partial C(H_2O)}{\partial x} + \varepsilon w\frac{\partial C(H_2O)}{\partial z} = -\sigma_{h_2o}C(H_2O) + \mathcal{D}\nabla^2 C(H_2O), \tag{6}$$

where ζ represents the perturbation vorticity of gravity waves, $\bar{u}$ is the horizontal component of the background flow velocity, ψ is the perturbation streamfunction of gravity waves, g is the gravitational force, $\bar{\rho}$ is the background density and ρ is the perturbation density.

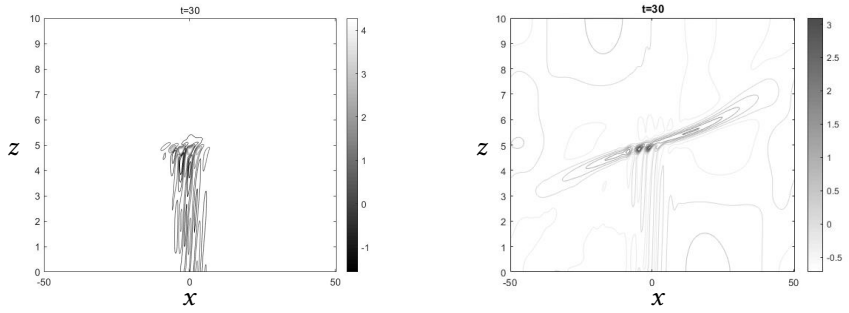

(a) (b)

Figure 1: Figure (a) shows $u(x, z, t)$ in the absence of chemical interaction at $t = 30$; whereas the sub Figure (b) shows $u(x, z, t)$ influenced by $C(O_3)$ and $C(H_2O)$ at $t = 30$.

Acknowledgements The Researchers would like to thank the Deanship of Graduate Studies and Scientific Research at Qassim University for financial support (QU-APC-2024-9/1).

References

[1] Ahmed S. Almohaimeed, *Mathematical modelling for gravity waves interactions coupled with localized water vapor and ozone in the atmosphere*, Frontiers in Earth Science **12** (2024) 1385305.

Book of abstracts of the 9th International Conference on
Advanced Computational Methods in ENgineering and Applied Mathematics
September, 15–19, 2025.

The Maxey-Riley-Gatignol equations for macroplastics in oceanic flows

Meike F. Bos[1], Irina I. Rypina[2], Larry J. Pratt[2] and Erik van Sebille[1]

[1] *Institute for Marine and Atmospheric research Utrecht, Utrecht University*

[2] *Woods Hole Oceanographic Institution, Woods Hole*

e-mails: m.f.bos@uu.nl, iryina@whoi.edu, lpratt@whoi.edu, e.vansebille@uu.nl

Abstract

Floating macroplastics in the ocean have a finite size and density lower than the water in which they are drifting. Due to their inertia, they do not perfectly follow the ocean currents and their motion might be better described by the Maxey-Riley-Gatignol equations. In this work, we tailor these equations to simulate subsurface buoyant macroplastics in the ocean. We implemented these equations in the Lagrangian simulation framework Parcels. With this implementation, we performed Lagrangian analysis simulations, where we studied the effect of inertia on the trajectories of macroplastics. We find that the drag force controls the trajectories of subsurface buoyant macroplastics in the North west European shelf, which makes the macroplastics behave very similar to surface-flow-following tracer particles.

Key words: Lagrangian analysis, macroplastics, Maxey-Riley-Gatignol equations, particle Reynolds number, ocean

1 Introduction

Macroplastics (plastic objects > 5 cm) make up most of the mass of plastic in the ocean [1]. The distribution of macroplastic varies widely in space and time [2]. However, what processes cause this large variability is not yet understood. In this work, we focus on how the macroplastics' inertia can affect its transport.

The macroplastics' finite size and density is different from the water in which they are drifting. This makes their behavior inherently different from water particles. For particles that are much smaller than the typical scales of the flows in which they are embedded, the motion can be described by the Maxey-Riley-Gatignol (MRG) equations [4, 5]. The MRG equations use Newtons second law to describe the velocity and position of the particle over time. Here, we tailor the MRG equation for subsurface macroplastics in oceanic flows (*i.e.* ignoring the effect of the wind on the particle), for which we perform sensitivity tests for the particle Reynolds number-dependent drag force and history force. We use the North West European shelf as test location, for which we used surface velocity fields with hourly temporal resolution from the Copernicus Marine Services [3].

2 The MRG equations for subsurface macroplastics

Our sensitivity tests for a spherical macroplastic with buoyancy $B = 0.68$ and a diameter $d = 25$ cm, show that the average Reynolds number $\langle \mathrm{Re}_p \rangle$ for such a particle in the NWES is around $300 - 500$, and thus well beyond the Stokes regime. Thus, we use a drag force with an effective viscosity that depends on the particle Reynolds number:

$$\mathbf{F}_{\mathrm{drag}}(\mathbf{u}_p, \mathbf{x}_p, t) = -3\pi\mu_{\mathrm{eff}} d(\mathbf{u}_p(t) - \mathbf{u}_f(\mathbf{x}_p, t)) \tag{1}$$

with $\mathbf{u}_p(t)$ the particle velocity at time t, $\mathbf{u}_f(\mathbf{x}_p, t)$ the fluid velocity at the position of the particle denoted by $\mathbf{x}_p$. μ_{eff} is given by [6]:

$$\mu_{\mathrm{eff}} = \nu \left(1 + \frac{\mathrm{Re}_p}{4\left(1 + \sqrt{\mathrm{Re}_p}\right)} + \frac{\mathrm{Re}_p}{60}. \right), \tag{2}$$

with μ the dynamic viscosity of seawater. This relation is valid for $\mathrm{Re}_p < 10^5$. As the ocean flow in the NWES is highly variable in space and time, so is the particle Reynolds number. Thus, we define a particle Reynolds number per particle that can change its value over time.

Our sensitivity tests show that due to the relatively large particle Reynolds number, the history term is negligible compared to the steady drag force.

Using the MRG equations with a drag force that depends on the particle Reynolds number and without the history force, we find that the trajectories of subsurface macroplastics are dominated by the drag force and thus very similar to tracer particles. Furthermore, we find that the flexible Reynolds number MRG equations used in this work are sensitive to the underlying resolution of the velocity field. For velocity fields with an hourly resolution, the trajectories of subsurface macroplastics are not significantly different from tracer particles, while for velocity fields with a daily resolution the trajectories are significantly different. This is because for a lower time resolution, some variations in the velocity field are averaged out, which leads to smaller particle Reynolds numbers and thus to an underestimation of the drag force. This underestimation will happen for any model with a finite resolution, and thus has to be accounted for in any MRG simulation of macro-objects in the ocean.

References

[1] M. Kaandorp et all., *Global mass of buoyant marine plastics dominated by large long-lived debris*, Nat. Geosci. **16** (2023) 689-694.

[2] C. Morales-Caselles et all, *An inshore–offshore sorting system revealed from global classification of ocean litter*, Nat. Sustain. **4** (2021) 484-493.

[3] Coperinus Marine Services, *Atlantic - European North West Shelf - Ocean Physics Analysis and Forecast*, https://doi.org/10.48670/moi-00054

[4] M.R. Maxey, J. J. Riley, *Equation of motion for a small rigid sphere in a nonuniform flow*, Phys. Fluids **26** (1983) 883-889.

[5] R. Gatignol *The faxen formulae for a rigid particle in an unsteady non-uniform Stokes flow* J. Mec. Theor. Appl 1 (1983) 143-160.

[6] F. M. White, *Solutions of the Newtonian Viscous-Flow Equations*, McGraw-Hill, 1991.

Book of abstracts of the 9th International Conference on
Advanced Computational Methods in ENgineering and Applied Mathematics
September, 15–19, 2025.

Maxey-Riley-Gatignol equations for tracking Lagrangian devices in chemical reactors

Vamika Rathi[1] and Daniel Ruprecht[1]

[1] *Lehrstuhl Computational Mathematics, Institut für Mathematik, Technische Universität Hamburg, Germany*

e-mails: vamika.rathi@tuhh.de, ruprecht@tuhh.de

Abstract

The Maxey–Riley–Gatignol equation (MaRGE) describes the motion of small, spherical inertial particles in fluids. MaRGE is an integro-differential equation due to the presence of the history force term—an integral over the entire time interval of the particle's motion—which makes it difficult and computationally expensive to solve. For this reason, the history force term is often neglected despite substantial evidence of its importance. We present a numerical solver for the 3D MaRGE based on methods developed by Daitche for the 2D case. An analytical solution for MaRGE in a simple vortex has been proposed by Candelier et al., which we extend to a 3D vortex to demonstrate the accuracy of our numerical solution. To track Lagrangian devices in reactors, we also develop a filtering algorithm that uses a simplified version of MaRGE as the prediction model.

Key words: MaRGE, history term, vortex field, tracking.

1 Introduction

Inertial particle dynamics is an important topic of study with applications in a wide range of systems ranging from the movement of sediment particles in water flow [1], to spread of wildfires [2]. The motion of inertial particles in fluids is modeled using Maxey-Riley-Gatignol equation (MaRGE) [3, 4] which can be written in non-dimensional from (here all quantities are dimensionless) as

$$\frac{\mathrm{d}\boldsymbol{v}}{\mathrm{d}t} = R\,\frac{\mathrm{D}\boldsymbol{u}}{\mathrm{D}t} - \frac{R}{S}(\boldsymbol{v}-\boldsymbol{u}) - R\sqrt{\frac{3}{S\pi}}\frac{\mathrm{d}}{\mathrm{d}t}\int_{t_0}^{t}\frac{1}{\sqrt{t-\tau}}(\boldsymbol{v}-\boldsymbol{u})\mathrm{d}\tau - (1-R)\boldsymbol{G}, \tag{1}$$

where $\dot{\boldsymbol{x}} = \boldsymbol{v}(t)$ is the particle's absolute velocity, $\boldsymbol{u}(\boldsymbol{x}(t),t)$ is the fluid velocity at particle's position $\boldsymbol{x}(t)$, $\mathrm{D}/\mathrm{D}t$ is the material derivative. R, S and $\boldsymbol{G}$ are the non-dimensional parameters given as

$$R = \frac{3m_f}{m_f + 2m_p}, \qquad S = \frac{1}{3}\frac{a^2/\nu}{T}, \qquad \boldsymbol{G} = \frac{T}{U}\boldsymbol{g}, \tag{2}$$

where m_p is mass of the particle, m_f is mass of the fluid displaced by the particle, ρ_f is the fluid density, ν is the kinematic viscosity and $\boldsymbol{g}$ is the gravitational force vector. The terms on the right hand side of (1) correspond to the acceleration of the particle in undisturbed fluid, the Stokes drag, the Basset history term and the buoyancy term. The history term is an

integral term which makes the computation of MaRGE difficult and expensive. Due to this reason it is often neglected in various applications despite its evident importance.

There have been some attempts to solve MaRGE in recent years for 2D flows. However we need to model particle trajectories in 3D flows. We present a numerical solver for the 3D MaRGe using the quadrature schemes for solving the history term and Adams-Bashforth methods for solving the full equations as proposed by Daitche [6]. For verification, we derive an analytical solution using techniques by Candelier et. al. [7] for a 3D vortex as test case.

For tracking Lagrangian devices in chemical reactors we develop filtering algorithms that use a simplified version of MaRGE as prediction model instead of the commonly used assumption of constant acceleration over a time step. We also use acceleration measurements instead of position measurements in the measurement model of our filtering algorithm.

Acknowledgements This project is funded by the Deutsche Forschungsgemeinschaft (DFG, German Research Foundation) – SFB 1615 – 503850735.

References

[1] Y. Niño, M. García, *Gravel Saltation: 2. Modeling*, Water Resour. Res. **30** (1994) 1915-1924.

[2] A. Mendez, M. Farazmand, *Quantifying Rare Events in Spotting: How Far Do Wildfires Spread?*, Fire Saf. J. **132** (2022) 103630.

[3] M.R. Maxey, J.J. Riley, *Equation of Motion for a Small Rigid Sphere in a Nonuniform Flow*, Phys. Fluids **26** (1983) 883–889.

[4] R. Gatignol, *The Faxén Formulae For A Rigid Particle In An Unsteady Non-Uniform Stokes Flow*, J. Mécan. Théor. Appl. **2** (1983) 143-160.

[5] R. Mei, R.J. Adrian, T.J. Hanratty, *Particle Dispersion in Isotropic Turbulence under Stokes Drag and Basset Force with Gravitational Settling*, J. Fluid Mech. **225** (1991) 481-495.

[6] A. Daitche, *Advection of Inertial Particles in the Presence of the History Force: Higher Order Numerical Schemes*, J. Comput. Phys **254** (2013) 93-106.

[7] F. Candelier, J.R. Angilella, M. Souhar, *On the Effect of the Boussinesq–Basset Force on the Radial Migration of a Stokes Particle in a Vortex*, Phys. Fluids **16** (2004) 1765-1776.

MS4: Implicit high-order time integration for hyperbolic PDEs

Organiser: Jochen Schütz (Hasselt University) and Peter Frolkovic (Slovak University of Technology)

Description: Traditionally, time integration for hyperbolic PDEs has been done using explicit time integration schemes. While these schemes are easier to analyze and implement, and very often yield highly efficient algorithms, they can suffer from severe stability restrictions when the underlying PDE becomes stiff due to, e.g., large wave speeds, large sources, geometries with high aspect ratio and the like. Recent years have hence seen much progress in the development and analysis of implicit time integration for hyperbolic (and related) PDEs. This minisymposium aims to bring together researchers that work on implicit, semi-implicit or implicit/explicit (IMEX) time integration for PDEs, with a particular focus on hyperbolic PDEs.

Book of abstracts of the 9th International Conference on
Advanced Computational Methods in ENgineering and Applied Mathematics
September, 15–19, 2025.

Compact implicit high resolution fast sweeping methods for some hyperbolic problems

Peter Frolkovič[1]

[1] *Department of Mathematics and Descriptive Geometry,*
Slovak University of Technology in Bratislava

e-mails: peter.frolkovic@stuba.sk

Abstract

Efficient numerical solvers for some hyperbolic equations using unconditionally stable non-oscillatory compact implicit numerical schemes are presented.

Key words: compact implicit scheme, fast sweeping method, hyperbolic problems

1 Introduction

We present a holistic approach to solve some hyperbolic problems using high-resolution implicit numerical methods. The approach consists of coupling the space and time discretizations and iterative algebraic solvers. We build on the implicit first order accurate method that can be used efficiently with an appropriate fractional time step method and fast sweeping method for numerical solutions of nonlinear hyperbolic systems [1]. The method is extended to essentially non-oscillatory form using higher-order reconstructions in space based on mixed space-time differences and a novel limiting in time [2]. For the case of linear advection with divergence free variable velocity field, we can show that the method is Local Extrema Diminishing for any choice of time steps [3]. The discretization methods exploit coupled space-time approximations that are tailored to the fast sweeping method to solve the resulting algebraic systems [1, 2]. We discuss possible variants that can bring the expected order of accuracy after a finite number of iterations like a deferred correction method or time splitting methods.

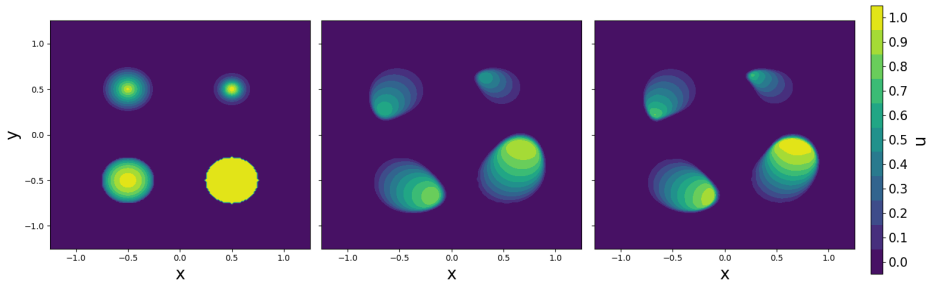

Figure 1: Comparison of the first order (the middle picture) and the high-resolution (the right picture) implicit scheme for an example of Burgers equation combined with rotational velocity for maximal Courant number equal 3.92 [3]. The left picture is the initial condition consisting of Gaussian and three non-smooth profiles. The results for both methods were obtained with the fast sweeping algebraic solver using only four nonlinear Gauss-Seidel iterations with four distinct orderings of unknowns.

Acknowledgements This work has been supported by VEGA 1/0314/23.

References

[1] E. Lozano, T. D. Aslam, "Implicit Fast Sweeping Method for Hyperbolic Systems of Conservation Laws", *Journal of Computational Physics*, 430, pp. 110039, 2021.

[2] P. Frolkovič, M. Žeravý, "High Resolution Compact Implicit Numerical Scheme for Conservation Laws", *Applied Mathematics and Computation*, 442, pp. 127720, 2023.

[3] D. Žáková and P. Frolkovič "Compact implicit high resolution numerical methods for solving transport problems with sorption isotherms", *arxiv*, 2025, in a revision

Book of abstracts of the 9th International Conference on
Advanced Computational Methods in ENgineering and Applied Mathematics
September, 15–19, 2025.

Unconditionally stable higher order semi-implicit level set method

Nikola Gajdošová[1] and Peter Frolkovič[2]

[1,2] *Department of Mathematics and Descriptive Geometry, Slovak University of Technology in Bratislava*

e-mails: nikola.gajdosova@stuba.sk, peter.frolkovic@stuba.sk

Abstract

We present semi-implicit higher order numerical methods to solve nonlinear level set equations for evolving interfaces driven by external velocity and speed in the normal direction. We introduce up to third order accurate unconditionally stable numerical schemes of a compact implicit form on structured grids. To approximate in time, we use finite Taylor series that are expressed in an implicit (backward) manner, where the time derivatives are replaced using the partial Lax-Wendroff procedure allowing for mixed temporal and spatial derivatives. We suggest different space discretizations for each term with mixed derivatives in the Taylor series including Weighted Essentially Non-Oscillatory form for the approximation of the normal velocity. The compact implicit part of the stencil of numerical schemes contains unknowns only in the upwind direction. Consequently, algebraic solvers like the fast sweeping method can be applied efficiently to solve the resulting algebraic systems. Several tests in the two-dimensional case will be presented that confirm the advantages of the proposed methods. Recently, we have explored applications of the above schemes with methods based on semi-implicit Runge–Kutta schemes.

Key words: higher order methods, compact schemes, semi-implicit methods, level set methods

1 Introduction

We focus on numerical methods that do not require restrictions on the choice of (grid) Courant number to be small enough to avoid instability of the solution computation. Typically, if the Courant number is greater than one, it means that the information propagates through more than one grid cell at each time step, it can make the solution with nonphysical results. Moreover, large time steps, and therefore large Courant numbers, are suitable in problems where the time dependent solution is approaching a stationary form. In order to derive a semi-implicit scheme with no stability restriction on time steps, we use techniques that are popular in proposing numerical methods for the solution of hyperbolic problems.

In particular, we consider the following nonlinear advection equation,

$$\partial_t \phi + \left(\mathbf{u} + \delta \frac{\nabla \phi}{|\nabla \phi|} \right) \cdot \nabla \phi = 0 \,, \quad \phi(\mathbf{x}, 0) = \phi^0(\mathbf{x}), \tag{1}$$

where $\phi = \phi(\mathbf{x}, t)$ for $\mathbf{x} \in R^2$ and $t > 0$ is the unknown level set function given at $t = 0$ by the given function ϕ^0. The vector field $\mathbf{u} = \mathbf{u}(\mathbf{x})$ prescribes the movement of all level sets by an external velocity, and δ is the speed in the normal direction given by the normalized gradient.

In the following example, we illustrate the behavior of the third order scheme for a solution of the advection equation when the velocity significantly changes its values in the computational domain. Namely, we choose the velocity $\mathbf{u}$ that varies exponentially and $\delta = 0$,

$$\mathbf{u} = (e^{2(x_2 - x_1)}, e^{2(x_2 - x_1)}).$$

The initial condition ϕ^0 is the distance function to the point $[-1, -1]$.

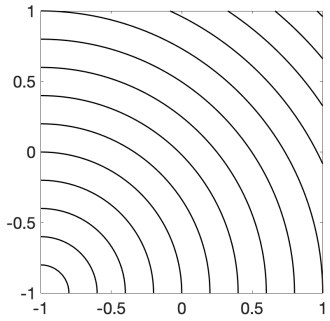

Figure 1: The initial condition for the example with exponentially varying velocity.

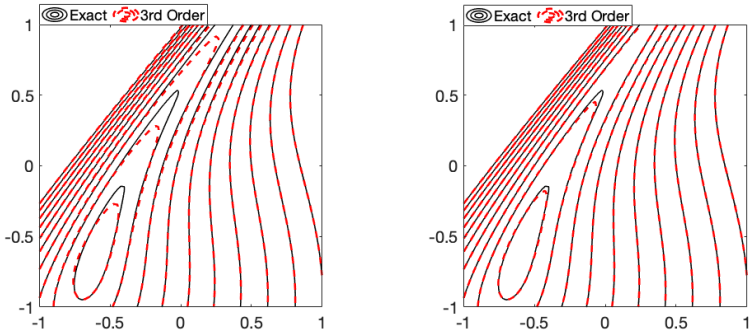

Figure 2: The example with time-dependent Dirichlet boundary conditions — the results with the exact solution (black) and the numerical solutions obtained with the 3rd order scheme (red dashed) at $t = 0.4$ using $I = 80$ and $N = 2$ with $C \approx 436$ (left) and $N = 8$ with $C \approx 109$ (right).

References

[1] Frolkovič, P., Mikula, K. (2018). *Semi-implicit second order schemes for numerical solution of level set advection equation on Cartesian grids.* Applied Mathematics and Computation, 329, p. 129–142.

[2] Frolkovič, P., Gajdošová, N. (2023). *Unconditionally stable higher order semi-implicit level set method.* Applied Mathematics and Computation, 466, 128460.

Book of abstracts of the 9th International Conference on
Advanced Computational Methods in ENgineering and Applied Mathematics
September, 15–19, 2025.

Low Mach number implicit-explicit schemes for the incompressible Cahn-Hilliard-Navier-Stokes equations

Andreu Martorell[1], Pep Mulet[1] and Dionisio F. Yáñez[1]

[1] *Departament de Matemàtiques, Universitat de València*

e-mails: andreu.martorell@uv.es, pep.mulet@uv.es, dionisio.yanez@uv.es

Abstract

We present a second-order implicit-explicit (IMEX) time-stepping scheme for the isentropic Cahn-Hilliard-Navier-Stokes equations in the low Mach number regime. These equations describe the dynamics of compressible binary fluid mixtures, such as foams or phase separation, under the influence of gravity.

The numerical scheme is based on finite differences on staggered grids and is specifically designed to address the challenges posed by the low Mach number limit, where the system approaches to an incompressible behavior. In this regime, standard explicit schemes suffer from severe time-step restrictions due to fourth-order diffusion terms and the stiffness induced by fast acoustic waves.

To overcome this, we employ an IMEX strategy which splits the governing equations into stiff and non-stiff components. The stiff terms, arising from pressure and fourth-order Cahn-Hilliard contributions, are treated implicitly, while the remaining are dealt explicitly.

Key words: Asymptotic preserving, low Mach number, implicit-explicit schemes, incompressible limit, isentropic compressible Cahn-Hilliard-Navier-Stokes

1 Introduction

In the current model [3], ρ represents the density of the mixture, $\mathbf{v}$ the bulk velocity and c describes the concentration difference of two species. In addition, parameters such as the diffuse interface thickness ε and the viscosity coefficients $\nu(c), \lambda(c)$ are considered.

The governing equations are the isentropic compressible Cahn-Hilliard-Navier-Stokes equations with gravitation in a low Mach number regime:

$$\begin{cases} \rho_t + \nabla \cdot (\rho \mathbf{v}) = 0, \\ (\rho \mathbf{v})_t + \nabla \cdot (\rho \mathbf{v} \otimes \mathbf{v}) + \dfrac{1}{\delta} \nabla p = \rho \mathbf{g} + \nabla \cdot \mathbb{T}, \\ (\rho c)_t + \nabla \cdot (\rho c \mathbf{v}) = \Delta \mu, \end{cases}$$

defined in $\Omega \times (0, T)$, where Ω is an open subset of $\mathbb{R}^3$. The first equation describes the continuity equation for the mixture, the second represents the conservation of bulk momenta, and the third is a Cahn-Hilliard type equation modelling the evolution of the mixture. The stress tensor is given by

$$\mathbb{T} = \nu(c)(\nabla \mathbf{v} + \nabla \mathbf{v}^T) + \lambda(c) \nabla \cdot \mathbf{v} \mathbb{I} + \frac{\varepsilon}{2} |\nabla c|^2 \mathbb{I} - \varepsilon (\nabla c \otimes \nabla c),$$

and the fluid pressure is modeled by the isentropic law

$$p(\rho) = \rho^{\gamma}.$$

Here, $\delta > 0$ represents the squared Mach number, $\mathbf{g}$ the gravitational acceleration, and the chemical potential is defined as

$$\mu = c^3 - c - \frac{\varepsilon}{\rho}\Delta c.$$

2 Numerical Challenges

Solving numerically this system poses significant challenges [1, 3]. The presence of fourth-order diffusion terms in the Cahn-Hilliard type equations and the stiffness induced by fast pressure waves, particularly when δ tends to zero, lead to stability constraints [1]. In addition, standard schemes become highly expensive since requeries small time steps,

$$\Delta t = O(\delta \Delta x),$$

where Δx is the step size.

3 Proposed Strategy

To address these difficulties, the goal is to design an asymptotic preserving method, that is, a scheme whose stability and accuracy is independent of the Mach number, and which converges to a consistent discretization of the model when $\delta \to 0$. Therefore, we employ an IMEX strategy which splits the governing equations into stiff and non-stiff components. The stiff terms, arising from pressure and fourth-order Cahn-Hilliard contributions, are treated implicitly, while the remaining are dealt explicitly. In addition, our method is based on MAC staggered meshes for providing symmetric schemes [2].

Acknowledgements This work has been supported by the research projects PID2023-146836NB-I00, granted by MCIN/ AEI /10.13039/501100011033, and CIAICO/2021/227, granted by GVA.

References

[1] P. Degond, M. Tang, *All speed scheme for the low Mach number limit of the isentropic Euler equations*, Commun. Comput. Phys. **10** (2011), 1–31.

[2] F. H. Harlow, J. E. Welch, *Numerical calculation of time-dependent viscous incompressible flow of fluid with free surface*, Phys. Fluids **8** (1965), 2182.

[3] P. Mulet, *Implicit-Explicit Schemes for Compressible Cahn–Hilliard–Navier–Stokes Equations*, J. Sci. Comput. **101** (2024), 36.

Book of abstracts of the 9th International Conference on
Advanced Computational Methods in ENgineering and Applied Mathematics
September, 15–19, 2025.

Filtered implicit second derivative time-stepping methods

Afsaneh Moradi[1]

e-mails: afsaneh.moradi@ovgu.de

Abstract

This work focuses on the construction and numerical analysis of novel time-filtered second-derivative methods for stiff equations. The proposed methods are developed by incorporating inexpensive pre-filtering and post-filtering steps into existing second-derivative schemes. We show that applying these filtering steps to second-derivative multistep or multi-stage methods results in new methods that combine features of both multistep and multi-stage approaches, referred to as second-derivative general linear methods (SGLMs). The well-established properties of SGLMs are utilized to analyze the accuracy and stability of the filtered methods and to design optimal new filters for time-stepping schemes. Several new embedded families of high-accuracy methods with low cognitive complexity and excellent stability characteristics are introduced. Finally, numerical experiments validate the stability and efficiency of the proposed methods.

Key words: second-derivative methods, time-filtering, high-order accuracy, stability analysis

1 Introduction

It is well-known that implementing and validating new high-order methods requires substantial effort and often necessitates major modifications to existing frameworks. To address this challenge, filtering algorithms have gained popularity in recent years as a means to develop high-order time-stepping methods with favorable stability properties that can be derived with minimal modifications. As a non-intrusive technique capable of pre- and post-processing computed values, first-derivative time filters have recently been proposed to enhance numerical accuracy [1]. The work in [1] leveraged the well-established properties of general linear methods (GLMs) to analyze the accuracy and stability of filtered methods. This understanding was also employed to design optimal new filters for widely-used first-derivative time-stepping methods, such as the fully implicit Euler method, the midpoint rule, and the backward differentiation formula (BDF) method.

Despite the success of these first-derivative time filters, a rigorous stability and convergence analysis for time-filtered second-derivative methods remains absent. Second derivative methods, which incorporate not only the first derivative $y'(t)$ but also the second time derivative $\dot{f} := y''(t) = f_y(y)f(y)$, have been effectively used in constructing A-stable high-order methods [2].

As a motivating example, consider the fully implicit second-order Taylor method (ITM) applied to the stiff ODE $y'(t) = f(y(t))$:

$$u_{n+1} = u_n + \Delta t f(u_{n+1}) - \frac{1}{2}\Delta t^2 \dot{f}(u_{n+1}),$$

where $n = 1, 2, \ldots, N$, $N\Delta t = T - t_0$, and Δt is the timestep. Here, u_n represents the approximation of the solution at time t_n. By adding a few extra lines of code, we obtain the following new scheme:

$$\text{ITM solver:} \quad u_{n+1} = u_n + \Delta t f(u_{n+1}) - \frac{1}{2}\Delta t^2 \dot{f}(u_{n+1}), \tag{1a}$$

$$\text{Post-filter:} \quad u_{n+1}^{\text{3rd}} = -\frac{1}{7}u_{n-1} + \frac{8}{7}u_n + \frac{6}{7}\Delta t f(u_{n+1}) - \frac{2}{7}\Delta t^2 \dot{f}(u_{n+1}). \tag{1b}$$

This new method achieves third-order accuracy and is A-stable.

Writing the methods obtained from pre- and post-filtering in the form of SGLMs enables the use of established order conditions and stability theory to optimize these methods. SGLMs provide a general representation for any combination of k-step and s-stage second-derivative methods

$$\begin{aligned} y^{(i)} = &\sum_{l=1}^{k} d_{il} u_{n-k+l} + \Delta t \left(\sum_{l=1}^{k-1} \widehat{a}_{il} f(u_{n-k+l}) + \sum_{j=1}^{s} a_{ij} f(y^{(j)}) \right) \\ &+ \Delta t^2 \left(\sum_{l=1}^{k-1} \widehat{\overline{a}}_{il} \dot{f}(u_{n-k+l}) + \sum_{j=1}^{s} \overline{a}_{ij} \dot{f}(y^{(j)}) \right), \quad 1 \le i \le s \end{aligned} \tag{2a}$$

$$\begin{aligned} u_{n+1} = &\sum_{l=1}^{k} \theta_l u_{n-k+l} + \Delta t \left(\sum_{l=1}^{k-1} \widehat{b}_l f(u_{n-k+l}) + \sum_{j=1}^{s} b_j f(y^{(j)}) \right) \\ &+ \Delta t^2 \left(\sum_{l=1}^{k-1} \widehat{\overline{b}}_l \dot{f}(u_{n-k+l}) + \sum_{j=1}^{s} \overline{b}_j \dot{f}(y^{(j)}) \right), \end{aligned} \tag{2b}$$

where u_{n-k+l} refers to approximate solutions at previous and current steps, while $y^{(i)}$ denotes intermediate stages used to compute the next solution value u_{n+1}. The method (1) takes the form of (2) with $k = 2$ and $s = 1$

$$\begin{gathered} d_{11} = 0, \quad d_{12} = 1, \quad a_{11} = 1, \quad \overline{a}_{11} = -\frac{1}{2}, \quad \widehat{a}_{11} = \widehat{\overline{a}}_{11} = 0, \\ \theta_1 = -\frac{1}{7}, \quad \theta_2 = \frac{8}{7}, \quad b_1 = \frac{6}{7}, \quad \overline{b}_1 = -\frac{2}{7}, \quad \widehat{b}_1 = \widehat{\overline{b}}_1 = 0. \end{gathered}$$

References

[1] V. DeCaria, S. Gottlieb, Z.J. Grant, W. Layton, *A general linear method approach to the design and optimization of efficient, accurate, and easily implemented time-stepping methods in CFD*, J. Comput. Phys. **455** 110927 (2022)

[2] J. Schütz, D.C. Seal, J. Zeifang, *Parallel-in-time high-order multiderivative IMEX solvers*, J. Sci. Comput. **90** 54 (2022).

Book of abstracts of the 9th International Conference on
Advanced Computational Methods in ENgineering and Applied Mathematics
September, 15–19, 2025.

Well-balanced second-order compact implicit numerical scheme for hyperbolic balance laws

Carlos Parés[1], Michal Žeravý[2] and Peter Frolkovič[2]

[1] *Department of Mathematical Analysis, Statistics and O.R., Applied Mathematics, University of Málaga*

[2] *Department of Mathematics and Descriptive Geometry, Slovak University of Technology in Bratislava*

e-mails: pares@uma.es, zeravymichal@gmail.com, peter.frolkovic@stuba.sk

Abstract

In this work, we present a second-order well-balanced implicit scheme to solve numerically hyperbolic systems of balance laws [1]. The scheme has a compact stencil which allows an efficient application of fast algebraic solvers like fast sweeping methods. The methods are well-balanced in the sense that they preserve exactly all the continuous stationary solutions in the one-dimensional case whenever local equilibria can be obtained analytically and they are able to preserve a family of given stationary solutions in the two-dimensional case. The method is applied to the shallow water equations in 1D and 2D: several numerical experiments confirm the properties of the proposed scheme.

Key words: Hyperbolic PDE systems, systems of balance laws, implicit methods, well-balanced methods, shallow-water equations

1 Introduction

Fully implicit time-discretization of hyperbolic systems can significantly reduce restrictions on the choice of time steps in numerical methods. The price to be paid may be the resolution of large fully coupled nonlinear algebraic systems to update the numerical solution. Therefore, several efforts have been done recently to reduce the complexity of such algebraic systems. Here, we focus on systems of balance laws:

$$\partial_t \mathbf{q} + \partial_x \mathbf{F}(\mathbf{q}) = \mathbf{S}(\mathbf{q})\partial_x H\,, \quad \mathbf{q}(x,0) = \mathbf{q}^0(x)\,, \quad x \in \Omega \subset \mathcal{R}\,, \quad t > 0\,, \tag{1}$$

where $\mathbf{q} = \mathbf{q}(x,t)$ is a vector of unknown functions with prescribed values at $t = 0$ by the given initial condition $\mathbf{q}^0$; $\mathbf{F}$=$\mathbf{F}(\mathbf{q})$ is the flux vector function; $\mathbf{S}$=$\mathbf{S}(\mathbf{q})$ is the source vector function; and $H = H(x)$ is a given smooth function. We assume that the Jacobian matrix $\frac{d\mathbf{F}}{dq}(\mathbf{q})$ of the flux vector function $\mathbf{F}(\mathbf{q})$ has m distinct real eigenvalues $\lambda^p(\mathbf{q})$, $p = 1, 2, \ldots, m$.

The 1d shallow-waters equation is the particular case corresponding to $m = 2$ and

$$\mathbf{q} = \begin{bmatrix} h \\ hu \end{bmatrix} = \begin{bmatrix} h \\ q \end{bmatrix}, \; \mathbf{F}(\mathbf{q}) = \begin{bmatrix} hu \\ hu^2 + \frac{1}{2}gh^2 \end{bmatrix} = \begin{bmatrix} q \\ \frac{q^2}{h} + \frac{1}{2}gh^2 \end{bmatrix}, \; \mathbf{S}(\mathbf{q}) = \begin{bmatrix} 0 \\ -gh \end{bmatrix}, \tag{2}$$

where h represents the thickness of the water layer; u, the depth-averaged velocity; and $q = hu$, the discharge. The function $H(x)$ represents in this case the depth measured from a reference level.

The stationary solutions $h^*(x)$, $q^*(x)$ of this system are implicitly given by the following algebraic equations:

$$q^* = \tilde{q}, \tag{3}$$

$$\frac{\tilde{q}^2}{2g(h^*)^2} + h^* + H = \tilde{E}, \tag{4}$$

where $\tilde{q}$ is a constant discharge and $\tilde{E}$ is a constant.

2 Second-order well-balanced methods

In order to derive the numerical method, first the scheme derived in [2] for systems of conservation laws is extended to systems of balance laws. A fractional time step method is used together with the Lax-Friedrichs splitting

$$\mathbf{F}^{\pm}(\mathbf{q}) = \frac{1}{2}(\mathbf{F}(\mathbf{q}) \pm \alpha \mathbf{q}), \tag{5}$$

where the constant parameter α is set as the maximal absolute value of the eigenvalues of the Jacobian matrix. A splitting $\mathbf{S} = \mathbf{S}^+ + \mathbf{S}^-$ is also required: we consider here the simplest choice $\mathbf{S}^{\pm} = \frac{1}{2}\mathbf{S}$. The scheme is formally second-order accurate in time and space, but space and time limiters are added to avoid unphysical oscillations in numerical solutions. The method produces nonlinear algebraic equations whose size is analogous to the first-order accurate fully implicit scheme.

The procedure for making the scheme well-balanced is based on the one described in [3]. The idea is to subtract from the scheme an adequate discretization of the equations satisfied by the stationary solutions. The resulting method preserves all the continuous stationary solutions given by (3)-(4).

Finally, an extension of the method to 2D problems is presented that is well-balanced in the sense that it preserves a family of given stationary solutions. Several numerical experiments confirm these properties of the proposed scheme.

Acknowledgements

The work of the 1st author is partially supported by grants PID2022-137637NB-C21 and PID2022-137637NB-C22 funded by MCIN/AEI/10.13039/501100011033 and by "ERDF A way of making Europe". The work of the 2nd and 3rd author is supported by the grant VEGA 1/0314/23.

References

[1] M. Žeravý, P. Frolkovič, C. Parés, *Well-balanced high-resolution compact implicit numerical scheme for hyperbolic balance laws*, submitted (2025).

[2] P. Frolkovič, M. Žeravý, *High resolution compact implicit numerical scheme for conservation laws*, App. Math. Comp.**442** (2023), 127720.

[3] C. Parés, C. Parés-Pulido, *Well-balanced high-order finite difference methods for systems of balance laws*, J. Comp. Phys.**425** (2021),109880.

Book of abstracts of the 9th International Conference on
Advanced Computational Methods in ENgineering and Applied Mathematics
September, 15–19, 2025.

Implicit Compact Approximate Taylor schemes

Arjun Thenery Manikantan[1] and Jochen Schütz[1]

[1] *Faculty of Sciences & Data Science Institute, Hasselt University*

e-mails: arjun.thenerymanikantan@uhasselt.be, jochen.schuetz@uhasselt.be

Abstract

We present the implicit Compact Approximate Taylor (implicit CAT) designed for stable numerical solutions of hyperbolic partial differential equations. The schemes are extensions of the explicit CAT schemes by Carrillo and Pares (J Sci Comput 80, 1832–1866 (2019)) to an implicit framework. This talk will analyze these schemes for linear hyperbolic equations, presenting rigorous stability results. We will discuss the extensions to implicit multi-derivative Runge-Kutta methods.

Key words: compact approximate Taylor, implicit,Lax-Wendroff, hyperbolic equations
MSC 2020: 65M12, 65M22

1 Introduction

Higher-order numerical schemes are of great interest when solving partial differential equations that require finely resolved solutions. Therefore, a wise combination of a high-order time integration scheme and a higher-order spatial discretization is the key to achieving it. Consider the conservation equation

$$u_t + f(u)_x = 0. \tag{1}$$

The most established scheme for solving (1) utilize the first derivative (u_t) to develop the numerical schemes for solving Eq. (1). However, there is quite a big class of schemes utilizing multiple derivatives ($u_t, u_{tt}, u_{ttt}, \ldots$) of equation (1) to construct higher-order numerical schemes. The temporal derivatives of Eq. (1) are expressed in terms of the fluxes through a so-called Lax-Wendroff procedure, being in fact motivated through the Cauchy–Kowalevskaya procedure

$$u_t = -f(u)_x, \quad u_{tt} = (-f(u)_x)_t = (-f(u)_t)_x = (f'(u)f(u)_x)_x\,;$$

higher derivatives can be found recursively. However, implementing them directly in their exact form is cumbersome as we include more temporal derivatives in the schemes, in particular for higher dimensions. Therefore, one of the possible ways is to use the approximations of the higher derivatives rather than their exact forms [1, 2].

In [2] a high-order method for solving conservation equations is termed the compact approximate Taylor (CAT). CAT uses a $2p+1$ compact stencil to achieve a $2p$−th order of accuracy. When applied to the linear equation ($f(u) = au$), the schemes reduce to the actual Lax-Wendroff scheme. Hence, the CAT scheme possesses the same stability properties as the Lax-Wendroff schemes. It was combined with flux-limiter and weighted essentially

non-oscillatory (WENO) scheme to mitigate spurious oscillations that can occur near discontinuities. The CAT scheme was further extended with Fast and Optimized WENO schemes in [4], for a system of balance laws in [7], and with an order-adaptive strategy in [5]. In [9], a semi-implicit CAT scheme was devised treating the source term implicitly. Incorporating intermediate stages, the idea of CAT was utilized to construct the explicit Jacobian-free multi-derivative Runge–Kutta (MDRK) schemes in [6].

However, explicit schemes have limited stability regions. A significant drawback of explicit methods when applied to singularly perturbed equations is the necessity for extremely small time steps to maintain numerical stability. Therefore, developing an implicit CAT is a possible way to mitigate timestep restrictions. There are approximate implicit Taylor [3] and implicit MDRK [8] schemes developed for solving ODEs. We utilize the ideas implemented in [3, 8] and aim at developing an unconditionally stable implicit CAT type method for conservation laws. As a foundation, we will perform a thorough stability analysis of the implicit CAT schemes on simple linear equations to understand the origins of potential stability problems. Later, the schemes will be extended to implicit MDRK methods for hyperbolic problems.

References

[1] D. Zorío, A. Baeza, and P. Mulet, "An Approximate Lax–Wendroff-Type Procedure for High Order Accurate Schemes for Hyperbolic Conservation Laws," *Journal of Scientific Computing*, vol. 71, pp. 246–273, 2017.

[2] H. Carrillo and C. Parés, "Compact approximate Taylor methods for systems of conservation laws," *Journal of Scientific Computing*, vol. 80, no. 3, pp. 1832–1866, 2019.

[3] A. Baeza, R. Bürger, M. del C. Martí, P. Mulet, and D. Zorío, "On approximate implicit Taylor methods for ordinary differential equations," *Computational and Applied Mathematics*, vol. 39, no. 4, p. 304, 2020.

[4] H. Carrillo, C. Parés, and D. Zorío, "Lax-Wendroff approximate Taylor methods with fast and optimized weighted essentially non-oscillatory reconstructions," *Journal of Scientific Computing*, vol. 86, no. 1, 2021.

[5] H. Carrillo, E. Macca, C. Parés, G. Russo, and D. Zorío, "An order-adaptive compact approximation Taylor method for systems of conservation laws," *Journal of Computational Physics*, vol. 438, p. 110358, 2021.

[6] J. Chouchoulis, J. Schütz, and J. Zeifang, "Jacobian-free explicit multiderivative Runge-Kutta methods for hyperbolic conservation laws," *Journal of Scientific Computing*, vol. 90, no. 96, 2022.

[7] H. Carrillo, E. Macca, C. Parés, and G. Russo, "Well-balanced adaptive compact approximate Taylor methods for systems of balance laws," *Journal of Computational Physics*, vol. 478, p. 111979, 2023.

[8] J. Chouchoulis and J. Schütz, "Jacobian-free implicit MDRK methods for stiff systems of ODEs," *Applied Numerical Mathematics*, vol. 196, pp. 45–61, 2024.

[9] E. Macca and S. Boscarino, "Semi-implicit-Type Order-Adaptive CAT2 Schemes for Systems of Balance Laws with Relaxed Source Term," *Communications on Applied Mathematics and Computation*, vol. 7, no. 1, pp. 151–178, 2025.

Book of abstracts of the 9th International Conference on
Advanced Computational Methods in ENgineering and Applied Mathematics
September, 15–19, 2025.

Unified numerical analysis for thermoelastic diffusion and thermo-poroelasticity of thin plates

Aamir Yousuf[1], Neela Nataraj[1] and Ricardo Ruiz-Baier[2]

[1] *Department of Mathematics, Indian Institute of Technology Bombay, India*

[2] *School of Mathematics, Monash University, Australia*

e-mails: aamir72@iitb.ac.in, neela@math.iitb.ac.in,
ricardo.ruizbaier@monash.edu

Abstract

We investigate a coupled hyperbolic-parabolic system modeling thermoelastic diffusion (resp. thermo-poroelasticity) in plates, consisting of a fourth-order hyperbolic partial differential equation for plate deflection and two second-order parabolic partial differential equations for the first moments of temperature and chemical potential (resp. pore pressure). The unique solvability of the system is established via Galerkin approach, and the additional regularity of the solution is obtained under appropriately strengthened data. For numerical approximation, we employ the Newmark method for time discretization of the hyperbolic term and a continuous interior penalty scheme for the spatial discretization of displacement. For the parabolic equations that represent the first moments of temperature and chemical potential (resp. pore pressure), we use the Crank–Nicolson method for time discretization and conforming finite elements for spatial discretization. The convergence of the fully discrete scheme with quasi-optimal rates in space and time is established. The numerical experiments demonstrate the effectiveness of the 2D Kirchhoff–Love plate model in capturing thermoelastic diffusion and thermo-poroelastic behavior in specific materials. We illustrate that as plate thickness decreases, the two-dimensional simulations closely approximate the results of three-dimensional problem. Finally, the numerical experiments also validate the theoretical rates of convergence.

Key words: thermoelastic diffusion, thermo-poroelasticity, Kirchhoff–Love.

1 Introduction

The authors in [1] formulated a model from the 3D for Thermoelastic diffusion in thin plates, under the assumption that body forces, external loads, and sources of heat and diffusion are absent. This model is based on the 2D Kirchhoff–Love hypotheses for thin plates, with classical Fourier's law for heat conduction and Fick's law for diffusion. An enhanced *novel* model considered in this article for Thermoelastic diffusion and Thermo-poroelasticity that include external loads f, heat source ϕ, and mass diffusion g and is presented as follows: the coupled

model aims to determine mid-surface deflection u, first moments of temperature θ and chemical potential (resp. pore pressure) p such that

$$u_{tt} - a_0\Delta u_{tt} + d_0\Delta^2 u + \alpha\Delta\theta + \beta\Delta p = f(\mathbf{x},t) \quad \text{in } \Omega\times(0,T], \tag{1a}$$
$$a_1\theta_t - \gamma p_t + b_1\theta - c_1\Delta\theta - \alpha\Delta u_t = \phi(\mathbf{x},t) \quad \text{in } \Omega\times(0,T], \tag{1b}$$
$$a_2 p_t - \gamma\theta_t - \kappa\Delta p - \beta\Delta u_t = g(\mathbf{x},t) \quad \text{in } \Omega\times(0,T], \tag{1c}$$
$$u = \partial_{\mathbf{n}} u = 0,\ \theta = 0,\ p = 0 \quad \text{on } \Gamma\times[0,T], \tag{1d}$$
$$u|_{t=0} = u^0,\ u_t|_{t=0} = u^{*0},\ \theta|_{t=0} = \theta^0,\ p|_{t=0} = p^0 \quad \text{in } \Omega, \tag{1e}$$

where $\mathbf{n}$ is the outward-pointing unit normal, $\partial_{\mathbf{n}} u = \nabla u\cdot\mathbf{n}$ is the outer normal derivative of u on $\partial\Omega$, u_t, θ_t, p_t (resp. u_{tt}) denote the first (resp. second)-order derivatives with respect to time.

We mention some key contributions of this work as: The present analysis is robust with respect to the coupling model parameter (between equation (1b) and (1c)) γ . Allowing γ to take values in $\mathbb{R}$ enables a unified analytical framework that accommodates both the thermoelastic diffusion and thermo-poroelastic thin plate models. The well-posedness of the fully coupled hyperbolic-parabolic thermoelastic diffusion and thermo-poroelastic systems is demonstrated under reasonable data regularity conditions. A consistent and stable fully discrete scheme is developed. Due to the coupling of second-order terms special care must be taken in the choice of compatible finite element spaces that plays a crucial role in the choice of the test functions in the proofs of stability and error estimates. Moreover, similar care is required when approximating coupling terms involving time derivatives of different orders. A novel concept of approximating the solution at the initial time step, while incorporating the approximation properties established is introduced to the literature, facilitating the development of a fully discrete scheme for general hyperbolic-parabolic coupled systems without any assumptions regarding the solution and its approximation at this time step. A priori error estimates are derived in the best approximation form in both L^2, H^1 and energy norm for displacement. These optimal error rates are also established in L^2 and H^1 norm for temperature and chemical potential/pore pressure. Also, the combination of Newmark–Crank–Nicolson time discretization schemes to approximate the second and first-order time derivatives, respectively yield quadratic convergence rates. The superconvergence of the projected error in the energy norm is established, in turn leading to lower H^s- order estimates with $s = 0, 1$ (resp. $s = 0$) for displacement u (resp. temperature θ and chemical potential/pore pressure p). While such superconvergence is expected in uncoupled problems, it is not straightforward in the current coupled problem since the polynomial degrees of the finite element spaces. This work also demonstrates that the Kirchhoff–Love plate model is effective in capturing Thermoelastic diffusion and Thermo-poroelastic behavior in specific materials (such as copper and flat layers of Berea sandstone, respectively). The findings indicate that as the plate thickness decreases, the two-dimensional simulations closely approximate the results from three-dimensional modeling, with a substantial reduction in computational time. This emphasises the efficiency and accuracy of 2D modeling for thin-plate structures. Numerical results are provided to validate theoretical estimates and illustrate the effective performance of the proposed scheme with different values of γ.

References

[1] Aouadi, M, *On thermoelastic diffusion thin plate theory*, Applied Mathematics and Mechanics, Springer, 2015.

MS5: Nonlinear Acoustic Waves: Modeling, Analysis, and Numerics

Organiser: Barbara Kaltenbacher (University of Klagenfurt) and Vanja Nikolić (Radboud University)

Description: The research on nonlinear acoustics has mainly been driven by numerous developing applications of ultrasound waves, including imaging, non-invasive therapy, and targeted drug delivery. In recent years, significant advances have been made in the mathematical aspects of nonlinear acoustics, and new, challenging open questions have been raised in the areas of accurate modeling, rigorous analysis, and efficient simulation. This minisymposium aims to bring together researchers working on this topic to encourage novel ideas, trends, and cooperation in this field.

Book of abstracts of the 9th International Conference on
Advanced Computational Methods in ENgineering and Applied Mathematics
September, 15–19, 2025.

Numerical algorithms for the 2D wave equation in heterogeneous media

Arshyn Altybay[1,2], Michael Ruzhansky[1,3], Mohammed Elamine Sebih[4] and Niyaz Tokmagambetov[2]

[1] *Department of Mathematics: Analysis, Logic and Discrete Mathematics, Ghent University, Belgium*

[2] *Institute of Mathematics and Mathematical Modeling, 125 Pushkin str., 050010 Almaty, Kazakhstan*

[3] *School of Mathematical Sciences, Queen Mary University of London, United Kingdom*

[4] *Laboratory of Geomatics, Ecology and Environment (LGEO2E), Mustapha Stambouli University of Mascara, 29000 Mascara, Algeria*

e-mails: arshyn.altybay@ugent.be, arshyn.altybay@gmail.com, michael.ruzhansky@ugent.be, m.ruzhansky@qmul.ac.uk, sebihmed@gmail.com, ma.sebih@univ-mascara.dz, tokmagambetov@math.kz

Abstract

In this study, we consider numerical simulations for the 2D wave equation in heterogeneous media. After establishing the theoretical well-posedness of the problem and deriving a priori estimates for both low and high regularity cases -thereby guaranteeing uniqueness and continuous dependence on the given data - we proceed to develop and analyse three numerical methods: a Finite Difference Method (FDM), a Finite Element Method (FEM), and a Physics-Informed Neural Network (PINN) approach. Numerical examples are presented to discuss the different techniques and support our findings. We then perform a comparative analysis of the three approaches to gain a deeper understanding of the respective advantages and limitations of each method in the numerical simulation of wave equations.

We consider the following wave equation„ which is of great importance in science and engineering.

$$\begin{cases} u_{tt}(t,x) - \sum_{j=1}^{d} \partial_{x_j} \left(h_j(x) \partial_{x_j} u(t,x) \right) = f(t,x), \quad (t,x) \in [0,T] \times \mathbb{R}^d, \\ u(0,x) = u_0(x), \quad u_t(0,x) = u_1(x), \quad x \in \mathbb{R}^d. \end{cases} \tag{1}$$

Here, the variation in coefficient h affects how the wave propagates through different medium regions. This can represent a medium with varying density, elasticity, underwater topography, bathymetry, or other properties. Equations of this type are widely used in various fields such as acoustics, seismology, medical imaging, oceanography, geophysics and other wave propagation phenomena, especially in cases where the environment has spatially varying characteristics.

Key words: wave equation, heterogeneous media, finite difference scheme, finite element method, PINN, numerical simulation

MSC 2020: 35L81, 35L05, 35D30, 35A35

Book of abstracts of the 9th International Conference on
Advanced Computational Methods in ENgineering and Applied Mathematics
September, 15–19, 2025.

Robust fully discrete error bounds for the Kuznetsov equation in the inviscid limit

Benjamin Dörich[1] **and Vanja Nikolić**[2]

[1] *Institute for Applied and Numerical Mathematics, Karlsruhe Institute of Technology, Germany*

[2] *Department of Mathematics, Radboud University, The Netherlands*

e-mails: benjamin.doerich@kit.edu, vanja.nikolic@ru.nl

Abstract

The Kuznetsov equation is a classical wave model of nonlinear acoustics that incorporates quadratic gradient nonlinearities. When its strong damping vanishes, it undergoes a singular behavior change, switching from a parabolic-like to a hyperbolic quasilinear evolution. In this talk, we discuss its finite element discretization as well as a semi-implicit fully discrete approximation that are robust with respect to the vanishing damping parameter and further include numerical examples which confirm our theoretical findings.

Key words: asymptotic-preserving error estimates, full discretization, Kuznetsov equation, nonlinear acoustics

1 Introduction

We consider the Kuznetsov equation on a bounded domain $\Omega \subset \mathbb{R}^d$, $d = 2, 3$,

$$(1 + \kappa \partial_t u)\partial_t^2 u - c^2 \Delta u - \beta \Delta \partial_t u + \ell \nabla u \cdot \nabla \partial_t u = f, \tag{1}$$

equipped with homogeneous Dirichlet boundary conditions and initial values. In the context of nonlinear acoustics, the function u represents the acoustic velocity potential, $c > 0$ denotes the speed of sound in the medium, and the damping parameter β is the sound diffusivity. The most interesting part in this equation is the already mentioned gradient nonlinearity as it is of the same order as the leading order terms, but does not have a sign. Hence, it cannot be treated by standard perturbation theory for lower order terms.

2 Robust space and time discretization

Setting all parameters (except β) to 1, we discretize in space by Lagrange finite elements V_h on a quasi-uniform triangulation with piecewise polynomials of degree k. We denote by $(\cdot, \cdot)$ the L^2-inner product and seek for a finite element solution $u_h \in C^2([0, T], V_h)$ such that

$$((1 + \partial_t u_h)\partial_t^2 u_h, \varphi_h) + (\nabla u_h, \nabla \varphi_h) + \beta(\nabla \partial_t u_h, \nabla \varphi_h) + (\nabla u_h \cdot \nabla \partial_t u_h, \nabla \varphi_h) = (f_h, \varphi_h),$$

holds for all $\varphi_h \in V_h$. We further discretize in time with step-size τ using a semi-implicit Euler method employing the discrete derivative ∂_τ defined by $\partial_\tau a^n = \frac{1}{\tau}(a^n - a^{n-1})$, and solve for u_h^{n+1}, $1 \le n \le N$, the linear system

$$((1 + \partial_\tau u_h^n)\partial_\tau^2 u_h^{n+1}, \varphi_h) + (\nabla u_h^{n+1}, \nabla \varphi_h) + \beta(\nabla \partial_\tau u_h^{n+1}, \nabla \varphi_h) + (\nabla u_h^n \cdot \nabla \partial_\tau u_h^{n+1}, \varphi_h) = (f_h^{n+1}, \varphi_h),$$

with appropriately chosen initial data u_h^0, u_h^1. Assuming that our solution is sufficiently smooth and that $\|f - f_h\|_{C^1(L^2)} \lesssim h^k$ holds, we can prove the following error bounds for h and τ sufficiently small, where discrete analogous to Sobolev's embedding, and a discrete version of the identity $(\nabla u \cdot \nabla \partial_t^2 u, \partial_t^2 u) = -\frac{1}{2}(\Delta u\, \partial_t^2 u, \partial_t^2 u)$ play a crucial role in the proofs.

Theorem *(a) For $k \ge 2$ and all $t \in [0, T]$ there is a constant independent of h and β such that*

$$\|\partial_t^2 u(t) - \partial_t^2 u_h(t)\|^2 + \|\nabla \partial_t u(t) - \nabla \partial_t u_h(t)\|^2 + \int_0^t \|\nabla u(s) - \nabla u_h(s)\|_{L^6}^2 \, \mathrm{d}s \lesssim h^{2k}.$$

(b) For some $\varepsilon > 0$ let $\tau \lesssim h^{1+d/6+\varepsilon}$, then it holds for $k \ge 2$

$$\|\partial_t^2 u(t_n) - \partial_\tau^2 u_h^n\|^2 + \|\nabla \partial_t u(t_n) - \nabla \partial_\tau u_h^n\|^2 + \tau \sum_{j=1}^n \|\nabla u(t_j) - \nabla u_h^j\|_{L^6}^2 \lesssim \left(\tau + h^k\right)^2,$$

with $n = 1, \dots, N+1$ and a constant that is independent of h, τ, and β.

Further, we can quantify the behavior of the numerical solutions in the limit $\beta \to 0$ and denote by u^β the solution of (1) for a fixed parameter $\beta > 0$ and by $u^{\beta=0}$ for $\beta = 0$. Motivated from the linear convergence

$$\|\partial_t u^\beta(t) - \partial_t u^{\beta=0}(t)\| + \|\nabla(u^\beta(t) - u^{\beta=0}(t))\| \le C\beta,$$

established in [2, Theorem 5.1], we consider the family $\{u_h^\beta\}_{\beta \in (0,\bar\beta]}$ of semi-discrete solutions and the family $\{u_{h,\beta}^n\}_{\beta \in (0,\bar\beta]}$ of fully discrete solutions. We prove the following discrete analogue under the conditions of the above theorem, i.e., for the spatially discrete problem we have

$$\|\partial_t u_h^\beta(t) - \partial_t u_h^{\beta=0}(t)\| + \|\nabla(u_h^\beta(t) - u_h^{\beta=0}(t))\| \le C\beta,$$

with $C > 0$ independent of β and h, as well as for the fully discrete problem

$$\|\partial_\tau u_{h,\beta}^n - \partial_\tau u_{h,\beta=0}^n\|_{L^2} + \|\nabla(u_{h,\beta}^n - u_{h,\beta=0}^n)\|_{L^2} \le C\beta,$$

for all $n = 1, \dots, N+1$, with $C > 0$ independent of β, h, and τ.

Acknowledgements Funded by the Deutsche Forschungsgemeinschaft (DFG, German Research Foundation) – Project-ID 258734477 – SFB 1173.

References

[1] B. Dörich and V. Nikolić, Robust fully discrete error bounds for the Kuznetsov equations in the inviscid limit. CRC 1173 Preprint 2024/1, Karlsruhe Institute of Technology, 2024.

[2] B. Kaltenbacher and V. Nikolić. Parabolic approximation of quasilinear wave equations with applications in nonlinear acoustics. *SIAM J. Math. Anal.*, 54(2):1593–1622, 2022.

Book of abstracts of the 9th International Conference on
Advanced Computational Methods in ENgineering and Applied Mathematics
September, 15–19, 2025.

A p-adaptive space-time discontinuous Galerkin method for nonlinear acoustics

Pascal Lehner[1], Christian Wieners[2] and Danielle Corallo[2]

[1] *Department of Mathematics, University of Klagenfurt; Universitätsstraße 65-67 , 9020 Klagenfurt, Austria*

[2] *Department of Mathematics, Karlsruhe Institute of Technology; Kaiserstr. 89-93, 76133 Karlsruhe, Germany*

e-mails: pascal.lehner@aau.at, christian.wieners@kit.edu, daniele.corallo@kit.edu

Abstract

In this talk we introduce a space-time discontinuous Galerkin method for a first-order-in-time nonlinear wave equation modeling nonlinear acoustics. The continuous system is derived in [1], where also its well-posedness is shown in suitable Sobolev spaces.

The discrete system presented here is based on a space-time method for symmetric Friedrichs systems, see [2]. To show its well-posedness we show coercivity of a linearized system and then apply an existence result for Newton's method. Convergence results with respect to a suitable norm are also discussed.

Key words: nonlinear acoustics, finite elements, space-time method, discontinuous Galerkin method, p-adaptive

1 Introduction

Many classical models of nonlinear acoustic, such as Westervelt's and Kuznetsov's equation, involve second-order time derivatives that appear in nonlinear terms. An alternative first-order-in-time model with nonlinearities restricted to spatial derivatives has been proposed and analyzed in [1]. The model is governed by parameters satisfying

$$\alpha,\ \beta,\ \gamma,\ \delta,\ \varepsilon,\ \zeta,\ \eta,\ \vartheta > 0,\ \gamma \neq \delta,$$

and takes the form

$$\begin{aligned} \alpha\partial_t p + \nabla\cdot\mathbf{v} - \beta\Delta p + \gamma p\nabla\cdot\mathbf{v} + \delta\nabla p\cdot\mathbf{v} &= p_S \\ \varepsilon\partial_t\mathbf{v} + \nabla p - \zeta\Delta\mathbf{v} + \frac{1}{2}\nabla\left(\eta\mathbf{v}^2 - \vartheta p^2\right) &= \mathbf{v}_S \end{aligned} \tag{1}$$

with suitable initial, boundary conditions and source terms p_S, v_S. p denotes derivation of pressure and v derivation of the velocity field from a ground state.

In this talk, we propose and analyze a space-time discontinuous Galerkin (DG) method for this model. To the best of our knowledge, this is the first application of a space-time DG method to nonlinear acoustics. Space-time methods are particularly attractive due to their natural support for adaptive refinement, parallel implementation, and suitability for inverse problems.

2 Numerical analysis

The proposed DG method for a suitable discontinuous space-time polynomial space Z_h is:

$$\text{Solve for } u_h \in Z_h \text{ such that } b_h(u_h, z_h) = \ell_h(z_h) \text{ for all } z_h \in Z_h \tag{2}$$

with

$$b_h(u_h, z_h) := m_h(u_h, z_h) + a_h(u_h, z_h) + d_h(u_h, z_h) + n_h(u_h, z_h)$$

and a suitable right hand side ℓ_h reflecting the boundary conditions. Here m_h stands for a space-time discretiation of the time derivatives, a_h for the of the linear wave operator $(\nabla, \nabla\cdot)$ as done in space-time methods for symetric Friedrich systems [2]. d_h stands for the discretization of the Laplacian terms with an interior penalty method, and n_h for the nonlinear terms.

The analysis is carried out with respect to the h-dependent norm

$$\|u_h\|_{Z_h} := \left(\frac{1}{2} \sum_{j=0}^{k} \|M^{\frac{1}{2}} [u_h]_j\|^2_{L^2(\Omega_h)} + \int_0^T c_A \|A_{\mathbf{n}} [u_h]\|^2_{L^2(\partial\Omega_h)} + c_\Theta |\!|\!| u_h |\!|\!|^2_h \, dt \right)^{\frac{1}{2}},$$

where Ω_h is the discrete space domain, $c_A, c_\theta > 0$, M, A_n are suitable matrices, $[\cdot]$ denotes a jump in space, $[\cdot]_j$ denotes a jump in time at timestep j, k is the number of time steps, and $|\!|\!| \cdot |\!|\!|_h$ is the usual norm of the broken Sobolev space $H^1(\Omega_h)$. After showing well-posedness of a linearized system by means of standard methods, using a generalized Newton-Kantorvich argument, one can show the following well-posedness and convergence result for (2) .

Theorem *Let $u = (p, v) \in U$ be a regular enough solution to the continuous system (1) and assume that $\|u\|_U, \|\ell_h\|_{Z_h'}$ are sufficiently small. Let $\chi \in (0, 1)$ and $\xi > 0$ be determined by space-time mesh and approximation space properties. For $\bar{h} > 0$ define*

$$D_{\bar{h},*} := \{u_h \in Z_h : \|u_h - u\|_{Z_h} < C_* h^\xi\}$$

with $C_* > 0$ independent of $\bar{h}$. Then, there exists a $\tilde{h} < \bar{h}$ such that for all $h < \tilde{h}$ (2) has a unique solution $u_h \in Z_h$ and $(1 + \chi)$-order of convergence in Newton's method with initial guess $u_{h,*} \in D_{h,*}$ holds. In particular, we have the following error estimate

$$\|u_h - u\|_{Z_h} \leq C_* h^\xi.$$

Acknowledgements Pascal Lehner is supported by the Austrian Science Fund (FWF) [10.55776/P36318].

References

[1] B. Kaltenbacher, P. Lehner, *A first order in time wave equation modeling nonlinear acoustics,* Journal of Mathematical Analysis and Applications, 543(2, Part 2):128933, 2025.

[2] D. Corallo, W. Dörfler, C. Wieners, *Space-Time Discontinuous Galerkin Methods for Weak Solutions of Hyperbolic Linear Symmetric Friedrichs Systems,* J Sci Comput, 94(1):27, 2022.

Book of abstracts of the 9th International Conference on
Advanced Computational Methods in ENgineering and Applied Mathematics
September, 15–19, 2025.

On the existence of strong solutions to a heat-conducting fluid system with general Dirichlet boundary conditions

Mostafa Meliani[1]

[1] *Department of Evolution Differential Equations, Institute of Mathematics of the Academy of Sciences of the Czech Republic*

e-mails: meliani@math.cas.cz

Abstract

In our talk, we will discuss the local existence of solutions to the Navier–Stokes–Fourier (NSF) system describing the motion of a compressible, viscous, and heat conducting fluid in the L^p–L^q class with inhomogeneous boundary conditions. The open system is allowed to receive incoming matter from the outside through (part of) the boundary which we refer to as an inflow boundary. This setup brings about a difficulty in estimating the regularity of the density ϱ which we remedy by assuming appropriate hypotheses on the velocity field, domain boundary and on the boundary and initial data of ϱ. The main result ensures the local well-posedness of the full NSF system which is shown through a linearization combined with a Banach fixed-point theorem.

Key words: Navier–Stokes–Fourier system, initial-boundary value problem, strong solutions, local existence, conditional regularity
MSC 2020: 35Q30, 35Q35, 76N06, 76N10

1 Introduction

There exist by now a wide literature on the existence of strong solutions to equations of compressible isothermal and non-isothermal fluids:

$$\begin{aligned}
&\partial_t \varrho + \boldsymbol{u}\cdot\nabla_x\varrho = -\varrho \operatorname{div}_x \boldsymbol{u},\\
&\partial_t \boldsymbol{u} + \boldsymbol{u}\cdot\nabla_x\boldsymbol{u} = \frac{1}{\varrho}[\operatorname{div}_x(\mathbb{S}(\boldsymbol{u})) - \nabla_x\theta - \theta\nabla_x\log(\varrho) + \nabla_x G,\\
&\partial_t \theta + \boldsymbol{u}\cdot\nabla_x\theta - \frac{\kappa}{\varrho c_v}\Delta_x\theta = \frac{1}{\varrho c_v}\mathbb{S}(\boldsymbol{u}) : \mathbb{D}_x\boldsymbol{u} - \frac{\theta}{c_v}\operatorname{div}_x \boldsymbol{u}.
\end{aligned} \tag{1.1}$$

Above,

$$\mathbb{S}(\boldsymbol{u}) = \mu(2\mathbb{D}_x\boldsymbol{u} - \frac{2}{d}\operatorname{div}_x \boldsymbol{u}\mathbb{I}) + \lambda \operatorname{div}_x \boldsymbol{u}\mathbb{I},$$

where $\mu > 0$ is the shear viscosity coefficient, $\lambda \geq 0$, the bulk viscosity coefficient, $\mathbb{D}_x\boldsymbol{u} = \frac{1}{2}\nabla_x\boldsymbol{u} + \frac{1}{2}\nabla_x\boldsymbol{u}^t$ is the symmetrized gradient, and $\mathbb{I}$, the identity matrix in $\mathbb{R}^3$. Additionally, ϱ is the mass density, $\boldsymbol{u}$, the velocity, p, the pressure, and θ, the temperature. The coefficients κ and c_v are medium-dependent constant.

In recent years, study of open fluid systems has gained some traction (i.e., when $\boldsymbol{u}\cdot n|_{\partial\Omega}$ is not sign constrained). In particular, existence of weak solutions was established [1]. Nevertheless, strong solutions are more desirable for certain practical applications, e.g., numerical analysis, optimization or control.

In our work [2], we set to establish the existence of strong solutions on a C^2-regular bounded domain $\Omega \subset \mathbb{R}^d$ ($d \leq 3$) in the L^p-L^q class aided by the theoretical framework of Denk–Hieber–Prüss [3].

2 Problem data

On the velocity field we impose the inhomogeneous Dirichlet boundary conditions:

$$\boldsymbol{u}|_{\partial\Omega} = \boldsymbol{u}_B \quad \text{on } [0,T]\times\partial\Omega. \tag{2.1}$$

We define the inflow subset of $[0,T]\times\partial\Omega$ as

$$\Sigma_{\text{in}} = \{(t,x) \in [0,T]\times\partial\Omega \quad | \quad \boldsymbol{u}_B(t,x)\cdot n < 0\}.$$

To simplify the presentation, we assume that $\Sigma_{\text{in}} = [0,T]\times\Gamma_{\text{in}}$, i.e, we assume that the inflow boundary Γ_{in} is time-independent. We assume that there exist a constant $c > 0$ such that

$$-\boldsymbol{u}_B \cdot n \geq c > 0 \qquad \text{on } [0,T]\times\Gamma_{\text{in}}. \tag{2.2}$$

As is well-known, we need to prescribe the mass density on the inflow part of the boundary

$$\varrho = \varrho_B > 0 \quad \text{on } [0,T]\times\Gamma_{\text{in}}. \tag{2.3}$$

We also prescribe Dirichlet boundary conditions for the temperature field:

$$\theta = \theta_B > 0 \quad \text{on } [0,T]\times\partial\Omega. \tag{2.4}$$

We additionally impose initial data

$$\varrho(0) = \varrho_0, \qquad \boldsymbol{u}(0) = \boldsymbol{u}_0, \qquad \theta(0) = \theta_0, \tag{2.5}$$

to be chosen in suitable function spaces, which for $\boldsymbol{u}$ and θ is dictated by the framework of Denk–Hieber–Prüss [3].

3 Main Results

Our main result is contained in the following theorem.

Theorem 3.1 *Let $p,q \in (1,\infty)$, such that $q > d$ and $\max\{\frac{2q}{q-1}, \frac{2q}{2q-d}\} < p$). Under appropriate conditions on the boundary $\partial\Omega$ and regularity assumptions on the initial and boundary data, there exists a strictly positive final time $T_* > 0$ such that the system* (1.1) *supplemented with the boundary conditions* (2.1)–(2.4) *and the initial conditions* (2.5) *has a unique solution:*

$$(\varrho,\boldsymbol{u},\theta) \in L^\infty(0,T_*;W^{1,q}(\Omega)) \cap W^{1,\infty}(0,T_*;L^q(\Omega)) \times \left(L^p(0,T_*;W^{2,q}(\Omega)) \cap W^{1,p}(0,T_*;L^q(\Omega))\right)^2.$$

Acknowledgements This work was supported by the Czech Sciences Foundation (GAČR), Grant Agreement 24-11034S. The Institute of Mathematics of the Academy of Sciences of the Czech Republic is supported by RVO:67985840.

References

[1] E. Feireisl, A. Novotný, *Mathematical of Open Fluid Systems*, Birkäuser, 2022.

[2] M. Meliani, *L^p–L^q existence for the open compressible MHD system*, arXiv:2502.18164, 2025.

[3] R. Denk, M. Hieber, and J. Prüss, *Optimal L^p-L^q-estimates for parabolic boundary value problems with inhomogeneous data*, Mathematische zeitschrift **257(1)** (2007) 193–224.

Book of abstracts of the 9th International Conference on
Advanced Computational Methods in ENgineering and Applied Mathematics
September, 15–19, 2025.

Robust error bounds for a combined DG-CG finite element method for the Westervelt equation

Sergio Gómez[1] and Vanja Nikolić[2]

[1] *Department of Mathematics and Applications, University of Milano-Bicocca, Via Cozzi 55, 20125 Milan, Italy*

[2] *Department of Mathematics, Radboud University, Heyendaalseweg 135, 6525 AJ Nijmegen, The Netherlands*

e-mails: sergio.gomezmacias@unimib.it, vanja.nikolic@ru.nl

Abstract

It is well-known that classical strongly damped models of nonlinear acoustics undergo a a singular behavior change as the damping vanishes, switching from a parabolic-like to a hyperbolic quasilinear evolution [2]. In this talk, we will discuss the influence of strong damping on finite element discretizations of acoustic models. We will focus on a space–time finite element method for Westervelt's quasilinear model of ultrasound waves in second-order formulation. The method combines conforming finite element spatial discretizations with a discontinuous-continuous Galerkin time stepping. Its analysis is challenged by the fact that standard Galerkin testing approaches for wave problems do not allow for bounding the discrete energy at all times. By means of redesigned energy arguments for a linearized problem combined with Banach's fixed-point argument, we show the well-posedness of the scheme, a priori error estimates, and robustness with respect to the strong damping parameter. Moreover, the scheme preserves the asymptotic preserving property of the continuous problem in the singular vanishing dissipation limit. The presentation is based on [1].

Key words: asymptotic-preserving methods, discontinuous-continuous Galerkin time stepping, Westervelt's equation

MSC 2020: 65M50, 65M60, 35L70

1 Introduction

Westervelt's equation is a classical model of nonlinear acoustic and ultrasonic wave propagation. It is especially attractive for simulating medical and industrial applications of ultrasound as it does not assume any directionality of the wave field. In this talk, based on [1], we will discuss a space–time finite element approach for its discretization in the framework of the DG–CG scheme introduced in [3] that combines continuous and discontinuous Galerkin time stepping methodologies.

We consider a space–time cylinder $Q_T = \Omega \times (0, T)$, where $\Omega \subset \mathbb{R}^d$ ($d \in \{1, 2, 3\}$) is an open, bounded polytopic domain with Lipschitz boundary $\partial\Omega$, and $T > 0$ is the final propagation time. We define the surfaces $\Sigma_0 := \Omega\times\{0\}$ and $\Sigma_T := \Omega\times\{T\}$. Given a medium-dependent

nonlinearity parameter $k \in \mathbb{R}$, a sound diffusivity coefficient $\delta \geq 0$, the speed of sound $c > 0$, a source term $f : Q_T \to \mathbb{R}$, and initial data u_0, $u_1 : \Omega \to \mathbb{R}$, we consider the following Westervelt IBVP: find the acoustic pressure $u : Q_T \to \mathbb{R}$, such that

$$\begin{cases} \partial_t((1+ku)\partial_t u) - c^2\Delta u - \delta\Delta(\partial_t u) = f & \text{in } Q_T, \\ u = 0 & \text{on } \partial\Omega \times (0,T), \\ u = u_0 \quad \text{and} \quad \partial_t u = u_1 & \text{on } \Sigma_0. \end{cases} \tag{1}$$

2 Main contributions

Our first main contribution pertains to expanding the theoretical framework of the DG–CG finite element methodology from [3] to accommodate quasilinear wave models in the form of (1). Specifically, we determine the sufficient conditions for the discretization and exact solution u, that ensure that the discrete solution $u_{h,\tau}$ satisfies the following *a priori* bounds:

$$\begin{aligned} \|\partial_t(u - u_{h,\tau})\|_{L^\infty(0,T;L^2(\Omega))} &\lesssim \left(\tau^m \|u\|_m + h^{\ell+1}\|u\|_\ell\right), \\ \|\nabla(u - u_{h,\tau})\|_{L^\infty(0,T;L^2(\Omega)^d)} &\lesssim \left(\tau^m \|u\|_{m,\tau} + h^{\ell}\|u\|_{\ell,h}\right), \end{aligned} \tag{2}$$

provided $h^{\ell+1-\frac{d}{2}} \lesssim \tau \lesssim h^{\frac{d}{2m}}$, $2 \leq m \leq q$, and $d/2 \leq \ell \leq p$, where p and q denote the degrees of approximation in space and time, respectively, and the norms on the right-hand side will be made precise in the talk; we refer to [1] details.

Secondly, our analysis guarantees that the constants in estimates (2) do not depend on the sound diffusivity δ. This fact paves the way for our second main theoretical contribution, which quantifies the δ-asymptotic behavior of discrete solutions of dissipative problems as $\delta \searrow 0$. More precisely, we will show that, for a properly set up discretization, the discrete solutions preserve the asymptotic behavior of the exact ones (established in [2]) in the vanishing dissipation limit as they converge to the discrete solution to the inviscid problem at a linear rate.

References

[1] S. Gómez, V. Nikolić, *Combined DG–CG finite element method for the Westervelt equation*, arXiv:2412.09095.

[2] B. Kaltenbacher, V. Nikolić, *Parabolic approximation of quasilinear wave equations with applications in nonlinear acoustics*, SIAM J. Math. Anal., 54(2): 2022.

[3] N. J. Walkington, *Combined DG-CG time stepping for wave equations*, SIAM J. Numer. Anal. 52(3): 2014.

Book of abstracts of the 9th International Conference on
Advanced Computational Methods in ENgineering and Applied Mathematics
September, 15–19, 2025.

Mathematical models and multiharmonic algorithms for contrast-enhanced ultrasound

Vanja Nikolić[1] **and Teresa Rauscher**[2]

[1] *Department of Mathematics, Radboud University*

[2] *Department of Mathematics, University of Klagenfurt*

e-mails: vanja.nikolic@ru.nl, teresa.rauscher@aau.at

Abstract

Contrast-enhanced ultrasound is a valuable tool in biomedical applications, using gas-filled microbubbles to enhance both diagnostic and therapeutic imaging. Once injected, microbubbles oscillate nonlinearly in response to ultrasound waves, making sound propagation through bubbly liquids a highly nonlinear problem. This behavior is modeled by a nonlinear acoustic wave equation coupled with a Rayleigh–Plesset-type describing bubble dynamics. We first look at the derivation of such coupled models from constitutive laws, then present an existence result for a Westervelt–Rayleigh–Plesset system. Finally, we present multiharmonic algorithms for time-periodic solutions that improve computational efficiency and demonstrate their performance through numerical experiments.

Key words: contrast-enhanced ultrasound, Helmholtz equation, iterative algorithms, nonlinear acoustics, Westervelt–Rayleigh–Plesset system

MSC 2020: 35L05, 35L72, 34A34, 35J05

1 Introduction

We consider the propagation of nonlinear acoustic waves in a liquid medium containing gas-filled microbubbles. The acoustic pressure field $p(x,t)$ is governed by a Westervelt-type equation, derived from the fundamental equations of fluid dynamics, which incorporates nonlinear propagation, dissipation, and a linear coupling to the microbubble volume oscillation $v(x,t)$:

$$\frac{1}{c^2}p_{tt} - \Delta p - \frac{b}{c^2}\Delta p_t - \frac{\beta}{\rho_0 c^4}(p^2)_{tt} = \rho_0 n_0 v_{tt}, \tag{1}$$

where c is the speed of sound in the liquid, b the damping coefficient, β the nonlinearity parameter, ρ_0 the mass density, and n_0 the bubble number density. The volume oscillation $v(x,t)$ is expressed in terms of the bubble radius $R(x,t)$ and its equilibrium value R_0 as

$$v(x,t) = \frac{4\pi}{3}\left(R(x,t)^3 - R_0^3\right). \tag{2}$$

The dynamics of the bubble radius are governed by Rayleigh–Plesset-type equations, which can be written in the unified form

$$\rho_0\left(RR_{tt} + \frac{3}{2}R_t^2\right) = p_{\text{int}} - p_{\text{ext}}, \tag{3}$$

where p_{int} is the internal gas pressure, and p_{ext} is the external pressure acting on the bubble, which includes the acoustic field p.

2 Local well-posedness analysis

We prove that the system defined by (1), (2), and (3), together with appropriate initial and boundary conditions, is locally well-posed in time under suitable assumptions on the initial pressure and bubble data. The full details and proof are provided in [1].

3 Periodic regime and multiharmonic Ansatz

Simulating such time domain systems is challenging due to different time scales between the wave equation and the nonlinear ODE, often requiring very small time steps; we address this by developing multiharmonic algorithms that efficiently compute time-periodic solutions via harmonic expansions. To approximate the problem we employ a multiharmonic Ansatz for the pressure and volume fields:

$$p \approx p^N = \mathfrak{R}\left\{\sum_{m=0}^{N} \exp(\imath m\omega t) p_m^N(x)\right\}, \quad v \approx v^N = \mathfrak{R}\left\{\sum_{m=0}^{N} \exp(\imath m\omega t) v_m^N(x)\right\}, \tag{4}$$

with $\omega = \frac{2\pi}{T}$. In this context we establish the existence of time-periodic solutions for a coupled Westervelt-ODE system and develop several multiharmonic algorithms for computing (p_m^N, v_m^N). These methods decompose the field into a sum of harmonics, which can be obtained as solutions of suitable Helmholtz problems and algebraic equations.

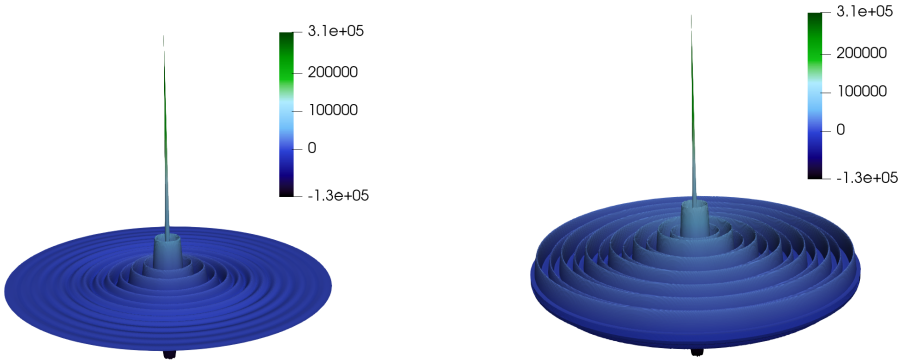

(a) Pressure with bubbles in the medium. (b) Pressure without bubbles in the medium.

Figure 1: $\mathfrak{R}(p(x, y, t_0))$ computed using a multiharmonic algorithm.

Acknowledgements This research was funded in part by the Austrian Science Fund (FWF) [10.55776/DOC78].

References

[1] V. Nikolić and T. Rauscher, *Mathematical models for nonlinear ultrasound contrast imaging with microbubbles*, SIAM J. Appl. Math. **85(2)** (2025) 961-982.

[2] V. Nikolić and T. Rauscher, *Multiharmonic algorithms for contrast-enhanced ultrasound*, arXiv preprint (arXiv:2504.13335) (2025).

MS6: New generation methods for numerical challenges in curl-div problems: Electromagnetism, MHD, and derived models

Organiser: D. Di Pietro (University of Montpellier), L. Beirao da Veiga (University of Milano-Bicocca), P. Antonietti (Politecnico di Milano) and J. Droniou (University of Montpellier)

Description: Electromagnetic models display specific structures that challenge their mathematical analysis. The well-posedness of stationary versions (such as magnetostatics) depend on the topology of the domain - typically, the number of holes in it. Transient versions comprise two types of equations: evolution and constraints (divergence condition on the fields), the latter being preserved by the former. When considering charged fluids, electromagnetic and Navier-Stokes equations are coupled, giving rise to complex non-linear magnetohydrodynamics equations that also present certain structures of interest, such as the preservation of helicity. Other nonlinear equations also arise in the context of generalised electromagnetic models, such as the Einstein equations.

Most of these structures and complexities stem from the fact that electromagnetic equations are based on "incomplete" operators: the curl and the divergence. The properties and relations between these two operators, which explain the aforementioned structures, are embedded into the de Rham complex and its cohomology. Designing robust and accurate numerical methods for electromagnetic (and related) models is a complex task, and it requires to properly represent at the discrete level the underlying mathematical structures. This necessitates suitable discretisations of the divergence and curl, and the resulting schemes often lead to indefinite linear systems that present severe computational challenges.

This minisymposium will focus on numerical and computational aspects of models involving the curl and divergence operators, with emphasis on electromagnetic and magnetohydrodynamics models. Topics covered include the design and analysis of numerical methods for these models, considerations around the preservation of structures at the discrete level, computational challenges, etc.

Book of abstracts of the 9th International Conference on
Advanced Computational Methods in ENgineering and Applied Mathematics
September, 15–19, 2025.

Topology-preserving discretisation of the magneto-frictional equations arising in the Parker conjecture

Mingdong He[1], Patrick E. Farrell[1], Kaibo Hu[2] and Boris D. Andrews[1]

[1] *Mathematical Institute, University of Oxford*

[2] *School of Mathematics, University of Edinburgh*

e-mails: mingdong.he@maths.ox.ac.uk, patrick.farrell@maths.ox.ac.uk, kaibo.hu@ed.ac.uk, boris.andrews@maths.ox.ac.uk

Abstract

The Parker conjecture, which explores whether magnetic fields in perfectly conducting plasmas can develop tangential discontinuities during magnetic relaxation, remains an open question in astrophysics. Helicity conservation provides a topological barrier during relaxation, preventing topologically nontrivial initial data relaxing to trivial solutions; preserving this mechanism discretely over long time periods is therefore crucial for numerical simulation. This work presents an energy- and helicity-preserving finite element discretization for the magneto-frictional system, for investigating the Parker conjecture.

Key words: magnetohydrodynamics, Parker conjecture, magnetic relaxation, magnetic helicity, finite element method
MSC 2020: 65N30, 65L60, 76W05

1 Background

The essential claim of the Parker conjecture [5, 6] is as follows:

> *For almost all possible flows, the magnetic field develops tangential discontinuities (i.e. current sheets) during ideal magnetic relaxation.*

Effective numerical investigation of the Parker conjecture requires effective simulation of magnetic relaxation.

In this work, we consider the magneto-frictional equations, a magnetic relaxation model with a diffusive fluid component and ideal magnetic component. This systems demonstrates a dissipated energy $\mathcal{E}$ and conserved helicity $\mathcal{H}$, defined

$$\mathcal{E} \coloneqq \int \|\mathbf{B}\|^2, \qquad \mathcal{H} \coloneqq \int \mathbf{A} \cdot \mathbf{B}, \tag{1}$$

where $\mathbf{A}$ is any potential for the magnetic field $\mathbf{B}$ satisfying $\mathbf{B} = \operatorname{curl} \mathbf{A}$. The Arnold equality [3], $C|\mathcal{H}| \leq \mathcal{E}$ for some constant $C > 0$, bounds the energy below by the helicity; this has the significant consequence that, despite the dissipation in the energy, initial data with nonzero $\mathcal{H}$ cannot relax to zero.

As $\mathcal{H}$ quantifies the knottedness of the magnetic field [4] this can be interpreted as a topological barrier. Failure to preserve helicity conservation discretely implies a failure to preserve this topological barrier, thus allowing the magnetic field to artificially relax to zero.

2 Our contributions

In this work, we design a finite-element discretisation of the magneto-frictional equations that, over general meshes, preserves both the dissipation of energy and conservation of helicity, and with it the topological barrier provided by the Arnold inequality. This scheme allows us to accurate reproduce the magnetic relaxation behaviour of this system over long time periods, a result which is crucial for numerical investigations into the Parker conjecture.

The construction relies on the systematic introduction of auxiliary variables [1]—the discretisation we propose is a mixed 4-field **B**−**B**−**E**−**j** discretisation—and finite element exterior calculus [2].

Acknowledgements We would like to thank Gunnar Hornig, Yang Liu, Pablo Brubeck Martinez, Zhongmin Qian, and Chris Smiet for helpful discussions.

This work was funded by the Engineering and Physical Sciences Research Council [grant numbers EP/R029423/1 and EP/W026163/1], the EPSRC Energy Programme [grant number EP/W006839/1], a CASE award from the UK Atomic Energy Authority, the Donatio Universitatis Carolinae Chair "Mathematical modelling of multicomponent systems", the European Research Council (ERC Starting Grant, project 101164551 GeoFEM), and by a Royal Society University Research Fellowship (URF\R1\221398). This work used the ARCHER2 UK National Supercomputing Service. No new data were generated or analysed during this work.

References

[1] B. D. Andrews and P. E. Farrell, *High-order conservative and accurately dissipative numerical integrators via auxiliary variables*, arXiv, (2024).

[2] D. N. Arnold, *Finite Element Exterior Calculus*, Society for Industrial and Applied Mathematics, 2018.

[3] V. I. Arnold, *The asymptotic Hopf invariant and its applications*, Vladimir I. Arnold–Collected Works: Hydrodynamics, Bifurcation Theory, and Algebraic Geometry 1965–1972, (1974), pp. 357–375.

[4] V. I. Arnold and B. A. Khesin, *Topological Methods in Hydrodynamics*, vol. 129 of Applied Mathematical Sciences, Springer, 2011.

[5] E. N. Parker, *Topological dissipation and the small-scale fields in turbulent gases*, Astrophysical Journal, **174** (1972), p. 499.

[6] D. I. Pontin and G. Hornig, *The Parker problem: existence of smooth force-free fields and coronal heating*, Living Reviews in Solar Physics, **17** (2020), p. 5.

Book of abstracts of the 9th International Conference on
Advanced Computational Methods in ENgineering and Applied Mathematics
September, 15–19, 2025.

GPU implementation of a hybridized discontinuous finite element solver for frequency-domain wave problems

Ahmed Chabib[1], Roland Greffe[2], Christophe Geuzaine[2] and Axel Modave[1]

[1] *POEMS, CNRS, Inria, ENSTA, Institut Polytechnique de Paris, 91120 Palaiseau, France*

[2] *Institut Montefiore, Université de Liège, Belgique*

e-mails: ahmed.chabib@ensta.fr, r.greffe@uliege.be, cgeuzaine@uliege.be, axel.modave@ensta.fr

Abstract

Numerical simulations of time-harmonic wave propagation phenomena are of paramount importance in industry and research. We deal with the finite element solution of large-scale problems by using graphics processing units (GPUs). Although using GPUs offers significant potential for accelerating computations, fully exploiting them remains challenging. We consider a hybridizable discontinuous Galerkin finite element method, called CHDG, with transmission variables on element interfaces, which is well-suited for efficient parallel computing. In this work, we propose and study different implementation strategies for efficient computations on GPUs.

Key words: Finite Element, GPU, Helmoltz, HDG, Waves

CHDG method

Discontinuous Galerkin finite element approaches [1] have demonstrated their ability to solve large-scale time-harmonic problems thanks to their robustness, flexibility, and their capability to leverage the computing power of parallel computers. To improve the properties of the global system, the problem can be reformulated by introducing interface variables, and eliminating the physical variables in a hybridization process [2]. The CHDG method [3] is a variant in which transmission variables are used as interface variables to accelerate the convergence of iterative solution procedures for time-harmonic problems.

To describe the method, we consider a general time-harmonic problem on a domain Ω:

$$-\imath\kappa p + \nabla\cdot\boldsymbol{u} = 0 \ \text{ in } \Omega, \qquad -\imath\kappa\boldsymbol{u} + \nabla p = 0 \ \text{ in } \Omega \qquad \text{and} \qquad p - \boldsymbol{n}\cdot\boldsymbol{u} = s_R \ \text{ on } \partial\Omega,$$

where p and $\boldsymbol{u}$ are the physical variables, κ is the wave number, $\boldsymbol{n}$ the outward unit normal vector, and s_R is a surface source. This problem is solved by using a finite element mesh of the domain with nodal polynomial basis functions [1]. In CHDG, a local physical problem is defined on each element. The local physical variables are coupled thanks to *outgoing* and *incoming* transmission variables, which are defined on each face F and for each element K as

$$g^{\oplus}_{K,F} := p_K + \boldsymbol{n}_K\cdot\boldsymbol{u}_K \qquad \text{and} \qquad g^{\ominus}_{K,F} := \begin{cases} g^{\oplus}_{K',F} & \text{if } F \not\subset \partial\Omega, \\ s_R & \text{if } F \subset \partial\Omega, \end{cases}$$

respectively, where K' is a neighboring element of K.

The resulting global system can be written in the abstract form as $\boldsymbol{M}(\boldsymbol{I} - \boldsymbol{\Pi S})\boldsymbol{g} = \boldsymbol{Mb}$, where $\boldsymbol{M}$ is the mass matrix, $\boldsymbol{\Pi}$ is an exchange matrix with data communication between neighboring elements, $\boldsymbol{S}$ is the scattering matrix that includes the solution of local problems, $\boldsymbol{b}$ is a right-hand side vector and $\boldsymbol{g}$ groups all the unknown outgoing variables, see [3].

GPU implementation

Our code is written in C++ with CUDA for GPU programming. The GPU kernels corresponding to the application of $\boldsymbol{M}$, $\boldsymbol{\Pi}$ and $\boldsymbol{S}$ are optimized separately. For the application of $\boldsymbol{S}$, we have investigated computation of the fly of the matrix at each call (OTF) and the precomputation and the storage of the matrix (I2O).

We observe that, I2O outperforms OTF in a benchmark using 8.106 tetrahedral elements and the fixed-point iteration on A100 GPU. The results show that, the computation time per element decreases for both strategies as the problem size increases. The time eventually plateaus with OTF, whereas it continues to improve with I2O. Nevertheless, the I2O approach requires more memory storage, which could be a limiting factor for GPU computing.

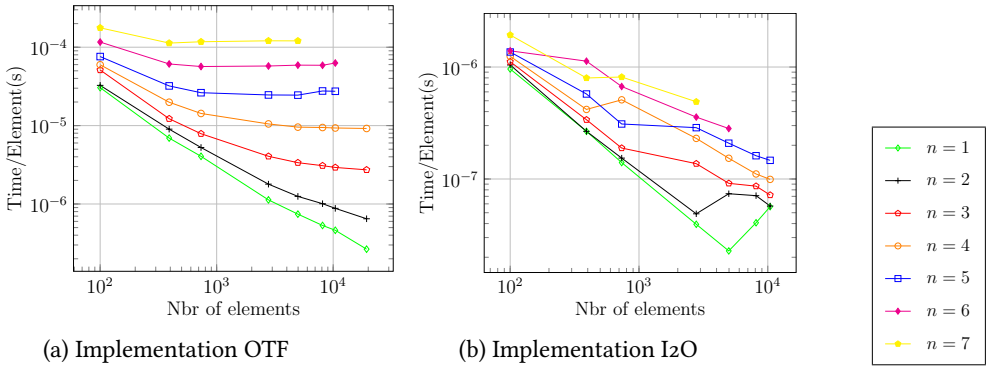

(a) Implementation OTF (b) Implementation I2O

Figure 1: Average time per fixed-point iteration and per element for the two implementations (OTF and I2O), for different polynomial degrees n

Acknowledgements This work was supported in part by the ANR JCJC WavesDG project (ANR-21-CE46-0010) and, in the context of France 2030, by the Exa-MA project (ANR-22-EXNU-0002). Computational resources have been provided by the Consortium des Équipements de Calcul Intensif (CÉCI), funded by the Fonds de la Recherche Scientifique de Belgique (F.R.S.-FNRS) under Grant No. 2.5020.11 and by the Walloon Region.

References

[1] J. S. Hesthaven & T. Warburton, *Nodal discontinuous Galerkin methods: algorithms, analysis, and applications*, Springer Science & Business Media (2007).

[2] B. Cockburn, J. Gopalakrishnan & R. Lazarov, Unified Hybridization of Discontinuous Galerkin, Mixed, and Continuous Galerkin Methods for Second Order Elliptic Problems, *SIAM J. Numer. Anal.* 47, 1319-1365 (2009)

[3] A. Modave & T. Chaumont-Frelet, A hybridizable discontinuous Galerkin method with characteristic variables for Helmholtz problems, *J. Comput. Phys.*, 493 (2023) 112459.

Book of abstracts of the 9th International Conference on
Advanced Computational Methods in ENgineering and Applied Mathematics
September, 15–19, 2025.

A hybridizable discontinuous Galerkin method with transmission variables for time-harmonic electromagnetic problems

T. Chaumont-Frelet[1], A. Rappaport[2] and A. Modave[2]

[1] *Inria, Univ. Lille, CNRS, UMR 8524 – Laboratoire Paul Painlevé, 59000 Lille, France*

[2] *POEMS, CNRS, Inria, ENSTA Paris, Institut Polytechnique de Paris, 91120 Palaiseau, France*

e-mails: theophile.chaumont@inria.fr, ari.rappaport@ensta-paris.fr, axel.modave@ensta-paris.fr

Abstract

We propose a new hybrization strategy for discontinuous Galerkin (DG) discretizations of time-harmonic Maxwell's equations. Instead of the "numerical trace" classically employed in hybridizable discontinuous Galerkin (HDG) methods, we employ "characteristic variables" to equivalently reformulate the discrete problem onto the mesh skeleton. We call the resulting numerical schemes CHDG. We show that although the CHDG linear system has more degrees of freedom that the standard HDG counterparts, it is more suited for fast iterative solvers. In particular, we rigorously establish that the CHDG linear system can alwats be solved with a simple fix point iteration, and present numerical examples indicating the iteration count for GMRES and CGNR iterations is drastically reduced for the CHDG linear system has compared to its HDG and DG counterparts.

Key words: Maxwell's equations, Discontinuous Galerkin methods, High-order methods, Hybridization, Iterative solvers
MSC 2020: 65F08, 65N22, 65N30

1 Introduction

For a three-dimensional domain $\Omega \subset \mathbb{R}^3$, and a fixed wavenumber $\kappa > 0$, we are willing to numerically simulate the electromagnetic field produced by a given incident field $\boldsymbol{s} : \partial\Omega \to \mathbb{C}^3$. Specifically, we are looking for $\boldsymbol{e}, \boldsymbol{h} : \Omega \subset \mathbb{C}^3$ solution to Maxwell's equation:

$$\left\{\begin{array}{rcll} i\kappa\boldsymbol{e} - \boldsymbol{\nabla}\times\boldsymbol{h} &=& \boldsymbol{o} & \text{in } \Omega, \\ i\kappa\boldsymbol{h} + \boldsymbol{\nabla}\times\boldsymbol{e} &=& \boldsymbol{o} & \text{in } \Omega, \\ -\boldsymbol{n}\times(\boldsymbol{n}\times\boldsymbol{e}) + \boldsymbol{n}\times\boldsymbol{h} &=& \boldsymbol{s} & \text{on } \partial\Omega, \end{array}\right.$$

where $\boldsymbol{n}$ is the unit normal to $\partial\Omega$ pointing outside Ω.

When the wavenumber κ becomes large, this problem is notoriously difficult for two reasons. On the one hand (i), the solution oscillates more and more as the wavenumber increases, requiring a fine mesh to correctly capture these oscillations and limit numerical dispersion errors. On the other hand (ii), the resulting linear system becomes highly indefinite, making the design of efficient iterative solver challenging [1].

2 Discontinuous Galerkin discretization

In this contribution, we consider a simplicial mesh $\mathcal{T}_h$ and a polynomial degree p, and focus on the associated discontinuous Galerkin discretizations. Specifically we look for piecewise polynomial ansatz $\boldsymbol{e}_h$ and $\boldsymbol{h}_h$ such that

$$
\begin{aligned}
i\kappa\big(\boldsymbol{e}_h, \boldsymbol{v}_h\big)_{\mathcal{T}_h} - \big(\boldsymbol{h}_h, \boldsymbol{\nabla}\times\boldsymbol{v}_h\big)_{\mathcal{T}_h} - \big\langle \boldsymbol{n}\times\widehat{\boldsymbol{h}}(\boldsymbol{e}_h,\boldsymbol{h}_h), \boldsymbol{v}_h\big\rangle_{\partial\mathcal{T}_h} &= 0,\\
i\kappa\big(\boldsymbol{h}_h, \boldsymbol{w}_h\big)_{\mathcal{T}_h} + \big(\boldsymbol{e}_h, \boldsymbol{\nabla}\times\boldsymbol{w}_h\big)_{\mathcal{T}_h} + \big\langle \boldsymbol{n}\times\widehat{\boldsymbol{e}}(\boldsymbol{e}_h,\boldsymbol{h}_h), \boldsymbol{w}_h\big\rangle_{\partial\mathcal{T}_h} &= 0,
\end{aligned}
$$

for all piecewise polynomial test fucntions $\boldsymbol{v}_h$ and $\boldsymbol{w}_h$. The upwind *numerical fluxes* are given by $\widehat{\boldsymbol{h}}(\boldsymbol{e}_h,\boldsymbol{h}_h)$ and $\widehat{\boldsymbol{e}}(\boldsymbol{e}_h,\boldsymbol{h}_h)$ defined by

$$
\begin{aligned}
\widehat{\boldsymbol{e}}_F &:= (\boldsymbol{e}_K + \boldsymbol{e}_{K'})/2 + \boldsymbol{n}_F\times(\boldsymbol{h}_K - \boldsymbol{h}_{K'})/2,\\
\widehat{\boldsymbol{h}}_F &:= (\boldsymbol{h}_K + \boldsymbol{h}_{K'})/2 - \boldsymbol{n}_F\times(\boldsymbol{e}_K - \boldsymbol{e}_{K'})/2,
\end{aligned}
$$

for each interior face $F = \partial K \cap \partial K'$, $K, K' \in \mathcal{T}_h$. For external faces, these definitions are modified to take into account the boundary condition and the incident field.

3 Hybridization

In the standard hybridization procedure, the auxiliary variable $\boldsymbol{\lambda}_h := \widehat{\boldsymbol{e}}(\boldsymbol{e}_h,\boldsymbol{h}_h)$ is introduced onto each mesh face. The resulting hybridizable discontinuous Galerkin (HDG) scheme can be formulated only in terms of $\boldsymbol{\lambda}_h$, and the physical fields $\boldsymbol{e}_h$ and $\boldsymbol{h}_h$ may be recovered from $\boldsymbol{\lambda}_h$ through a post-processing by solving local problems.

Here, we follow an alternative approach where the auxiliary variable is defined by $\boldsymbol{g}_h := -\boldsymbol{n}\times(\boldsymbol{n}\times\boldsymbol{e}_h) + \boldsymbol{n}\times\boldsymbol{h}_h$ on the boundary of each element $K \in \mathcal{T}_h$. The key idea behind this definition is that the resulting local problems linking $\boldsymbol{g}_h$ to the physical field $\boldsymbol{e}_h$ and $\boldsymbol{h}_h$ correspond to scattering operators that are well behaved. This approach was first introduced for the Helmholtz equation [2], and the result presented here for Maxwell's equations are from [3].

4 Key results

The advantage of the alternative hybridization strategy over the standard one is that the resulting linear system can be solved with a simple fixed-point iteration. Besides, numerical experiments indicate that the resulting linear system is better suited for CGNR and GMRES iteration. Both of these aspects will be highlighted in the presentation.

References

[1] O.G. Ernst and M.J. Gander, *Why it is difficult to solve Helmholtz problems with classical iterative methods*, Numerical Analysis of Multiscale problems (2011) 325–363.

[2] A. Modave and T. Chaumont-Frelet, *A hybridizable discontinuous Galerkin method with characteristic variables for Helmholtz problems*, J. Comput. Phys. **493** (2023) 112459.

[3] A. Rappaport, T. Chaumont-Frelet and A. Modave, *A hybridizable discontinuous Galerkin method with characteristic variables for Helmholtz problems*, arXiv:2505.04288 (2025).

Book of abstracts of the 9th International Conference on
Advanced Computational Methods in ENgineering and Applied Mathematics
September, 15–19, 2025.

Finite elements for symmetric and traceless tensors in three dimensions

Kaibo Hu[1], Ting Lin[2] and Bowen Shi[3]

[1] *Mathematical Institute, University of Oxford*

[2] *School of Mathematical Sciences, Peking University*

[3] *Oden Institute for Computational Engineering & Sciences, University of Texas at Austin*

e-mails: kaibo.hu@maths.ox.ac.uk, lintingsms@pku.edu.cn, bowenshi@utexas.edu

Abstract

We construct a family of finite element sub-complexes of the conformal complex on tetrahedral meshes and show its exactness on contractible domains. This complex includes vector fields and symmetric and traceless tensor fields, interlinked through the conformal Killing operator, the linearized Cotton-York operator, and the divergence operator, respectively. This leads to discrete versions of transverse traceless (TT) tensors, i.e., symmetric, traceless and divergence-free matrix fields, in continuum mechanics and general relativity. We show the inf-sup stability of the $H(\mathrm{div})$-conforming finite element symmetric and traceless tensors paired with discontinuous vectors.

Key words: Hilbert complexes, Finite Element Exterior Calculus, transverse-traceless tensors, conformal deformation complex, inf-sup condition,

1 Conformal Complexes

Hilbert complexes are sequences of linear spaces connected by linear operators, where the composition of consecutive operators vanishes. The de Rham complex is a fundamental example, while the Bernstein-Gelfand-Gelfand (BGG) construction yields complexes for tensor fields, such as symmetric and traceless matrices ($\mathbb{S} \cap \mathbb{T}$) [2, 1]. These appear in problems like incompressible Stokes flow, where the stress variable $\boldsymbol{\sigma} := \mathrm{def}(\boldsymbol{u})$ is symmetric and traceless due to incompressibility ($\mathrm{div}\, \boldsymbol{u} = 0$), and in general relativity (GR), where transverse-traceless (TT) tensors describe gravitational waves.

We study the *conformal deformation complex* in three dimensions:

$$\boldsymbol{CK} \xrightarrow{\subset} H^1(\Omega;\mathbb{R}^3) \xrightarrow{\mathrm{dev}\,\mathrm{def}} H(\mathrm{cott},\Omega;\mathbb{S}\cap\mathbb{T}) \xrightarrow{\mathrm{cott}} H(\mathrm{div},\Omega;\mathbb{S}\cap\mathbb{T}) \xrightarrow{\mathrm{div}} L^2(\Omega;\mathbb{R}^3) \to \mathbf{0}, \quad (1)$$

where $\mathbb{S}\cap\mathbb{T}$ denotes symmetric and traceless tensors, dev def is the conformal Killing operator, and $\boldsymbol{CK} := \ker(\mathrm{dev}\,\mathrm{def})$ is the 10-dimensional conformal Killing field. The spaces are defined using standard Sobolev notations:

$$H(\mathrm{cott},\Omega;\mathbb{S}\cap\mathbb{T}) := \{\boldsymbol{\sigma} \in L^2(\Omega;\mathbb{S}\cap\mathbb{T}) : \mathrm{cott}\,\boldsymbol{\sigma} \in L^2(\Omega;\mathbb{S}\cap\mathbb{T})\},$$
$$H(\mathrm{div},\Omega;\mathbb{S}\cap\mathbb{T}) := \{\boldsymbol{\sigma} \in L^2(\Omega;\mathbb{S}\cap\mathbb{T}) : \mathrm{div}\,\boldsymbol{\sigma} \in L^2(\Omega;\mathbb{R}^3)\}.$$

The operator cott is a third-order differential operator related to the linearized Cotton-York tensor, and div applies row-wise. In GR, this complex encodes TT tensors ($H(\mathrm{div}, \Omega; \mathbb{S} \cap \mathbb{T}) \cap \ker(\mathrm{div})$) and York splits, with exactness implying TT tensors can be expressed via Cotton-York potentials. The complex also applies to Cosserat elasticity and trace-free Korn inequalities.

2 Finite Element Discretization

We construct a finite element sub-complex [3]:

$$\boldsymbol{CK} \xrightarrow{\subset} \boldsymbol{U}_{k+1,h} \xrightarrow{\mathrm{dev}\,\mathrm{def}} \Sigma^{\mathrm{cott}}_{k,h} \xrightarrow{\mathrm{cott}} \Sigma^{\mathrm{div}}_{k-3,h} \xrightarrow{\mathrm{div}} \boldsymbol{V}_{k-4,h} \to \boldsymbol{0}$$

on triangulation. In particular, we construct a conforming finite element pair $\Sigma^{\mathrm{div}}_{k,h} \times \boldsymbol{V}_{k-1,h} \subset H(\mathrm{div}, \Omega; \mathbb{S} \cap \mathbb{T}) \times L^2(\Omega; \mathbb{R}^3)$ satisfying the algebraic condition:

$$\mathrm{div}\, \Sigma^{\mathrm{div}}_{k,h} = \boldsymbol{V}_{k-1,h},$$

and the inf-sup condition:

$$\inf_{\boldsymbol{v} \in \boldsymbol{V}_{k-1,h} \setminus \{0\}} \sup_{\boldsymbol{\sigma} \in \Sigma^{\mathrm{div}}_{k,h} \setminus \{0\}} \frac{\int_\Omega \mathrm{div}\, \boldsymbol{\sigma} \cdot \boldsymbol{v}}{\|\boldsymbol{\sigma}\|_{H(\mathrm{div},\Omega)} \|\boldsymbol{v}\|_{L^2(\Omega)}} \geq C > 0,$$

with C independent of mesh size h. This ensures exact preservation of the TT structure.

Our work addresses the smoothness conditions required for the inf-sup stability, enabling structure-preserving discretizations for applications in GR and fluid mechanics.

Acknowledgements The work of KH was supported by a Royal Society University Research Fellowship (URF\R1\221398) and an ERC Starting Grant (project 101164551, GeoFEM). The work of TL was supported by NSFC project 123B2014.

References

[1] D. N. Arnold, K. Hu, *Complexes from Complexes*, Foundations of Computational Mathematics, volume=21, number=6, pages=1739–1774, Springer, 2021.

[2] A. Čap, K. Hu, *BGG Sequences with Weak Regularity and Applications*, Foundations of Computational Mathematics, pages=1–40, Springer, 2023.

[3] K. Hu, T. Lin, B. Shi, *Finite Elements for Symmetric and Traceless Tensors in Three Dimensions*, arXiv preprint arXiv:2311.16077, 2023.

Book of abstracts of the 9th International Conference on
Advanced Computational Methods in ENgineering and Applied Mathematics
September, 15–19, 2025.

Multi-GPU Discontinuous Galerkin Solver for Maxwell's Equations

Orian Louant[1], Matteo Cicuttin[2], Clément Smagghe[1] and Christophe Geuzaine[1]

[1] *Department of Electrical Engeneering and Computer Science, University of Liège, Belgium*

[2] *Department of Mathematical Sciences, Politecnico di Torino, Italy*

e-mails: orian.louant@uliege.be, matteo.cicuttin@polito.it, Cle.Smagghe@student.uliege.be, cgeuzaine@uliege.be

Abstract

This work presents the performance and scaling of the multi-GPU extension of the GmshDG discontinuous Galerkin solver for solving Maxwell's equations in the time domain. Our implementation shows good weak and strong scaling performance up to a hundred GPUs.

Key words: Maxwell's equations, Discontinuous Galerkin Methods, GPU computing.

1 Introduction

Modern supercomputers increasingly rely on Graphics Processing Units (GPUs), a trend likely to continue. GPUs offer high performance and low cost per GFLOP, making them ideal for scientific computing. In computational electromagnetics, GPU use began with finite-difference time-domain (FDTD) [1] and discontinuous Galerkin (DG) methods [2]. DG is especially suited for GPUs, combining the flexibility of the finite element method mesh with explicit FDTD time-stepping and parallelism.

This work presents a multi-GPU implementation of a time-explicit DG method for Maxwell's equations, optimized to efficiently exploit modern heterogeneous clusters with hundreds of GPUs. On that hardware, the solver achieves good strong and weak scaling performance up to around a hundred GPUs.

2 Multi-GPU Discontinuous Galerkin solver

Initially, GmshDG* focused on maximizing single-GPU performance [3] to ensure high efficiency in both cost and energy consumption. However, due to the limited memory capacity of GPUs, typically an order of magnitude smaller than that of a CPU nodes, a multi-GPU implementation is essential for solving large-scale problems.

The DG method allows parallelization both at the level of a mesh element and at the level of a

*https://gitlab.onelab.info/gmsh/dg/

single degree of freedom, and is thus well suited for multi-GPU parallelization via mesh partitioning. Communication between subdomains however is required at element interfaces to evaluate numerical fluxes, making inter-partition data exchange a critical performance factor at scale. As GPU compute power and memory bandwidth continue to increase, communication speeds and latency create a bottleneck. Therefore, achieving strong scaling performance requires careful optimization to minimize communication and overlap it with computation wherever possible.

Figure 1 presents the strong and weak scaling performance of GmshDG on up to 128 GPUs on the LUMI supercomputer[†]. The implementation demonstrates solid scalability, achieving a strong scaling efficiency of 80% and a weak scaling efficiency of 88%.

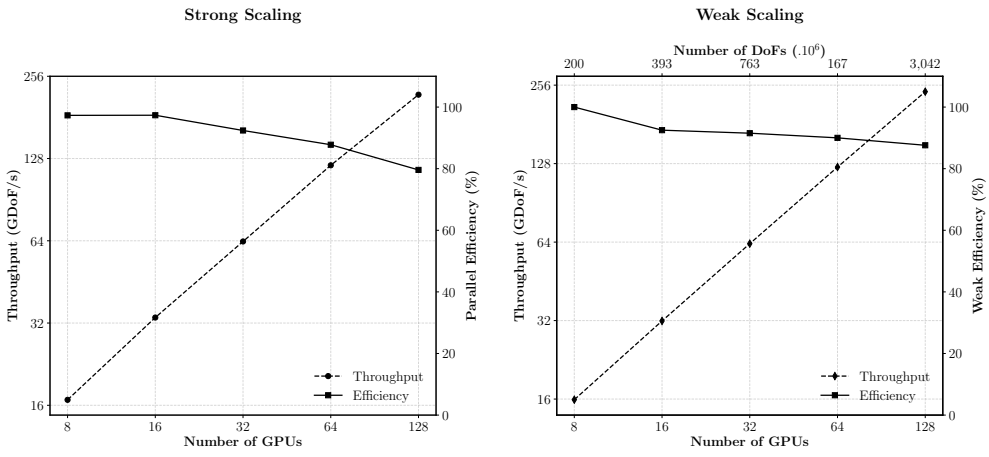

Figure 1: Strong (left) and weak (right) scaling of GmshDG up to 128 GPUs.

References

[1] Takada, N., Shimobaba, T., Masuda, N., Ito, T., *High-speed FDTD simulation algorithm for GPU with compute unified device architecture.* 2009 IEEE Antennas and Propagation Society International Symposium

[2] A. Klockner, T. Warburton, J. Bridge, J. S. Hesthaven, *Nodal discontinuous Galerkin methods on Graphics processors*, J. Comp. Phys. 228, 2009.

[3] M. Cicuttin, A. Royer, P. Binde, C. Geuzaine, *Electrostatic discharge simulation using a GPU-accelerated DGTD solver targeting modern graphics processors*, IEEE Transactions on Magnetics, 58(9), 2022.

[†] `https://lumi-supercomputer.eu`

Book of abstracts of the 9th International Conference on
Advanced Computational Methods in ENgineering and Applied Mathematics
September, 15–19, 2025.

A Reynolds- and Hartmann-semirobust hybrid method for magnetohydrodynamics

Daniele A. Di Pietro, Jérôme Droniou and Vito Patierno

IMAG, Univ Montpellier, CNRS, Montpellier, France,

e-mails: daniele.di-pietro@umontpellier.fr, jerome.droniou@umontpellier.fr, vito.patierno@umontpellier.fr

Abstract

In this work we develop a novel method for magnetohydrodynamics on convex domains robust with respect to the Reynolds and Hartmann numbers.

The starting point is a weak formulation of magnetohydrodynamics where an H1-based form is considered for all diffusive terms. Both scalar- and vector-valued variables are discretized using polynomial functions inside the elements and on the faces in the spirit of [1, 2]. Concerning vector-valued fields, face variables are taken in full polynomial spaces, whereas element variables are taken in the Raviart-Thomas-Nédélec space. This choice leads, in particular, to the pointwise satisfaction of the mass conservation and Gauss's law. Crucial attention has been put into designing the trilinear form, as its skew-symmetry properties are crucial in the proof of the convergence theorem.

A thorough stability and convergence analysis for the space semi-discrete problem is carried out. Specifically, we prove energy error estimates of order h^{k+1} for the version of the scheme corresponding to a polynomial degree $k \geq 0$. Using techniques inspired by [3], such estimates are additionally robust with respect to the pressure and semirobust with respect to the Reynolds and Hartmann numbers, meaning that the constants in the right-hand side remain bounded in the whole range of value for such dimensionless numbers provided that the velocity and magnetic fields are smooth enough.

References

[1] L. Botti and F. C. Massa. HHO methods for the incompressible Navier-Stokes and the incompressible Euler equations. In: J. Sci. Comput. 92.28 (2022). doi: 10.1007/s10915-022-01864-1.

[2] L. Botti, M. Botti, D. A. Di Pietro, and F. C. Massa. Stability, convergence, and pressure-robustness of numerical schemes for incompressible flows with hybrid velocity and pressure. Math. Comp., 2024. Accepted for publication. arXiv preprint 2404.12732 [math.NA].

[3] L. Beirão da Veiga, D. A. Di Pietro, and K. B. Haile. A Péclet-robust discontinuous Galerkin method for nonlinear diffusion with advection. Math. Models Methods Appl. Sci., 2024, 34(9):1781–1807. DOI: 10.1142/S0218202524500350.

Book of abstracts of the 9th International Conference on
Advanced Computational Methods in ENgineering and Applied Mathematics
September, 15–19, 2025.

The Discrete De Rham method for the exterior calculus Einstein's equations

Jia Jia Qian[1]

[1] *School of Mathematics, Monash University, Australia*

e-mails: jia.qian@monash.edu

Abstract

Einstein's field equations (EFEs) are a system of partial differential equations modeling the interactions of gravity and matter on a 4-dimensional spacetime manifold. Decomposing the domain into "space" and "time" transforms the EFEs into a set of constraint and evolution equations defined on the 3-dimensional spatial surfaces. There are various ways to go about this decomposition, with the BSSNOK formulation and its derivatives being a classic approach in numerical relativity. However, due to the form and complexity of the equations, the standard discretisation method remains to be finite differencing. We present a formulation of the EFEs that gives the unknowns an exterior calculus structure, enabling the application of methods based on the (exterior calculus) de Rham complex, such as the discrete de Rham (DDR) method. Taking advantage of the features of DDR, we design two arbitrary order schemes, and present numerical results on generic polytopal meshes.

Key words: discrete de Rham complex, Einstein's field equations, exterior calculus, general relativity, numerical relativity,

1 Introduction

General relativity describes the relations and interactions between gravity and matter using the curvature of spacetime. The entire theory is captured by the metric g, a symmetric $(0,2)$-tensor, from which one can derive the Riemann curvature tensor and its various contractions. The vacuum spacetime Einstein's equations are

$$G_{\mu\nu} \coloneqq R_{\mu\nu} - \frac{1}{2} R g_{\mu\nu} = 0, \tag{1}$$

where $R_{\mu\nu}$ is the Ricci tensor, and R is the scalar curvature. A standard $3+1$ spacetime decomposition lets us recast these 4-dimensional equations into an initial value problem, containing both constraint and evolution equations. In contrast to similar problems such as the Maxwell's equations and the Yang–Mills equations, the usual $3+1$ Einstein's equations are a set of *tensor equations*, which do not lend itself easily to certain classes of numerical methods.

2 Exterior calculus Einstein's equations

We present a 3 + 1 exterior calculus version of Einstein's equations [1], based on the formulation first proposed in [2], written using differential forms from the exterior calculus de Rham complex

$$\{0\} \longrightarrow \Lambda^0(\Omega) \xrightarrow{\mathrm{d}} \Lambda^1(\Omega) \xrightarrow{\mathrm{d}} \Lambda^2(\Omega) \xrightarrow{\mathrm{d}} \Lambda^3(\Omega) \longrightarrow \{0\}$$

where d is the exterior derivative. In 3 dimensions, this is equivalent to the vector de Rham complex by using *vector proxies*, an identification of scalar and vector fields with 0-forms and 1-forms.

The main idea behind this formulation consists in rewriting the 4-dimensional spacetime equation (1) using 4-dimensional exterior calculus, after which the 3+1 split [4] will naturally produce a set of equations evolving 3-dimensional differential forms, using the 3-dimensional derivative. For example, denoting by $\mathbf{n}$ the normal vector field ($\mathbf{n}^\flat$ the corresponding 1-form) to our 3-dimensional space, any spacetime differential form ω breaks down into

$$\omega = -\mathbf{n}^\flat \wedge \bar{\omega} + \hat{\omega},$$

where $\bar{\omega}$, $\hat{\omega}$ are *purely spatial forms*.

This rewrite of the EFEs enables the design of schemes using methods based on the discretisation of the de Rham complex, such as the (exterior calculus) DDR method [3]. The main advantages of using DDR over standard finite differencing is the flexibility on the underlying mesh, and the possibility of higher order approximations. For general relativity in particular, where simulations often contain singularities (e.g. black holes), this method opens up advanced techniques such as non-conforming mesh refinements that allow to better capture the steep solutions at a lower cost. We will introduce, to our knowledge, one of the first polytopal schemes for the Einstein's equations, complete with numerical simulations for two exact vacuum solutions, the Kasner and Gowdy wave solution, with both natural and periodic boundary conditions (torus) where appropriate.

References

[1] Oliynyk, T. A., and Qian, J. J., *A polytopal discrete de Rham scheme for the exterior calculus Einstein's equations*, arXiv preprint arXiv:2505.00286 (2025).

[2] Olivares, H., I. M. Peshkov, E. R. Most, F. M. Guercilena, and L. J. Papenfort, *New first-order formulation of the Einstein equations exploiting analogies with electrodynamics*, Phys. Rev. D, 105.12, (2022).

[3] Bonaldi, F., Di Pietro, D. A., Droniou, J., and Hu, K, *An exterior calculus framework for polytopal methods*, Journal of the European Mathematical Society, page 55p (2024).

[4] Fecko, Marián, *On 3+ 1 decompositions with respect to an observer field via differential forms*, J. Math. Phys., 4542–4560(38) (1997).

Book of abstracts of the 9th International Conference on
Advanced Computational Methods in ENgineering and Applied Mathematics
September, 15–19, 2025.

Primal finite element schemes of the $\mathbf{H}(\mathrm{d}) \cap \mathbf{H}(\boldsymbol{\delta})$ problems

Shuo Zhang[1,2]

[1] *Academy of Mathematics and System Sciences, Chinese Academy of Sciences*

[2] *School of Mathematical Sciences, University of Chinese Academy of Sciences*

e-mails: szhang@lsec.cc.ac.cn

Abstract

Two families of primal finite element methods are presented for the $\mathbf{H}(\mathbf{d}) \cap \mathbf{H}(\boldsymbol{\delta})$ problems, one for the elliptic problem established on $\mathbf{H}(\mathbf{d}) \cap \mathbf{H}(\boldsymbol{\delta})$ and the other for the Hodge Laplacian equation.

Keywords: $\mathbf{H}(\mathbf{d}) \cap \mathbf{H}(\boldsymbol{\delta})$, *primal discretization, nonconforming finite element scheme*

The discretization of the $\mathbf{H}(\mathbf{d}) \cap \mathbf{H}(\boldsymbol{\delta})$ elliptic problems necessitates suitable in-pair discretisations of the "incomplete" operators divergence and curl. Due to difficulties come across in constructing primal discretizations, the mixed element scheme based on the continuous and discrete de Rham complex have been well accepted standard methods. Though, for the mixed element scheme, the differential and the codifferential operators are not simultaneously local, and it remains a question what a function operated by both differential and the codifferential operators can be like. There have been kinds of primal scheme for $\mathbf{H}(\mathbf{d}) \cap \mathbf{H}(\boldsymbol{\delta})$, which are generally the Crouzeix-Raviart type vector fields or interior penalty techniques are used.

This talk presents two families of primal finite element methods, one for the elliptic problem established on $\mathbf{H}(\mathbf{d}) \cap \mathbf{H}(\boldsymbol{\delta})$ and the other for the Hodge Laplacian equation. Both the two families are nonconforming, and new kinds of continuity other than Crouzeix-Raviart type are imposed. The basis of our construction is the adjoint relationship below.

Theorem *([1]) Denote* $\mathbf{T}\boldsymbol{\mu} := (\mathbf{d}^k\boldsymbol{\mu}, \boldsymbol{\delta}_k\boldsymbol{\mu})$ *and* $\mathbb{T}(\boldsymbol{\eta}, \boldsymbol{\tau}) := \boldsymbol{\delta}_{k+1}\boldsymbol{\eta} + \mathbf{d}^{k-1}\boldsymbol{\tau}$. *Then* $(\mathbf{T}, H\Lambda^k \cap H_0^*\Lambda^k)$ *and* $(\mathbb{T}, H_0^*\Lambda^{k+1} \times H\Lambda^{k-1})$ *are a pair of adjoint operators.*

The finite element spaces are then constructed aiming at establishing discrete adjoint connections. The constructions for the two types of model problems are different, reflecting the different sources of ellipticity, by the aid of the 0^{th} order terms for the $\mathbf{H}(\mathbf{d}) \cap \mathbf{H}(\boldsymbol{\delta})$ elliptic problem, and by filtering the cohomology space for the Hodge Laplacian.

Acknowledgements This work is partially supported by NSFC (12271512, 11871465).

References

[1] S. Zhang, *A primal finite element scheme of the Hodge Laplace problem*, arXiv 2208.00575.

[2] S. Zhang, *A primal finite element scheme of the* $\mathbf{H}(\mathbf{d}) \cap \mathbf{H}(\boldsymbol{\delta})$ *elliptic problem*, arXiv 2207.12003.

MS7: Model reduction via moment closures with application to complex transport phenomena based on kinetic theory and free-surface flows

Organiser: Julian Köllermeier (Ghent University and University of Groningen)

Description: Many high-dimensional applications involving kinetic descriptions of complex transport phenomena, such as non-equilibrium gas flows, polydisperse and polykinetic sprays, and radiative heat transfer, require model reduction to allow for efficient simulations of the multiscale underlying physics. Free-surface flows with complex velocity profiles are another application area that benefits from reduced models. Moment closures are one way to derive lower-dimensional PDEs that enable this efficiency while allowing for analytical derivation with physical insight. This minisymposium covers recent advances in moment closure techniques for diverse applications. The focus is not only on the derivation and analysis of the closures but also on the numerical schemes and simulation results.

Book of abstracts of the 9th International Conference on
Advanced Computational Methods in ENgineering and Applied Mathematics
September, 15–19, 2025.

High-Order Velocity Moment Coupling for Polydisperse Liquid Fuel Sprays

Kevin A. Brooks[1] and Clinton P. T. Groth[1]

[1] *Institute for Aerospace Studies, University of Toronto*

e-mails: kevin.brooks@mail.utoronto.ca, groth@utias.utoronto.ca

Abstract

This study presents an extension to existing polydisperse spray models through the modelling of a velocity variance with respect to drop size. By introducing higher-order size-velocity correlations, we demonstrate the capacity to obtain more accurate solutions to benchmark shock-tube problems. Results are presented for one-dimensional simulations comparing a classical solution to the proposed extension with both using 10 equations. The authors would like to note that this method can also be applied to systems outside the scope of sprays, such as gas kinetic systems.

Key words: Computational, Moments, Multi-Equation Models, Velocity-Size Correlation

1 Introduction

Practical engineering sprays exist in a phase space which is characterized by variable drop velocities and sizes in addition to physical space and time. The kinetic equation for sprays is given by the Williams-Boltzmann equation, given here in 1 dimension of physical space as

$$\frac{\partial \mathcal{F}(x,t,v,S)}{\partial t} + v\frac{\partial \mathcal{F}(x,t,v,S)}{\partial x} = 0 \tag{1}$$

where v is total velocity, and S is a selected size parameter [1]. The presented equation only considers transport; other effects can be included through the addition of source terms. Using the method of moments, it is possible to integrate over the velocity and size space to yield a set of partial differential equations which can be solved in just space and time.

2 Modelling Velocity Variance as a Distribution

Most studies involving sprays with multiple drop sizes (polydisperse) have neglected the correlation between drop velocity variance and drop size [4]. Empirical evidence suggests that velocity variance and drop size are correlated [2].

We propose a polydisperse Gaussian model which assigns 3 size moments, 4 momentum moments, and 3 energy moments; this model specifies a distribution of pressure which is similar to the distribution used for number density. The number of equations matches that of the partially polydisperse Gaussian closure, used here for comparison, with 5 size moments, 4 momentum moments, and 1 energy moment. Using finite difference approximations, it can

be shown that the proposed polydisperse Gaussian model is non-hyperbolic for cases with low velocity variance; thus, its application is limited.

To ensure hyperbolicity is maintained, a shock-tube problem is defined with a high velocity variance. The simulation is run with a 1000-cell uniform mesh using an HLL approximate finite volume solver [5]. The polydisperse descriptions use Beta distributions as kernel functions, as described by Yuan *et. al.* [3]. The polydisperse description solves multiple problems simultaneously: a collection of right-moving shocks, and a collection of left-moving shocks.

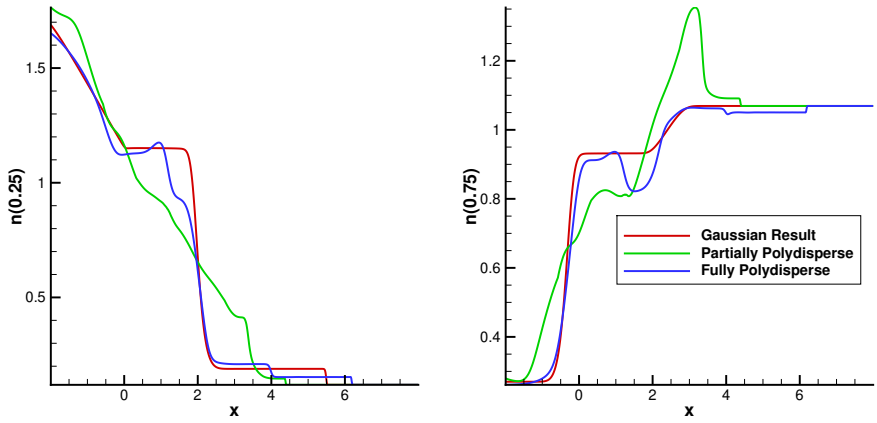

(a) Extracted slice $S = 0.25$ (b) Extracted slice $S = 0.75$

Figure 1: Simultaneous solution to shock tube problem using polydisperse moment method.

Restricting the simulation to 10 equations per cell, it is clear that the proposed fully polydisperse Gaussian model produces a result which is closer to the expected Gaussian solution.

Acknowledgements Computational resources were provided by the SciNet High Performance Computing Consortium at the University of Toronto and the Digital Research Alliance of Canada through funding from the Canada Foundation for Innovation (CFI) and the Province of Ontario, Canada. The first author also received support in the form of an Ontario Graduate Scholarship (OGS) from the Province of Ontario and University of Toronto.

References

[1] F. A. Williams , *Spray Combustion and Atomization*, Phys. Fluids. **1** (1958) 541 – 545

[2] R. Sellens , *Prediction of the Drop Size and Velocity Distribution in a Spray, Based on the Maximum Entropy Formalism*, Part. Part. Syst. Charact. **6** (1989) 17 – 27

[3] C. Yuan, F. Laurent, R. O. Fox, *An extended quadrature method of moments for population balance equations*, J. of Aerosol Sci., **51** (2012) 1–23

[4] T. Leung, C. P. T. Groth, *Moment Closure Description of Polydisperse, Polykinetic and Evaporating Liquid Sprays*, ICCFD, **11**, 2022.

[5] A. Harten, P. D. Lax, B. Leer, *On Upstream Differencing and Godunov-Type Schemes for Hyperbolic Conservation Laws*, SIAM Rev., **25** (1983) 35 – 61

Book of abstracts of the 9th International Conference on
Advanced Computational Methods in ENgineering and Applied Mathematics
September, 15–19, 2025.

Modelling the friction effect in the shallow water moment equations for granular flows

Julio Careaga[1], Qian Huang[2] and Julian Koellermeier[1,3]

[1] *Bernoulli Institute, University of Groningen*

[2] *Institute of Applied Analysis and Numerical Simulation, University of Stuttgart*

[3] *Department of Mathematics, Computer Science and Statistics, Ghent University*

e-mails: j.c.careaga.solis@rug.nl, qian.huang@mathematik.uni-stuttgart.de, julian.koellermeier@ugent.be

Abstract

Shallow-water moment equations (SWME) emerge as a generalization of the classical shallow water equations to vertically variable velocity profiles. The SWME are derived from the mass conservation and momentum balance equations under the assumption that the fluid velocity is described by a polynomial expansion in the vertical coordinate. The moments, which are the coefficients of the polynomial expansion, together with the water height and mean velocity are modelled by a coupled system of nonlinear transport equations. In this work, we study the friction term arising in the momentum and moment equations, which results as a remaining term from the treatment of the viscous-stress tensor. We propose a modelling procedure to incorporate general friction terms to the SWME particularly addressing the case of granular flows. Moreover, we develop a finite volume numerical scheme for correctly approximating the stiffness of the friction source terms. Numerical simulations are presented for different models of friction, including the case of wet-dry fronts.

Keywords: Shallow Water Moment Equations, Granular flows, Friction Effect

1 Shallow-water moment equations with friction

Under the assumption of shallowness of a water body, the well-known Navier-Stokes equations accounting for the mass conservation and momentum balance of the fluid can be reduced. The shallow-water moment equations (SWE) are then formulated assuming that the water velocity is given by a polynomial expansion in the vertical coordinate, which is scaled to the normalized coordinate $\zeta \in [0, 1]$, see [1]. This ansatz allows for a more general description of the velocity profile, including vertical variations and a more physically correct bottom velocity.

We let $h(x, t)$ be the water height and $u_m(x, t)$ be the depth-averaged velocity, with x and t being the horizontal coordinate and time, respectively. The flow velocity is then assumed to be defined by the polynomial expansion

$$u(x, \zeta, t) = u_m(x, t) + \alpha_1(x, t)\phi_1(\zeta) + \alpha_2(x, t)\phi_2(\zeta) + \cdots + \alpha_N(x, t)\phi_N(\zeta),$$

where the coefficients $\alpha_1, \alpha_2, \ldots, \alpha_N$ are the so-called moments, and the functions $\phi_1, \phi_2, \ldots, \phi_N$ are scaled Legendre polynomials. The hyperbolic shallow water moment equations for Newtonian or Granular flows can be then written as a hyperbolic system of the type:

$$\partial_t \boldsymbol{U} + \boldsymbol{A}\partial_x \boldsymbol{U} = \mathrm{S}(\boldsymbol{U}, x), \qquad \boldsymbol{U} = (h, hu_m, h\alpha_1, h\alpha_2, \ldots, h\alpha_N) \in \mathbb{R}^{N+2}, \tag{1}$$

where $\boldsymbol{A} \in \mathbb{R}^{N+2\times N+2}$ is the system matrix, see [2], and $\mathrm{S} \in \mathbb{R}^{N+2}$ is the source term, which includes the friction terms at the bottom $\tau_{xz}|_{\mathrm{b}}$, and at the water surface $\tau_{xz}|_{\mathrm{s}}$, and an additional bulk friction term given by

$$\mathcal{T}_{\mathrm{bulk},j} = \int_0^1 \tau_{xz}(\zeta)\phi_j'(\zeta)\,\mathrm{d}\zeta, \qquad \text{for } j = 1, \ldots, N.$$

The function τ_{xz} is related to the viscous-stress tensor and depends on the viscosity of the fluid. Unlike standard shallow water equations, the additional bulk friction term $\mathcal{T}_{\mathrm{bulk},j}$ requires the information of the stress related function τ_{xz} for all values $\zeta \in [0, 1]$. In the case of Granular flows, the definition of τ_{xz} at the boundaries, and the calculation of $\mathcal{T}_{\mathrm{bulk},j}$ may become non-trivial depending on the definition of the viscosity.

In this work, we have established a formal procedure for modelling the friction term τ_{xz} in granular flows for general viscosity functions. The procedure consists of defining τ_{xz} directly from the viscous-stress tensor, compute the dimensionless version of it in the transformed ζ-coordinate, and then calculate $\mathcal{T}_{\mathrm{bulk},j}$ with a quadrature rule in the general case. To approximate (1), we propose a finite volume scheme based on the so-called PVM methods [3], and a splitting approach to handle stiffness of the source S for small values of h and general forms of τ_{xz}. Numerical examples of different cases such as the classical Newtonian friction and Savage-Hutter friction model for the case of wet-dry fronts are also included in this work.

Acknowledgements This work is supported by the *Dutch Research Council (NWO)* through the ENW Vidi project *HiWAVE* with file number VI.Vidi.233.066.

References

[1] J. Kowalski, M. Torrilhon, *Moment Approximations and Model Cascades for Shallow Flow*, Commun. in Comput. Phys. **25** (2019), 669–702.

[2] J. Koellermeier and M. Rominger, *Analysis and Numerical Simulation of Hyperbolic Shallow Water Moment Equations*, Commun. in Comput. Phys. **28** (2020), 1038–1084.

[3] M. J. Castro Díaz and E. Fernández-Nieto, *A Class of Computationally Fast First Order Finite Volume Solvers: PVM Methods*, SIAM J. Sci. Comput. **34** (2012), A2173–A2196.

Book of abstracts of the 9th International Conference on
Advanced Computational Methods in ENgineering and Applied Mathematics
September, 15–19, 2025.

Asymptotic Analysis of Shallow Water Moment Models

Mieke Daemen[1], Julio Careaga [1] and Julian Koellermeier[1,2]

[1] *Bernoulli Institute, University of Groningen*

[2] *Department of Mathematics, Computer Science and Statistics, Ghent University*

e-mails: m.e.f.daemen@rug.nl, j.c.careaga.solis@rug.nl,
Julian.koellermeier@ugent.be

Abstract

The shallow-water moment equations (SWME) represent an extension of the shallow-water equations (SWE) for modeling free-surface flows. Unlike the SWE, which assume a constant vertical velocity, the SWME allow the possibility of a non-uniform vertical velocity profile. Within the SWME framework, the vertical velocity profiles are approximated using polynomial expansions. One cost associated with the SWME is the increased number of variables that must always be incorporated, even in scenarios where the flow approaches an equilibrium state that could be characterized by fewer variables. To simplify the SWME in cases proximate to these equilibria, we conduct an asymptotic expansion for small deviations around various equilibria. We are investigating whether this process yields closed-form equations for the perturbations from equilibrium. Initial results for a case with high slip indicate that such a simplified solution can indeed be found. Furthermore, we also investigate hyperbolicity in our research. For future research, we will focus on different equilibrium cases.

Keywords: Free-surface flows, Shallow Water Moment Equations, asymptotic analysis

1 Shallow-Water Moment Equations with Bottom Friction

The shallow-water equations (SWE) are hyperbolic partial differential equations modeling free-surface flows with horizontal scales larger than vertical scales, commonly used in oceanic and river flow simulations. Since the SWE lack vertical information, we employ the shallow-water moment equations (SWME) system with bottom friction [1]. The SWME approximate vertical velocity profiles using polynomial expansions. Our objective is to examine the vertical velocity profiles around various equilibria in a system with bottom friction.

Let $u_m(x,t)$ be the depth-averaged velocity that is independent of the vertical scale, and let $h(x,t)$ be the water height. Within the SWME framework, the velocity is expanded around the average as: $u(t,x,\xi) = u_m(x,t)+\alpha_1(x,t)\phi_1(\xi)+\cdots+\alpha_N(x,t)\phi_N(\xi)$, where $\zeta = (z-b)/h \in [0,1]$ is a scaled vertical variable and α_i and ϕ_i for $i = 1,\dots,N$ denote coefficients and scaled Legendre polynomials, respectively [1].

In [1], applying higher-order depth integration to the incompressible Navier Stokes equations with hydrostatic pressure yields closed evolution equations for variables h, u_m, α_i, for

$i = 1 \ldots, N$. For example N = 2, this system reads:

$$\partial_t \begin{pmatrix} h \\ hu_m \\ h\alpha_1 \\ h\alpha_2 \end{pmatrix} + \partial_x \begin{pmatrix} hu_m \\ hu_m^2 + \frac{1}{3}h\alpha_1^2 + \frac{1}{5}h\alpha_2^2 + g\frac{h^2}{2} \\ 2hu_m\alpha_1 + \frac{4}{5}\alpha_1\alpha_2 \\ 2hu_m\alpha_2 + \frac{2}{3}h\alpha_1^2 + \frac{2}{7}h\alpha_2^2 \end{pmatrix} = \begin{pmatrix} 0 \\ 0 \\ (u_m - \frac{1}{5}\alpha_2)\partial_x(h\alpha_1) + \frac{1}{5}\alpha_1\partial_x(h\alpha_2) \\ \alpha_1\partial(h\alpha_1) + (u_m + \frac{\alpha_2}{7})\partial_x(h\alpha_2)) \end{pmatrix} - \frac{\nu}{\lambda}\begin{pmatrix} 0 \\ u_m + \alpha_1 + \alpha_2 \\ 3(u_m + \alpha_1 + \alpha_2) \\ 5(u_m + \alpha_1 + \alpha_2) \end{pmatrix} - \frac{\nu}{h}\begin{pmatrix} 0 \\ 0 \\ 12\alpha_1 \\ 60\alpha_2 \end{pmatrix}. \tag{1}$$

where λ and ν denote the friction parameters slip length and viscosity, respectively.

2 Applying Asymptotic Analysis to a Specific Example

In [2], the coefficients α_1 and α_2 in the $N = 2$ system 1 are approximated under the assumption that $\nu = \frac{\nu_0}{\varepsilon}$ and $\lambda = \frac{\lambda_0}{\varepsilon}$, where ε is a small value. Note that $\varepsilon \to 0$, corresponds to a stable equilibrium in [3], where all the moment variables are equal to zero. Asymptotic expressions are developed for the coefficients up to order $i = 1, 2$: $\alpha_i = \alpha_i^{(0)} + \varepsilon\alpha_i^{(1)} + \varepsilon^2\alpha_i^{(2)} + \ldots$ and substituted in Equation (1). By using a magnitude of orders analysis approximations for moments up to order $O(\varepsilon^2)$-can be found:

$$\alpha_1 \approx \varepsilon\frac{-u_m h}{4\lambda_0} + \varepsilon^2\frac{\lambda_0}{48\nu_0}\left(\frac{-g}{4}\partial_x(h^4) + 3\frac{\nu_0}{\lambda_0}u_m h^2\right), \quad \alpha_2 \approx \varepsilon\frac{-u_m h}{12\lambda_0} + \varepsilon^2\frac{\lambda_0}{720\nu_0}\left(\frac{-g}{4}\partial_x(h^4) + 19\frac{\nu_0}{\lambda_0}u_m h^2\right).$$

The presentation will cover the extension of this method to problems with an arbitrary number of moments, hyperbolicity analysis, and analysis of various types of equilibria.

Acknowledgements This work is part of the project *HiWAVE* with file number VI.Vidi.233.066 of the *ENW Vidi* research programme, funded by the *Dutch Research Council (NWO)*.

References

[1] J. Kowalski, M. Torrilhon, *Moment Approximations and Model Cascades for Shallow Flow*, Commun. in Comput. Phys. **25** (2019).

[2] D. Wang, *Extensions and Simulations of Shallow Water Equations*, MSc thesis, University of Singapore (2023).

[3] Q. Huang, J. Koellermeier, W. Yong, *Equilibrium stability analysis of hyperbolic shallow water moment equations*, Math. Meth. Appl. Sci. **45** (2022).

Book of abstracts of the 9th International Conference on
Advanced Computational Methods in ENgineering and Applied Mathematics
September, 15–19, 2025.

High-Order Flux Reconstruction Methods for Hyperbolic Moment Closures

Clinton P. T. Groth[1]

[1] *Institute for Aerospace Studies, University of Toronto*

e-mails: groth@utias.utoronto.ca

Abstract

Moment closure methods based on maximum-entropy principals offer efficient and effective strategies for predicting high-speed non-equilibrium gaseous flows with shocks ranging from the near-equilibrium continuum regime well into the so-call transition regime, without necessitating the solution of the underlying high-dimensional Boltzmann kinetic equation. In the present study, a high-order flux reconstruction (FR) scheme is considered for the solution of both the second- and fourth-order maximum-entropy closures associated with a representative one-dimensional kinetic equation and relaxation-time approximation for the collision operator. A limiting technique is considered for the high-order FR schemes so as to effectively manage shocks and discontinuities while avoiding unwanted oscillations and preserving accuracy. The potential effectiveness of the proposed high-order FR schemes with limiting are demonstrated via application to a range of problems, including those with shocks, and future application to the multi-dimensional case is discussed.

Key words: kinetic theory, moment closure methods, hypebolic systems, high-order methods, flux reconstruction, shocks

Book of abstracts of the 9th International Conference on
Advanced Computational Methods in ENgineering and Applied Mathematics
September, 15–19, 2025.

Moment models for free-surface flows and their energy conservation properties

Julian Koellermeier[1,2]

[1] *Department of Mathematics, Computer Science and Statistics, University of Ghent*

[2] *Bernoulli Institute, University of Groningen*

e-mails: julian.koellermeier@ugent.be

Abstract

Shallow Water Moment Equations (SWME) are extensions to the well-known Shallow Water Equations (SWE) for the numerical simulation of free-surface flows. In contrast to the SWE, which typically assume a constant depth-averaged vertical velocity profile, the SWME allow for vertical variations of the velocity profile, by assuming a polynomial profile and then deriving additional evolution equations for the polynomial coefficients via higher order depth integration. Different versions of the SWME have been derived, e.g., to mitigate a potential loss of hyperbolicity, or to include more physical effects like sediment transport. In this work, we compare existing models that appear in the recent literature. We then focus on the derivation of an energy equation as an extension to the standard energy equation for the SWE. We show how different SWME models may or may not allow for an analytical energy equation derivation, which opens up possibilities for numerically preserving this energy equation.

Keywords: Free-surface flows, Shallow Water Moment Equations, energy equation

1 Shallow Water Equations and energy conservation

Shallow flows are occurring in a wide range of free-surface flow scenarios, ranging from ocean or river waves to avalanches and mud flows. These shallow flows are characterized by situations in which the surface wave length is much larger than the waer depth. For the purpose of this work, we assume a simple 1D setting and neglect friction terms. Those can readily be found in the respective literature.

The most commonly used model to simulate such flows are the Shallow Water Equations (SWE). They assume a constant velocity and are derived using depth-averaging of the underlying Navier-Stokes equations. In a 1D setting with known bottom topography term b, the system of two PDEs for the water height h and the depth-averaged velocity u_m reads

$$\partial_t h + \partial_x (h u_m) = 0, \qquad \partial_t (h u_m) + \partial_x \left(h u_m^2 + \frac{1}{2} g h^2 \right) = -g h \partial_x b, \tag{1}$$

It is well known that for the SWE (1) an energy equation can be derived as

$$\partial_t \left(\frac{h u_m^2}{2} + g \frac{h^2}{2} + g h b \right) + \partial_x \left(\frac{h u_m^3}{2} + g h u_m (h + b) \right) = 0, \tag{2}$$

in which the energy is a conserved quantity and an entropy function with entropy flux $f = \frac{h u_m^3}{2} + g h u_m (h + b)$. This allows tailored numerical methods to preserve energy discretely.

2 Shallow Water Moment Equations and energy conservation

The SWME model is based on the vertical velocity expansion $u(t,x,z) = u_m + \sum_{i=0}^{N} \alpha_i \phi_i \left(\frac{z-h_b}{h}\right)$, where $\zeta = \frac{z-b}{h} \in [0,1]$ is a scaled vertical variable and α_i and ϕ_i for $i = 1,\dots,N$ are the polynomial coefficients and the orthogonal Legendre polynomials on $[0,1]$, respectively, see [1].

Evolution equations for the variables h, u_m, α_i for $i = 1,\dots,N$ are derived via higher-order depth integration of the underlying Navier-Stokes equations, resulting in

$$\partial_t h + \partial_x (h u_m) = 0, \qquad \partial_t (h u_m) + \partial_x \left(h u_m^2 + h \sum_{j=1}^{N} \frac{\alpha_j^2}{2j+1} + \frac{1}{2} g h^2 \right) = -g h \partial_x b, \tag{3}$$

$$\partial_t (h\alpha_i) + \partial_x \left(h \left(2 u_m \alpha_i + \sum_{j,k=1}^{N} A_{ijk} \alpha_j \alpha_k \right) \right) = u_m \partial_x (h\alpha_i) - \sum_{j,k=1}^{N} B_{ijk} \alpha_k \partial_x (h\alpha_j), \tag{4}$$

with $A_{ijk} = (2i+1) \int_0^1 \phi_i \phi_j \phi_k d\zeta$ and $B_{ijk} = (2i+1) \int_0^1 \phi_i' \left(\int_0^\zeta \phi_j d\zeta \right) \phi_k d\zeta$.

Different variants of the full SWME (3)-(4) exist by approximating the coefficients A_{ijk} and B_{ijk}, see [2, 3]. As one example, using $A_{ijk} = 0, B_{ijk} = 0$ leads to the so-called Shallow Water Linearized Moment Equations (SWLME). For those, an energy equation reads [4]

$$\partial_t \left(\frac{h u_m^2}{2} + \frac{h}{2} \sum_{i=1}^{N} \frac{\alpha_i^2}{2i+1} + g \frac{h^2}{2} + g h b \right) + \partial_x \left(\frac{h u_m^3}{2} + h u_m \frac{3}{2} \sum_{i=1}^{N} \frac{\alpha_i^2}{2i+1} + g h u_m (h+b) \right) = 0. \tag{5}$$

In our work, we will dive deeper into the derivation of energy equations for other versions of the SWME that may lead to energy conserving numerical schemes.

Acknowledgements This publication is part of the project *HiWAVE* with file number VI.Vidi.233.066 of the *ENW Vidi* research programme, funded by the *Dutch Research Council (NWO)*.

References

[1] J. Kowalski, M. Torrilhon, *Moment Approximations and Model Cascades for Shallow Flow*, Commun. in Comput. Phys. **25** (2019).

[2] J. Koellermeier, M. Rominger, *Analysis and Numerical Simulation of Hyperbolic Shallow Water Moment Equations*, Commun. in Comput. Phys. **28** (2020).

[3] J. Koellermeier, E. Pimentel-García, *Steady states and well-balanced schemes for shallow water moment equations with topography*, Appl. Math. Comput. **427** (2022).

[4] C. Caballero-Cárdenas, I. Gómez-Bueno, A. Del Grosso, J. Koellermeier, T. Morales de Luna, *A semi-implicit exactly fully well-balanced relaxation scheme for the Shallow Water Linearized Moment Equations*, Comput. Meth. Appl. Mech. Eng. **437** (2025).

Book of abstracts of the 9th International Conference on
Advanced Computational Methods in ENgineering and Applied Mathematics
September, 15–19, 2025.

Sparse kinetic distribution estimation

Georgii Oblapenko[1], Lambert Theisen[1], Michael Herty[2] and Manuel Torrilhon[1]

[1] *Applied and Computational Mathematics, RWTH Aachen, Aachen, Germany*

[2] *Institute of Geometry and Applied Mathematics, RWTH Aachen, Aachen, Germany*

e-mails: oblapenko@acom.rwth-aachen.de, theisen@acom.rwth-aachen.de, herty@igpm.rwth-aachen.de, mt@acom.rwth-aachen.de

Abstract

In the present work, sparse reconstructions of kinetic distributions on the basis of given moments thereof are investigated via optimization-based approaches and low-rank representation methods. The developed methods are applied to model kinetic distributions arising in various kinetic theory problems.

Key words: Boltzmann equation, kinetic theory, low-rank decomposition, sparsity
MSC 2020: Mathematics Subject Classification, separated by comma (optional)

1 Introduction

Accurate modeling of rarefied gas flows is highly relevant to a wide variety of applications, ranging from nano-scale devices to atmospheric re-entry and satellite propulsion [1]. Classical fluid models fail to correctly describe the physics of rarefied gases, whereas numerical methods such as Direct Simulation Monte Carlo (DSMC) [1] are oftentimes prohibitively expensive. Moment methods extend classical fluid models to stronger rarefaction regimes by modeling the evolution of higher-order moments of the underlying distribution function [2]; however, a closure relation is required to express the fluxes in terms of the known moments. Numerous methods have been developed for such closures, with some of them relying on a reconstruction of the underlying velocity distribution function (VDF), from which any required moment can be directly computed.

In the present work, we investigate two approaches for moment-constrained distribution function reconstruction that impose sparsity in the ansatz used to represent the VDF. Imposition of sparsity not only regularizes the under-determined problem of reconstructing a high-dimensional distribution function from a limited number of moments, but also serves to reduce the memory constraints associated with such a reconstruction, especially in case of multi-dimensional velocity distribution functions.

2 Optimization-based sparse reconstruction

The first approach is based on the following ansatz for the distribution function f:

$$f(v) = \sum f_i \delta(v - v_i). \tag{1}$$

Here v_i are fixed velocities, and $f_i \geq 0$ are the unknown expansion weights. These can be determined by solving an optimization problem for the discrete entropy with linear moment constraints. The standard approach of enforcing sparsity by adding an L_1 regularization term is not applicable in this case, as $\sum_i |f_i| = \sum_i f_i$ corresponds to the number density, a conserved moment. Therefore, we will investigate pre-conditioning techniques that allow for improved convergence and imposition of sparsity via introduction of additional fixed weights w_i:

$$f(v) = \sum w_i f_i \delta(v - v_i). \tag{2}$$

Additionally, a variance-reduced approach will also be studied, in which only the deviation of f from an equilibrium distribution is reconstructed.

3 Moment-preserving low-rank decomposition

Complementary to sparsity, we exploit the empirical observation that many non-equilibrium VDFs exhibit pronounced *low-rank* structure in velocity space [3]. Instead of penalizing the rank, we *enforce* it by restricting the admissible set to a fixed-rank manifold $\mathcal{M}_{\mathrm{LR}}$ and minimize the squared moment mismatch

$$f^{(*)} = \arg\min_{f \in \mathcal{M}_{\mathrm{LR}}} \left\| M_\alpha - \int \psi_\alpha(v) f(v)\, \mathrm{d}v \right\|^2.$$

This reduces to a classical tensor-completion problem [4], which we tackle with projected gradient descent and direct optimization of CP, Tucker, and tensor-train (TT) factorizations.

Acknowledgements The authors acknowledge the support of the Deutsche Forschungsgemeinschaft (DFG, German Research Foundation) through 442047500/SFB1481 “Sparsity and Singular Structures” within the project B04 (Sparsity fördernde Muster in kinetischen Hierarchien).

References

[1] G. Bird, *Molecular gas dynamics and the direct simulation of gas flows* , Oxford University Press, 1994.

[2] H. Grad, *On the kinetic theory of rarefied gases*, Commun. Pure Appl. Math. **2(4)** (1949) 331–407.

[3] A. V. Chikitkin, E. K. Kornev, and V. A. Titarev, *Numerical solution of the Boltzmann equation with S-model collision integral using tensor decompositions*, Comput. Phys. Commun. **264** (2021) 107954.

[4] H. Rauhut, R. Schneider, and Ž. Stojanac, *Tensor completion in hierarchical tensor representations*, Compressed Sensing and Its Applications: MATHEON Workshop 2013 (2015) 419–450.

Book of abstracts of the 9th International Conference on
Advanced Computational Methods in ENgineering and Applied Mathematics
September, 15–19, 2025.

Intrinsic Dimension Estimating Autoencoder (IDEA) Using CancelOut layer and a Projected Loss Application to Vertically Resolved Shallow Flow Simulations

Antoine Oriou[1,3], Julian Koellermeier[1,2] and Philipp Krah[4]

[1] *Department of Mathematics, Computer Science and Statistics, University of Ghent*

[2] *Bernoulli Institute, University of Groningen*

[3] *CentraleSupélec, University Paris-Saclay*

[4] *Groupe Théorie et Simulation Numérique, IRFM - CEA Cadarache*

e-mails: antoine.oriou@student-cs.fr, ,

Abstract

This paper investigates the use of an autoencoder neural network to estimate the intrinsic dimension underlying a dataset. We introduce the Intrinsic Dimension Estimating Autoencoder (IDEA), a versatile model capable of identifying the intrinsic dimension across a wide range of datasets whose samples lie on either linear or nonlinear manifolds. Beyond estimating the intrinsic dimension, IDEA is also able to reconstruct the original dataset after projecting it onto the corresponding latent space.

We apply this model to data generated from the numerical solution of a vertically resolved one-dimensional free-surface flow, following a pointwise discretization of the vertical velocity profile in the horizontal direction, vertical direction, and time. IDEA succeeds in estimating the dataset's intrinsic dimension, and then reconstructs the original solution by working directly within the projection space identified by the network.

In addition, we assess the performance of IDEA on a series of theoretical benchmarks to validate its robustness. These experiments allow us to test its reconstruction ability and compare its performance with state-of-the-art intrinsic dimension estimators. The benchmarks show good accuracy and high versatility of our approach.

Keywords: Autoencoder, Intrinsic dimension, Cancel-out layer, Free-surface flow.

1 Intrinsic dimension of a dataset

The intrinsic dimension (ID) of a dataset is a fundamental quantity that refers to the minimum number of parameters required to represent the data with satisfactory accuracy. We consider datasets represented as matrices $M \in \mathcal{M}_{n,p}(\mathbb{R})$ where, following standard machine learning notation, n denotes the number of samples and p the number of features. Such a dataset corresponds to a collection of points in $\mathbb{R}^p$, where p is the embedded dimension.

The objective is to determine whether there exists a lower-dimensional space of dimension $d < p$ from which the original data can be accurately reconstructed. To this end, we leverage an autoencoder, a deep learning model approximating the identity function via

$g_\phi(f_\theta(x)) \approx x$, where $f_\theta : \mathbb{R}^p \to \mathbb{R}^d$ is the encoder and $g_\phi : \mathbb{R}^d \to \mathbb{R}^p$ is the decoder, with $d \ll p$. ϕ and θ denote the parameters of the model (see Figure 1).

Within the network, the input is compressed into a latent space of dimension d, called the bottleneck. Thus, if the reconstruction remains accurate, this suggests that the ID of the data is at most d. Our goal is therefore to guide the autoencoder toward using the smallest possible latent dimension without degrading reconstruction quality. This is achieved through a regularization strategy that combines an innovative projected loss term and an adapted architecture of the bottleneck based on the CancelOut layer proposed in [1].

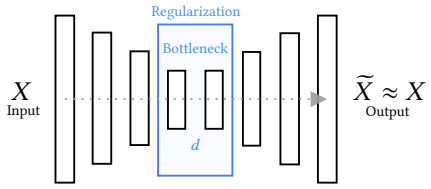

Figure 1: Architecture of IDEA

2 Application to the vertically resolved free-surface flow

Shallow flow models are widely used in applications such as weather forecasting and simulation-based natural hazard assessment [2]. We consider a vertically resolved one-dimensional free-surface shallow flow PDE model, which describes the evolution of the horizontal component of the vertical velocity profile $u(t, x, \zeta)$ and the free surface height $h(t, x)$ over time and along the x axis, where $\zeta \in [0, 1]$ denotes the vertical coordinate.

While the solution can be discretized pointwise in the ζ direction, often only a few macroscopic variables can describe the full vertical velocity profile, in which case their number corresponds to the ID of the profiles. One example is the vertical average $u_m(t, x)$, which could be computed purely from the reduced shallow water equations. However, such simple models often fail to capture important vertical dynamics in realistic settings.

To address this limitation, we propose using IDEA to learn a compact and informative latent representation of the vertical velocity profile. Specifically, we apply our model to data generated from a pointwise numerical discretization of the vertically resolved system, on a grid of size $n_t \times n_x \times n_\zeta$, as in [2]. The resulting solution is transformed into a dataset represented as a matrix $M \in \mathcal{M}_{n_x \times n_t, n_\zeta}(\mathbb{R})$. IDEA successfully balances computational efficiency and reconstruction accuracy by learning a precise mapping of the full solution into a lower-dimensional latent space of size $1 < d < n_\zeta$, thus identifying the ID of the velocity profiles.

Acknowledgements This publication is part of the project *HiWAVE* with file number VI.Vidi.233.066 of the *ENW Vidi* research programme, funded by the *Dutch Research Council (NWO)*.

References

[1] V. Borisov, J. Haug, G. Kasneci, *CancelOut: A Layer for Feature Selection in Deep Neural Networks*, in Proc. ECML PKDD, Springer (2019), pp. 72–83.

[2] J. Kowalski, M. Torrilhon, *Moment Approximations and Model Cascades for Shallow Flow*, Commun. in Comput. Phys. **25** (2019).

Book of abstracts of the 9th International Conference on
Advanced Computational Methods in ENgineering and Applied Mathematics
September, 15–19, 2025.

Moment Approximations to Shallow Flows with Non-Hydrostatic Pressure

Robin Paar[1] **and Manuel Torrilhon**[2]

[1] *Research Training Group EDDy, RWTH Aachen University*

[2] *Chair of Applied and Computational Mathematics, RWTH Aachen University*

e-mails: paar@eddy.rwth-aachen.de, mt@acom.rwth-aachen.de

Abstract

Today, the well-known Shallow Water Model has a wide range of applications from weather forecasting to debris flow. It can be used whenever the shallowness allows a vertical-averaging. One of the biggest advantages are the low computational cost but it comes with the price of losing vertical information, e.g., the flows velocity profile. To overcome this limitation the Shallow Moment Models are introduced. The vertical velocity profile is assumed to be polynomial. These models are also computational advantageous but keep information in the vertical direction despite averaging. We focus on the case of non-hydrostatic pressure, which was introduced before as Dispersive Shallow Moment Model (DSM) and generalize this model in the linear case. Furthermore, we show what are the difficulties to derive the same model for the non-linear case. For the linear model we present some numerical results both in the static and non-static case and compare to the classic Shallow Moment Model.

Key words: Dispersive model, Free-surface flows, Non-hydrostatic pressure, Moment approximation, Shallow flow

1 The Linear Dispersive Shallow Moment Model

The Shallow Moment Models are introduced to describe flows better than the classical Shallow Flow Models. They are computational cheap and overcome the disadvantage of losing vertical information through depth averaging. They can be seen as a generalization of Shallow Flow Models and fill the gap between them and the fully resolved flow. The starting point to derive this models are the mapped free surface Euler equations with different assumptions on pressure and stress. The common approach is to assume the vertical velocity profile to be an expansion of orthogonal polynomials. With this approach it is possible to keep the vertical information during the averaging and combine an higher accuracy with the advantage of low computational costs. There is a wide range of physically assumption that lead to different models for different applications. They are first introduced with a hydrostatic pressure and surface stresses [1]. It is also possible to combine the approach with various kinds of models like Multilayer Methods [3].
We follow here the work of [2] and consider a non-hydrostatic pressure. We generalize the introduced Dispersive Shallow Moment Model (DSM) in the linear case and write it down in a

more concise way. We assume that the pressure consists of a hydrostatic part and a deviation, i.e., $p = p_{\text{hyd}} + q$. We decompose the velocity and pressure deviation in the form

$$\boldsymbol{U}(t,x,y,\zeta) = \boldsymbol{U}_m(t,x,y) + \sum_{j=1}^{N} \boldsymbol{\Lambda}_j(t,x,y)\phi_j(\zeta), \tag{1}$$

where t is the time, $(x, y, \zeta = \frac{z-h_b(x,y)}{h(t,x,y)})$ are the spatial coordinates, h is the fluid height and h_b stand for the bottom topography, $\boldsymbol{U} = (u, v, w, q)^T$ denotes the vector of velocity $\boldsymbol{u} = (u, v, w)^T$ and pressure deviation q, $\boldsymbol{U}_m$ are the depth averaged quantities and $\boldsymbol{\Lambda}_j = (\alpha_j, \beta_j, \gamma_j, \kappa_j)^T$ denotes the coefficient vector of the orthogonal Legendre polynomials on $[0, 1]$ for $j = 1, \dots, N$. The averaging for an arbitrary order N gives the equations

$$\begin{cases} \partial_t \boldsymbol{u}_m + (\boldsymbol{u}_0 \cdot \tilde{\nabla})\boldsymbol{u}_m + g\tilde{\nabla}h + \tilde{\nabla}q_m = -g\tilde{\nabla}h_b + A_0(q_m, \{\kappa_j\}_j)\boldsymbol{e}_\zeta, & i = 0 \\ \partial_t \boldsymbol{\Lambda}_i + (\boldsymbol{u}_0 \cdot \tilde{\nabla})\boldsymbol{\Lambda}_i + \tilde{\nabla}\kappa_i = (2i+1)A_i(q_m, \{\kappa_j\}_j)\boldsymbol{e}_\zeta, & i \geq 1 \end{cases},$$

where we have in addition a Poisson problem to determine the pressure coefficients derived from the divergence free condition

$$\begin{cases} \tilde{\Delta}p = -B_0(A_0, \{(2j+1)A_j\}_j), & i = 0, \\ \tilde{\Delta}\kappa_i = -B_i(A_0, \{(2j+1)A_j\}_j), & i \geq 1 \end{cases}$$

with $\tilde{\nabla} = (\partial_x, \partial_y, \frac{1}{h_0}\partial_\zeta)$,$\tilde{\Delta} = \tilde{\nabla} \cdot \tilde{\nabla}$, a constant vector $\boldsymbol{u}_0$ and the operators A_k, B_k, $k = 0, \dots, N$.

2 Extension to the Non-Linear Model

It is in a similar way possible to derive a general non-linear Dispersive Shallow Moment Model. Here one of the key difficulties are the derivation of the pressure equations since the differential operators do not commute in this case. In addition the operators A_k, B_k have a more complicated form. We show some current results in the development of such a model and give an outlook to further investigations.

Acknowledgements This work is funded by the Deutsche Forschungsgemeinschaft (DFG, German Research Foundation) – 320021702/GRK2326 – Energy, Entropy, and Dissipative Dynamics (EDDy).

References

[1] J. Kowalski, M. Torrilhon, *Moment approximation and model cascades for shallow flow*, Commun. in Comput. Phys. **25** (2019)

[2] U. Scholz, J. Kowalski, M. Torrilhon, *Dispersion in Shallow Moment Equations*, Commun. Appl. Math. Comput. **6** (2023).

[3] J.Garres-Díaz, C. Escalante, T. Morales de Luna, M.J. Castro Díaz, *A general vertical decomposition of Euler equations: Multilayer-moment models*, Applied Numerical Mathematics **183** (2022).

Book of abstracts of the 9th International Conference on
Advanced Computational Methods in ENgineering and Applied Mathematics
September, 15–19, 2025.

Moment Approximations to Magnetic Rotating Shallow Flows

Michael Redle[1], Julian Koellermeier[2,3] and Manuel Torrilhon[1]

[1] *Chair of Applied and Computational Mathematics, RWTH Aachen University*

[2] *Department of Mathematics, Science and Statistics, University of Ghent*

[3] *Bernoulli Institute, University of Groningen*

e-mails: redle@acom.rwth-aachen.de, julian.koellermeier@ugent.be, mt@acom.rwth-aachen.de

Abstract

Originally introduced to describe a transition region in stars, the magnetic rotating shallow water (MRSW) model is now used for a number of solar physics and geophysical applications. Derived from the 3-D incompressible ideal magnetohydrodynamic system, the shallow nature of these applications motivates depth-averaging of both the velocities and magnetic fields. This is advantageous in terms of computational efficiency—but at the loss of vertical information, thus limiting the predictive power of the MSRW model. To overcome this problem, we employ higher-order vertical moments, but now in the context of conductive fluids. In doing so, the new approximation maintains non-constant vertical profiles of the horizontal magnetic fields in addition to those of the horizontal velocities, while still remaining in the simplified 2-D framework corresponding to depth integration. Through 1-D numerical results for MRSW moment systems up to third-order, we show that these moment approximations for MRSW reduce model error in certain parameter regimes. Furthermore, we demonstrate that these models have the potential to increase the predictive power of conductive shallow flow models without significantly sacrificing computational efficiency.

Key words: Free-surface flows, Magnetohydrodynamics, Moment approximation

1 The Magnetic Rotating Shallow Water Moment Equations

The rotating shallow water magnetohydrodynamic equations, also referred as magnetic rotating shallow water (MRSW) equations, describe the behavior of a thin layer, conductive fluid with a free surface. Since their introduction in the context of solar tachocline, the thin layer of the Sun between the convective and radiative zones [1], the number of applications has vastly grown; some examples include neutron star atmosphere dynamics and accreting matter flows, and exoplanets with magnetically active atmospheres. While these applications can be described by the fully 3-D incompressible magnetohydrodynamic system, the 'shallow fluid' assumption leads to a reduced complexity 2-D model through depth averaging, thus significantly lowering computational cost.

This comes at the cost of losing vertical information. To mitigate these losses without returning back to the expensive 3-D model, we follow the work of [2] and extend the derivation of the shallow water moment equations to now account for magnetic field effects. That is, we expand the velocities and magnetic fields about their depth-averaged quantities:

$$\mathbf{W}(t,x,y,z) = \mathbf{W}_m(t,x,y) + \sum_{i=1}^{M} \mathbf{\Psi}_i(t,x,y)\phi_i\left(\frac{z - Z(t,x,y)}{h(t,x,y)}\right), \tag{1}$$

where t is time, (x,y,z) denotes the spatial coordinate, $\mathbf{W} = (u,v,a,b)^\top$, $\mathbf{u} = (u,v)^\top$ denotes the velocities, $\mathbf{b} = (a,b)^\top$ is the magnetic field, h is the fluid height, with Z denoting the bottom topography, and $\mathbf{\Psi}_i = (\alpha_i, \beta_i, \gamma_i, \eta_i)^\top$ are the polynomial coefficients to the orthogonal Legendre polynomials ϕ_i on $[0,1]$ for $i = 1,\dots,M$.

Doing higher-order depth-averaging results in the arbitrary-order hierarchical model we will refer to as the MRSW moment equations. For example, the 1-D system for $M = 1$ reads

$$\begin{pmatrix} h \\ hu_m \\ hv_m \\ ha_m \\ hb_m \\ h\alpha_1 \\ h\beta_1 \\ h\gamma_1 \\ h\eta_1 \end{pmatrix}_t + \begin{pmatrix} hv_m \\ hu_m v_m + \frac{1}{3}h\alpha_1\beta_1 - ha_m b_m - \frac{1}{3}h\gamma_1\eta_1 \\ hv_m^2 + \frac{1}{3}h\beta_1^2 - hb_m^2 - \frac{1}{3}h\eta_1^2 + \frac{g}{2}h^2 \\ ha_m v_m + \frac{1}{3}h\beta_1\gamma_1 - hb_m u_m - \frac{1}{3}h\alpha_1\eta_1 \\ 0 \\ hu_m\beta_1 + hv_m\alpha_1 - ha_m\eta_1 - hb_m\gamma_1 \\ 2hv_m\beta_1 - 2hb_m\eta_1 \\ ha_m\beta_1 + hv_m\gamma_1 - hb_m\alpha_1 - hu_m\eta_1 \\ 0 \end{pmatrix}_y = \begin{pmatrix} 0 \\ fhv_m - (a_m - \gamma_1)(hb_m)_y \\ -fhu_m - ghZ_y - (b_m - \eta_1)(hb_m)_y \\ -(u_m - \alpha_1)(hb_m)_y \\ -(v_m - \beta_1)(hb_m)_y \\ u_m(h\beta_1)_y - a_m(h\eta_1)_y - 2\gamma_1(hb_m)_y \\ v_m(h\beta_1)_y - b_m(h\eta_1)_y - 2\eta_1(hb_m)_y \\ a_m(h\beta_1)_y - u_m(h\eta_1)_y - 2\alpha_1(hb_m)_y \\ b_m(h\beta_1)_y - v_m(h\eta_1)_y - 2\beta_1(hb_m)_y \end{pmatrix}, \tag{2}$$

where f is the Coriolis parameter, g denotes the gravitational constant, and the divergence-free condition on the magnetic field in 1-D reads $(hb_m)_y = 0$.

2 Influence of the magnetic field vertical expansion

The derivation of the magnetic field vertical expansions parallels those of the velocity. This is due to the so-called 'vertical coupling' terms appearing almost identically. Due to the free surface boundary conditions on the magnetic field ($\mathbf{b}\cdot\mathbf{n} = 0$), the magnetic divergence-free condition remains identical to that of the MRSW system. The one place where the vertical coupling differs naturally results in the appearance of the so-called Godunov-Powell source (see, e.g., $(hb_m)_y$ terms in source of (2)), which has proven useful in numerical simulations as it helps 'advect away' the divergence error of the magnetic field. However, the addition of the magnetic field makes the MRSW moment system lose global hyperbolicity at a lower order ($M = 1$) than the shallow water moment system, which loses this property at $M = 2$.

Acknowledgement. This work is partially funded by German Research Foundation (DFG) Research Unit FOR5409 (grant #463312734), and by the Dutch Research Council (NWO) under the project HiWAVE (file #VI.Vidi.233.066) of the ENW Vidi research programme.

References

[1] P. Gilman, *Magnetohydrodynamic "shallow water" equations for the solar tachocline*, Astrophys. J. **544** (2000).

[2] J. Kowalski, M. Torrilhon, *Moment approximations and model cascades for shallow flow*, Commun. in Comput. Phys. **25** (2019).

Book of abstracts of the 9th International Conference on
Advanced Computational Methods in ENgineering and Applied Mathematics
September, 15–19, 2025.

Spline Shallow Water Moment Equations

Ullika Scholz[1] and Julian Koellermeier[2,3]

[1] *Applied and Computational Mathematics, RWTH Aachen University*

[2] *Department of Mathematics, Computer Science and Statistic, Ghent University*

[3] *Bernoulli Institute, University of Groningen*

e-mails: scholz@acom.rwth-aachen.de, julian.koellermeier@ugent.be

Abstract

A reduced-order model for free-surface flows is presented: The Spline Shallow Water Moment Equations (SSWME), which use spline ansatz functions in a moment approach for shallow flow. The locally supported ansatz function allow for a flexible representation of velocity profiles with high order derivatives or even layer-wise structures. Another advantage is the possibility of an adaptive approach. In this talk, hierarchies of SSWME models using different number of basis functions and different degrees will be derived and analyzed. Also, regularized hyperbolic versions of the equations will be shown. Finally, numerical simulations show high accuracy and robustness of the new models.

Keywords: Free-surface flows, hyperbolicity, Shallow Water Moment Equations, splines

1 Introduction

Standard reduced models for free-surface flow such as the classical Shallow Water Equations (SWE) do not provide information about the vertical changes in the velocity profile. To efficiently model flows with a complex velocity profile shape (such as granular or mud flows) without fully resolving the vertical axis, the recently proposed moment method [1] uses an expansion around the averaged velocity u_m written as

$$u(x,t,\zeta) = u_m(x,t) + \sum_{j=1}^{N} \alpha_j(x,t)\phi_j(\zeta) \tag{1}$$

for the velocity profile in vertical direction $\zeta \in [0,1]$ to derive the *Shallow Water Moment Equations* (SWME) hierarchy. The SWME are a coupled PDE system for the coefficients α_j of the expansion (1) that uses Legendre polynomials as ansatz functions ϕ_i. Higher-order SWME models incorporating a larger number of equations have been shown to capture complex profile shapes [1]. Up to now, the application of SWME was limited to global polynomial bases only, clearly limiting its flexibility.

For gas dynamics, the usefulness of piecewise polynomial spline basis functions for moment models was demonstrated in [2]. It showed that accurate models with beneficial analytical properties like conservation and hyperbolicity can be derived using piecewise defined splines with local support.

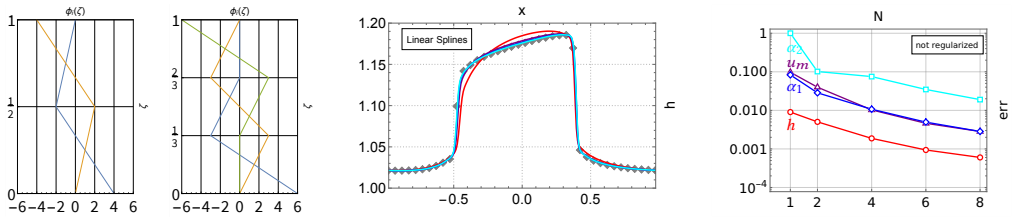

(a) (b) (c)

Figure 1: (a): Two constrained linear spline bases L2, L3 satisfying (2) on equidistant grids: L2 uses $N = 2$ splines (left); L3 uses $N = 3$ splines (right). (b): Results of the smooth wave experiment with N=2 (red) N=4 (purple) N=6 (blue) and N=8 (cyan) spline moments for the variable height h. (c): Relative L_1 error in water height h (red), mean velocity u_m (purple), linear coefficient α_1 (blue), or quadratic coefficient α_2 (cyan) for different numbers of splines N. The error decreases the more splines are used.

2 Spline Shallow Water Moment Equations

The standard B-splines do not fulfill the zero-mean condition

$$\forall i \in \{1, \dots, N\} : \int_0^1 \phi_i(\zeta) d\zeta = 0 \tag{2}$$

which, without further restriction on the coefficients, contradicts the assumption that u_m is the vertical average of u in the expansion (1). Therefore new ansatz functions are formulated (Figure 1(a)), the so-called constrained splines, where (2) is guaranteed by construction. The resulting hierarchy of PDE systems called SSWME can be seen as a generalization of the SWME. The SSWME generally have a less sparse system matrix due to the lack of orthogonality of the basis functions. Similiar to the Legendre systems, imaginary eigenvalues of the system matrix occur, which we correct using hyperbolic linearization techniques [3]. In numerical simulations of dam breaks and smooth waves, the SSWME show convergence with respect to the number of splines (Figures 1(b) and 1(c)) and higher accuracy than the SWME systems when ground friction is much larger than the internal friction of the fluid.

Acknowledgements This work is part of the project *HiWAVE* with file number VI.Vidi.233.066 of the *ENW Vidi* research programme, funded by the *Dutch Research Council (NWO)* under the grant *https://doi.org/10.61686/CBVAB59929*.

References

[1] J. Kowalski, M. Torrilhon, *Moment Approximations and Model Cascades for Shallow Flow*, Comm. Computational Physics **3** (2019) 669–702.

[2] J. Koellermeier, U. Scholz, *Spline moment models for the one-dimensional Boltzmann–Bhatnagar–Gross–Krook equation*, Physics of Fluids **32** (2020) 102009.

[3] J. Koellermeier, M. Rominger, *Analysis and Numerical Simulation of Hyperbolic Shallow Water Moment Equations*, Comm. Computational Physics **3** (2020) 1038–1084.

Book of abstracts of the 9th International Conference on
Advanced Computational Methods in ENgineering and Applied Mathematics
September, 15–19, 2025.

Application of the R13 moment system to shock wave dynamics with viscous and non-equilibrium corrections

Satyvir Singh[1] **and Manuel Torrilhon**[1]

[1] *Institute for Applied and Computational Mathematics, RWTH Aachen University, Germany*

e-mails: singh@acom.rwth-aachen.de, mt@acom.rwth-aachen.de

Abstract

Accurate modeling of shock wave dynamics in rarefied gas flows remains a fundamental challenge, particularly under conditions where viscous and non-equilibrium effects are pronounced. In this study, we investigate the application of the regularized 13-moment (R13) system to simulate shock wave phenomena in supersonic flows past a spiked blunt body, where conventional Navier–Stokes–Fourier (NSF) equations fail to capture essential non-equilibrium features. The R13 system, derived from Grad's moment method, incorporates higher-order moments such as stress and heat flux evolution, enabling enhanced representation of non-equilibrium transport phenomena [1, 2]. The governing R13 equations are numerically solved using a high-order modal discontinuous Galerkin (DG) method, which provides accurate resolution of steep gradients, shock structures, and complex flow features [3]. Additionally, we conduct a detailed numerical analysis of a steady monatomic gas flow near the point of regular reflection of a strong oblique shock wave from a symmetry plane—highlighting the model's robustness in capturing multiscale and multidimensional shock interactions under rarefied conditions. We systematically examine the influence of key parameters—Mach number, Knudsen number, and spike geometry—on shock stand-off distance, thermodynamic profiles, and non-equilibrium stress and heat flux characteristics. Validation against benchmark results and kinetic-based solutions confirms that the R13-DG framework offers significant improvements over classical continuum models. This work underscores the effectiveness of high-order moment methods for high-fidelity simulations of shock-dominated flows in transitional regimes and complex geometries.

Key words: R13 moment system, shock wave dynamics, discontinuous Galerkin method, non-equilibrium effects, Knudsen number.

References

[1] M. Torrilhon, H. Struchtrup, *Regularized 13-moment equations: shock structure calculations and comparison to Burnett models*, J. Fluid Mech. **513** (2004) 171–198.

[2] M. Torrilhon, *Modeling nonequilibrium gas flow based on moment equations*, Annu. Rev. Fluid Mech. **48** (2016) 429–458.

[3] S. Singh, H. Song, M. Torrilhon, *Modal discontinuous Galerkin simulations for Grad's 13 moment equations: Application to Riemann problem in continuum-rarefied flow regime*, J. Comput. Theor. Trans. **53** (2024) 398–422.

Book of abstracts of the 9th International Conference on
Advanced Computational Methods in ENgineering and Applied Mathematics
September, 15–19, 2025.

Adaptive simulation of One-Dimensional Shallow Water Moment Equations

Rik Verbiest[1] and Julian Koellermeier[1,2]

[1] *Bernoulli Institute, University of Groningen*

[2] *Department of Mathematics, Computer Science and Statistics, Ghent University*

e-mails: r.verbiest@rug.nl, Julian.koellermeier@ugent.be

Abstract

Models for shallow free surface flow often assume that the velocity is constant over the water height, which reduces the modelling complexity considerably. The Shallow Water Moment Equations are an extension of the standard shallow water equations that allow for a vertically changing velocity profile. The modelling complexity of a shallow water moment model is determined by its order. A shallow water moment model with higher-order includes more variables and equations and therefore has more modelling complexity, compared to a lower-order shallow water moment model. Often, the flow is characterized by both subdomains that require high modelling complexity and subdomains that can sufficiently accurately be modelled with low modelling complexity. Moreover, these subdomains might change in time as the water flows through the domain. This motivates the need for adaptivity in the simulation of shallow free surface flows. We propose a padded buffer cell approach for the coupling of the varying-order shallow water moment equations. The domain decomposition is performed based on a decomposition of the higher-order shallow water moment model. Numerical results of the collision of a dam-break wave with a smooth wave yield accurate results, while achieving a speedup compared to a non-adaptive model with fixed modelling complexity.

Keywords: Free surface flows, multiscale modelling, Shallow Water Moment Equations

1 Introduction

The Shallow Water Moment Equations (SWME) were introduced in [1] as an extension of the Shallow Water Equations. They allow vertical variability in the lateral velocity by introducing additional variables that describe the vertical velocity profile. In the SWME, the velocity $u(t,x,z)$ is modelled as an expansion in the Legendre polynomials ϕ_i of order M:

$$u(t,x,z) = u_m(t,x) + \sum_{i=1}^{M} \alpha_i(t,x)\phi_i\left(\frac{z-h_b(t,x)}{h(t,x)}\right), \tag{1}$$

with mean velocity $u_m(t,x)$, bottom topography $h_b(t,x)$, water height $h(t,x)$ and basis coefficients $\alpha_i(t,x)$. The higher the order M, the more variables and equations are included in the model, thus increasing the modelling complexity but also the computational effort. In many applications, some subdomains in the x-space need to be modelled by a high-order SWME

model to yield accurate results, while other subdomains can be modelled by a low-order SWME model. This motivates the need for a time- and space-dependant order $M = M(t, x)$. The adaptive simulation of the SWME consists of two main steps: 1) Decompose the domain into a set of subdomains, each modelled by a SWME model of a certain order; 2) Couple the different order SWME models at the subdomain boundary interfaces.

2 Domain Decomposition

Ideally, the domain decomposition should be based on the error that is made by the finite order $M(t, x)$ of the SWME moment model. Since the error is not known a priori, accurate error estimators need to be constructed. We propose two sets of error estimators: 1) The first set of error estimators includes the direct computation of the difference between a higher-order SWME model and a lower-order SWME model by using the hierarchical structure of the SWME; 2) The second set of error estimators is heuristically based and includes the fluid gradients, the values of the highest order additional variable α_M and the friction effects.

3 Boundary Interface Coupling

For the coupling of the different-order subdomains, we propose a padded buffer cell approach in combination with a standard finite volume scheme for non-conservative systems [2]. Assume that Ω_M and Ω_{M+1} are two neighbouring subdomains that are modelled by the SWME of order M and order $M + 1$, respectively, resulting in the situation illustrated in Figure 1. To

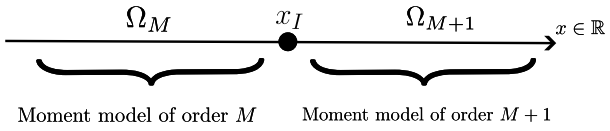

Figure 1: Example of a domain decomposition.

compute the flux at the boundary interface $x = x_I$, the adjacent boundary interface cell is padded with an additional coefficient such that it has the same number of variables as the other cell bordering the boundary interface. The advantage of this approach is that it straightforwardly allows to leverage the hierarchical structure of the models and make use of the same overarching finite volume scheme in the entire domain.

Acknowledgements This work is part of the project *HiWAVE* with file number VI.Vidi.233.066 of the *ENW Vidi* research programme, funded by the *Dutch Research Council (NWO)*.

References

[1] J. Kowalski, M. Torrilhon, *Moment Approximations and Model Cascades for Shallow Flow*, Commun. in Comput. Phys. **25** (2019).

[2] R. Verbiest, J. Koellermeier, *Spatially Adaptive Moment Model using Padded Buffer Cell for Linear Hierarchical Moment Equations*, accepted (2025).

Book of abstracts of the 9th International Conference on
Advanced Computational Methods in ENgineering and Applied Mathematics
September, 15–19, 2025.

A New Class of Nonlinear Closures Based on Orthogonal Polynomials

E. Yilmaz[1], G. Oblapenko[1] and M. Torrilhon[1]

[1] *Applied and Computational Mathematics (ACoM), RWTH Aachen University, Germany*

e-mails: yilmaz@acom.rwth-aachen.de, oblapenko@acom.rwth-aachen.de, mt@acom.rwth-aachen.de

Abstract

In the present work, an approach to the moment closure problem on the basis of orthogonal polynomials derived from Gram matrices is proposed. Its properties are studied in the context of the moment closure problem arising in gas kinetic theory, for which the proposed approach is proven to have multiple attractive mathematical properties. Numerical studies are carried out for model gas particle distributions and the approach is compared to other moment closure methods, such as Grad's closure and the maximum-entropy method. The proposed "Gramian" closure is shown to provide very accurate results for a wide range of distribution functions.

Key words: hyperbolic moment closures, kinetic gas theory, orthogonal polynomials
MSC 2020: 82C40, 35L60, 35Q70

1 Introduction

The kinetic theory of gases provides a fundamental description of particle dynamics via the Boltzmann equation, which governs the evolution of the distribution function $f(x, t, c)$ in phase space.While this equation accurately describes gas behavior across a wide range of regimes, its main challenge lies in the computational expense, which arises from the high dimensionality of phase space and the nonlinear nature of the collision term. A well-established model reduction strategy is the *method of moments*, which replaces the kinetic description with a system of partial differential equations governing the moments of the distribution function. These moments are defined as

$$u_k = \int_{\mathbb{R}} c^k f(c)\, dc, \quad k = 0, 1, \ldots, M.$$

Projecting the Boltzmann equation onto these moments yields a system of the form

$$\partial_t u_k + \partial_x u_{k+1} = s_k,$$

where s_k are the moments of the collision operator. However, the system is inherently open: each equation depends on a higher-order moment, necessitating a *closure relation* to approximate u_{M+1} in terms of known quantities.

Classical approaches to closure include Grad's method, which relies on Hermite polynomial expansions around equilibrium, and the maximum-entropy method, which derives the distribution function by maximizing entropy under moment constraints. While these techniques have been successful, they also present challenges: Grad's closure may lose hyperbolicity far from equilibrium, while maximum-entropy methods often require computationally expensive optimization and lack closed-form flux expressions.

In recent work, a new class of closures, called *Gramian closures*, has been proposed. These closures are constructed using orthogonal polynomials derived from a *Gramian matrix* associated with the moments. This approach leads to explicit formulas for the unknown moment u_{M+1}, avoiding the need for reconstructing the underlying distribution function. The Gramian closure is extended by introducing a parameter that provides additional control over mathematical properties such as hyperbolicity and equilibrium preservation. These closures are especially attractive due to their analytical structure and efficient evaluation. In this study, we investigate the mathematical formulation and numerical performance of Gramian and extended Gramian closures. To assess their accuracy, we compare them to established methods such as Grad's and maximum entropy closures on a set of test problems. The numerical results demonstrate that Gramian closures provide competitive predictions across a wide range of scenarios, making them a promising alternative for efficient kinetic modeling.

Acknowledgements This work was supported by the German Research Foundation (DFG) within the research unit FOR5409.

References

[1] Grad, H. On the kinetic theory of rarefied gases. *Communications on Pure and Applied Mathematics*, 2(4):331–407, 1949.

[2] Levermore, C. D. Entropy-based moment closures for kinetic equations. *Transport Theory and Statistical Physics*, 26(4–5):591–606, 1997.

[3] Torrilhon, M. Modeling nonequilibrium gas flow based on moment equations. *Annual Review of Fluid Mechanics*, 48:429–458, 2016.

[4] Yilmaz, E., Oblapenko, G., and Torrilhon, M. On nonlinear closures for moment equations based on orthogonal polynomials. *arXiv preprint arXiv:2407.05894*, 2024.

[5] Fox, R. O., Laurent, F. Hyperbolic Quadrature Method of Moments for the One-Dimensional Kinetic Equation. *SIAM Journal on Applied Mathematics*, 82:750–771, 2022.

MS8: Recent Trends in Mathematical Software

Organiser: Andrew Dienstfrey (National Institute of Standards and Technology) and Amparo Gil (Universidad de Cantabria)

Description: Numerical software lies at the foundation of nearly all scientific computing applications. This minisymposium will showcase recent advances in the development and analysis of numerical algorithms across a range of problem areas including: numerical linear algebra, Monte Carlo methods for PDEs, and numerical software for special functions and Gauss quadrature. This minisymposium is being organized by members of the International Federation of Information Processing Working Group 2.5 on Numerical Software.

Book of abstracts of the 9th International Conference on
Advanced Computational Methods in ENgineering and Applied Mathematics
September, 15–19, 2025.

Implementation of Gaussian Quadrature with Even Node Distribution for the Unit Sphere

Hiroshi Fujiwara[1]

[1] *Graduate School of Informatics, Kyoto University*

e-mails: fujiwara@acs.i.kyoto-u.ac.jp

Abstract

This talk presents numerical implementation and accuracy of a quadrature rule for the unit sphere proposed by S. L. Sobolev, which is a Gaussian type quadrature rule based on spherical harmonic functions. In order to distribute the sampling nodes evenly, the use of a regular polyhedral group was proposed. We focus on the use of the icosahedral group, and find nodes which are not localized up to a certain degree.

Key words: numerical quadratures, unit sphere, spherical harmonics, icosahedral group, high-accurate computation
MSC 2020: 65D32, 33C55

1 Introduction

In the present research, we implement a quadrature rule for the unit sphere proposed by S. L. Sobolev [1]. Gaussian-type quadrature rules are effective for achieving high accuracy, and on the sphere it has been proposed to use spherical harmonic functions as the basis. The use of regular polyhedral groups has also been proposed in order to reduce the number of unknowns; specifying one node as a seed results in multiple sample nodes generated by the group action. Solving a system of nonlinear equations

$$\sum_{j=1}^{J} \sum_{g \in G_{20}} w_j Y_n^m(g\eta_j) = \sqrt{4\pi}\delta_{n0}\delta_{m0}, \qquad |m| \le n \le N$$

where G_{20} is the regular icosahedral group, Y_n^m is the spherical harmonic function, and N is a desired degree of the Gaussian type quadrature rule, we obtain the sampling nodes $\{g\eta_j\,;\, g \in G_{20}, 1 \le j \le J\}$ associated with the weights $\{w_j\}$. A design of its numerical procedure has been described in [2].

2 Numerical Results

When the degree is 60, the number of unknowns are 63. If we use the vertices, the midpoints of edges, and the centers of the faces of an inscribed icosahedron, the number of nodes are 1,262 with efficiency [3] of 0.982. Although a method that does not employ any of them has not been described in [2], it has 1,260 nodes with higher efficiency of 0.990. We found 13

distributions in the former case, and 20 distributions in the latter case. Figure 1 illustrates one of distributions of nodes in the latter case, where no nodes lie on the vertices, the midpoints of edges, on the centers of the faces of the icosahedron indicated by red segments.

In order to verify its accuracy, we apply the obtained results to numerical computation of

$$\int_{S^2} \frac{1}{4\pi} \frac{1-s^2}{(1-2s\eta\cdot\xi+s^2)^{3/2}} d\sigma_\xi = 1, \qquad \eta = \left(\frac{1}{9}, \frac{4}{9}, \frac{8}{9}\right), \quad s = \frac{1}{2},$$

where $d\sigma_\xi$ is the surface element of the unit sphere. Figure 2 shows the comparison of error decays of the implemented rule (light blue) and conventional methods (purple and green) with 100 decimal digits computation with multiple-precision arithmetic [4]. Among them, the implemented rule achieves the highest accuracy, and its errors decay almost exponentially with respect to the number of sampling nodes.

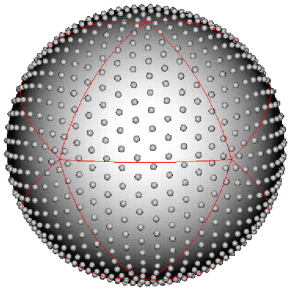

Figure 1: Example of distribution of nodes (Degree 60). The red segments indicate the reference icosahedron

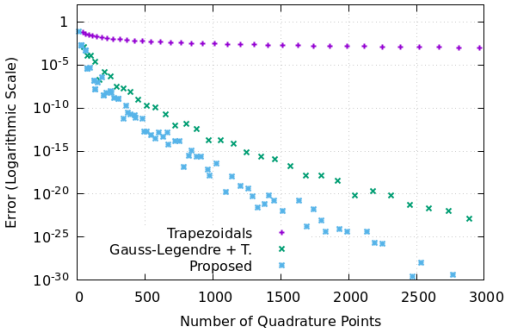

Figure 2: Comparison of error decays

Acknowledgements This work has been partially supported by JSPS KAKENHI Grant Number JP24K00539.

References

[1] S. L. Sobolev, *Cubature Formulas on the Sphere Invariant under Finite Groups of Rotations*, Sov. Math. **3** (1962) 1307–1310.

[2] C. Ahrens, G. Beylkin, *Rotationally Invariant Quadratures for the Sphere*, Proc. Roy. Soc. A **465** (2009) 3103–3125.

[3] A. McLaren, *Optimal Integration on a Sphere*, Math. Comput. **17** (1963) 361–383.

[4] H. Fujiwara, *Extended precision floating-point arithmetic library*, `https://www-cm.acs.i.kyoto-u.ac.jp/~fujiwara/exflib`.

Book of abstracts of the 9th International Conference on
Advanced Computational Methods in ENgineering and Applied Mathematics
September, 15–19, 2025.

Algorithm-based Resilience in Scalable Conjugate Gradient Methods

Viktoria Mayer[1] and Wilfried N. Gansterer[2]

[1] *UniVie Doctoral School Computer Science DoCS, Faculty of Computer Science, University of Vienna*

[2] *Faculty of Computer Science, University of Vienna*

e-mails: viktoria.mayer@univie.ac.at, wilfried.gansterer@univie.ac.at

Abstract

The growing complexity of modern supercomputers in combination with energy constraints tends to increase the frequency of hardware failures and soft errors. The generic approach for improving resilience against various types of failures is the Checkpoint-Restart concept, where the entire state of a computation is periodically saved. Applying checkpointing of the entire state to *scalable* Preconditioned Conjugate Gradient (PCG) algorithms, which hide or avoid global synchronizations of parallel computations, significantly increases memory and communication cost compared to the standard PCG algorithm as more data must be communicated and stored redundantly.

Exact state reconstruction (ESR) strategies are algorithm-based alternatives to the generic Checkpoint-Restart concept which can significantly reduce memory and communication cost by exploiting algorithm-specific properties and relationships. However, existing ESR strategies focus only on increasing resilience of PCG against node failures, and they are not applicable for implicit preconditioner types. Additional limitations exist when trying to achieve resilience of scalable PCG algorithms against *soft errors*: Generic checkpointing requires new specific soft error detection mechanisms for most scalable PCG variants to avoid saving potentially corrupted data, and existing ESR strategies are not effective against soft errors.

In this presentation, we discuss algorithm-based resilience strategies for scalable PCG variants. The focus is on a novel ESR strategy which supports arbitrary preconditioners and allows for recovery from many simultaneous node failures as well as from soft errors. For any PCG algorithm, this novel strategy only checks and checkpoints two vectors and can be combined with any error detection mechanism that verifies the correctness of the state of the standard PCG solver. Thus, this novel approach is applicable to any PCG algorithm mathematically equivalent to standard PCG. Theoretical analysis and experimental evaluations confirm that the proposed ESR strategy increases resilience while retaining the performance and memory advantages of existing ESR strategies over generic checkpointing.

Key words: algorithmic fault tolerance, communication-hiding/communication-avoiding conjugate gradient algorithms, extreme-scale parallel computing, node failures, soft errors

MSC 2020: 65F10, 65F50, 65Y05, 65Y20, 68W10

Book of abstracts of the 9th International Conference on
Advanced Computational Methods in ENgineering and Applied Mathematics
September, 15–19, 2025.

The Walk on Spheres Monte Carlo Algorithm for Solving Partial Differential Equations

Michael Mascagni[1]

[1] *Department of Computer Science, Florida State University and NIST, USA*

Abstract

The stochastic representation to the solutions of partial differential equations (PDEs) and integral equations (IEs) has been known for decades. These representations have lead to a variety of Monte Carlo methods for the numerical solution of both PDEs and IEs, among them is a method called the Walk on Spheres (WoS) algorithm. WoS has been quite successful in solving linear elliptic and parabolic PDEs with Dirichlet boundary conditions in a very cost effective way. This numerical analysis work was taken up by the computer graphics community, who are experts in Monte Carlo through their use of it in image rendering via ray tracing. Their interest stems from the fact that WoS and ray tracing both permit the representation of the geometry of the problem in a very compact and computational efficient way via Bounding Volume Hierarchy. This has lead to the expansion of the scope and efficiency of WoS in a wide variety of ways which will be presented here.

Book of abstracts of the 9th International Conference on
Advanced Computational Methods in ENgineering and Applied Mathematics
September, 15–19, 2025.

Symbiosis of Scalar and Matrix Polynomials

Aaron Melman[1]

[1] *Department of Applied Mathematics, Santa Clara University*

e-mails: amelman@scu.edu

Abstract

Many properties of matrix polynomials are derived from analogous properties of scalar polynomials, but matrix polynomials can in turn be used to obtain new results for scalar polynomials, which constitute the very concept that they generalize. We consider two examples of this symbiosis. The first (from [1]) consists of explicit simple upper bounds on the magnitudes of scalar polynomial zeros that are close approximations of the Cauchy radius. The latter is an upper bound that is optimal among all bounds depending only on the moduli of the coefficients, but it has the disadvantage of requiring the solution of a nonlinear equation, making an explicit approximation useful. The second example (from [2]) is the construction of a (scalar) polynomial whose zeros are powers of the (unknown) zeros of a given polynomial. Using matrix polynomials provides an efficient and elegant way to accomplish this.

Key words: matrix polynomial, bounds, polynomial zeros, powers of zeros
MSC 2020: 15A18, 30C15, 65H04

1 Introduction

We give two examples of the way in which matrix polynomials can be used to obtain (new) results for scalar polynomials.

2 Efficient approximation to the Cauchy radius

While, in general, it is certainly true that bounds on the magnitudes of scalar polynomial zeros have become less important now that polynomial zeros can be computed very efficiently, a high quality and simple explicit bound is still useful. Implicit bounds significantly outperform explicit ones, but have the disadvantage that they need to be computed numerically. Although the bounds we obtain here are explicit, they are related to an implicit bound (the Cauchy radius) to such an extent that they approach it in effectiveness. These bounds are obtained by embedding scalar polynomials into the larger framework of their generalization to matrix polynomials.

We now derive a quadratic matrix polynomial whose eigenvalues are the zeros of a given scalar polynomial of even degree. If the scalar polynomial is of odd degree, we instead consider the polynomial $zp(z)$ with no discernible detrimental effect on the results. The complex

polynomial p of even degree n can be expressed as

$$\begin{aligned} p(z) &= z^n + a_{n-1}z^{n-1} + \ldots + a_1 z + a_0 \\ &= \left(z^2 + a_{n-1}z + a_{n-2}\right) z^{n-2} + \left(a_{n-3}z + a_{n-4}\right) z^{n-4} \\ &\qquad + \left(a_{n-5}z + a_{n-6}\right) z^{n-6} + \cdots + \left(a_3 z + a_2\right) z^2 + \left(a_1 z + a_0\right) \\ &= \det \begin{pmatrix} z^2 & & & & & a_1 z + a_0 \\ -1 & z^2 & & & & a_3 z + a_2 \\ & \ddots & \ddots & & & \vdots \\ & & -1 & z^2 & & a_{n-5}z + a_{n-6} \\ & & & -1 & z^2 & a_{n-3}z + a_{n-4} \\ & & & & -1 & z^2 + a_{n-1}z + a_{n-2} \end{pmatrix}, \end{aligned}$$

which can be written as $\det\left(\mathrm{I}z^2 - A_1 z - A_0\right)$. By applying the matrix polynomial version of the Cauchy radius and its enhancements to this quadratic matrix polynomial, we explicitly obtain an upper bound on the zeros of p.

3 Polynomials whose zeros are powers of a given polynomial's zeros.

Given a complex polynomial, we use linear algebra to obtain a polynomial of the same degree, whose zeros are integer powers of the (unknown) zeros of the given polynomial. Other than simple curiosity, there also exist practical reasons for considering such polynomials, as the properties of the new polynomial's coefficients may allow the applications of certain results that depend on such properties that may be absent from the original polynomial. The result is contained in the following theorem, whose proof relies on the construction of the (block) companion matrix of a matrix polynomial. A polynomial can always be modified to satisfy the requirements of the theorem by using a proper multiplier.

Theorem *Let $p(z) = \sum_{j=0}^{n} a_j z^j$ be a complex polynomial of degree n with companion matrix $C(p)$, let $k \neq n$ be a positive integer, and let $k \mid n$. Then the kth power of the zeros of p are the eigenvalues of the $k \times k$ matrix polynomial P of degree n/k with (block) companion matrix $C(P) = C^k(p)$. They are the zeros of the monic scalar polynomial* $\det\left(P(z)\right)$*, which is of degree n.*

References

[1] A. Melman, *An efficient approximation to the Cauchy radius*, Numer. Algorithms **96** (2024) 1–11.

[2] A. Melman, *Polynomials whose zeros are powers of a given polynomial's zeros*, Amer. Math. Monthly **129** (2022) 276–280.

Book of abstracts of the 9th International Conference on
Advanced Computational Methods in ENgineering and Applied Mathematics
September, 15–19, 2025.

Improving the quality of numerical software for distribution functions

Amparo Gil[1], Javier Segura[2] and Nico M. Temme[3]

[1] *Departamento de Matemática Aplicada y CC. de la Computación, Universidad de Cantabria. 39005-Santander, Spain.*

[2] *Departamento de Matemáticas, Estadística y Computación, Universidad de Cantabria, 39005 Santander, Spain.*

[3] *Valkenierstraat 25, 1825 BD Alkmaar, the Netherlands ,*

e-mails: amparo.gil@unican.es, javier.segura@unican.es, nic@temme.net

Abstract

Special functions are fundamental in probability theory, as they appear in the definitions of many probability distributions. The use of numerical and asymptotic methods commonly employed to compute special functions enables the development of stable and accurate algorithms for evaluating numerous distribution functions. We review recent developments in this field, focusing in particular on advances in numerical software for computing Beta distribution functions, which outperform previous implementations in Matlab and R.

Key words: Beta distributions, numerical computation, inversion, Matlab software
MSC 2020: 33B15, 33F05, 33C15, 65D20

Acknowledgements This work has been supported by project PID2021-127252NB-I00 funded by MCIN/AEI/10.13039/501100011033/ FEDER, UE.

References

[1] V. Egorova, A. Gil, J. Segura, N.M. Temme , *Algorithms for the inversion of the noncentral beta distribution function.* Submitted.

[2] V. Egorova, A. Gil, J. Segura, N.M. Temme , *A numerical algorithm for the computation of the noncentral beta distribution function.* Numerical Algorithms 99, 17911804 (2025).

[3] A. Gil, J. Segura, N.M. Temme , *New asymptotic representations of the noncentral t distribution.* Studies in Applied Mathematics 151 (2023) 857-882

Book of abstracts of the 9th International Conference on
Advanced Computational Methods in ENgineering and Applied Mathematics
September, 15–19, 2025.

Numerical investigation of finite element formulations for ICRH plasma heating

Jules Zaleski[1], Bernard Reman[2], Philippe Lamalle[2] and Christophe Geuzaine[1]

[1] *Department of Electrical Engineering and Computer Science, University of Liège, Belgium*

[b] *Laboratory for Plasma Physics, Royal Military Academy, Brussels, Belgium*

e-mails: j.zaleski@uliege.be, Bernard.Reman@mil.be,
philippe.lamalle.erm@pm.me, cgeuzaine@uliege.be

Abstract

This work presents a numerical investigation of finite element formulations to model Ion Cyclotron Resonance heating (ICRH) of fusion plasmas in the frequency domain. Both local and nonlocal modelling approaches of wave-particle interactions are considered, respectively using a complex permittivity tensor (case of a single wave mode along the equilibrium magnetic field) or a dedicated new integral kernel (for arbitrary wave excitations).

Key words: Finite Element Method, High frequency electromagnetic waves, Plasma heating

1 Introduction

To simulate the impact of warm plasma on ICRH, the main approach for decades has been to use spectral solvers with a finite number of excitation modes. Recent plasma modelling approaches [1] based on an integral representation of the particle interactions are amenable to the finite element method (FEM), which could greatly facilitate the modelling of more complex geometries, using locally adapted meshes.

2 FEM modelling of warm plasma

In the frequency domain, the FEM formulation of the Maxwell-Vlasov equation consists in finding the electric field $\boldsymbol{E}$ such that

$$\frac{i}{2}\int_V \left[\frac{1}{\omega\mu_0}(\nabla\times\boldsymbol{E})\cdot(\nabla\times\boldsymbol{F})^* - \omega\varepsilon_0\boldsymbol{E}\cdot\boldsymbol{F}^*\right] dV + \sum_\beta W_\beta(\boldsymbol{E},\boldsymbol{F}) = \frac{1}{2}\int_V \boldsymbol{j}_s\cdot\boldsymbol{F}^*\, dV \qquad (1)$$

holds for suitable test functions $\boldsymbol{F}$, at a given angular frequency ω and for a given source current density $\boldsymbol{j}_s$. The plasma contribution is taken into account for each particle species β through W_β.

Figure 1 shows initial results for a 2D configuration, where the electric field is discretized using high-order Whitney edge elements for the in-plane components, and high-order Lagrange elements for the out-of-plane component [2]. An out-of-plane current density $j_s^z = \sin(k_\parallel y)$ is imposed on a line strap antenna on the right, which leads to a single antenna mode ($k_\parallel$). In this configuration, the local approximation of W_β through a complex permittivity tensor is used and serves as a validation of the new integral kernel. The full paper will compare both approaches and detail how the new integral kernel (which is logarithmically singular) is integrated along the static magnetic field lines in the plasma reactor.

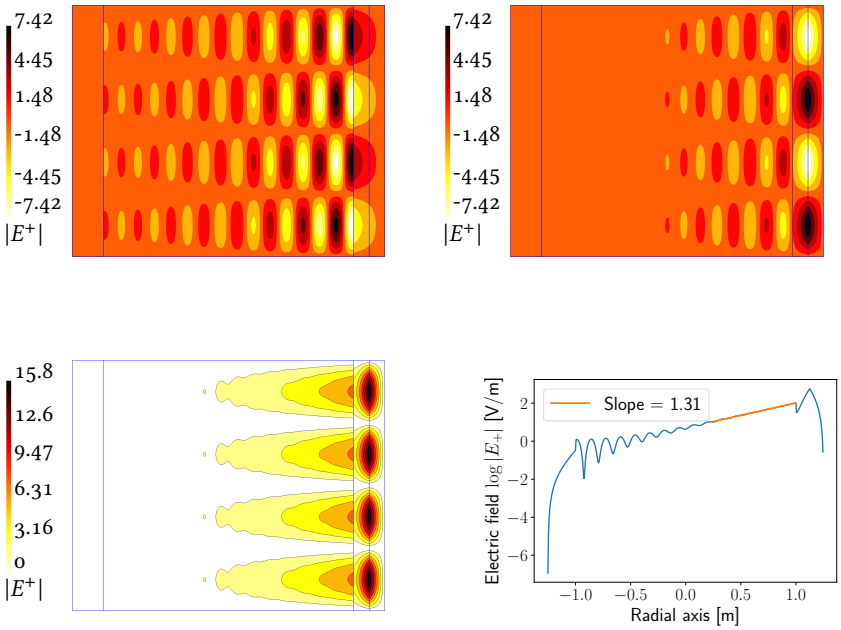

Figure 1: Solution $E^+ := (E_z + iE_x)/\sqrt{2}$ at $f = 51.8$ MHz with an in-plane static magnetic flux density with constant amplitude $B^y_{\text{stat}} = 3.45$ T, with three particle species: electrons (0 keV, $n_{\text{elec}} = 3 \cdot 10^{19}$ m^3), hydrogen ($T_H = 2$ keV, 5 % $\cdot\, n_{\text{elec}}$) and deuterium (0 keV, 95 % $\cdot\, n_{\text{elec}}$). Top left: $\Re(E^+)$. Top right: $\Im(E^+)$. Bottom left: $|E^+|$. Bottom right: horizontal absorption profile. The slope of the absorption profile is validated against the analytical dispersion relation.

Acknowledgements Jules Zaleski is a FRIA grantee of the Fonds de la Recherche Scientifique – FNRS.

References

[1] P.U. Lamalle, Dielectric kernels for maxwellian tokamak plasmas, *AIP Conf. Proc.*, 2254, 100001 (2020).

[2] A. Royer, E. Béchet, et C. Geuzaine, « GMSH-FEM: An Efficient Finite Element Library Based on GMSH », 14th WCCM-ECCOMAS Congress 2020, vol. 1400-Software, High Performance Computing, (2021).

MS9: Advanced Numerical Methods for Flow and Related Problems

Organiser: Marius Paul Bruchhäuser (Helmut Schmidt University Hamburg), Nils Margenberg (Helmut Schmidt University Hamburg), Richard Schussnig (Ruhr University Bochum)

Description: Accurate and efficient numerical solution methods for large-scale flow simulations remain a challenging task. Flow phenomena arise in numerous scientific and engineering fields including mechanics, environmental science, biology, and medicine. Ongoing progress in these fields is closely linked to the evolution of increasingly complex models.

Handling these problems demands innovative numerical and computational methods. With the increasing availability of high performance computing hardware, efficient computational methods for large-scale flow simulations become crucial in order to achieve optimal performance and save cost and time. The achievement of this goal further depends on the numerical discretisation, which is required to be accurate, stable and should be able to capture fine scales and complex physics. In this regard, standard or naive approaches often prove inadequate.

This minisymposium consists of contributions to the mathematical and computational innovations in the complex simulations associated with flow and related problems. The main focus is on the development and rigorous analysis of state-of-the-art numerical methods and solvers using high performance and extreme scale computing techniques. Modern techniques like highly parallel scalable domain decomposition methods, matrix-free multigrid methods, goal-oriented space-time adaptivity and adaptive stabilized methods are of particular interest.

Book of abstracts of the 9th International Conference on
Advanced Computational Methods in ENgineering and Applied Mathematics
September, 15–19, 2025.

Stabilisation of the Navier–Stokes equations on under-resolved meshes via enstrophy preservation

Boris D. Andrews[1], Matin Shams[1] and Patrick E. Farrell[1,2]

[1] *Mathematical Institute, University of Oxford*

[2] *Faculty of Mathematics and Physics, Charles University*

e-mails: boris.andrews@maths.ox.ac.uk, matin.shams@st-hughs.ox.ac.uk, patrick.farrell@maths.ox.ac.uk

Abstract

The typical energy estimate for the Navier–Stokes equations provides a bound for the gradient of the velocity; energy-stable numerical methods that preserve this estimate preserve this bound. However, the bound scales with the Reynolds number (Re) causing solutions to be numerically unstable (i.e. exhibit spurious oscillations) on under-resolved meshes. The dissipation of enstrophy on the other hand provides, in the transient 2D case, a bound for the gradient that is independent of Re.

We propose a finite-element integrator for the Navier–Stokes equations that preserves the evolution of both the energy and enstrophy, implying gradient bounds that are, in the 2D case, independent of Re. Our scheme is a mixed velocity–vorticity discretisation, making use of a discrete Stokes complex. While we introduce an auxiliary vorticity in the discretisation, the energy- and enstrophy-stability results both hold on the primal variable, the velocity; our scheme thus exhibits greater numerical stability at large Re than traditional methods.

We conclude with a demonstration of numerical results, and a discussion of the existence and uniqueness of solutions.

Keywords: stabilisation, enstrophy, structure preservation, finite element exterior calculus, Stokes complex

1 Background

We consider the incompressible NS equations,

$$\dot{\mathbf{u}} = \mathbf{u} \times \operatorname{curl} \mathbf{u} - \nabla p - \frac{1}{\mathrm{Re}} \operatorname{curl}^2 \mathbf{u}, \qquad 0 = \operatorname{div} \mathbf{u}, \tag{1}$$

for velocity $\mathbf{u}$, pressure p, and Reynolds number Re. The typical energy estimate $\partial_t [\frac{1}{2} \int \|\mathbf{u}\|^2] = -\frac{1}{\mathrm{Re}} \int \|\operatorname{curl} \mathbf{u}\|^2$ provides a bound for the gradient of the velocity; energy-stable numerical methods that preserve this estimate preserve this bound. However, the bound scales with Re, causing solutions to be numerically unstable (i.e. exhibit spurious oscillations) on under-resolves meshes with mesh number much smaller than $\sqrt{\mathrm{Re}}$.

Alternatively, the dissipation of enstrophy $\partial_t [\frac{1}{2} \int \|\operatorname{curl} \mathbf{u}\|^2] = -\frac{1}{\mathrm{Re}} \int \|\operatorname{curl}^2 \mathbf{u}\|^2$ in the transient 2D case provides a bound for the gradient that is independent of Re. We propose a finite-element discretisation for the transient Navier–Stokes equations that preserves the evolution of both the energy and enstrophy, implying gradient bounds that are, in the 2D case, independent of Re.

2 Our contributions

Our scheme is a mixed velocity–vorticity discretisation (designed through the framework presented in [1]) relying on the existence of a discrete Stokes complex:

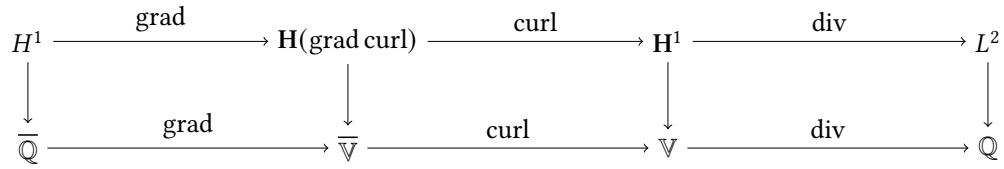

Our proposed semi-discretisation is as follows: find $(\theta, \boldsymbol{\omega}, \mathbf{u}, p) \in \overline{\mathbb{Q}} \times \overline{\mathbb{V}} \times \mathbb{V} \times \mathbb{Q}$ such that

$$\int \dot{\mathbf{u}} \cdot \mathbf{v} = \int (\mathbf{u} \times \boldsymbol{\omega}) \cdot \mathbf{v} + p(\operatorname{div} \mathbf{v}) - \frac{1}{\mathrm{Re}} \operatorname{curl} \boldsymbol{\omega} \cdot \mathbf{v}, \qquad 0 = \int (\operatorname{div} \mathbf{u}) q, \tag{2a}$$

$$\int \operatorname{curl} \boldsymbol{\omega} \cdot \operatorname{curl} \boldsymbol{\chi} = \int \operatorname{curl} \mathbf{u} \cdot \operatorname{curl}^2 \boldsymbol{\chi} - \nabla\theta \cdot \boldsymbol{\chi}, \qquad 0 = -\int \boldsymbol{\omega} \cdot \nabla\eta, \tag{2b}$$

for all $(\eta, \boldsymbol{\chi}, \mathbf{v}, q) \in \overline{\mathbb{Q}} \times \overline{\mathbb{V}} \times \mathbb{V} \times \mathbb{Q}$. The auxiliary variable $\boldsymbol{\omega}$ is a discretely divergence-free approximation to the vorticity $\operatorname{curl} \mathbf{u}$. This preserves discrete forms of energy dissipation and the evolution of enstrophy,

$$\partial_t \left[\frac{1}{2} \int \|\mathbf{u}\|^2 \right] = -\frac{1}{\mathrm{Re}} \int \|\operatorname{curl} \mathbf{u}\|^2, \tag{3a}$$

$$\partial_t \left[\frac{1}{2} \int \|\operatorname{curl} \mathbf{u}\|^2 \right] = -\int \mathbf{u} \cdot (\boldsymbol{\omega} \cdot \nabla\boldsymbol{\omega}) - \frac{1}{\mathrm{Re}} \int \|\operatorname{curl} \boldsymbol{\omega}\|^2; \tag{3b}$$

as quadratic structures, these are preserved to the fully discrete level when using any Gauss–Legendre timestepping scheme. Notably, while we introduce an auxiliary vorticity $\boldsymbol{\omega}$, the energy and enstrophy stability results both hold on the primal variable $\mathbf{u}$.

In 2 dimensions, the equivalent scheme makes use of a discrete 2D Stokes complex. In this case, the enstrophy evolution result (3b) becomes a dissipation law, providing a Re-robust $\mathbf{H}^1$ bound for $\mathbf{u}$, consequently offering greater numerical stability even in the ideal limit $\mathrm{Re} = \infty$. In contrast to existing stabilisation techniques, this necessitates the introduction of no artificial viscosities or penalty terms.

Acknowledgements This work was funded by the Engineering and Physical Sciences Research Council [grant number EP/W026163/1], the EPSRC Energy Programme [grant number EP/W006839/1], a CASE award from the UK Atomic Energy Authority, and by the Donatio Universitatis Carolinae Chair "Mathematical modelling of multicomponent systems".

References

[1] B. D. Andrews and P. E. Farrell, *Enforcing conservation laws and dissipation inequalities numerically via auxiliary variables*, arXiv, (2025).

Book of abstracts of the 9th International Conference on
Advanced Computational Methods in ENgineering and Applied Mathematics
September, 15–19, 2025.

Flux-Based Interface Coupling in Non-Overlapping Domain Decomposition Methods

Nawfel Benatia[1] and Christophe Geuzaine[1]

[1] *Department of Electrical Engineering and Computer Science, University of Liège, Belgium*

e-mails: nawfel.benatia@uliege.be, cgeuzaine@uliege.be

Abstract

We propose a novel Flux-Based Domain Decomposition Method (FDDM) that reformulates non-overlapping domain decomposition by leveraging numerical fluxes within a variational framework. This enables a global fixed-point iteration that converges robustly without relaxation or parameter tuning.

Key words: Flux-Based Domain Decomposition, Discontinuous Galerkin, Robin Transmission Conditions, Fixed-Point Iteration, Optimized Schwarz Method

1 Introduction

Domain Decomposition (DD) methods provide an efficient framework for the numerical solution of large-scale partial differential equations (PDEs) by dividing the computational domain into smaller subdomains that can be solved independently, often in parallel. A central challenge in DD lies in ensuring compatibility across subdomain interfaces, typically through the exchange of interface data to reproduce the global solution accurately.
Classical Schwarz methods overcome this by prescribing Dirichlet or Neumann boundary conditions on the interfaces. However, they exhibit two significant drawbacks [1]: (i) they often fail to converge for wave propagation problems (e.g., Helmholtz equations), even when subdomains overlap, and (ii) they typically break down entirely in non-overlapping settings, even for elliptic problems. To address these limitations, Lions [2] (for elliptic PDEs) and Després [3] (for Helmholtz equations) introduced Robin (impedance) transmission conditions of the form

$$\partial_{\boldsymbol{n}} u + Tu = g$$

where $\partial_{\boldsymbol{n}} u$ and u denote the normal derivative and the trace of the solution on the interface, respectively, and T is a suitable impedance operator (possibly non-local). These Robin conditions restore convergence in both elliptic and wave propagation problems, even without overlap, and are the foundation of Optimized Schwarz Methods (OSM).

Recent developments in Hybrid Discontinuous Galerkin (HDG) discretizations exploit numerical fluxes for the weak imposition of continuity across element interfaces. Inspired by this paradigm, we propose a novel Flux-Based Domain Decomposition Method (FDDM) in which numerical fluxes impose continuity across subdomain interfaces, embedding Robin-type behavior directly into the variational formulation.

2 Flux-Based Domain Decomposition

The Characteristic–Hybridized Discontinuous Galerkin (CHDG) [4] method uses characteristic variables as hybrid unknowns on each element interface. By statically condensing out interior degrees of freedom, CHDG yields a reduced system defined solely on the mesh skeleton. Crucially, the DG numerical dissipation renders the resulting interface operator a strict contraction in the energy norm, guaranteeing rapid, parameter-free convergence of fixed-point iterations.

Extending this perspective, we treat each CHDG element as a macro-subdomain within the global FDDM framework. Local solves on each subdomain generate interface fluxes that serve as coupling data. The global interface problem reduces to finding the characteristic trace vector λ = characteristic hybrid variables such that:

$$(\mathcal{I} - \mathcal{T}_{\mathrm{FDDM}})\lambda = b_{\mathrm{FDDM}}, \quad \text{with } \mathcal{T} := \Pi \circ \mathcal{S}_{\mathrm{FDDM}}, \tag{1}$$

where $\mathcal{S}_{\mathrm{FDDM}}$ is the element scattering map (local solve), Π is the exchange operator assembling interface contributions, and b_{FDDM} collects boundary and source terms.

By construction, $\mathcal{T}_{\mathrm{FDDM}}$ is a strict contraction. Consequently, the fixed-point iteration

$$\lambda^{k+1} = \mathcal{T}_{\mathrm{FDDM}}\lambda^k + b_{\mathrm{FDDM}},$$

converge.
For comparison, classical non-overlapping OSM yields an analogous interface equation [3]

$$(\mathcal{I} - \mathcal{T}_{\mathrm{OSM}})g = b_{\mathrm{OSM}}, \tag{2}$$

with g denoting Robin traces and $\mathcal{T}_{\mathrm{OSM}}$ only a weak contraction in general. Even after optimizing impedance parameters, one typically requires relaxation to ensure convergence.

Acknowledgements This research was funded by the Win2Wal R&D funding program under the project EXPANSION (Convention No. 2010161). The authors gratefully acknowledge this support.

References

[1] É. Parolin, *Non-overlapping domain decomposition methods with non-local transmission operators for harmonic wave propagation problems*, PhD Thesis, 2020.

[2] P.-L. Lions, *On the Schwarz alternating method. III: a variant for nonoverlapping subdomains*, Third international symposium on domain decomposition methods for partial differential equations. **6** (1990) 202–223.

[3] B. Després, *Méthodes de décomposition de domaine pour la propagation d'ondes en régime harmonique. Le théorème de Borg pour l'équation de Hill vectorielle*, PhD thesis. Université Paris IX Dauphine, 1991

[4] A. Modave, T. Chaumont-Frelet, *A hybridizable discontinuous Galerkin method with characteristic variables for Helmholtz problems*, Journal of Computational Physics **493** (2023) 112459.

Book of abstracts of the 9th International Conference on
Advanced Computational Methods in ENgineering and Applied Mathematics
September, 15–19, 2025.

Goal-Oriented Space-Time Adaptivity for Nonstationary Incompressible Flow Problems

Marius Paul Bruchhäuser[1], Nils Margenberg[1] and Markus Bause[1]

[1] *Chair of Numerical Mathematics, Helmut Schmidt University Hamburg*

e-mails: bruchhaeuser@hsu-hh.de, margenbn@hsu-hh.de, bause@hsu-hh.de

Abstract

The Dual Weighted Residual (DWR) Method has attracted researchers' interest in many fields of application problems since it was introduced by Becker and Rannacher at the turn of the last millennium. With regard to an efficient numerical approximation of the underlying model problem, the DWR approach yields an a posteriori error estimator measured in goal quantities of physical interest, that can be used for adaptive mesh refinement in space and time. Here, we apply this goal-oriented error control to nonstationary Navier-Stokes equations. The performance properties of the underlying algorithm are studied by means of well-known benchmarks for nonstationary flow problems. Furthermore, we give insight into the application of the DWR approach in combination with efficient iterative solver technologies using a flexible geometric multigrid preconditioner.

Keywords: Dual Weighted Residual Method, Geometric Multigrid Method, Goal-Oriented Error Control, Navier-Stokes Equations, Space-Time Adaptivity
MSC 2020: 65M50, 65M55, 65M60,

1 Introduction

We investigate here the following time-dependent incompressible Navier-Stokes equations

$$\begin{aligned} \partial_t \boldsymbol{v} - \nu\Delta\boldsymbol{v} + \boldsymbol{v}\cdot\nabla\boldsymbol{v} + \nabla p &= \boldsymbol{f} \quad \text{in } Q && = \Omega\times I,\\ \nabla\cdot\boldsymbol{v} &= 0 \quad \text{in } Q && = \Omega\times I,\\ \boldsymbol{v} &= \boldsymbol{v}_D \text{ on } \Sigma_D && = \Gamma_D\times I,\\ \nu\partial_{\boldsymbol{n}}\boldsymbol{v} - p\,\boldsymbol{n} &= \boldsymbol{0} \quad \text{on } \Sigma_{\text{outflow}} && = \Gamma_{\text{outflow}}\times I,\\ \boldsymbol{v}(0) &= \boldsymbol{v}_0 \text{ on } \Sigma_0 && = \Omega\times\{0\}, \end{aligned} \tag{1}$$

on a space-time domain $Q = \Omega \times I$, where $\Omega \subset \mathbb{R}^d$, with $d = 2$ or $d = 3$, is a polygonal or polyhedral bounded domain with Lipschitz boundary $\partial\Omega$ and $I = (0,T), 0 < T < \infty$, is a finite time interval. For this problem, we derive an a posteriori error representation based on the DWR method. This representation is given in terms of a user-chosen goal functional J, for instance, the deformation of a solid-point, the computation of a drag or lift coefficient or simply the control with respect to some global error norm. For the adaptve mesh refinement process, we split the total error representations into local, cell-wise error indicators in space and time, cf. [4]

$$J(\boldsymbol{u}) - J(\boldsymbol{u}_{\tau h}) = \underbrace{J(\boldsymbol{u}) - J(\boldsymbol{u}_\tau)}_{=:\eta_\tau} + \underbrace{J(\boldsymbol{u}_\tau) - J(\boldsymbol{u}_{\tau h})}_{=:\eta_h}.$$

For the efficient solution of the higher order space-time finite element approximation a parallelized geometric multigrid (GMG) method based on a cell-wise Vanka smoother is applied. This GMG solver serves as a preconditioner of the generalized minimal residual (GMRES) method used within the Newton's method. Each Newton step requires solving a large, sparse, nonsymmetric, and indefinite linear system due to the saddle–point structure of the Navier–Stokes equations. The implementation of the adaptive algorithm described in this work is distributed via MPI, exploiting `deal.II`'s [1] MPI parallel capabilities to perform error estimation, marking, refinement, and multigrid setup concurrently across processes.

Acknowledgements Computational resources (HPC cluster HSUper) have been provided by the project hpc.bw, funded by dtec.bw - Digitalization and Technology Research Center of the Bundeswehr. dtec.bw is funded by the European Union - NextGenerationEU.

References

[1] P. C. Africa, D. Arndt, W. Bangerth, B. Blais, M. Fehling, R. Gassmöller, T. Heister, L. Heltai, S. Kinnewig, M. Kronbichler, M. Maier, P. Munch, M. Schreter-Fleischhacker, J. P. Thiele, B. Turcksin, D. Wells, V. Yushutin, *The deal.II library, Version 9.6*, J. Numer. Math. **32(4)** (2024) 369–380.

[2] M. P. Bruchhäuser, M. Bause, *A cost-efficient space-time adaptive algorithm for coupled flow and transport*, Comput. Methods Appl. Math. **23(4)** (2023) 849–875.

[3] M. P. Bruchhäuser, U. Köcher, M. Bause, *On the implementation of an adaptive multirate framework for coupled transport and flow*, J. Sci. Comput. **93(59)** (2022) 1–29.

[4] M. P. Bruchhäuser, *Goal-oriented space-time adaptivity for a multirate approach to coupled flow and transport*, Ph.D. thesis, Helmut-Schmidt-University/University of the Federal Armed Forces Hamburg, 2022.

[5] U. Köcher, M. P. Bruchhäuser, M. Bause, *Efficient and scalable data structures and algorithms for goal-oriented adaptivity of space–time FEM codes*, Software X **10:100239** (2019).

Book of abstracts of the 9th International Conference on
Advanced Computational Methods in ENgineering and Applied Mathematics
September, 15–19, 2025.

Intrinsic Surface Meshing Using Geodesic Distances for High-Order Methods

Tim Gabriel[1], Jean Bragard[2], Jean-François Remacle[3] and Christophe Geuzaine[1]

[1] *Department of Electrical Engineering and Computer Science, Montefiore Institute , University of Liège, Belgium*

[2] *Department of Physics and Applied Mathematics, Institute of Data Science and Artificial Intelligence , University of Navarra, Spain*

[3] *Institute for Mechanical, Materials and Civil Engineering , Catholic University of Louvain, Belgium*

e-mails: tim.gabriel@uliege.be, jbragard@unav.es, jean-francois.remacle@uclouvain.be, cgeuzaine@uliege.be

Abstract

We present an intrinsic meshing process for accurately approximating complex surfaces. Starting from a high-resolution triangulation, intrinsic mesh operations based on geodesic distances adapt the mesh without geometric approximation. Intrinsic elements can then be approximated by high-order polynomial elements suitable for numerical simulations. We demonstrate the effectiveness of this new approach by simulating the membrane potentials on the left atrium of a human heart.

Key words: intrinsic meshing, geodesic distance, high-order method, mesh coarsening

Accurately and efficiently approximating complex geometries is essential for the success of numerical simulations, particularly when dealing with surfaces that exhibit multiscale features or strong curvature gradients. In this work, we incorporate the concept of intrinsic triangulation [1] into an adaptive meshing framework, introducing a novel approach to intrinsic mesh generation for arbitrary input surfaces.

The method begins with a high-resolution triangulation of the target surface, serving as the geometric ground truth. From this starting point, we apply a sequence of intrinsic local mesh optimization operations—such as edge swaps, collapses, splits, and point insertions—guided by geodesic distances computed via a continuous Dijkstra algorithm [2]. These operations construct an intrinsic mesh, a segmentation of the original surface in which each edge represents the shortest geodesic path between two vertices (see Figure 1).

Crucially, this segmentation introduces no geometric approximation: all vertices, edges, and faces of the intrinsic mesh lie exactly on the original surface. The resulting intrinsic mesh could be used as-is in polytopal numerical methods such as HHO; but it also constitutes an ideal intermediate representation for simplicial high-order numerical methods. Here, a high-order polynomial triangle is fitted to each intrinsic face, producing a mesh suitable for standard finite element solvers.

As an application, Figure 2 illustrates the simulation of membrane potential propagation on the surface of a human left atrium [3]. The intrinsic high-order mesh allows the use of fewer but larger curved elements, leading to improved convergence while keeping the number of degrees of freedom low.

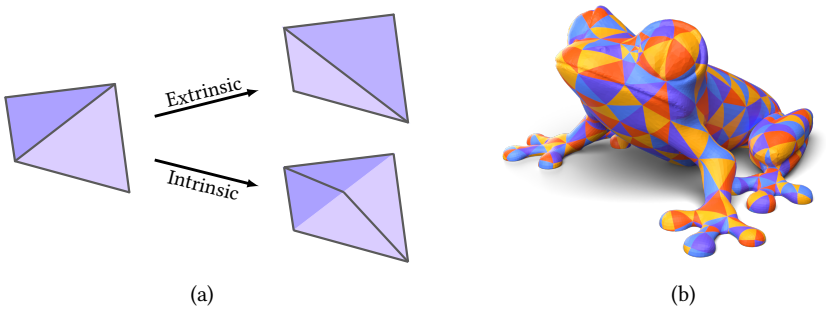

Figure 1: Intrinsic framework: (a) the swap edge operation and (b) an example of mesh.

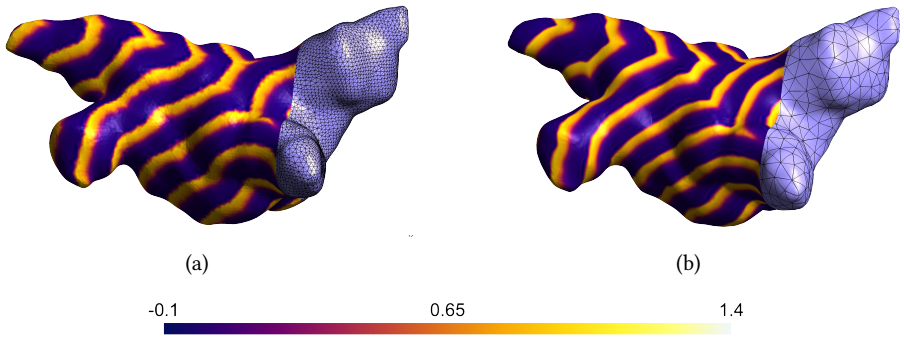

Figure 2: Simulation of membrane potential pulse propagation on the left atrium using (a) the initial mesh and (b) a 7th-order mesh with elements five times larger.

References

[1] N. Sharp, Y. Soliman, K. Crane, *Navigating intrinsic triangulations*, ACM Transactions on Graphics (TOG), **38** (2019) 1–16.

[2] J. Mitchell, D. Mount, C. Papadimitriou, *The discrete geodesic problem*, SIAM Journal on Computing, **16** (1987) 647–668.

[3] J. Bragard et al., *Cardiac computational modelling*, Revista Española de Cardiología (English Edition), **74(1)** (2021) 65–71.

Book of abstracts of the 9th International Conference on
Advanced Computational Methods in ENgineering and Applied Mathematics
September, 15–19, 2025.

GPU-Accelerated Substructured Optimized Schwarz Solver for the Helmholtz Equation

Roland Greffe[1], Ahmed Chabib[2], Axel Modave[2] and Christophe Geuzaine[1]

[1] *Department of Electrical Engeneering and Computer Science, University of Liège, Belgium*

[2] *POEMS, CNRS, Inria, ENSTA, Institut Polytechnique de Paris*

e-mails: r.greffe@uliege.be, ahmed.chabib@ensta.fr, axel.modave@ensta.fr, cgeuzaine@uliege.be

Abstract

This work discusses a GPU-accelerated implementation of a Domain Decomposition Method (DDM) for the finite element solution of the Helmholtz equation, based on the existing CPU implementation of an optimized substructured Schwarz algorithm in Gmsh-DDM. The design choices made in order to adapt the solver to efficiently exploit multiple GPUs are discussed, as well as initial convergence and scalability results.

Key words: Helmholtz equation, finite element method, Domain Decomposition Methods, GPU computing

1 Introduction

Solving large-scale 3D Helmholtz problems with high-order finite elements remains a major challenge: direct solvers are prohibitively costly in memory and time, while iterative methods often struggle to converge. Among existing approaches, domain decomposition methods (DDMs) stand out as a powerful and flexible solution, blending the strengths of both direct and iterative techniques [1].

One of the main advantages of DDMs is their ability to decompose a large problem into smaller subproblems that can be solved independently and thus in parallel, which is why they are often used in High Performance Computing (HPC) applications. However, current implementations are limited to CPUs rather than Graphical Processing Units (GPUs), which is an issue as current HPC machines are beginning to shift towards having most of their computational power on GPUs.

2 GPU-accelerated DDM solver

Our strategy to adapt DDMs to GPUs is three-fold: 1) instead of using DDMs as a preconditioner for the large Helmholtz system, we use a substructured, non-overlapping approach that reformulates the Helmholtz problem in terms of a (much) smaller number of interface unknowns; 2) we split the computational mesh into very small subdomains, so that high arithmetic intensity dense algebra can be used on each subdomain; 3) we use optimized interface

conditions between the subdomains to minimize the number of iterations of the Krylov subspace solver. However, using small subdomains comes at a cost as the number of iterations of a one-level DDM increases with the number of subdomains. The hope is that this will be compensated by the speed-up gained by the use of GPUs.

Efficiently porting the substructured DDM on GPU in the GmshDDM library[1] implies moving all the computationally intensive parts on GPU and minimizing copies between host and device memory. To this end, the LU factorizations of the subdomain matrices used by the direct solvers have been converted into a single batched LU factorization, which is then used to solve all the local linear systems in parallel [2]. The Krylov subspace method is fully implemented on GPU through PETSc[2], with a custom preconditioner making use of the subdomain direct solves directly on GPU as well, with batched matrix-vector multiplications.

Figure 1 shows the weak scalability of this approach on a reference Helmholtz problem: a rectangular waveguide discretized with fifth order quadrangular finite elements. A layered partitioning is used, with 2400 subdomains per GPU, combined with a restarted GMRES(100) Krylov solver. Each GPU manages 1.452.121 DOFs and each subdomains contains 24 elements.

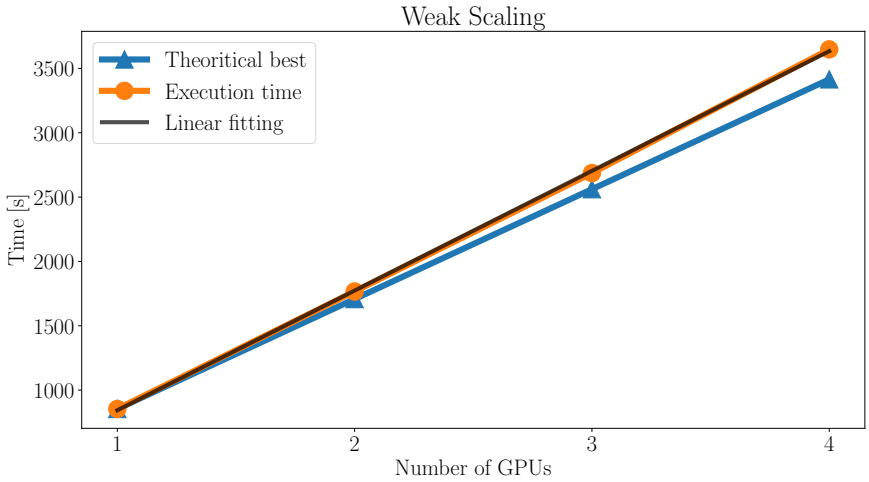

Figure 1: Weak scaling of an Helmoltz Waveguide problem solved with 2400 subdomains per GPU on up to 4 NVIDIA A100 40GB with a GMRES restart value of 100.

Acknowledgements Roland Greffe is a FRIA grantee of the Fonds de la Recherche Scientifique – FNRS.

References

[1] V. Dolean, P. Jolivet, F. Nataf, *An Introduction to Domain Decomposition Methods: Algorithms, Theory, and Parallel Implementation*, Society for Industrial and Applied Mathematics, Philadelphia, PA, 2015.

[2] A. Abdelfattah, N. Beams, R. Carson, et al., *MAGMA: Enabling exascale performance with accelerated BLAS and LAPACK for diverse GPU architectures*, The International Journal of High Performance Computing Applications, **38**(5), pp. 468–490, 2024.

[1] https://gitlab.onelab.info/gmsh/ddm/
[2] https://petsc.org/

Book of abstracts of the 9th International Conference on
Advanced Computational Methods in ENgineering and Applied Mathematics
September, 15–19, 2025.

Two-level Schwarz preconditioners with an algebraic multiscale coarse spaces for large-scale heterogeneous problems

Filipe Cumaru[1], Alexander Heinlein[1] and Hadi Hajibeygi[2]

[1] *Delft Institute of Applied Mathematics, Delft University of Technology*

[2] *Department of Geoscience and Engineering, Delft University of Technology*

e-mails: f.a.cumarusilvaalves@tudelft.nl, a.heinlein@tudelft.nl, h.hajibeygi@tudelft.nl

Abstract

The Schwarz framework enables the construction of multilevel preconditioners for linear systems arising from the discretization of elliptic problems. In this context, a global problem defined in a coarse space ensures robustness and scalability. An effective coarse space captures problematic error modes, such as those related to the null space or potential heterogeneities. In this talk, we discuss an algebraic multiscale coarse space and present its parallel implementation in the FROSch (Fast and Robust Overlapping Schwarz) package within the Trilinos software framework. We compare the parallel performance of our algebraic multiscale coarse space with other algebraic coarse space options available in FROSch. Finally, we investigate the use of local inexact solvers to reduce the computational cost of applying the preconditioner while maintaining robustness.

Key words: two-level Schwarz preconditioners, multiscale coarse space, heterogeneous problems, parallel computing

1 Introduction

We consider the scalar diffusion problem

$$\begin{aligned} -\nabla \cdot (\alpha(x)\nabla u(x)) &= f(x) \qquad && \text{in } \Omega \subset \mathbb{R}^d, \\ u &= u_D(x) \qquad && \text{on } \partial\Omega, \end{aligned} \tag{1}$$

for $d = 2, 3$ and with scalar coefficient function $\alpha : \mathbb{R}^d \to \mathbb{R}$ with $0 < \alpha_{min} \leq \alpha \leq \alpha_{max} < \infty$, for $\alpha_{min}, \alpha_{max} \in \mathbb{R}^+$, which is highly heterogeneous possibly containing jumps.

We discretize eq. (1) using linear or bilinear/trilinear finite elements on a computational domain Ω and employ a preconditioned Krylov subspace method to solve the resulting system of linear equations $Ax = b$. Then, we partition the rows of A based on a non-overlapping domain decomposition of Ω and extend the subdomains algebraically in a recursive manner to obtain overlapping subdomains. The two-level additive Schwarz preconditioner reads

$$M_{OAS,2}^{-1} = \Phi A_0^{-1} \Phi^\top + \sum_{i=1}^{N} R_i^\top A_i^{-1} R_i, \tag{2}$$

where R_i is the restriction matrix of the i-th overlapping subdomain, $A_i = R_i A R_i^\top$ the corresponding local subdomain matrix, and $A_0 = \Phi^\top A \Phi$ is the coarse problem matrix determined by the coarse basis functions, which form the columns of Φ. The coarse problem is required for numerical scalability of domain decomposition methods.

We apply an algebraic formulation of the multiscale finite element method (MsFEM) [3, 1] to compute the coarse basis functions in Φ in eq. (2). The MsFEM basis functions are energy-minimizing extensions of trace functions defined on the interface of the non-overlapping subdomains into the interior. This allows the coarse space to better capture variations in α. The method is implemented in the FROSch package within Trilinos [2].

2 Numerical results

The results for a 3D model problem are shown in fig. 1. We have employed the conjugate gradient method with the preconditioner in eq. (2) to a stopping criterion $||r^{(k)}||_2/||r^{(0)}||_2 < 10^{-6}$, where $r^{(0)}$ and $r^{(k)}$ are the initial and k-th unpreconditioned residuals, respectively. Cubic non-overlapping subdomains were used with $H/h = 16$, where H and h are the subdomain and the grid size, respectively. The performance of our approach is compared to the algebraic GDSW and RGDSW coarse spaces available on FROSch.

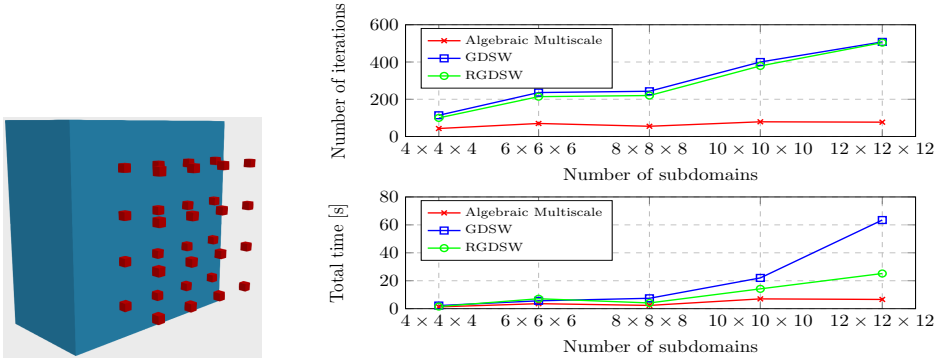

(a) (b)

Figure 1: Coefficient distribution (a) and the weak scalability results for the preconditioner in eq. (2) (b). In (a), $\alpha(x) = 10^5$ in the red regions, and $\alpha(x) = 1$ elsewhere.

References

[1] F. A. C. S. Alves, A. Heinlein, H. Hajibeygi, *A computational study of algebraic coarse spaces for two-level overlapping additive Schwarz preconditioners*, arXiv pre-print, **DOI:** 10.48550/arXiv.2408.08187 (2024).

[2] M. Mayr, A. Heinlein, C. Glusa, S. Rajamanickam *et al.*, *Trilinos: Enabling Scientific Computing Across Diverse Hardware Architectures at Scale*, arXiv preprint arXiv:2503.08126 (2025).

[3] Y. Wang, H. Hajibeygi, H. A. Tchelepi, *Algebraic multiscale solver for flow in heterogeneous porous media*, J. Comput. Phys. **259** (2014) 284–303.

Book of abstracts of the 9th International Conference on
Advanced Computational Methods in ENgineering and Applied Mathematics
September, 15–19, 2025.

An *hp* Multigrid Approach for Tensor-Product Space-Time Finite Element Discretizations of the Stokes Equations

Nils Margenberg[1], Peter Munch[2] and Markus Bause[1]

[1] *Chair of Numerical Mathematics, Helmut Schmidt University Hamburg*

[2] *Faculty of Mathematics, Technical University Berlin*

e-mails: margenbn@hsu-hh.de, p.muench@tu-berlin.de, bause@hsu-hh.de

Abstract

We propose a monolithic *hp* space-time multigrid method for the Stokes equations, discretized using tensor-product space-time finite elements. We employ an inf-sup stable pressure-velocity pair in space. The discontinuous Galerkin time discretization yields a fully variational space-time formulation. Our multigrid scheme performs both geometric and polynomial coarsening in space and time and leverages matrix-free techniques from the `deal.II` library. A space-time cell-wise Vanka smoother addresses the challenge of constructing efficient smoothers for the coupled system. Numerical experiments on problems with $> 10^{12}$ degrees of freedom confirm excellent scalability and throughput exceeding 10^8 dofs/s.

Key words: Space-time finite elements, space-time multigrid, matrix-free, higher-order finite elements

MSC 2020: 65M60, 65M55, 65F10, 65Y05

1 *hp* Multigrid Method for Space-Time Finite Elements

We present a monolithic *hp* space-time multigrid method for tensor-product space-time finite element discretizations of the *Stokes equations*, which in first-order form read:

$$\begin{aligned} -\nu\Delta\mathbf{u} + \nabla p &= \mathbf{f} \quad \text{in } \Omega \times (0,T), \\ \nabla \cdot \mathbf{u} &= 0 \quad \text{in } \Omega \times (0,T), \end{aligned}$$

subject to appropriate boundary and initial conditions, where $\nu > 0$ denotes the kinematic viscosity, $\mathbf{u}$ is the velocity field, and p the pressure [1]. Geometric and polynomial coarsening of the space–time mesh is performed, and the entire algorithm is expressed through rigorous mathematical mappings. The temporal domain $(0,T)$ is partitioned into slabs $I_n = (t_n, t_{n+1}]$, and the spatial domain $\Omega \subset \mathbb{R}^d$ is discretized using tensor-product finite elements. For the discretization, we use *inf-sup stable* of the form:

$$\mathcal{V}_h = \mathbb{Q}_{r+1}(\Omega_h)^d, \quad \mathcal{Q}_h = \mathbb{P}_r^{\text{disc}}(\Omega_h),$$

for velocity and pressure, respectively, where $\mathbb{Q}_{r+1}$ denotes the space of continuous polynomials of degree $r+1$ on hexahedral meshes, and $\mathbb{P}_r^{\text{disc}}$ the space of discontinuous polynomials of degree r.

In time, we employ a discontinuous Galerkin (DG(k)) discretization with piecewise polynomials of order k. The key novelty of this work is the application of *hp* multigrid techniques in space and time, facilitated and accelerated by the matrix-free capabilities of the `deal.II` library (cf. Figure 1). While multigrid methods are well-established for stationary problems, their application in space-time formulations encounter unique challenges, particularly in constructing suitable smoothers. To overcome these challenges, we employ a space-time cell-wise Vanka smoother. Extensive tests on high-performance computing platforms demonstrate the efficiency of our *hp* multigrid approach on problem sizes exceeding a trillion degrees of freedom (dofs), sustaining throughputs of hundreds of millions of dofs per second.

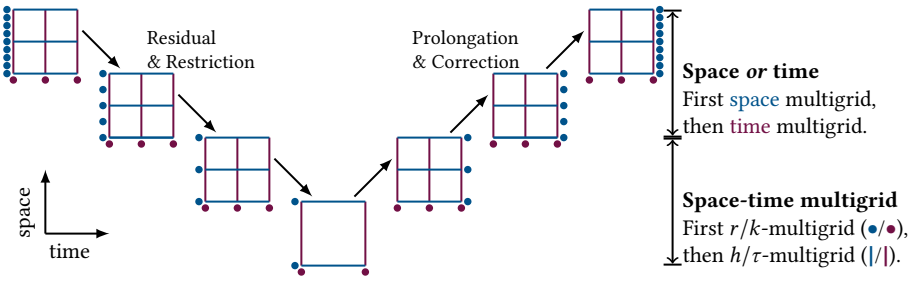

Figure 1: Sketch of the *hp* space-time multigrid method. The corrections are transferred by the prolongation operators and the residual is transferred by the restriction operators. On each level the error is smoothened by application of the Vanka smoother. Coarsening is done first in space then in time. Polynomial coarsening is done before geometric coarsening.

The methodology has also been applied to acoustic wave equations [2]. Extensive empirical evidence, provided through scaling and convergence tests on high-performance computing platforms, demonstrated high performance on perturbed meshes and problems with heterogeneous and discontinuous coefficients. The results show that the space-time multigrid method can effectively solve complex problems in high-fidelity simulations and show great potential for use in coupled problems.

Acknowledgements Computational resources (HPC cluster HSUper) have been provided by the project hpc.bw, funded by dtec.bw - Digitalization and Technology Research Center of the Bundeswehr. dtec.bw is funded by the European Union - NextGenerationEU.

References

[1] N. Margenberg, P. Munch, M. Bause, *An hp multigrid approach for tensor-product space-time finite element discretizations of the Stokes equations*, SIAM J. Sci. Comput., under review (2025), pp. 1–23; arXiv:2502.09159

[2] N. Margenberg, P. Munch, *A Space-Time Multigrid Method for Space-Time Finite Element Discretizations of Parabolic and Hyperbolic PDE*, Springer Scientific Computing, under review (2024), pp. 1–33; arXiv:2408.04372

Book of abstracts of the 9th International Conference on
Advanced Computational Methods in ENgineering and Applied Mathematics
September, 15–19, 2025.

To overlap or not to overlap? A large-scale investigation for Helmholtz problems with multiple sources

Boris Martin[1], Pierre Jolivet[2] and Christophe Geuzaine[1]

[1] *Montefiore Institute, University of Liège*

[2] *CNRS, LIP6, Université Paris Sorbonne*

e-mails: boris.martin@uliege.be, pierre@joliv.et, cgeuzaine@uliege.be

Abstract

Solving large-scale 3D time-harmonic problems is notoriously difficult: direct solvers are robust but unscalable, and classical iterative methods degrade at high frequencies. Hybrid solvers based on domain decomposition methods (DDMs), which iteratively solve smaller subproblems, offer a scalable alternative. We compare two DDMs: the overlapping ORAS preconditioner and the non-overlapping OSM substructuring method. Tests on up to 32768 CPU cores show that non-overlapping methods are roughly twice as efficient on realistic benchmarks, especially when solving for multiple right-hand sides, as in Full Waveform Inversion.

Key words: Domain decomposition methods, Helmholtz equation, High-performance scientific computing, Optimized Restricted Additive Schwarz, Optimized Schwarz Method,
MSC 2020: 35J05, 65N55, 68W10, 35-04, 86-08

1 Introduction

Full Waveform Inversion (FWI) in the frequency-domain is a seismic imaging technique that aims to reconstruct the subsurface properties of the Earth from seismic data. It is a challenging problem, especially in 3D, due to the large size and ill-conditioning of the linear systems arising from a FEM or FD discretization of the PDE of interest, such as the Helmholtz equation. DDMs have been suggested as a promising approach to solve these large systems efficiently. Overlapping methods such as ORAS have been shown to outperform sparse direct solvers in [1]. In this talk we compare this approach to non-overlapping, substructured Optimized Schwarz Methods (OSM) [2]. We show numerically that our approach is twice as efficient in both time and memory on the realistic geophysics benchmark proposed in [3].

2 Summary of the results

We solved the Helmholtz equation on a h-adaptive tetrahedral mesh (with $P3$ elements) for 64 RHS. Table **??** summarizes our results with the highest frequencies f we simulated. It shows that the OSM approach is consistently faster despite a higher iteration count. Figure 1 shows the weak scaling of both approaches: for a constant subdomain size and a number of subdomains proportional f^3, the computational time grows as $O(f)$.

Problem solved			Time spent (s)				Cumulated	
f (Hz)	DOFs (M)	$N_{\text{subdomains}}$	Solves	GMRES	SpMM	Total	CPU-h	Its.
OSM:								
5.00	326.4	4,096	226.3	22.9	21.6	291.1	662.5	249
5.00	326.4	8,192	130.5	18.8	14.7	182.4	830.2	318
5.00	326.4	16,384	70.5	13.3	8.6	99.5	905.6	346
6.25	630.1	8,192	303.1	29.4	28.7	378.6	1,723.3	318
6.25	630.1	16,384	142.0	20.7	16.4	205.5	1,870.7	357
ORAS:								
5.0	326.4	8,192	223.8	110.6	98.5	363.7	1,655.2	244
5.0	326.4	16,384	160.6	89.2	82.6	256.9	2,338.2	344
6.25	630.1	16,384	311.1	162.3	147.2	502.6	4,574.7	347

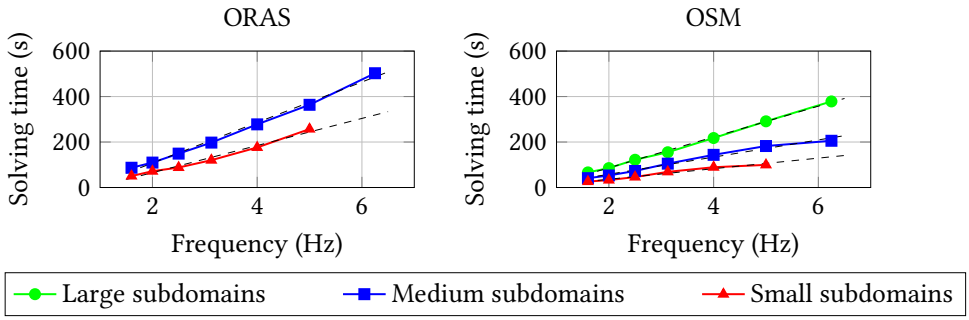

Figure 1: Weak scaling comparison of OSM and ORAS with constant subdomain size. Dashed lines represent affine functions fitting each curve.

References

[1] P.-H. Tournier, P. Jolivet, V. Dolean, H. S. Aghamiry, S. Operto, and S. Riffo, *Three-dimensional finite-difference & finite-element frequency-domain wave simulation with multi-level optimized additive Schwarz domain-decomposition preconditioner: A tool for FWI of sparse node datasets*, arXiv preprint arXiv:2110.15113, 2021. arxiv.org/abs/2110.15113

[2] B. Martin, P. Jolivet, and C. Geuzaine, *Comparison of substructured non-overlapping domain decomposition and overlapping additive Schwarz methods for large-scale Helmholtz problems with multiple sources*, arXiv preprint arXiv:2506.16875, 2025. arxiv.org/abs/2506.16875

[3] A. Górszczyk and S. Operto, *GO_3D_OBS: the multi-parameter benchmark geomodel for seismic imaging method assessment and next-generation 3D survey design (version 1.0)*, Geosci. Model Dev. **14** (2021), no. 3, 1773–1799. DOI: 10.5194/gmd-14-1773-2021

Book of abstracts of the 9th International Conference on
Advanced Computational Methods in ENgineering and Applied Mathematics
September, 15–19, 2025.

Pressure-robustness for (nearly) incompressible flows

Alexander Linke[2], Christian Merdon[1] and Marwa Zainelabdeen[1]

[1] *Research Group Numerical Mathematics and Scientific Computing, Weierstrass Institute for Applied Analysis and Stochastics*

[2] *Scientific Computing, University of Kaiserslautern-Landau (RPTU)*

e-mails: alexander.linke@rptu.de, christian.merdon@wias-berlin.de, marwa.zainelabdeen@wias-berlin.de

Abstract

The talk starts with a refined stability analysis of mixed problems that focusses on semi norms and related equivalence properties. The observations are motivated by the concept of pressure-robustness for the incompressible Stokes problem, which characterizes discretizations that allow for discrete velocity estimates that are independent of the pressure.

The second part focusses on the compressible Stokes problem and discretizations that are provable convergent on unstructured grids and preserve pressure-robustness when the Mach number goes to zero.

Key words: Navier–Stokes Equations, Mixed Finite Element Methods, Mixed Problems, Pressure-Robustness

MSC 2020: 65N12, 65N30, 76D05, 76D07

1 Summary

Starting with a more abstract setting, consider a mixed problem of the form

$$\begin{aligned} a(u,v) + b(v,p) &= F(v) \quad \forall v \in V, \\ b(u,q) &= G(q) \quad \forall q \in Q, \end{aligned}$$

formulated on Hilbert spaces V and Q with bilinearforms $a : V \times V \to \mathbb{R}$ and $b : V \times Q \to \mathbb{R}$ and linear forms $F \in V^\star$ and $G \in Q^\star$. The bilinearform a is symmetric and elliptic with constant $\alpha > 0$, while the operator b is bounded and surjective, i.e., satisfies an inf-sup condition with inf-sup constant $\beta > 0$, such that the mixed problem is well-posed. This setting allows for the refined stability estimates [1]

$$\|u\|_V \leq \frac{1}{\alpha}\|F\|_{K^\star} + \frac{1}{\beta}\left(\frac{\|a\|}{\alpha}\right)^{1/2}\|G\|_{Q^\star} \quad \text{and} \quad \|p\|_Q \leq \frac{1}{\beta}\left(\frac{\|a\|}{\alpha}\right)^{1/2}\|F\|_{(K_a^\perp)^\star} + \frac{\|a\|}{\beta^2}\|G\|_{Q^\star}$$

with operator semi norms $\|F\|_K^\star$ and $\|F\|_{(K_a^\perp)^\star}$ for the spaces $K := \{v \in V : b(v,q) = 0 \text{ for all } q \in Q\}$ and $K_a^\perp := \{v \in V : a(v,w) = 0 \text{ for all } w \in K\}$, respectively.

For the Stokes model problem with

$$a(u,v) = \int_\Omega \nabla u : \nabla v \, dx \quad \text{and} \quad b(v,p) = -\int_\Omega \nabla \cdot v \, p \, dx$$

and divergence constraint with $G = 0$, one obtains

$$\|\nabla \mathbf{u}_h\|_0 =: \|\mathbf{u}_h\|_{\mathrm{V}} \leq \|\nabla \mathbf{u}\|_0 + \frac{1}{\nu}\|b(\bullet, p)\|_{\mathrm{K}^\star}.$$

Observe, that $\|b(\bullet, p)\|_{\mathrm{K}^\star} = 0$ represents the L^2-rthogonality of divergence-free functions and pressures gradients which is usually not preserved in classical finite element methodsand can causes a locking phenomenon for $\nu \to 0$. Indeed, in a Galerkin discretization with discrete spaces $V_h \subset V$ and $Q_h \subset Q$ the pressure term gets replaced by $\|b(\bullet, p)\|_{\mathrm{K}_h^\star}$ for the space of discretly divergence free functions K_h and only vanishes for divergence-free methods with $\mathrm{div}(V_h) = Q_h$. Alternatively, pressure-robust discretizations can be achieved by introducing a reconstruction operator Π in the right hand side F, such that $\|b(\Pi\bullet, p)\|_{\mathrm{K}_h^\star}$ appears and vanishes if Π maps K_h to a divergence-free space.

The second part of the talk explains how the concept of pressure-robustness can be extended to the compressible Stokes problem. Given an equation of state, e.g. $p(\varrho) = c\varrho^\gamma$ for $\gamma \geq 1$, the compressible Stokes problem seeks a velocity $\mathbf{u}$ and a positive density ϱ such that

$$\begin{aligned} a(u,v) + b(v, p(\varrho)) &= F(v) \quad \forall v \in V, \\ \int_\Omega \varrho \mathbf{u} \cdot \nabla w &= 0 \quad \forall w \in W^{1,\infty}(\Omega) \end{aligned}$$

and $\int_\Omega \varrho \, dx = M$ for a given mass $M > 0$. A force balance balance $F = b(\bullet, p(\varrho))$ leads to a hydrostatic solution with $\mathbf{u} = \mathbf{u}$ and discretizations that preserve this regime therefore require $\|b(\Pi\bullet, p(\varrho))\|_{\mathrm{K}_h^\star} = 0$. This motivates to employ pressure-robust designs also for the compressible Stokes problem. A short summary of stability and convergence results and some supporting numerical examples conclude the talk.

References

[1] N. Gauger, A. Linke, C. Merdon, *Refined stability estimates for mixed problems by exploiting semi norm arguments*, https://arxiv.org/abs/2506.11566 (2025).

[2] M. Akbas, T. Gallouet, A. Gassmann, A. Linke and C. Merdon,

A gradient-robust well-balanced scheme for the compressible isothermal Stokes problem, CMAME 367 (2020).

Book of abstracts of the 9th International Conference on
Advanced Computational Methods in ENgineering and Applied Mathematics
September, 15–19, 2025.

TerraNeo: High-Performance Simulation of Geodynamical Fluids with Mesh-Free Finite-Element Methods and Code Generation

Marcus Mohr[1], Daniel Bauer[2], Andreas Burkhart[3], Fabian Böhm[2], Ponsuganth Ilangovan[1], Nils Kohl[1] and Barbara Wohlmuth[3]

[1] *Department of Geo- and Environmental Sciences, LMU Munich*

[2] *Department of Computer Science, Friedrich-Alexander-University of Erlangen-Nuremberg*

[3] *School of Computation, Information and Technology, TU Munich*

e-mails: marcus.mohr@lmu.de, daniel.j.bauer@fau.de, burk@ma.tum.de, fabian.boehm@fau.de, p.ilango@lmu.de, nils.kohl@lmu.de, wohlmuth@ma.tum.de

Abstract

In this contribution we report on the high-performance Finite-Element framework HyTeG (Hybrid Tetrahedral Grids) and its associated code generator HOG. We focus on the demonstrator application TerraNeo for simulating convection in the Earth's mantle and demonstrate that HyTeG allows to scale realistic scenarios up to 61,444 cores and solve problems for global resolutions of 3 km with 10^{11} (1 E11) DoFs.

Keywords: Code Generation, Computational Geoscience, Mantle Convection, Mesh-Free Methods, Multigrid

1 Application

The uplift of the Himalya mountain range, the volcanic activity around the Pacific ring of fire, earthquakes triggered by built-up of stress at tectonic plate margins, are all surface expressions of convective processes within the Earth's mantle. Via the latter our planet rids itself of excess energy left from its formation and heat generated by radioactive decay. A detailed understanding of these processes is, thus, of fundamental interest to Geophysics and computational experiments are the primary tool to achieve this.

While the mantle is composed of rocks, these deform on geologic time-scales of millions of years similar to a fluid. Due to the slow speeds and extreme viscosities the process can be modelled by an extended compressible Stokes equation in combination with an equation for the conservation of energy. The mantle has a thickness of about 3.000 km. However, features of interest, such as rising plumes and subducting slabs, are on the order of a few km requiring extremely fine resultions. The resulting large number of degrees of freedom (DoFs) in combination with a large number of time-steps to cover millions of years of simulated time constitute a major computational challenge.

2 Software Framework

In this contribution we will report on the TerraNeo project[1] whose goal it is to create software to support mantle convection simulations with 1 km global resolution. In order to achieve this we make use of the open source Finite-Element framework HyTeG, [3] It combines the flexibility of an unstructured coarse base mesh with the performance benefits of a structured fine mesh. The refinement process naturally leads to a hierarchy of meshes lending itself for the implementation of geometric multigrid solvers. HOG, the associated code generator, [1], creates optimized C++ code for the evaluation of (bi-)linear forms, allows to easily extend HyTeG to new PDE problems, while avoiding the necessity for hand-tuning code.

The bulk of the computational effort in the convection model goes into solving the Stokes system. HyTeG offers multiple iterative approaches for this, such as e.g. a monolithic multigrid method with Uzawa-type smoother or a classic pressure-correction scheme. For realistic Earth-like models, which feature strong, localised viscosity contrasts we currently prefer multigrid preconditioned FGMRES solvers, see [2]. The energy equation, which is of advection-diffusion type is handled with a semi-lagrangian approach as detailed in [4]. With this we were able demonstrate excellent weak scaling of TerraNeo for realistic scenarios on the Hawk supercomputer at the Supercomputing Center Stuttgart (HLRS) on up to 61,444 cores and could solve a problem with nearly 10^{11} DoFs, giving a global resolution of 3 km.

Acknowledgements This work has been partially supported by the German Federal Ministry of Research, Technology and Space (BMFTR) (16ME0649 - SCALEXA: CoMPS) and the German Research Foundation (DFG) via the research training group UPLIFT (GRK 2698) - 440512084. Computing resources were provided by the Institute of Geophysics of LMU Munich, funded by DFG - 495931446 and 518204048, the Supercomputing Center Stuttgart (HLRS).

References

[1] F. Böhm, D. Bauer, N. Kohl, Chr. Alappat, D. Thönnes, M. Mohr, H. Köstler, and Ulrich Rüde, *Code Generation and Performance Engineering for Matrix-Free Finite Element Methods on Hybrid Tetrahedral Grids*, SIAM J. Sci. Comp. **47(1)** (2025) B131–B159.

[2] A. Burkhart, N. Kohl, B. Wohlmuth, and J. Zawallich, *A robust matrix-free approach for large-scale non-isothermal high-contrast viscosity stokes flow on blended domains with applications to Geophysics*, arXiv **2506.04157** (2025).

[3] N. Kohl, D. Thönnes, D. Drzisga, D. Bartuschat, and U. Rüde, *The HyTeG finite-element software framework for scalable multigrid solvers*, Int. J. Parallel, Emergent and Distributed Systems **34(5)** (2019) 477–496.

[4] N. Kohl, M. Mohr, S. Eibl, and U. Rüde, *A Massively Parallel Eulerian-Lagrangian Method for Advection-Dominated Transport in Viscous Fluids*, SIAM J. Sci. Comp. **44(3)** (2022) C260–C285.

[5] P. Ilangovan, N. Kohl, and M. Mohr, *Highly Scalable Geodynamic Simulations with HyTeG*, Geoscientific Model Development (2025), under review.

[1] https://terraneo.fau.de

Book of abstracts of the 9th International Conference on
Advanced Computational Methods in ENgineering and Applied Mathematics
September, 15–19, 2025.

Monolithic convex limiting and implicit pseudo-time stepping for calculating steady-state solutions of the Euler equations

Paul Moujaes[1] **and Dmitri Kuzmin**[1]

[1] *Institute of Applied Mathematics (LS III), TU Dortmund University*
Vogelpothsweg 87, D-44227 Dortmund, Germany

e-mails: paul.moujaes@math.tu-dortmund.de, kuzmin@math.tu-dortmund.de

Abstract

In this work, we discretize the Euler equations of gas dynamics in space using a continuous Galerkin finite element method and a monolithic convex limiting (MCL) strategy. For the backward Euler time stepping, we show that the resulting nonlinear system has an invariant domain preserving (IDP) solution. Our proof involves constructing a fixed-point iteration that meets the requirements of a Krasnoselskii-type theorem. Our iterative solver for the nonlinear discrete problem employs a more efficient fixed-point iteration. The matrix of the associated linear system is a robust low-order Jacobian approximation that exploits the homogeneity property of the flux function. The limited antidiffusive terms are treated explicitly. We use positivity preservation as a stopping criterion for nonlinear iterations. The first iteration yields the solution of a linearized semi-implicit problem. This solution possesses the discrete conservation property but is generally not IDP. Further iterations are performed if any non-IDP states are detected. The existence of an IDP limit is guaranteed by our analysis. To facilitate convergence to steady-state solutions, we perform adaptive explicit underrelaxation at the end of each time step. The calculation of appropriate relaxation factors is based on an approximate minimization of nodal entropy residuals. The performance of proposed algorithms and alternative solution strategies is illustrated by the convergence history for standard two-dimensional test problems.

Key words: convex limiting, hyperbolic conservation laws, implicit schemes, positivity preservation, steady-state computations

Book of abstracts of the 9th International Conference on
Advanced Computational Methods in ENgineering and Applied Mathematics
September, 15–19, 2025.

Computational Hemodynamic Analysis of Stenosed Coronary Arteries: Non-Newtonian Flow Dynamics and Magnetohydrodynamic Effects Using OpenFOAM

Nimra muqaddass[1]

[1] *IMT School for Advanced Studies Lucca, Italy*

e-mails: nimra.muqaddass@imtlucca.it

Abstract

Hemodynamic changes from severe coronary artery stenosis significantly affect cardiovascular health, requiring advanced computational tools to predict flow dynamics. This study uses CFD analysis with the Casson model to simulate non-Newtonian blood flow in a 100 mm arterial segment with 70% stenosis (2.9 mm diameter). The pimpleFoam solver in OpenFOAM resolves transient, incompressible laminar flow with no-slip walls and zero-gradient pressure outlet. We analyze momentum and pressure distribution through the stenosis and the impact of an external magnetic field using Lorentz force in the momentum equations. Our findings show an increased momentum and pressure drop within the stenosis compared to upstream conditions. An external magnetic field (1.2 T) reduces peak velocity and flattens the velocity profile. *Key words: Non-Newtonian CFD, OpenFOAM Modeling, Magnetic Drug Targeting, Cardiovascular Biomechanics*

1 Introduction

Cardiovascular disease is a major global health issue, particularly due to hemodynamic disorders like stenosis that impact morbidity and mortality. Blood flow disturbances increase wall shear stress (WSS) and disrupt pressure distributions, which can harm endothelial tissue [1]. Recent studies highlight the role of computational fluid dynamics (CFD) in diagnosing cardiovascular issues and guiding treatments ([2], [4]). Non-Newtonian models, such as Casson rheology, provide greater accuracy in predicting WSS and flow in stenotic areas compared to traditional Newtonian models [5], [6]. Additionally, magnetohemodynamic (MHD) research indicates that magnetic fields can influence flow and shear stress, offering new treatment possibilities ([?]). This study integrates MHD and CFD to enhance stenosis management strategies, aiming to improve interventions like stent placement and magnetic drug targeting.

2 More

The flow of blood in arteries is described by the modified Navier–Stokes equations, incorporating Casson non-Newtonian viscosity and the Lorentz force from an external magnetic field. The mass and momentum conservation equations are:

$$\nabla \cdot \mathbf{U} = 0 \tag{1}$$

$$\frac{\partial \mathbf{U}}{\partial t} + (\mathbf{U} \cdot \nabla)\mathbf{U} = -\frac{1}{\rho}\nabla p + \nabla \cdot \left[\nu_{\text{eff}}(\dot{\gamma}) \left(\nabla \mathbf{U} + (\nabla \mathbf{U})^T\right)\right] + \frac{1}{\rho}\mathbf{F}_{\text{Lorentz}} \tag{2}$$

Table 1: Boundary conditions and inlet velocity for pulsatile Casson flow

Boundary Type	Velocity Condition	Pressure Condition
Inlet	Pulsatile velocity $v_m(t)$	-
Outlet	`zeroGradient`	`fixedValue` $p = 0$
Walls	No-slip ($\mathbf{U} = 0$)	`zeroGradient`
Pulsatile Velocity: $v_m(t) = \frac{\bar{v}_m}{a_0}\left\{a_0 + \sum_{i=1}^{5}\left[a_i \cos(i\omega t) + b_i \sin(i\omega t)\right]\right\}$		

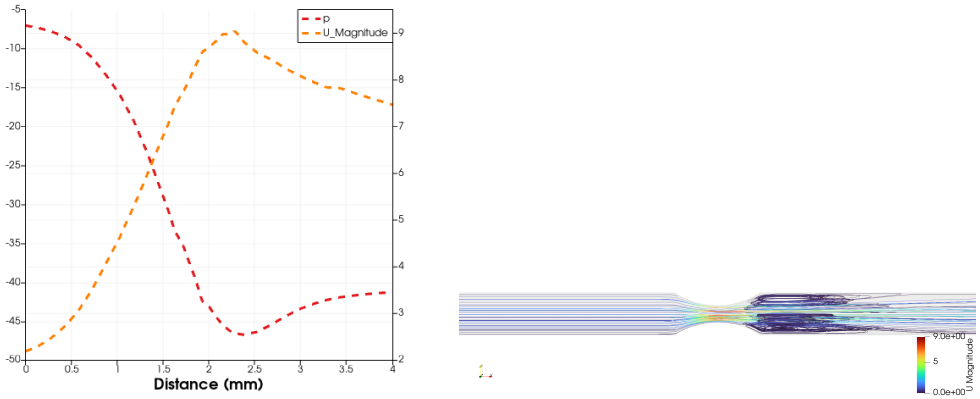

(a) $U_{magnitude}$ and p at stenosis.

(b) Velocity streamlines.

References

[1] J. Smith, L. R. Thompson, and A. K. Gupta, *Hemodynamic biomarkers in arterial stenosis: A CFD-based investigation under pulsatile flow*, J. Biomed. Eng. **49** (2022) 120–133.

[2] R. Johnson, F. Liu, and M. Santoro, *Computational hemodynamics for the clinical assessment of vascular disease: Review and trends*, Comput. Biol. Med. **158** (2023) 106970.

[3] E. Witten, *Supersymmetry and Morse theory*, J. Diff. Geom. **17** (1982) 661–692.

[4] Y. Wang, M. S. Ali, and T. M. Chan, *Multi-cycle analysis of pulsatile blood flow through stenosed arteries using Casson and Carreau-Yasuda models*, Phys. Fluids **36** (2024) 021901.

[5] H. Lee, S. Kumar, and E. Tanaka, *Casson model-based prediction of wall shear stress and recirculation in stenotic arteries*, J. Theor. Appl. Mech. **61** (2023) 550–562.

[6] A. Patel, R. Amini, and S. Y. Lee, *Non-Newtonian blood flow modeling in stenotic vessels using OpenFOAM: Influence of viscosity models*, Comput. Fluids **263** (2024) 105769.

Book of abstracts of the 9th International Conference on
Advanced Computational Methods in ENgineering and Applied Mathematics
September, 15–19, 2025.

Axisymmetric mass conservative flow and transport and a reduced basis approach for heterogeneous catalysis

Jürgen Fuhrmann[1], Sebastian Matera[2], Christian Merdon[1] and Daniel Runge[1]

[1] *Research Group Numerical Mathematics and Scientific Computing, Weierstrass Institute for Applied Analysis and Stochastics*

[2] *Multiscale Modeling from the Electron to the Reactor, Fritz-Haber-Institut der Max-Planck-Gesellschaft*

e-mails: juergen.fuhrmann@wias-berlin.de, matera@fhi-berlin.mpg.de, christian.merdon@wias-berlin.de, daniel.runge@wias-berlin.de

Abstract

This talk presents a physically consistent simulation of axisymmetric fluid flow and transport. In the three-dimensional setting, a mass-conservative discretization is achieved by employing divergence-free finite element methods for the flow velocity in a suitable finite volume discretization for the transport. A replication of this approach in cylindrical coordinates is not straightforward. Therefore, a possible modification is presented that ensures desired qualitative properties, i.e. mass conservation and the minimax principles. Moreover, we show a priori error estimates in suitable weighted Sobolev norms. Numerical experiments confirm the theoretical results and exhibit the expected convergence rates. In the case of heterogeneous catalysis with nonlinear reaction boundary conditions, our discretization is utilized in the construction of a reduced basis which enables a more efficient solution of the forward problem for varying kinetic models.

Key words: Axisymmetry, Mass Conservation, Reduced Basis, Flow and Transport
MSC 2020: 65N08, 65N15, 76D07, 76M10, 35B50

1 Summary

Given a polygonal domain $\Omega \subset \mathbb{R}^2$ whose rotation around the z-axis defines a solid of revolution $\widehat{\Omega} \subset \mathbb{R}^3$, we consider a species concentration c on Ω dissolved in a fluid whose motion in terms of its velocity $\boldsymbol{u}$ and pressure p on Ω is described by the axisymmetric Stokes system

$$-\nu\left(\Delta_{\mathrm{cyl}} u_r - \frac{u_r}{r^2}\right) + \frac{\partial p}{\partial r} = f_r, \quad -\nu\Delta_{\mathrm{cyl}} u_z + \frac{\partial p}{\partial z} = f_z, \quad \mathrm{div}_{\mathrm{cyl}}(\boldsymbol{u}) := \mathrm{div}_{(r,z)}\boldsymbol{u} + \frac{u_r}{r} \quad = 0 \qquad (1)$$

where $\Delta_{\mathrm{cyl}} := \frac{\partial^2}{\partial r^2} + \frac{1}{r}\frac{\partial}{\partial r} + \frac{\partial^2}{\partial z^2}$, $\mathrm{div}_{(r,z)} := \frac{\partial u_r}{\partial r} + \frac{\partial u_z}{\partial z}$, and (f_r, f_z) is a given volume force.

Given the solution $\boldsymbol{u}$ to (1), the concentration of the dissolved species c obeys

$$\mathrm{div}_{\mathrm{cyl}}(\boldsymbol{j}) = -D\Delta_{\mathrm{cyl}} c + \boldsymbol{u}\cdot\nabla_{(r,z)} c = s \quad \text{where} \quad \boldsymbol{j} := -D\nabla_{(\mathrm{r},\mathrm{z})} c + \boldsymbol{u}c, \qquad (2)$$

where $\nabla_{(r,z)} := \left(\frac{\partial c}{\partial r}, \frac{\partial c}{\partial z}\right)$ and ν, D are assumed constant.

In [1], a proper functional analytical setting in weighted Sobolev spaces is provided, stating that an axisymmetric weak solution $\widehat{c} \in H^1(\widehat{\Omega})$ of the transport equation corresponds to a weak solution $c \in H^1_1(\widehat{\Omega}) := \left\{v : \int_\Omega r\, \partial^\alpha v \mathrm{d}r\mathrm{d}z < \infty \text{ for all } \alpha \in \mathbb{N}^2 \text{ with } |\alpha| \leq 1\right\}$ of (2). Similarly, an axisymmetric velocity field $\widehat{\boldsymbol{u}}$ that solves the three-dimensional Stokes problem corresponds to a two-dimensional velocity field $\boldsymbol{u}$ that solves (1).

Our contribution is concerned with the physical consistency of the resulting numerical approximation c_h of c, resp. $\widehat{c}$, i.e. the conservation of mass and the validity of the min/max principle in the numerical discretization of this axisymmetric reformulation. Achieving this is fundamentally tied to whether the velocity $\widehat{\boldsymbol{u}}$ and its discrete approximation $\widehat{\boldsymbol{u}}_h$ respect the divergence constraint $\mathrm{div}(\widehat{\boldsymbol{u}}) = 0$, which is equivalent to $\mathrm{div}_{(r,z)}(r\,\boldsymbol{u}) = 0$. Following ideas from [2], we employ a post-processed low-order Bernardi–Raugel finite element method for the approximation of $\boldsymbol{u}$. To that end, we apply an $H(\mathrm{div}, \Omega)$-conforming standard interpolation operator Π to the discrete velocity $\boldsymbol{u}_h$ such that the resulting $H(\mathrm{div}, \Omega)$-conforming field $\Pi(r\,\boldsymbol{u}_h)$ satisfies the divergence constraint $\mathrm{div}_{(r,z)}(\Pi(r\,\boldsymbol{u}_h)) = 0$ by commutating diagram properties. The post-processed velocity $\Pi(r\,\boldsymbol{u}_h)$ is then included in the finite volume method with a classical upwinding approximation of the fluxes across the control volume edges.

Since only few results are available for finite volume and finite element methods in the axisymmetric setting, we deliver a complete a priori error analysis in the spirit of [4, 3] and proof of inf-sup stability of the post-processed Bernardi-Raugel method based on [5].

The discretization can be used to compute discrete Green's-like functions for the drift-diffusion operator with respect to a part of the boundary. These functions can be combined to a small number of reduced basis functions which allow for efficiently solving the transport equation with a non-linear boundary reaction as it appears in heterogeneous catalysis. By this, the global non-linear problem reduces to a smaller non-linear problem [6].

References

[1] C. Bernardi, M. Dauge, Y. Maday, *Spectral Methods for Axisymmetric Domains*, Gauthier-Villars, 1999.

[2] C. Merdon, J. Fuhrmann, A. Linke, T. Streckenbach, F. Neumann, M. Khodayari, H. Baltruschat, *Inverse modeling of thin layer flow cells for detection of solubility, transport and reaction coefficients from experimental data*, Electrochimica Acta **211** (2016) 01–10.

[3] R. Eymard, T. Gallouët, R. Herbin, *Finite volume methods*, In Do Young Kwak, editor, Handbook of numerical analysis, North-Holland, 2000 713–1020.

[4] T. Gallouët, R. Herbin, M. H. Vignal, *Error Estimates on the Approximate Finite Volume Solution of Convection Diffusion Equations with General Boundary Conditions*, SIAM Journal on Numerical Analysis **37** (2000) 111–136.

[5] Y.-J. Lee, H. Li, *On Stability, Accuracy, and Fast Solvers for Finite Element Approximations of the Axisymmetric Stokes Problem by Hood–Taylor Elements*, SIAM Journal on Numerical Analysis **49** (2011) 668–691.+

[6] S. Matera, C. Merdon, D. Runge, *Reduced Basis Approach for Convection-Diffusion Equations with Non-linear Boundary Reaction Conditions*, In E. Franck, J. Fuhrmann, V. Michel-Dansac, L. Navoret, editor, FVCA X—Volume 1, Elliptic and Parabolic Problems, Springer Nature Switzerland, (2023) 335–343.

Book of abstracts of the 9th International Conference on
Advanced Computational Methods in ENgineering and Applied Mathematics
September, 15–19, 2025.

Matrix-Free Methods for Finite-Strain Elasticity: Automatic Code Generation with No Performance Overhead

Michał Wichrowski[1,2], Mohsen Rezaee-Hajidehi[3], Jože Korelc[4], Martin Kronbichler[5] and Stanisław Stupkiewicz[3]

[1] *Interdisciplinary Center for Scientific Computing, Heidelberg University, Heidelberg, Germany*

[2] *Faculty of Mathematics, Informatics and Mechanics, University of Warsaw, Warsaw, Poland*

[3] *Institute of Fundamental Technological Research, Polish Academy of Sciences, Warsaw, Poland*

[4] *Faculty of Civil and Geodetic Engineering, University of Ljubljana, Slovenia*

[5] *Applied Numerics, Faculty of Mathematics, Ruhr University Bochum, Germany*

e-mails: mt.wichrowsk@uw.edu.pl, mrezaee@ippt.pan.pl, joze.Korelc@fgg.uni-lj.si, martin.kronbichler@rub.de, sstupkie@ippt.pan.pl

Abstract

This study explores matrix-free tangent evaluations in finite-strain elasticity with the use of automatically-generated code for the quadrature-point level calculations. The code generation is done via automatic-differentiation (AD) with AceGen. We compare hand-written and AD-generated codes under two computing strategies: on-the-fly evaluation and caching intermediate results. The comparison reveals that the AD-generated code achieves superior performance in matrix-free computations.

Keywords: Automatic differentiation, Finite Elements, Finite-strain elasticity, High-performance computing, Matrix-free
MSC 2020: (optional)

1 Introduction

Matrix-free methods offer significant computational performance benefits by avoiding explicit matrix storage, particularly for higher-order finite elements [3]. These methods rely on optimized loops to evaluate operator actions, alleviating the memory bottleneck often seen in traditional finite element (FE) computations. However, deriving and implementing the complex tangent operators required for nonlinear problems, such as finite-strain elasticity, can be a formidable challenge.

This work [4] explores the applicability of automatically generated code within matrix-free nonlinear solvers, focusing on finite-strain elasticity. We employ Automatic Differentiation (AD) using the AceGen system [2] to generate efficient C++ code for the computationally intensive quadrature-point calculations involved in both the residual and tangent operator evaluations. AceGen's hybrid symbolic-numerical approach automates the FE method, minimizing human error and development time.

We compare the performance of AD-generated code against hand-written implementations for a compressible neo-Hookean hyperelastic model, using results from [1] as a baseline. Different strategies, including on-the-fly computation and caching intermediate results (e.g., the fourth-order tangent tensor), are evaluated. Table 1 summarizes key performance metrics for various evaluation strategies on a test problem (3D, $\mathbb{Q}_2$ elements, 75k DoFs). Our findings indicate that AD-generated code, particularly when leveraging AD-specific techniques to compute matrix-vector products directly (AD On-the-fly), achieves superior performance with no discernible overhead compared to optimized hand-written code.

Table 1: Performance metrics for different caching strategies in the quadrature loop for the compressible neo-Hookean model. Timings of matrix-vector product (vmult), floating point operations (FLOPs) per point, processing rate in GFLOP/s, and total cache size for $\mathbb{Q}_2$ elements in 3D on a mesh with one refinement level (75,072 degrees of freedom).

Formulation	Timing [ms]	FLOP/point	[GFLOP/s]	Cache [Mb]
AD On-the-fly	3.43	3287	25.3	2
AD Cached Tensor	3.33	1566	18.5	18
Manual Scalar (Ref.) [1]	4.71	3148	14.8	4
Manual Scalar (Curr.) [1]	4.11	2138	13.2	5
Manual Cached Tensor [1]	4.44	1588	13.5	29

This demonstrates that AD is a viable and highly efficient approach for developing matrix-free solvers for complex nonlinear solid mechanics problems.

Acknowledgements This work was partially supported by the EU through the EffectFact project (No. 101008140) and the EuroHPC Joint Undertaking Centre of Excellence dealii-X (No. 101172493).

References

[1] D. Davydov, M. Kronbichler, S. Stupkiewicz, *Matrix-free finite element computations for finite-strain hyperelasticity with a multigrid solver*, Computational Mechanics **66**(3) (2020) 657–680.

[2] J. Korelc, *Multi-language and multi-environment generation of nonlinear finite element codes*, Engineering with Computers **18**(4) (2002) 312–327.

[3] M. Kronbichler, K. Kormann, *A generic interface for parallel cell-based finite element operator application*, ACM Trans. Math. Software **45**(4) (2019) Paper No. 39, 38 pp.

[4] M. Wichrowski, M. Rezaee-Hajidehi, J. Korelc, M. Kronbichler, S. Stupkiewicz, *Matrix-Free Methods for Finite-Strain Elasticity: Automatic Code Generation with No Performance Overhead*, arXiv preprint arXiv:2505.15535 (2025).

Open Session

Book of abstracts of the 9th International Conference on
Advanced Computational Methods in ENgineering and Applied Mathematics
September, 15–19, 2025.

Inverse Source Problem for Pseudoparabolic Equation with Memory Term and Damping

Shakir Aidos[1]

[1] *Department of Mathematics, Al-Farabi Kazakh National University, Almaty, Kazakhstan*

[2] *Institute of Mathematics and Mathematical Modeling, Almaty, Kazakhstan,*

e-mails: ajdossakir@gmail.com

Abstract

In this work, we study the inverse problem of determining, along with solution $u(x,t)$ of a pseudo-parabolic equation with memory (convolution term) and a damping term, also an unknown coefficient $f(t)$ determining the external effect (the free term). In the investigating inverse problem, the overdetermination condition is given in integral form, which represents the average value of a solution tested with some given function over all the domain. By reducing the considering inverse problem to an equivalent nonlocal direct problem. The applicability of the Faedo-Galerkin method to the inverse problem is analyzed. We establish the global and local in time existence and uniqueness of a weak solution of the studing problem.

Key words: Inverse problem, nonlinear pseudoparabolic equation, memory term, solvability

MSC 2020: 35D30, 35R30

1 Introduction

Let Ω be a bounded domain in $\mathbf{R}^d$, $d \geq 2$ with smooth boundary $\partial\Omega$, and $Q_T = \{(x,t) : \ x \in \Omega, \ 0 < t \leq T\}$ is a cylinder with lateral Γ_T. Let us consider the following inverse problem of finding the pair of functions $(u(x,t), f(t))$, which satisfy the pseudoparabolic equation with memory term and damping

$$u_t - \kappa\Delta u_t - \lambda\Delta u - \int_0^t K(t-s)\Delta u(x,s)ds = \gamma\,|u|^{q-2}\,u + f(t)\cdot g(x,t), \ \text{ in } \ Q_T, \tag{1}$$

the initial condition

$$u(x,0) = u_0(x) \ \text{ in } \ \Omega, \tag{2}$$

the boundary condition

$$u(x,t) = 0 \ \text{ on } \ \Gamma_T, \tag{3}$$

and the integral overdetermination condition

$$\int_\Omega u(x,t)\omega(x)dx = h(t), \ \ t \in [0,T]. \tag{4}$$

Here, the coefficient κ, λ are given positive numbers, γ is the coefficient of the damping term might be positive $\gamma > 0$ either negative $\gamma < 0$. The functions $g(x,t)$, $u_0(x)$, $\omega(x)$ and $h(t)$ are given. The exponent q is given positive number such that

$$1 < q < \infty. \tag{5}$$

The main goal [1] of this paper is to show existence and uniqueness of weak solution to the inverse problem (1)-(4).

Acknowledgements This research work has been funded by Grant number AP19676624 the Ministry of Science and Higher Education of the Republic of Kazakhstan.

References

[1] Kh. Khompysh, A. Shakir, A. Kabidoldanova , *Inverse problems for nonlinear Navier-Stokes-Voigt system with memory* Chaos, solitons and fractals **177(12)** (2023).

Book of abstracts of the 9th International Conference on
Advanced Computational Methods in ENgineering and Applied Mathematics
September, 15–19, 2025.

A Differentiation–free Method for the solution of initial value problems

Richard O. Akinola[1], Ezekiel O. Omole[2], Joshua Sunday[1] and Eleojor R. Akor[1]

[1] *Department of Mathematics, Faculty of Natural Sciences, University of Jos*

[2] *Department of Physical Sciences, Mathematics Programme, Landmark University*

e-mails: roakinola@gmail.com, omolez247@gmail.com, joshuasunday2000@gmail.com, eleojorachelakor@gmail.com

Abstract

Shampine [1], in his 1993 article, stated that matrices arising from the numerical approximation of stiff initial value problems (IVPs) using Linear Multistep Methods are mostly ill-conditioned. In this paper, we present a new block hybrid method with a better condition number and show that, in the absence of round-off errors, it gives approximately the same solution as an existing method in the literature that is ill-conditioned. We demonstrate computationally how an LU-type preconditioned Quasi Minimal Residual with a fixed default tolerance reduces the condition number of both the old and new methods, with the latter resulting in the smallest minimum norm of the residual.

Key words: Block hybrid methods, non-singular, $A(\alpha)$-stable, ill-conditioning, Integration of systems of equations.
MSC 2020: 65D30, 65L04, 65L05, 65L06.

References

[1] L. F. Shampine *Ill–conditioned matrices and the integration of stiff ODEs.* Journal of Computational and Applied Mathematics, **48**(1993), 279–292.

Book of abstracts of the 9th International Conference on
Advanced Computational Methods in ENgineering and Applied Mathematics
September, 15–19, 2025.

Operational Quadrature Methods for Approximating Fractional Integrals with Applications

Omar Alsayyed[1]

[1] *Department of Mathematics, The Hashemite University, Zarqa 13133, Jordan*

e-mails: omarm_re@hu.edu.jo

Abstract

Fractional integrals are central in modeling memory effects in complex systems, yet their nonlocal and weakly singular structure poses significant numerical challenges. This work develops a class of convolution quadrature (CQ) methods for approximating Caputo and Riemann–Liouville fractional integrals. Based on discretizing Laplace-domain representations using linear multistep methods, CQ methods yield stable and high-order approximations. We analyze convergence properties, derive error estimates, and demonstrate their efficiency in fractional diffusion and relaxation problems. Numerical experiments validate the theoretical findings and confirm the practical benefits of the CQ approach.

Key words: Convolution quadrature, fractional integrals, anomalous diffusion, numerical analysis.

1 Introduction

Fractional calculus extends differentiation and integration to non-integer orders, enabling the modeling of systems with memory, nonlocality, and anomalous transport. A fundamental operator is the Riemann–Liouville fractional integral of order $\alpha > 0$, defined by

$$(I^\alpha f)(t) = \frac{1}{\Gamma(\alpha)} \int_0^t (t-\tau)^{\alpha-1} f(\tau)\, d\tau.$$

Such operators arise in fractional diffusion, viscoelasticity, and heat conduction with memory. However, standard numerical quadratures often fail to handle the singular kernel efficiently, especially over long time intervals.

Convolution quadrature (CQ), introduced by Lubich [3], provides a systematic way to approximate convolution integrals via the Laplace transform of the kernel and the generating function of an underlying ODE method. When applied to fractional integrals, CQ yields accurate and robust schemes that respect both the nonlocal nature and singular behavior of the operator.

2 Method and Main Results

Let f be defined on $[0,T]$ and consider a uniform time grid $t_n = n\tau$. The CQ method approximates the fractional integral $I^\alpha f(t_n)$ by a discrete convolution:

$$I^\alpha f(t_n) \approx \sum_{j=0}^{n} \omega_j f(t_{n-j}),$$

where the weights ω_j are computed using the Laplace transform $\widehat{k}(s) = s^{-\alpha}$ and a linear multistep method with generating function $\delta(\zeta)$. Specifically,

$$\sum_{j=0}^{\infty} \omega_j \zeta^j = \left(\frac{\delta(\zeta)}{\tau}\right)^{-\alpha}.$$

Weights are efficiently evaluated via FFT or contour integration. If the multistep method is of order p and $f \in C^{p+1}[0,T]$, then the CQ approximation, with suitable corrected terms, satisfies

$$|I^\alpha f(t_n) - \sum_{j=0}^{n} \omega_j f(t_{n-j})| \le C\tau^p t_n^{\alpha-p} \|f^{(p)}\|_\infty,$$

for a constant C independent of τ.

3 Applications

CQ also applies to solving fractional differential equations like the Caputo diffusion equation [1]:

$$\partial_t^\alpha u(t) + Au(t) = f(t), \quad u(0) = 0,$$

where A is a sectorial operator. The CQ discretization yields a stable and convergent scheme without explicit evaluation of the fractional kernel.

Further, we apply the scheme to time-fractional diffusion problems with finite element spatial discretization. The CQ approach accurately resolves slow diffusion and long-time memory effects. Applications in viscoelasticity, where stress-strain relations involve fractional integrals, further illustrate the method's practical value.

In conclusion, Convolution quadrature offers a robust, high-order framework for approximating fractional integrals and solving time-fractional models. It efficiently handles singular kernels and long memory effects while preserving stability. Recent works include adaptive strategies and extensions to multi-term and variable-order models [2].

References

[1] L. Banjai and C.G. Makridakis, *A posteriori error analysis for approximations of time-fractional subdiffusion problems*, Math. Comp. **91** (2022) 1711–1737.

[2] M. Lopez-Fernandez and S. Sauter, *Generalized convolution quadrature with variable time stepping*, IMA J. Numer. **33** (2013) 1156–1175.

[3] C. Lubich, *Convolution quadrature and discretized operational calculus. I*, Numer. Math. **52** (1988) 129–145.

Book of abstracts of the 9th International Conference on
Advanced Computational Methods in ENgineering and Applied Mathematics
September, 15–19, 2025.

Combining Subdivision Schemes and Machine Learning for Geometric Modeling

A. Arhandou[1], A. Lamnii[1] and M.-Y. Nour[2]

[1] *ENSATe, University of Abdelmalek Essaadi*

[2] *University Lorraine, CNRS, Inria, LORIA, F-54000 Nancy, France.*

e-mails: arhandou.amine@etu.uae.ac.ma, ,

Abstract

Subdivision schemes are widely used in geometric modeling to generate smooth surfaces from coarse meshes. Traditional methods, such as Loop, Catmull-Clark, and B-spline subdivisions, rely on predefined refinement rules. Recent advances in machine learning have opened new possibilities for improving these methods by learning optimal refinement patterns from data.

This study explores the integration of machine learning techniques with classical subdivision schemes to enhance shape approximation and computational efficiency. A neural network-based approach is proposed to predict optimal refinement structures, allowing for adaptive and data-driven mesh refinement.

The proposed approach is evaluated on benchmark geometric datasets and compared with standard subdivision methods in terms of smoothness, computational performance, and approximation error. Potential applications include computer graphics, animation, and engineering simulations.

Key words: Subdivision Schemes, Machine Learning, Geometric Modeling, Computational Efficiency

1 Introduction

Subdivision schemes play a crucial role in geometric modeling by generating smooth surfaces from coarse meshes. These methods, including Loop, Catmull-Clark, and B-splines, are widely used in animation, computer graphics, and numerical simulations [1, 2]. However, traditional schemes follow fixed refinement rules, which may not always be optimal.

Recent advancements in machine learning have enabled data-driven methods for geometric modeling [3]. This work investigates the integration of machine learning techniques with classical subdivision schemes to improve adaptability and computational performance.

2 Methodology

A hybrid approach is proposed where a neural network is trained to predict optimal refinement structures based on geometric features. Key steps include:

- Implementing standard subdivision schemes (Loop, Catmull-Clark, B-splines).

- Training a neural network to learn efficient refinement patterns [4].
- Evaluating the hybrid approach on benchmark datasets.

3 Results and Discussion

Preliminary results indicate that the proposed method enhances surface approximation while reducing computational overhead. The adaptive refinement strategy learned by the neural network leads to more efficient mesh generation compared to traditional fixed-rule methods. Comparative metrics such as smoothness, error reduction, and computation time are analyzed [5].

4 Conclusion and Future Work

This study demonstrates the potential of combining subdivision schemes with machine learning to improve geometric modeling. Future work will refine the neural network architecture, extend the method to more complex surfaces, and explore applications in real-time rendering and engineering simulations.

References

[1] Nira Dyn. *Linear subdivision schemes for the refinement of geometric objects.* European Mathematical Society, 2007.

[2] Kestutis Karciauskas and Jörg Peters. Guided subdivision surfaces: modeling, shape and refinability. *arXiv*, 2017.

[3] B Victorri. *Modélisation et intelligence artificielle.* Springer, 2005.

[4] Baoxing Zhang, Yunkun Zhang, and Hongchan Zheng. A symmetric non-stationary loop subdivision with applications in initial point interpolation. *Symmetry*, 16(3):379, 2024.

[5] Niels Bügel, Lucia Romani, and Jiří Kosinka. A point-normal interpolatory subdivision scheme preserving conics. *Computer Aided Geometric Design*, 111:102347, 2024.

Book of abstracts of the 9th International Conference on
Advanced Computational Methods in ENgineering and Applied Mathematics
September, 15–19, 2025.

Transient Thermo-fluid Behavior of Airflow in Porous SiC Structures for Concentrated Solar Power Plants

Millaray Alejandra Vásquez Aburto[1], Masoud Behzad[1] and Cristóbal Sarmiento-Laurel[1]

[1] *School of Industrial Engineering, Faculty of Engineering and Science, Diego Portales University, Santiago, 8370191, Chile,*

e-mails: , masoud.behzad@mail.udp.cl;behzadmasoud@gmail.com, cristobal.sarmiento@udp.cl

Abstract

This study analyzes the thermal response of a SiC porous absorber under two solar radiation profiles: gradual variation and sharp drop-recovery, simulating cloud-passing events. At 45 seconds, when radiation returns to normal, the fluid outlet temperature recovers to 44.2% under gradual change, compared to 39.2% under sharp change These results indicate that gradual radiative transitions reduce thermal lag and improve recovery performance. The findings highlight the importance of moderating solar input fluctuations and enhancing thermal buffering in CSP systems. Such strategies can improve thermal stability and overall efficiency during transient operating conditions.

Key words: Porous, SiC, Transient, Solar thermal

1 Introduction

Increasing operating temperatures is essential for enhancing the efficiency of concentrated solar power plant (CSP) systems. Porous Silicon Carbide (SiC) volumetric absorbers are particularly well-suited for air-based CSP applications. Their large exchange area is ideal for compensating the low thermal conductivity of air, the working fluid in these systems. Additionally, the porous structure allows deep penetration of solar radiation, enabling radiative heat transfer to occur not only at the inlet surface but also within the volume of the medium, thereby promoting efficient volumetric absorption of energy.

Given the inherently transient nature of solar radiation, it is essential to evaluate the dynamic performance of SiC porous absorbers under transient flux conditions [1], [2]. The cloud-passing event is critical because of the sudden and significant drop in solar irradiance over a short period, which can strongly affect the thermofluid behavior within the absorber. This study investigates key temperature responses, including the solid and air temperature, under different cloud-passing scenarios over a short time span. The results provide insight into the absorber's thermal inertia and its ability to mitigate rapid irradiance fluctuations.

2 Methodology

In ANSYS CFX the porous domain is modeled with isotropic porosity, where momentum loss is described by directional resistance coefficients (Darcy and Forchheimer terms), including a streamwise multiplier for transverse effects. A non-thermal equilibrium energy model is applied, solving separate energy equations for the solid and fluid phases, linked through interfacial heat transfer defined by an overall volumetric heat transfer coefficient. Temperature-dependent thermophysical properties, such as viscosity and thermal conductivity, are incorporated using volume-average solid and fluid temperatures. Permeability and heat transfer coefficients are calculated using standard correlations for laminar flow in square ducts.

3 Results

Both the solid inlet and air outlet temperatures recover faster under gradual radiation variation (Data Set 1), supporting the view that smoother radiative input changes help maintain thermal continuity and reduce system inertia delays. These findings suggest that CSP plants should moderate sharp solar input fluctuations, for example through heliostat defocusing or receiver shielding. Flow rates can be dynamically adjusted to minimize thermal lag during transient conditions, while thermal buffering can be enhanced by increasing solid thermal mass or incorporating storage elements near the receiver. Additionally, predictive control systems that anticipate radiation changes can improve system responsiveness, reduce thermal stress, and enhance overall energy conversion efficiency under variable solar conditions.

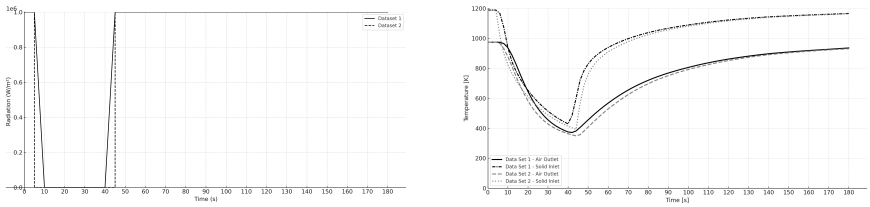

(a) Radiation profile showing a sharp drop and recovery versus a gradual drop and recovery

(b) Air outlet temperature and solid inlet temperature under different radiation profiles

Figure 1: Key input–output variations in a SiC porous absorber.

Acknowledgements This work acknowledges the financial support from ANID/FONDECYT Iniciación No. 11230698.

References

[1] B. Herrmann, M. Behzad, J. M. Cardemil, W. R. Calderón-Muñoz, R. M. Fernández, *Conjugate heat transfer model for feedback control and state estimation in a volumetric solar receiver*, Sol. Energy. **198** (2020) 343–354, https://doi.org/10.1016/j.solener.2020.01.062.

[2] S. Sharma, P. Talukdar, *Dynamic Performance Characteristics of a Porous Volumetric Solar Receiver Under Transient Flux Conditions*, J. Sol. Energy Eng. **145(4)** (2023) 041009, https://doi.org/10.1115/1.4056622.

Book of abstracts of the 9th International Conference on
Advanced Computational Methods in ENgineering and Applied Mathematics
September, 15–19, 2025.

Computational model of freezing front propagation in samples of porous media

Michal Beneš[1], Alexandr Žák[1] and Tissa H. Illangasekare[2]

[1] *Faculty of Nuclear Sciences and Physical Engineering, Czech Technical University in Prague*

[2] *CESEP, Colorado School of Mines, Golden*

e-mails: michal.benes@fjfi.cvut.cz, zakal@centrum.cz, tissa@mines.edu

Abstract

The freezing of water in porous media depends on various characteristics such as pore size, distribution of grains or boundary conditions. In this contribution we describe a numerical model of freeze/thaw process of a soil sample on the laboratory scale. The model is based on the balance laws for mass, momentum and energy in the porous structure. We investigate the dependence of this model on initial conditions, material properties and boundary conditions. This contributes to understanding of freeze/thaw processes observed under laboratory conditions.

Key words: freezing, thawing, finite-element method, porous media, Stefan problem
MSC 2020: 74N20, 74F10, 76S05, 80A22

1 Introduction

Soil freeze-thaw cycles not only influence structures, roads, buildings, and other critical infrastructure, but make part of phenomena accompanying climate changes.

Freezing and thawing in a porous medium is controlled by the heat transfer, mostly between the soil surface and atmosphere. The difference between the specific volume of water and ice causes expansion or shrinkage of pores, leading to the displacement of grains and flow of water between them. Transport through the interface film between ice and grains contributes to additional structural changes. Consequently, the porous medium expands wherever it can, mostly upwards, and creates a variety of surface patterns observable by the naked eye.

Recent modeling results are related to specific thermo-hydro-mechanical effects of soil freezing and use currently available numerical methods. Some are partly connected to the multiphysics approach of this research [1]. Recently [2], the polycrystalline structure of ice in pores was related to the buildup of stresses during soil freezing, whereas the role of solutes during freezing is not yet clarified.

Pore-scale model was introduced in [4], assuming geometrically symmetric pores in 2D. A general pore-scale phase-field model of freezing was derived and analyzed in detail in [5]. Laboratory aspects have been studied in [6].

2 Model summary

The presentation describes the modeling of freezing and thawing in a fully saturated porous medium with general geometry of pores. During the phase transition the grains remain intact but participate in the heat transfer and in mechanical interaction due to the difference in specific volumes of liquid and solid phase. Freezing and thawing inside the porous medium is accompanied by complex processes affected by the material composition, micro-scale interfaces between phases within the medium, bulk properties of the presented phases, and ambient physical conditions. Volumetric change of the liquid presented in pores subjected to phase change conditions is a crucial phenomenon.

In this contribution we consider a fully saturated porous medium sample similar to those discussed in [6]. The models discussed are based on balance laws for *mass, momentum and energy.* which are evaluated in the bulk of *the grain matrix, the water contained in pores, the ice contained in pores, and along the ice-water phase boundary in pores.* The detailed description of resulting PDE's is provided in [3, 4, 5]. The system of equations is weakly formulated and solved by the finite-element method in the geometry of the soil sample and its laboratory container. Computational results are compared to the laboratory measurements.

Acknowledgements The authors were partly supported by the project 25-18265S of the Czech Science Foundation, and by the CTU under the grant No. SGS23/188/OHK4/3T/14.

References

[1] H.S. Suh, W.C. Sun, *Multi-phase-field microporomechanics model for simulating ice-lens growth in frozen soil*, International Journal for Numerical and Analytical Methods in Geomechanics, **46**(12) (2022) 2307–2336.

[2] D. Gerber, L.A. Wilen, E.R. Dufresne, R.W. Style, *Polycrystallinity enhances stress buildup around ice*, Physical Review Letters **131** (2023) 208201.

[3] A. Žák, M. Beneš, T. H. Illangasekare, *Analysis of model of soil freezing and thawing*, IAENG International Journal of Applied Mathematics, **43**(3) (2013) 127–134.

[4] A. Žák, M. Beneš, T. H. Illangasekare, A.C. Trautz, *Mathematical model of freezing in a porous medium at micro-scale*, Communications in Computational Physics, **24**(2) (2018) 557–575.

[5] A. Žák, M. Beneš, T. H. Illangasekare, *Pore-scale model of freezing inception in a porous medium*, Computer Methods in Applied Mechanics and Engineering, **414** (2023) 116–166.

[6] M. Sobotková, A. Žák, M. Beneš, M. Sněhota, *Experimental and numerical investigation of water freezing and thawing in fully saturated sand*, J. Hydrol. Hydromech., **72**(3) (2024) 336–348.

Book of abstracts of the 9th International Conference on
Advanced Computational Methods in ENgineering and Applied Mathematics
September, 15–19, 2025.

Geodesic distance map generation algorithms for the geometrical inspection of flexible parts

Alex Bolyn[1] **and Eric Béchet**[1]

[1] *Department of aerospace and mechanical engineering, University of Liège*

e-mails: a.bolyn@uliege.be, eric.bechet@uliege.be

Abstract

In order to inspect flexible parts, we developed a Fast Marching method algorithm to obtain geodesic distances on manifolds represented by point cloud. This algorithm generates distance map using triangles built on the fly from a k-Nearest Neighbours graph. We show that the accuracy is similar to the mesh-based Fast Marching method [2]. However, this first order scheme is not sufficient for an inspection of part. Thus, a version approximating locally the wavefront as curved is proposed and shows an order of convergence of 2, which makes it suitable for the accurate inspection of flexible parts.

Key words: flexible part, geodesic distance, inspection, point cloud
MSC 2020: 68U05

1 Introduction

Mechanical parts such as car body parts or fuselage skin panels are considered as flexible (compliant) parts as their shapes significantly change under applied loads (gravity, supports, residual stresses, etc.). As the inspection relies on a specific shape, dedicated apparatus and procedures are required. However, given that the deformation is elastic and the thickness is sufficiently small, the intrinsic geometry is conserved. It means that it is possible to use geodesic distances for inspection instead of conventional Euclidean ones (same idea in [1]).

Our work consists in finding an algorithm that generates precise geodesic distance maps (or geodesic distance fields) directly on the point cloud obtained by a 3D scanner. We define a geodesic distance map as a scalar field in which each point has the shortest distance along the surface from a specific source, such as a point or another geometric feature (edge, hole, etc.). Using these fields or maps allows us to make multiple measurements at the same time, which can be used to validate the part according to GD&T. The input data for this algorithm is the point cloud itself to prevent the use of a mesh generation algorithm, which avoids increasing the time of computation and the number of error sources.

2 Algorithms

First, a graph is built using the k-Nearest Neighbours algorithm to help the propagation of the wavefront along the point cloud. In a way, this graph can be seen as a substitute for a mesh,

except that the stencil size can be locally adapted. Also, the algorithm does not simply walk on the graph but uses it to build triangles on the fly to apply an extrapolation scheme that is similar in essence to the one found in the FMM (which is first order) [2]. This last property gives the advantage, compared to the mesh version, that there is no particular geometrical case to handle.

Our algorithm is shown to be as accurate as the FMM. However, since the extrapolation used is linear, it does not provide sufficient precision for the metrology (as presented in the next section). Therefore, we propose a new version of the FMM to have an accuracy of order 2 by interpreting locally the wavefront as curved. The idea is to reduce the error due to the curvature of the distance field itself, which is one of the main error sources in the first-order version. Nevertheless, the error due to the discretisation of the explicit geometry becomes significant and must be compensated as well.

3 Results and discussion

We tested our algorithms on different test cases (point or planar source on plane or cylinder), and it results that the errors on the distance are the same as the original FMM with mesh. However, the error on the distances for the FMM algorithm decreases with an order 1 as the point density increases, whereas the error on a distance field due to the noise on the points usually increases with an order 2. This implies that there is an absolute minimum precision, which is actually not enough for metrology (even without noise, more than 10^3 points per unit length are required to reach at least a relative error of 0.1% on a curved surface).

Using our second version of the FMM algorithm drastically reduces the error due to the approximation of the wavefront: it converges at a rate of 2 (in the case of a convex flat surface, the accuracy even reaches machine precision), making it possible to reach a smaller error for a lower point cloud density. However, some corrections based on the curvature of the surface must be applied in the computation to compensate for the discretisation error at lower point density.

4 Conclusion

We successfully transpose the Fast Marching Method on point cloud, and we propose an order 2 version which interprets locally the curvature of the geodesic distance field. This new algorithm shows promising results for geometrical part inspection because it allows us to have good precision at a lower point density, where the noise due to the 3D scanner accuracy would have a lower impact.

References

[1] H. Radvar-Esfahlan and S.A. Tahan, *Nonrigid geometric metrology using generalized numerical inspection fixtures*, Precision Engineering, Vol. 36, pp. 1-9, 2011.

[2] R. Kimmel and J. Sethian, *Computing geodesic paths on manifolds*, Proc. Natl. Acad. Sci., Vol. 95, pp. 8431-8435, 1998.

Book of abstracts of the 9th International Conference on
Advanced Computational Methods in ENgineering and Applied Mathematics
September, 15–19, 2025.

Extended homogenization methods for foil windings

Jonas Bundschuh[1], Silas Weinert[1], Yvonne Späck-Leigsnering[1] and Herbert De Gersem[1]

[1] *Institute for Accelerator Science and Electromagnetic Fields (TEMF), Technical University of Darmstadt*

e-mails: jonas.bundschuh@tu-darmstadt.de, silas.weinert@stud.tu-darmstadt.de, spaeck@temf.tu-darmstadt.de, degersem@temf.tu-darmstadt.de

Abstract

The large number of turns in foil windings and the small thickness of the foil require many mesh elements in conventional finite element simulations. This renders models quickly computationally infeasible. With the use of homogenization approaches the small-scale structure in the foil winding domain does not need to be resolved by the finite element mesh. Starting from a standard foil winding model, this contribution examines three extensions: incorporating capacitive effects, thermal effects, and interleaved configurations, without sacrificing the computational efficiency of the foil winding model.

Key words: Capacitive effects, foil windings, homogenization, interleaved foil windings, thermal effects

1 Introduction

Foil windings are constructed by winding a thin, insulated metal foil. They are preferred over litz wire because of their higher fill-factor, better thermal properties and lower costs [1]. A foil winding may consist of hundreds of turns with thin conductors and even thinner insulation layers. Three exemplary foil windings are shown in Fig. 1(a), and the representation of a foil winding in the computational domain is shown in Fig. 1(b).

In a standard finite element procedure, the mesh resolves each turn of the foil and insulation layer separately. Due to the small thickness of the foil, this quickly leads to extremely large meshes and, thus, to prohibitively long simulation times. As a remedy, the standard foil winding model was proposed in [2].

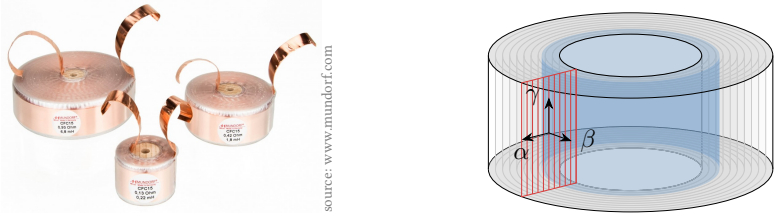

(a) (b)

Figure 1: (a) shows three foil windings, and (b) shows the representation of a foil winding with a local coordinate system on a cross section (red) and with cut $\Gamma(\alpha)$ (blue).

2 Standard foil winding model

The standard foil winding model replaces the foil winding domain with an artificial, homogenized material and approximates the voltage distribution perpendicular to the turns by the voltage function Φ that is constant per turn. The model is derived from the magnetoquasistatic approximation of Maxwell's equations, thus including resistive and inductive effects. With the magnetic vector potential $\mathbf{A}$, it reads

$$\nabla \times (\nu \nabla \times \mathbf{A}) + \sigma \partial_t \mathbf{A} - \sigma \Phi \zeta = 0, \tag{1a}$$

$$b \int_{\Gamma(\alpha)} \sigma \left(-\partial_t \mathbf{A} + \Phi \zeta\right) \cdot \zeta \, \mathrm{d}S = I, \tag{1b}$$

with the homogenized reluctivity ν and the homogenized conductivity σ, the distribution function ζ, the foil thickness b, the cuts $\Gamma(\alpha)$ (see Fig. 1(b)), and the current I [2]. Extensions are presented in the following.

3 Capacitive effects

The standard model assumes that the same current I flows through every turn of the foil winding. This assumption is no longer valid for elevated frequencies when capacitive effects become relevant. Therefore, (1b) is extended with the term $\int_{\Gamma(\alpha)} \partial_t \varepsilon \left(\frac{1}{b}\Phi - \frac{1}{2}\nabla\Phi \cdot \mathbf{e}_\alpha\right) \mathrm{d}S$ that comes up for the capacitive effects and uses the homogenized permittivity ε [3].

4 Thermal effects

A thermal homogenized model is used to examine the thermal behavior of the foil winding. Like the standard foil winding model, it replaces the foil winding domain with an artificial homogenized material. The Joule losses from the magnetic model are the heat source for the thermal model, and the electric conductivity depends on the temperature. This leads to a magnetic-thermally coupled model, which is solved by a weak coupling scheme.

5 Interleaved foil windings

For an interleaved foil winding, multiple foils are wound together such that adjacent turns belong to distinct windings. The standard foil winding model is adapted for interleaved foil windings. Each foil is represented by an individual voltage function defined on the shared foil winding domain and underlies a separate equation (1b) constraining the current.

References

[1] E. L. Barrios et al., *High-frequency power transformers with foil windings: maximum interleaving and optimal design*, IEEE Trans. Power Electron **30** (2015) 5712–5723.

[2] H. De Gersem et al., *A finite element model for foil winding simulation*, IEEE Trans. Magn. **37** (2001) 3427–3432.

[3] J. Bundschuh et al., *Homogenization of foil windings with globally supported polynomial shape functions*, IEEE J. Multiscale Multiphys. Comput. Tech. **9** (2024) 179–187.

Book of abstracts of the 9th International Conference on
Advanced Computational Methods in ENgineering and Applied Mathematics
September, 15–19, 2025.

A Krylov Subspace and Core Transformation Algorithm for Computing Recurrence Coefficients of Multiple Orthogonal Polynomials

Amin Faghih[1], Michele Rinelli[1], Marc Van Barel[1], Raf Vandebril[1] and Robbe Vermeiren[1]

[1] *Department of Computer Science, KU Leuven*

e-mails: amin.faghih@kuleuven.be, michele.rinelli@kuleuven.be, marc.vanbarel@kuleuven.be, raf.vandebril@kuleuven.be, robbe.vermeiren@kuleuven.be

Abstract

In this research, we develop algorithms for computing the recurrence coefficients corresponding to multiple orthogonal polynomials on the step-line. Multiple orthogonal polynomials generalize classical orthogonal polynomials but still satisfy a short-term recurrence relation. We exploit the connection with numerical linear algebra to reformulate the computation of the recurrence coefficients as an inverse eigenvalue problem. We consider two approaches: the first is based on the link with block Krylov subspaces and results in a biorthogonal Lanczos process with multiple starting vectors; the second consists of applying a sequence of Gaussian elimination matrices on the diagonal matrix of nodes to construct the banded Hessenberg matrix containing the recurrence coefficients. We analyze the accuracy and stability of the algorithms with numerical experiments on the ill-conditioned inverse eigenvalue problem related to Kravchuk and Hahn polynomials, as well as on other better conditioned examples.

Key words: Banded Hessenberg matrix, biorthogonal Lanczos, Gaussian elimination, inverse eigenvalue problem, multiple orthogonal polynomials.

1 Introduction

Recently, there has been a renewed interest in multiple orthogonal polynomials (MOPs), which are an extension of the classical notion of orthogonal polynomials. This extension originates from simultaneous rational approximation, particularly from Hermite-Padé approximation, where multiple functions are approximated by rational functions with the same denominator [3]. MOPs are polynomials in one variable with orthogonality relations with respect to r measures $\mu_1, \mu_2, \ldots, \mu_r$ [5]. In this research, we mainly deal with positive discrete measures on $\mathbb{R}$ [1], which also arise in quadrature rules for continuous measures [4].

Let $\mathbf{n} = (n_1, n_2, \ldots, n_r) \in \mathbb{N}^r$ be a multi-index with size $|\mathbf{n}| = n_1 + n_2 + \cdots + n_r$. There exist two types of multiple orthogonal polynomials. Type I MOPs are tuples of polynomials $(A_{\mathbf{n},1}, \ldots, A_{\mathbf{n},r})$, where $\deg A_{\mathbf{n},j} \leq n_j - 1$ for $j = 1, \ldots, r$, that satisfy the orthogonality conditions

$$\int_{\mathbb{R}} \sum_{j=1}^{r} A_{\mathbf{n},j}(x) x^k d\mu_j(x) = 0, \quad 0 \leq k \leq |\mathbf{n}| - 2.$$

A type II multiple orthogonal polynomial $P_{\mathbf{n}}$ is a polynomial of degree at most $|\mathbf{n}|$ that satisfies

$$\int_{\mathbb{R}} P_{\mathbf{n}}(x) x^k d\mu_j = 0, \quad 0 \leq k \leq n_j - 1, \quad 1 \leq j \leq r.$$

In 1969, Golub and Welsch [2] illustrated that in Gaussian quadrature (i.e., the case $r = 1$), the nodes and weights can be expressed in terms of eigenvalues and first components of the eigenvectors of a Jacobi matrix, respectively. This Jacobi matrix contains the coefficients appearing in the three-term recurrence relation corresponding to the set of orthogonal polynomials. MOPs satisfy several recurrence relations as well. In this research, we focus on the so-called step-line recurrence, an $(r + 2)$-term relation in which the multi-indices follow a specific path in $\mathbb{N}^r$. We propose numerical algorithms to compute this recurrence relation and recover the corresponding multiple orthogonal polynomials (MOPs).

The Golub-Welsch approach was extended to multiple Gaussian quadrature [4], where the goal is to approximate integrals of the kind

$$\int_{\mathbb{R}} f(x) d\mu_j(x), \qquad j = 1, 2, \ldots, r,$$

using the same quadrature nodes and weights. Since we have now $r + 2$-term recurrence relations, a banded upper Hessenberg matrix H_N takes the role of the Jacobi matrix [5]. As a consequence, the type I and type II MOPs are linked to the right and left eigenvectors of the recurrence matrix H_N, respectively; see, e.g., [4].

The interplay between numerical linear algebra and classical analysis is mutually beneficial. Numerical linear algebra provides effective procedures for solving linear algebraic problems and provides a natural framework to study the numerical stability of algorithms and the conditioning of problems. For example, it plays a central role in the problem of computing the nodes and weights related to multiple Gaussian quadrature [4]. We will be concerned with the opposite problem: given the nodes and weights of some discrete measures, we desire to retrieve the corresponding recurrence matrix. As explained in the previous paragraph, the nodes and weights are linked to the eigenvalues and eigenvectors of this recurrence matrix. Hence, we have an instance of an inverse eigenvalue problem (IEP).

References

[1] J. Arvesú, J. Coussement, and W. Van Assche, *Some discrete multiple orthogonal polynomials*, In Proc. 6th Int. Symp. Orthogonal Polynomials, Special Functions and Their Applications (Rome, 2001), vol. 153 (2003), 19–45.

[2] G. H. Golub and J. H. Welsch, *Calculation of Gauss quadrature rules*, Math. Comp. **23** (1969), 221–230.

[3] W. Van Assche, *Padé and Hermite-Padé approximation and orthogonality*, Surv. Approx. Theory **2** (2006), 61–91.

[4] W. Van Assche, *A Golub-Welsch version for simultaneous Gaussian quadrature*, Numer. Algor. (2024), to appear.

[5] W. Van Assche and E. Coussement, *Some classical multiple orthogonal polynomials*, J. Comput. Appl. Math. **127** (2001), 317–347.

Book of abstracts of the 9th International Conference on
Advanced Computational Methods in ENgineering and Applied Mathematics
September, 15–19, 2025.

An Upwind Picard-Newton iterative method for the 2-T heat conduction equations

Xudeng Hang[1] and Guangwei Yuan[1]

[1] *LCP, Institute of Applied Physics and Computational Mathematics*

e-mails: hang_xudeng@iapcm.ac.cn, yuan_guangwei@iapcm.ac.cn

Abstract

The paper proposes an Upwind Picard-Newton(UPN) iteration method for the nonlinear two-temperature heat conduction equations.Numerical experiments show that the new UPN iterative method is fast in convergence and efficient in time.

Key words: diffusion equation, Picard-Newton iteration,finite volume method
MSC 2020: 65M08;65M22

1 Introduction

Non-equilibrium diffusion equations should be solved in an implicit balanced way[1],[2]. By a linearization-discretization approach[3] , an upwind Picard-Newton iterative method is constructed to accelerate the solution procedure.

2 The upwind Picard-Newton(UPN) method

Consider the nonlinear 2T conduction equations

$$\begin{cases} \frac{\partial E(u)}{\partial t} - \nabla \cdot \kappa(u,v)\nabla u = ac\sigma(v)\left(v^4 - u^4\right) \\ \frac{\partial e(v)}{\partial t} - \nabla \cdot \lambda(v)\nabla v = -ac\sigma(v)\left(v^4 - u^4\right) \end{cases} \tag{1}$$

where $E(u)$ is a function of u, $\kappa(u,v)$is the conduction coefficient, $e(v)$ is a function of v, $\lambda(v)$is a function of v, and $a = 7.5656 \times 10^{-3}$,$c = 2.9979 \times 10^4$.

Denote $\Sigma^{(s)} = ac\sigma^{(s)}(u^{(s)2} + v^{(s)2})(u^{(s)} + v^{(s)})$ and linearize the 2T equations to

$$\begin{cases} \frac{E^{(s)} - E^n + E'^{(s)}(u^{(s+1)} - u^{(s)})}{\Delta t} - \nabla \cdot \left(\kappa^{(s)}\nabla u^{(s+1)} + \dot{\kappa}_1^{(s)}\nabla u^{(s)}(u^{(s+1)} - u^{(s)})\right) = \Sigma^{(s)}(v^{(s+1)} - u^{(s+1)}) \\ \frac{e^{(s)} - e^n + e'^{(s)}(v^{(s+1)} - v^{(s)})}{\Delta t} - \nabla \cdot \left(\lambda^{(s)}\nabla v^{(s+1)} + \dot{\lambda}_2^{(s)}\nabla v^{(s)}(v^{(s+1)} - v^{(s)})\right) = -\Sigma^{(s)}(v^{(s+1)} - u^{(s+1)}) \end{cases} \tag{2}$$

Let

$$\begin{aligned} F_1 &= \left(\frac{\kappa_{L\sigma}^{(s)} d_{K\sigma}\dot{\kappa}_{K\sigma 1}^{(s)}/\kappa_{K,\sigma}^{(s)}}{\kappa_{K\sigma}^{(s)} d_{L\sigma} + \kappa_{L\sigma}^{(s)} d_{K\sigma}} + \frac{\kappa_{K\sigma}^{(s)} d_{L\sigma}\dot{\kappa}_{L\sigma 1}^{(s)}/\kappa_{L,\sigma}^{(s)}}{\kappa_{K\sigma}^{(s)} d_{L\sigma} + \kappa_{L\sigma}^{(s)} d_{K\sigma}}\right) F_\sigma^{(s)} \\ G_2 &= \left(\frac{\lambda_{L\sigma}^{(s)} d_{K\sigma}\dot{\lambda}_{K\sigma 2}^{(s)}/\lambda_{K,\sigma}^{(s)}}{\lambda_{K\sigma}^{(s)} d_{L\sigma} + \lambda_{L\sigma}^{(s)} d_{K\sigma}} + \frac{\lambda_{K\sigma}^{(s)} d_{L\sigma}\dot{\lambda}_{L\sigma 2}^{(s)}/\lambda_{L,\sigma}^{(s)}}{\lambda_{K\sigma}^{(s)} d_{L\sigma} + \lambda_{L\sigma}^{(s)} d_{K\sigma}}\right) G_\sigma^{(s)} \end{aligned} \tag{3}$$

where $F_\sigma^{(s)} = \frac{\kappa_{K,\sigma}^{(s)}\kappa_{L\sigma}^{(s)}}{\kappa_{K\sigma}^{(s)}d_{L\sigma}+\kappa_{L\sigma}^{(s)}d_{K\sigma}}(u_K^{(s)} - u_L^{(s)}), G_\sigma^{(s)} = \frac{\lambda_{K,\sigma}^{(s)}\lambda_{L\sigma}^{(s)}}{\lambda_{K\sigma}^{(s)}d_{L\sigma}+\lambda_{L\sigma}^{(s)}d_{K\sigma}}(v_K^{(s)} - v_L^{(s)})$, and K, L are the cells with common edge σ , $d_{K\sigma}$ is the distance from the cell center of K to σ.Then the flux approximations are

$$f_\sigma = \frac{\kappa_{K,\sigma}^{(s)}\kappa_{L\sigma}^{(s)}}{\kappa_{K\sigma}^{(s)}d_{L\sigma} + \kappa_{L\sigma}^{(s)}d_{K\sigma}}(u_K^{(s+1)} - u_L^{(s+1)}) + \begin{cases} F_1(u_K^{(s+1)} - u_K^{(s)}), if & F_1 \geq 0 \\ F_1(u_L^{(s+1)} - u_L^{(s)}), if & F_1 < 0 \end{cases} \tag{4}$$

$$g_\sigma = \frac{\lambda_{K,\sigma}^{(s)}\lambda_{L\sigma}^{(s)}}{\lambda_{K\sigma}^{(s)}d_{L\sigma} + \lambda_{L\sigma}^{(s)}d_{K\sigma}}(v_K^{(s+1)} - v_L^{(s+1)}) + \begin{cases} G_2(v_K^{(s+1)} - v_K^{(s)}), if & G_2 \geq 0 \\ G_2(v_L^{(s+1)} - v_L^{(s)}), if & G_2 < 0 \end{cases} \tag{5}$$

The flux discretization constructs the UPN method, which begins with the Picard iteration, and shifts to the UPN method when the variation of the solution on the edge σ is sufficient small.

3 Numerical experiments

Consider a model problem with exact solutions

$$\begin{aligned} u(x,y,t) = v(x,y,t) &= 2T_t(0.1, \left[(z^2+r^2) - 5t\right]) \\ T_t(\varepsilon, s) &= \frac{e^{-s}-e^s+\varepsilon}{e^s+e^{-s}} + 1 = \frac{e^{-2s}-1+\varepsilon e^{-s}}{1+e^{-2s}} + 1 \end{aligned} \tag{6}$$

Numerical experiments show that the nonlinear iteration reduce to about 1/3, and the time cost reduce to about 40% of the Picard iteration

Table 1: Comparison of the iterations and time

T=0.6	Nonlinear Iters	Linear Iters	Solution time(s)
Picard	12934	7.41×10^5	775
UPN	4965	2.23×10^5	275

Acknowledgements This work has been partially supported by the Natural Science Foundation of China (No.12471340).

References

[1] D.A. Knoll, R.B. Lowrie, J.E. More, *Numerical analysis of time integration errors for nonequilibrium radiation diffusion*, J. Comp. Phys.**226** (2007) 1332-1347.

[2] D.A. Knoll, L. Chacon, L.G. Margolin, V.A. Mousseau, *On Balanced Approximations for Time Integration of Multiple Time Scale Systems*, J. Comp. Phys.,**185** (2003) 583.

[3] G. Yuan, X. Hang, *Accelerating Nonlinear Iteration for Nonlinear Parabolic Equations*, JCM, **24** (2006) 412-424.

Book of abstracts of the 9th International Conference on
Advanced Computational Methods in ENgineering and Applied Mathematics
September, 15–19, 2025.

A mathematical definition for electromagnetic forces

François Henrotte[1] and Christophe Geuzaine[1]

[1] *Montefiore Institute, University of Liège, B-4000 Liège, Belgium*

e-mails: francois.henrotte@uliege.be, cgeuzaine@uliege.be

Abstract

This paper proposes a mathematical definition for electromagnetic forces based on a shape derivative. It is further argued that shape calculus and differential geometry form the appropriate mathematical background to formulate the fundamental mechanism of the electromechanical coupling.

Key words: Magnetic forces, reluctance forces, shape derivative, magnetic energy, metric tensor

1 Introduction

In a recent paper [1], we studied the problem of electromagnetic forces from the point of view of their finite element computation. The objective was there to provide practical rules and formulae for their evaluation in electromechanical models. In this complementary paper, we aim at giving a clear and complete mathematical definition for electromagnetic forces. We start from their fundamental thermodynamic definition and carefully review the different mathematical steps of their derivation, invoking the concept of shape derivative [2, 3]. The elusive role played by the metric tensor, and the origin of reluctance forces are also elucidated along the way.

2 Magnetic energy

For the sake of clarity, only the magnetic energy of the system is considered in this derivation. Let

$$\mathbf{V} : E^3 \to E^3$$

be a smooth vector field on the 3-dimensional Euclidean space E^3. This vector field defines a smooth flow map (diffeomorphism) $T_s : E^3 \to E^3$, which is the solution of the family of initial value problems

$$\frac{\mathrm{d}}{\mathrm{d}s} T_s(x) = \mathbf{V}(T_s(x)) \quad , \quad T_s(0) = x.$$

With this map, one can express the magnetic energy in configuration s as

$$E(s) = \int_{E^3} \epsilon_{\mathrm{loc}}(s, T_{-s}x, b(s,x)).$$

The 3-form valued function ϵ_{loc} is the energy density. It depends on three arguments, which one explains from right to left.

The magnetic energy density obviously depends on the magnetic flux density $b(s,x)$, a 2-form, as the latter is the thermodynamic magnetic state variable.

It also depends on material features, such as the local magnetic permeability of the material and the possible presence of material discontinuities. As these features are attached to material points, they are convected by the flow T_s. The function ϵ_{loc} must therefore be evaluated in $T_{-s}x$, as the system system deforms, to produce the correct local value at a point x in the space E^3.

The metric tensor g is the geometric quantity that determines distances between points. It is a symmetric two times covariant tensor. As the system is deformed by the flow, the metric tensor $g(s)$ that encodes the distance between *material* points has to change to reflect the distortion. This yields the concept of strain tensor

$$\varepsilon(s) = g(s) - g(0) \quad , \quad \frac{\mathrm{d}\varepsilon}{\mathrm{d}s} = \frac{\mathrm{d}}{\mathrm{d}s} g(s).$$

Similarly, the volume form ω is the 3-form whose integral over a region of space gives the volume of that region. It obviously also depends on the metric tensor, and one has $\omega(s) = \sqrt{|g(s)|}\omega(0)$, where $|g(s)|$ stands for the determinant of the tensor $g(s)$. The metric tensor $g(s)$ and the volume form $\omega(s)$ combine to form the Hodge operator $\star_s$, which plays a pivotal role in the geometric expression of the magnetic energy density. The first argument of the ϵ_{loc} function thus accounts for the dependency in s induced by the Hodge operator $\star_s$. Now, the variation of the energy of the system reads

$$\begin{aligned}\frac{\mathrm{d}}{\mathrm{d}s}E(s) &= \int_{E^3} \frac{\mathrm{d}}{\mathrm{d}s}\epsilon_{\text{loc}}(s, T_{-s}x, b(s,x)) \\ &= \int_{E^3} \Big(\frac{\partial \epsilon_{\text{loc}}}{\partial s}(s, T_{-s}x, b(s,x)) - \frac{\partial \epsilon_{\text{loc}}}{\partial x}(s, T_{-s}x, b(s,x)) \cdot \mathbf{V} + \frac{\partial \epsilon_{\text{loc}}}{\partial b}(s, T_{-s}x, b(s,x)) \wedge \frac{\partial b}{\partial s} \Big),\end{aligned}$$

and it shall be demonstrated in the full paper that the three terms represent respectively: the work delivered by the Laplace force, the work delivered by the reluctance forces, and the variation of the magnetic energy.

References

[1] Henrotte, François and Geuzaine, Christophe, *Electromagnetic forces and their finite element computation*, Int J Numer Model 2024, 37(5), https://doi.org/10.1002/jnm.3290

[2] Hiptmair, R., Li, J., em Shape derivatives in differential forms I: an intrinsic perspective, Annali di Matematica 192, 1077–1098 (2013), https://doi.org/10.1007/s10231-012-0259-9

[3] P. Panchal, R. Hiptmair, and S. Kurz, *"Holding the fields constant" a shape-calculus approach to electromagnetic forces*, Mathematical Models and Methods in Applied Sciences 2025 35:10, 2181-2205.

Book of abstracts of the 9th International Conference on
Advanced Computational Methods in ENgineering and Applied Mathematics
September, 15–19, 2025.

On qualitative aspects of discrete dislocation dynamics model based on evolving curves

Miroslav Kolář[1], Michal Beneš[1] and Petr Pauš[2]

[1] *Faculty of Nuclear Sciences and Physical Engineering, Czech Technical University in Prague*

[2] *Faculty of Information Technology, Czech Technical University in Prague*

e-mails: Miroslav.Kolar@fjfi.cvut.cz, Michal.Benes@fjfi.cvut.cz, Petr.Paus@fit.cvut.cz

Abstract

We describe the fundamentals of discrete dislocation dynamics (DDD) and we discuss our approach to modeling DDD by means of curvature driven flow of curves. We also discuss the numerical approximation scheme based on the flowing finite volume method and show several computational examples of important dislocation mechanisms including the cross-slip effect.

Key words: cross-slip, curvature driven flow, dislocation, tangential redistribution

1 Introduction

Dislocation dynamics (DD) has become a standard tool for analyzing deformation microstructures. Fundamentals of dislocation theory have been established in 1930s and later verified by first TEM experiments in 1950s. The ultimate objective of DD is to fill the gap between fully continuous models in the macroscopic scale based on crystal plasticity, and atomistic models in nanoscale usually treated by the molecular dynamics methods.

In crystalline solids, dislocations represent irregularities or defects in the crystal structure. Such defects are usually of the line character and the typical unit of length of such defects is microns. These line defects are the subject of both external forces applied on the crystal and also various internal mechanisms, and they evolve in the so-called slip planes.

Several dislocation dynamics computational codes are available these days. Such tools are usually tailored to handle a bulk with large quantity of dislocations, and therefore a more or less simplistic description of dislocations is necessary. Recently, the increasing interest of the material science community has been in the detailed and precise modeling of fundamental mechanisms involving single or very few dislocations. Such a topic is typically referred to as a discrete dislocation dynamics (DDD).

2 Discrete dislocation dynamics

In our approach to DDD, a single dislocation carrying the plastic flow in its respective slip plane is represented as an evolving planar curve. The experimentally observed fact is that the motion of the dislocations is of a non-Newtonian type and can be schematically described as

$$\text{normal velocity} = \text{curvature} \; + \; \text{external force}.$$

Here the curvature term is used to approximate the self-stress of the dislocation generated by a line tension. The external force term is responsible for other dislocation mechanisms. We treat this kind of evolution equation by the direct (Lagrangian) approach resulting in the system of two degenerate parabolic equations for parametrization of the single dislocation curve. We solve this problem numerically by means of the flowing finite-volume method, and we improve the stability of the numerical scheme by the suitable choice of the external tangential velocity appropriately redistributing the discretization points along the dislocation.

We demonstrate our approach in several computational examples covering the fundamental dislocation mechanisms and we show how we applied our method together with the geodesic description of curves to investigate the so-called cross-slip effect [1], which is considered as one of the key mechanisms of microplasticity.

Acknowledgements This work was supported by the Ministry of Education, Youth and Sports of the Czech Republic under the OP RDE Grant No. CZ.02.1.01/ 0.0/0.0/16 019/0000778 "Centre for Advanced Applied Sciences", group MATE. The first author was partly supported by the International Research Fellowship of Japan Society for Promotion of Science.

References

[1] Kolář, Miroslav and Pauš, Petr and Kratochvíl, Jan and Beneš, Michal, *Improving method for deterministic treatment of double cross-slip in FCC metals under low homologous temperatures*, Computational Materials Science **189** (2021) 110251.

Book of abstracts of the 9th International Conference on
Advanced Computational Methods in ENgineering and Applied Mathematics
September, 15–19, 2025.

Efficient Numerical Techniques for Fractional Laplacian Differential Equation with Distributed Order Fractional Term

Yashveer Kumar[1], Juan Acebron[2] and Jose Monteiro[3]

[1] *INESC-ID Lisboa, Rua Alves Redol 9, Lisbon, Portugal, 1000-029,*

[2] *INESC-ID, Department of Mathematics, Carlos III University of Madrid, Spain,*

[3] *INESC-ID, IST, Universidade de Lisboa, Portugal,*

e-mails: yashveerkumar.rs.mat18@inesc-id.pt, juan.acebron@ist.utl.pt, jcm@inesc-id.pt

Abstract

This work presents a novel numerical method for solving fractional Laplacian differential equation described by distributed order fractional derivative. The method utilizes orthogonal polynomials and their associated operational matrices to efficiently and accurately approximate the solutions of such complex equations. The proposed scheme transforms the governing problem into a system of algebraic equations by exploiting the spectral properties of orthogonal polynomials. Numerical results validate the accuracy and robustness of the approach and demonstrate its applicability in nonlocal fractional model.

Key words: Distributed order fractional derivative, Fractional Laplacian, Fractional differential equations, Orthogonal polynomial, Operational matrix method

1 Introduction

Fractional differential equations are effective in modeling anomalous diffusion, memory effects, and multiscale phenomena. The distributed-order and fractional Laplacian adds spatial nonlocality and spectral complexity, making analytical solutions challenging and motivating efficient numerical methods.

Fractional Laplacian equations have gained attention for modeling nonlocal and anomalous behavior in areas such as physics, finance, biology, and image processing. The operator $(-\Delta)^s$, with $s \in (0,1)$, generalizes the classical Laplacian and is defined by [1,2]:

$$(-\Delta)^s u(X) = C_{n,s}\,\text{P.V.}\int_{\mathbb{R}^n} \frac{u(X)-u(Y)}{|X-Y|^{n+2s}}\,dY,$$

where P.V. denotes the Cauchy principal value. This operator captures long-range spatial interactions and is key to many fractional diffusion models. Orthogonal basis functions are effective tools for numerically solving fractional-order models. To our knowledge, this is the new application of an operational matrix method [3] using orthogonal functions to solve fractional Laplacian equations with distributed-order terms.

2 Numerical Method

We approximate the spatial and temporal components using orthogonal polynomials:

$$u(X,t) \approx \sum_{i=0}^{N} \sum_{k=0}^{M} c_{ik} T_i(X) T_k(t),$$

where $X \in \mathbb{R}^n$ and $T_n(\cdot)$ are orthogonal polynomials. Using operational matrices of fractional derivatives and integrals for polynomials, the DO-FDE is reduced to an algebraic system.

3 Conclusion

A orthogonal polynomial-based operational matrix method is developed for solving fractional Laplacian differential equation with distributed order fractional term. The results demonstrate good accuracy with low computational cost. The proposed scheme is accurate, computationally efficient, and can be extended to higher dimensions and more complex boundary conditions. It is also well-suited for implementation in a parallel computing environment, which is one of my future research goals. Work on higher-dimensional cases is currently in progress and will be reported in the near future.

Acknowledgements This work was partially supported by national funds through FCT URA-HPC - 2022.08838.PTDC and FCT, Fundação para a Ciência e a Tecnologia, under project UIDB/50021/2020 (DOI: 10.54499/UIDB/50021/2020).

References

[1] L. Caffarelli, L. Silvestre, *An extension problem related to the fractional Laplacian*, Communication in partial differential equations **32** (2007) 1245–1260.

[2] G. Acosta, J.P. Borthagaray, *A fractional Laplacian equation: regularity of solutions and finite element approximations*, SIAM Journal on Numerical Analysis **55** (2017) 472–495.

[3] Y. Kumar, V.K. Singh, *Computational approach based on wavelets for financial mathematical model governed by distributed order fractional differential equation*, Mathematics and Computers in Simulation **190** (2021) 531–569.

Book of abstracts of the 9th International Conference on
Advanced Computational Methods in ENgineering and Applied Mathematics
September, 15–19, 2025.

Wavelet collocation method for the solution of optimal control problems governed by diffusion equations on metric graphs

Ritu Kumari[1] **and Mani Mehra**[1]

[1] *Department of Mathematics, Indian Institute of Technology Delhi, New Delhi-110016, India*

e-mails: ritsrishu98@gmail.com, mmehra@maths.iitd.ac.in

Abstract

This article develops a shifted Legendre wavelet collocation method to solve optimal control problems governed by diffusion equations on metric graphs. By applying the method of calculus of variations, the problem is reformulated into a system of boundary value problems. Approximating the state and control variables using shifted Legendre wavelets reduces the system to linear algebraic equations. Further, a numerical example is taken which demonstrates the efficiency of the proposed method.

Key words: shifted Legendre wavelets, optimal control problems, metric graphs, collocation method, diffusion equation

1 Introduction

Optimal control problems (OCPs) aim to minimize a prescribed cost functional over a set of admissible control strategies, subject to dynamic constraints typically expressed by differential equations [1]. Many real-world systems are more naturally modeled on metric graphs rather than in traditional Euclidean domains. Notable examples include gas transport in pipeline networks [2], water wave propagation in open channel systems governed by Burgers' equation [3], and fluid flow through canal networks described by the Saint-Venant equations [4]. These scenarios are effectively represented by partial differential equations (PDEs) defined on metric graphs. Motivated by such applications, we investigate the optimal control of diffusion equations on a metric star graph. Specifically, we consider a graph $\mathcal{G} = (V, E)$, where $V = \{v_i\}_{i=0}^{N}$ denotes the set of vertices and E the set of edges. In this work, $\mathcal{G}$ is taken as a star graph with three edges, and the problem is formulated as follows:

$$\min_{y,u} \mathcal{J} = \int_0^T \int_0^{l_i} (y_i - y_i^d)^2 - (u_i - u_i^d)^2 dx dt \tag{1}$$

subject to

$$\begin{aligned}
&\frac{\partial y_i}{\partial t} - \frac{\partial^2 y_i}{\partial x^2} = u_i^d, && \text{in} \quad (0, l_i) \times (0, T), \quad i = 1, 2, 3,\\
&y_i(x, 0) = y_i^0(x), && x \in (0, l_i), \quad i = 1, 2, 3,\\
&y_i(0, t) = y_j(0, t), && i \neq j \quad i, j = 1, 2, 3, \quad t \in (0, T),\\
&\sum_{i=1}^{3} \frac{\partial y_i}{\partial x}(0, t) = 0, && t \in (0, T),\\
&y_i(l_i, t) = 0, && t \in (0, T), \quad i = 1, 2, 3.
\end{aligned}$$

We call this optimal problem as DOCP. We find the necessary optimality conditions for the DOCP and use the wavelet collocation method [5] for approximating the values of the optimal state $\mathbf{x}(\mathbf{t})$ and optimal control $\mathbf{u}(\mathbf{t})$.

2 Numerical Illustration

We particularly extend here the work of [6], where diffusion equations on metric star graphs were solved using a finite difference method. In contrast, the proposed approach achieves comparable accuracy with significantly fewer collocation points, whereas the method in [6] required a much larger number of spatial and temporal discretization steps. We illustrate through an example that the proposed method attains the same accuracy as [6] using only 8 spatial and temporal points, whereas their approach requires 20 spatial and 100 temporal points.

Example *Consider $l_i = 1$ and $T = 1$ for the DOCP. The desired state and desired control are given as*

$$y_1^d = y_2^d = (1-t)^2\left(\sin \pi x + \cos \frac{\pi}{2}x\right), \quad y_3^d = (1-t)^2\left(-2\sin \pi x + \cos \frac{\pi}{2}x\right),$$

$$u_1^d = u_2^d = -2(1-t)\left(\sin(\pi x) + \cos\left(\frac{\pi}{2}x\right)\right) - (1-t)^2\left(-\pi^2 sin(\pi x) - \frac{\pi^2}{4}\cos\left(\frac{\pi}{2}x\right)\right),$$

$$u_3^d = -2(1-t)\left(-2\sin(\pi x) + \cos\left(\frac{\pi}{2}x\right)\right) - (1-t)^2\left(2\pi^2 \sin(\pi x) - \frac{\pi^2}{4}\cos\left(\frac{\pi}{2}x\right)\right).$$

Table 1: Error E_{y_i} in the approximation of the optimal state (y_i), via the proposed method and method in [6] for $N_1 \times N_2$ (spatial × temporal) number of collocation points.

Proposed method			**Finite difference [6]**		
$N_1 \times N_2$	$E_{y_1} = E_{y_2}$	E_{y_3}	$N_1 \times N_2$	$E_{y_1} = E_{y_2}$	E_{y_3}
8×8	5.97×10^{-3}	3.16×10^{-3}	20×100	1.85×10^{-3}	3.70×10^{-3}
16×16	4.49×10^{-4}	2.36×10^{-4}	40×100	4.64×10^{-4}	9.28×10^{-4}

References

[1] Donald E Kirk, *Optimal control theory: an introduction*, Courier Corporation, 2004.

[2] Marc C Steinbach, *On PDE solution in transient optimization of gas networks*, Journal of computational and applied mathematics, 2007.

[3] H. Yoshioka, K. Unami, and M. Fujihara, *Burgers type equation models on connected graphs and their application to open channel hydraulics*, Kyoto University Research Information Repository, 2014.

[4] G. Q. Xu and N. E. Mastorakis, *Differential equations on metric graph*, Wseas Press Boston, 2010.

[5] R. Kumari, M. Mehra, and N. Kumar, *Müntz–Legendre wavelet collocation method for loaded optimal control problem*, International Journal of Systems Science, 2024.

[6] V. Mehandiratta, and M. Mehra, *A difference scheme for the time-fractional diffusion equation on a metric star graph*, Applied Numerical Mathematics, 2020.

Book of abstracts of the 9th International Conference on
Advanced Computational Methods in ENgineering and Applied Mathematics
September, 15–19, 2025.

Efficient Mesh Generation and Application for Large-Scale Multiphysics Coupled Simulations

Li Liao[1], Wei Wang[1] and Zhiming Gao[1]

[1] *Institute of Applied Physics and Computational Mathematics, Beijing*

[2] *CAEP Software Center for High Performance Numerical Simulation,*

e-mails: liliao@iapcm.ac.cn, wang_wei@iapcm.ac.cn, gao_zhiming@iapcm.ac.cn

Abstract

This paper investigates characteristic-based parallel generation techniques for unstructured meshes, achieving highly concurrent generation of two types of unstructured meshes at the billion-element scale and addressing the I/O bottleneck in large-scale unstructured mesh applications. Furthermore, a multi-resolution mesh technology is developed to resolve the spatial scale differences in multiphysics coupling codes. These advances significantly enhance the accuracy and scalability of multiphysics coupling programs.

Key words: multiphysics coupling, unstructured mesh generator, large-scale numerical simulation, multi-resolution mesh

1 Introduction

The scale of computable meshes in multiphysics coupled simulations based on unstructured grids is limited by two main factors: (1) high initialization I/O and memory overhead, and (2) differing mesh resolution requirements for different physical processes. This paper introduces a set of mesh generation and management methods for multiphysics coupled simulations. The methods enable efficient large-scale mesh generation and allow the physical processes utilize meshes of different resolutions as required.

2 High-Concurrency Generation Techniques for Characteristic Unstructured Meshes

Structured hexahedral and ray-based meshes are widely used in scientific simulations (see Figure 1). Traditional file-based mesh loading causes high memory use and long I/O times. To address this, we developed a parallel structured mesher that generates both mesh types at runtime, supporting billions of elements and enabling efficient, region-based partitioning with optimal face-to-cell ratios. This reduces initialization time by up to 100x, for example, generating 400 million ray-based meshes in just 0.02 seconds on 57,344 cores and increases coordinate precision from single to double precision compared to mesh files.

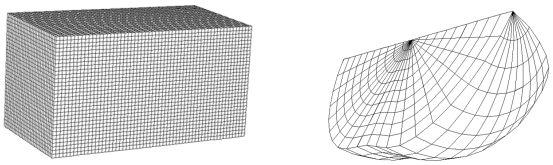

Figure 1: Two types of unstructured meshes used in scientific numerical simulations.

3 Multi-Resolution Meshes in Multiphysics Coupling

The structured mesher is applied in several ALE and Eulerian multi-physics codes built on JASMIN [1] and JAUMIN[2] frameworks. Different physical processes require different mesh resolutions: for example, fluid dynamics needs high-resolution meshes, while neutron transport becomes computationally infeasible at high resolutions. To solve this, overlapping meshes with varying resolutions are generated (see Figure 2): high-resolution for fluid dynamics and radiation, low-resolution for neutron transport. Data exchange is handled by the parallel mesh coupler JASMIN3C, bridging the scale gap. In ALE reactor dynamics simulations with non-uniform mesh resolutions (23.92 million cells for mechanics, 460,000 for neutrons), computation time dropped from 3.32 to 1.11 hours. This parallel mesh generation technology greatly enhances the accuracy and scalability of multiphysics coupling.

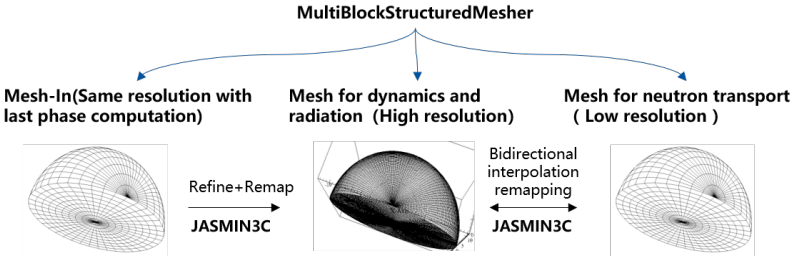

Figure 2: Meshes with different resolution are generated for multi-physics application.

References

[1] Z. Mo, A. Zhang, X. Cao, Q. Liu, X. Xu, H. An, W. Pei, S. Zhu, *JASMIN: a parallel software infrastructure for scientific computing*, Frontiers of Computer Science in China **4**(4) (2010) 480–488.

[2] Q. K. Liu, Z. Y. Mo, A. Q. Zhang, *JAUMIN: A programming framework for large-scale numerical simulation on unstructured meshes*, CCF Transactions on High Performance Computing **1**(1) (2019) 35–48.

Book of abstracts of the 9th International Conference on
Advanced Computational Methods in ENgineering and Applied Mathematics
September, 15–19, 2025.

Direct and inverse source problems for the fractional heat equation with phase lag

Frederick Maes[1] **and Karel Van Bockstal**[2]

[1] *Department of Electronics and Information Systems, Ghent University*

[2] *Department of Mathematics: Analysis, Logic and Discrete Mathematics, Ghent University*

e-mails: frederick.maes@ugent.be, karel.vanbockstal@ugent.be

Abstract

In this contribution, the fractional heat equation supplied with phase-lag parameters is addressed. The well-posedness result for the direct problem for the fractional single-phase-lag problem is studied first. The existence of a weak solution is discussed based on Rothe's method. The uniqueness is proven by the variational approach. In order to motivate some of the used assumptions, the one-dimensional case will be studied. Afterwards, attention is put on inverse source problems of determining a space-dependent source in the single- and dual-phase-lag setting. Several properties, of independent interest, of the multivariate Mittag-Leffler function are used in the analysis of the problems and will therefore be presented.

Key words: direct problem, fractional heat equation, inverse source problem, Mittag-Leffler function, phase lag

MSC 2020: 26A33, 35A01, 35A02, 35R11, 65M12, 33E12

1 Problem formulation

The fractional dual-phase-lag heat equation for the unknown temperature profile

$$u\colon Q_T \to \mathbb{R}^d,$$

where $Q_T = \Omega \times (0,T]$, $t > 0$ and $\Omega \subset \mathbb{R}^d$ is a Lipschitz continuous domain, is given by

$$\left[1 + \tau_q^\alpha \mathcal{D}_t^\alpha\right](\rho c \partial_t u + au) + \nabla \cdot \left(-\boldsymbol{k}\left[1 + \tau_\theta^\beta \mathcal{D}_t^\beta\right](\nabla u)\right) = p. \tag{1}$$

In (1), the mass density, specific heat and thermal conductivity are given by ρ, c and $\mathbf{k}$ respectively, p is a source term, $a > 0$ and τ_q^α and τ_θ^β are the positive lagging-parameters. The operator $\mathcal{D}_t^\gamma$ is the Caputo derivative operator of order γ. The fractional orders of differentiation are assumed to satisfy $\alpha, \beta \in (0,1)$. The fractional partial differential equation (1) is supplied with (homogeneous) Dirichlet boundary conditions on $\Sigma_T = \partial\Omega \times (0,T]$, and initial conditions $u(\mathbf{x},0) = \overline{u}_0(\mathbf{x})$, $\partial_t u(\mathbf{x},0) = \overline{u}_1(\mathbf{x})$.

For the direct problem associated to (1) we restrict attention to the fractional version of the Cattaneo-Vernotte equation, i.e. we set $\tau_\theta^\beta = 0$, obtaining the fractional single-phase-lag heat equation. For the studied inverse source problems, we assume that the source can be written as $p(\mathbf{x},t) = g(t)f(\mathbf{x})$, where g is a known function, and f is to be recovered from the final-in-time measurement $u_T(\mathbf{x}) = u(\mathbf{x},T)$.

2 Main results

Let $g_\alpha(t) = \frac{t^{-\alpha}}{\Gamma(1-\alpha)}, t > 0, \alpha \in (0,1)$ be the Riemann-Liouville kernel. Under the assumptions $F \in \mathrm{L}^2\left([0,T], \mathrm{L}^2(\Omega)\right), \overline{u}_0 \in \mathrm{H}_0^1(\Omega)$ and $\overline{u}_1 \in \mathrm{L}^2(\Omega)$, we proved in [2] the existence of a weak solution to the (direct) single-phase-lag problem satisfying

$$u \in \mathrm{L}^\infty\left((0,T), \mathrm{H}_0^1(\Omega)\right) \cap \mathrm{C}\left([0,T], \mathrm{L}^2(\Omega)\right),$$

for which $\partial_t u \in \mathrm{L}^2\left((0,T), \mathrm{L}^2(\Omega)\right)$ and $\partial_t\left(g_\alpha * (\partial_t u - \overline{u}_1)\right) \in \mathrm{L}^2\left((0,T), \mathrm{H}_0^1(\Omega)^*\right)$. Here $*$ denotes the convolution operator. The used approach is based on Rothe's method and a semi-discretisation in time.

Under the extra assumption that $\partial_t u \in \mathrm{L}^\infty\left((0,T), \mathrm{L}^2(\Omega)\right)$ such a weak solution is shown to be unique. This additional information is motivated by means of the Fourier method for the problem in the $d = 1$ dimensional setting and relies on a crucial bound

$$\left|E_{(\alpha_1,\ldots,\alpha_m),\beta}(z_1,\ldots,z_m)\right| \leq \frac{C}{1+|z_1|}$$

for the multivariate Mittag-Leffler function where $\beta > 0$ and $0 < \alpha_m < \cdots < \alpha_2 < \alpha_1 < 2$, in some region of the complex plane for z_1 and for $-K \leq z_j < 0, j = 2,\ldots,m$. This bound is of independent interest and was used in [3] in a different context. The direct problem in the dual-phase-lag setting is more complicated and remains open for now.

For the considered inverse source problem, we showed in [1], under standard assumptions on the physical parameters, that there exists at most one couple

$$(u, f) \in \mathrm{C}\left([0,T], \mathrm{H}_0^1(\Omega)\right) \times \mathrm{L}^2(\Omega),$$

that solves the fractional dual-phase-lag heat equation with $\alpha, \beta \in (0,1)$, given the final-in-time measurement u_T, in case the temporal part $g \in \mathrm{C}([0,T])$ of the source does not admit zero and shares its sign with its derivative $g' \in \mathrm{C}((0,T])$ for all $t \in (0,T]$. Several sub-models, obtained by a comparison between the phase-lags, are considered as well. In the dominant parabolic model, a relaxation of the condition on g is possible due to the complete monotonicity property of the occurring multivariate Mittag-Leffler function. This relaxation is not possible in the dominant hyperbolic model. Some form of sharpness of the used conditions on g is achieved by means of counterexamples.

References

[1] F. Maes, M. Slodička, *Some inverse source problems of determining a space dependent source in fractional-dual-phase-lag type equations*, Mathematics **8**(8) (2020) 16.

[2] F. Maes, K. Van Bockstal, *Existence and uniqueness of a weak solution to fractional single-phase-lag heat equation*, Fract. Calc.Ãppl. Anal. **26**(4) (2023) 1663–1690.

[3] H. De Bie, P. Lian, F. Maes, *Bounds for the kernel of the (κ,α)-generalized Fourier transform*, J. Funct. Anal **288**(4) (2025) 110755.

Book of abstracts of the 9th International Conference on
Advanced Computational Methods in ENgineering and Applied Mathematics
September, 15–19, 2025.

Fluid flow through porous wall and the Darcy interface condition

Eduard Marušić-Paloka[1]

[1] *Department of mathematics, University of Zagreb*

e-mails: emarusic@math.hr

Abstract

When a thin porous interface (a sieve) is submerged in container filled with viscous fluid, an effective interface condition is needed for simulations. Supposing that the sieve has periodic structure and using homogenization techniques, we rigorously derive a macroscopic interface condition in the form of Darcy law across the sieve. More precisely, the velocity is proportional to the (large) stress jump across the sieve. We check that the derived problem is well posed and justify the obtained model via error estimate.

Key words: porous interface, viscous fluid, homogenization, boundary layer, asymptotic analysis

1 Introduction

Fluid flows through domains that contain thin porous objects like filters, sieves or membranes appear in various application, from machine engineering to biology and medicine. Finding a correct macroscopic model has been a subject of many papers (see, for instance [7], [1], [2], [8]).

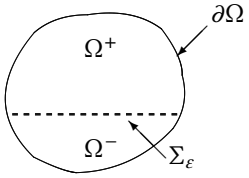

$\Omega = \Omega^+ \cup \Omega^-$

(ε is the porosity)

In previous works (cited above) the proposed condition was of the Dirichlet type. More precisely, imposing the constant value of the velocity on the interface Σ, with (constant) value determined by the total inflow through the exterior boundary.
In the present paper we make step forward. Starting from the Stokes system

$$-\mu\,\Delta \mathbf{u}^\varepsilon + \nabla p^\varepsilon = 0 \quad , \quad \operatorname{div} \mathbf{u}^\varepsilon = 0 \quad \text{in} \quad \Omega \tag{1}$$

$$\mathbf{u}^\varepsilon = \mathbf{f} \quad \text{on} \quad \partial\Omega \quad , \quad \mathbf{u}^\varepsilon = 0 \quad \text{on} \quad \Sigma_\varepsilon \quad , \tag{2}$$

using the homogenization and boundary layer techniques, we compute the corrector to that first order approximation. It turns out that the corrector, not only improves the approximation, but changes the perspective to the effective interface condition. The sum of the zero-order approximation and its first-order corrector $(\mathbf{v}, q)$ satisfies the Darcy interface law

$$\boxed{\mathbf{v} = \mathbf{K}_\varepsilon\,[\mathbf{T}(\mathbf{v}, q)\mathbf{n}]_\Sigma \quad \text{on} \quad \Sigma} \quad . \tag{3}$$

The derived macroscopic velocity approximation on the interface $\mathbf{v}$ (both parts, tangential and normal) turns out to be proportional to the jump of the stress

$$\mathbf{T}(\mathbf{v}, q)\,\mathbf{n} = [q\,\mathbf{I} - 2\mu\mathbf{D}(\mathbf{v})]\;\mathbf{n}$$

across the sieve. The proportionality is given by a tensor, representing the permeability of the boundary $\mathbf{K}_\varepsilon$.
We show that the obtained problem, with non-standard boundary condition, is well posed.
We justified the proposed effective boundary condition by an error estimate in terms of ε, expressed in the norms of the appropriate functional spaces.

Acknowledgements The authors have been supported by the Croatian Science Foundation under the project AsyAn (IP-2022-10-1091).

References

[1] C.Conca, Étude d'un fluide traversant une paroi perforée. I. Comportement limite près de la paroi, J.Math.Pures et Appl., 66 (1987), 1-43.

[2] C.Conca, Étude d'un fluide traversant une paroi perforée. II. Comportement limite loin de la paroi, J.Math.Pures et Appl., 66 (1987), 45-69.

[3] E.Marušić-Paloka, Rigorous derivation of the Darcy boundary condition on the porous wall, Mathematical methods in the applied sciences, 46 (2023), 9; 11021-11042. 19.

[4] E.Marušić-Paloka, I.Pažanin, Rigorous justification of the effective boundary condition on a porous wall via homogenization, Zeitschrift für angewandte Mathematik und Physik, 72 (2021), 146, 22

[5] E.Marušić-Paloka, I. Pažanin,

[6] E.Marušić-Paloka, I. Pažanin,The effective boundary condition on a porous wall, International journal of engineering science, 173 (2022), 103638, 12 Fluid flow through a sieve and the Darcy interface condition, submitted

[7] E.Sanchez-Palencia, Un problème d'écoulement lent d'un fluide visqueux incompressible au travers d'une paroi finement perforée, in D.Bergman et al., Les métodes de l'homogénéisation: Théorie et applications en physique, Collections de la direction des études et recherches d'électricité de France, No 57, 1985, 371-400, Eyrolles, Paris.

[8] G.A.Zampogna, F.Gallaire, Effective stress jump across membranes, Journal of Fluid Mechanics, 892 (2020), A9

Book of abstracts of the 9th International Conference on
Advanced Computational Methods in ENgineering and Applied Mathematics
September, 15–19, 2025.

Direct and Inverse Problem for Gas Diffusion in Polar Firn

Sophie Moufawad[1], Nabil Nassif [1] and Faouzi Triki[2]

[1] *Department of Mathematics, American University of Beirut (AUB), Beirut, Lebanon*

[2] *Laboratoire Jean Kuntzmann, UMR CNRS 5224, Université Grenoble-Alpes, 38401 Saint-Martin-d'Hères, France.*

e-mails: sm101@aub.edu.lb, nn12@aub.edu.lb,
faouzi.triki@univ-grenoble-alpes.fr

Abstract

Simultaneous use of partial differential equations in conjunction with data analysis has proven to be an efficient way to obtain the main parameters of various phenomena in different areas, such as medical, biological, and ecological. In the ecological field, the study of climate change (including global warming) over the past centuries requires estimating different gas concentrations in the atmosphere, mainly CO_2. This is possible by using gas concentrations obtained from deep polar ice (Firn) along with the proper mathematical tools.

The mathematical model of gas trapping in Firn consists of a parabolic partial differential equation that is almost degenerate at one boundary extreme. In this work, we first consider all the coefficients to be constants, except the diffusion coefficient that is to be reconstructed. Then, we consider both the diffusion coefficient and the gas volume fractions to be functions of the depth z.

We present the theoretical aspects of existence and uniqueness for such direct problems and build a robust simulation algorithm. Consequently, we formulate the inverse problem that attempts to recover the diffusion coefficients using given generated data, by defining an objective function to be minimized. An algorithm for computing the gradient of the objective function is proposed and its efficiency is tested using different minimization techniques available in MATLAB's optimization toolbox.

Key words: Climate change, existence and uniqueness of PDE solution, finite element semi-discretization, optimization solvers for inverse problem, time-dependent advection-diffusion PDE.

MSC 2020: 35A01, 35A02, 35A15, 35G16, 35M13, 35R30, 65M22, 65M32, 65M60.

1 Introduction

Antarctic and Greenland polar snow and ice constitute a unique archive of past climates and atmospheres. Based on a good understanding of the mechanisms controlling gas trapping in deep polar ice, and therefore of the processes of densification and pore closure in firns (typically over the first hundred meters of the polar cap), several models have been derived.

We consider the model [2] where the concentration ρ_α^o of a gas α in open pores satisfies an initial-value, time-dependent advection-diffusion partial differential equation on a one-space dimension segment $[0, z_F]$ with Dirichlet boundary condition at 0 and a mixed one at

z_F, where $\rho_\alpha^{\text{atm}}(0) = 0$. For $z \in (0, z_{\text{F}}), t > 0$:

$$\begin{cases} \dfrac{\partial}{\partial t}[\rho_\alpha^{\text{o}} f] + \dfrac{\partial}{\partial z}[\rho_\alpha^{\text{o}} f(v + w_{\text{air}})] + \rho_\alpha^{\text{o}}(\tau + \lambda) = \dfrac{\partial}{\partial z}\left[D_\alpha\left(\dfrac{\partial \rho_\alpha^{\text{o}}}{\partial z} - \rho_\alpha^{\text{o}}\dfrac{M_\alpha g}{RT}\right)\right], \\ \rho_\alpha^{\text{o}}(0,t) = \rho_\alpha^{\text{atm}}(t), \ t > 0, \\ D_\alpha(z_F)\left(\dfrac{\partial \rho_\alpha^{\text{o}}}{\partial z}(z_{\text{F}}, t) - \dfrac{M_\alpha g}{RT}\rho_\alpha^{\text{o}}(z_{\text{F}}, t)\right) = 0, \\ \rho_\alpha^{\text{o}}(z, 0) = 0 \end{cases} \tag{1}$$

Moreover, $D_\alpha(z)$ is the effective diffusion coefficient of the gas α in the firn (m^2/yr) and is given by

$$D_\alpha(z) = \begin{cases} D_{\text{eddy}}(z) + r_\alpha c_f D_{\text{CO2, air}}(z) & \text{if } z \le z_{\text{eddy}}, \\ r_\alpha D_{\text{CO2, air}}(z), & \text{if } z > z_{\text{eddy}}, \end{cases} \tag{2}$$

where z_{eddy}, r_α, and c_f are known constants, and $D_{\text{eddy}}(z)$ and $D_{\text{CO2, air}}(z)$ are diffusion coefficients.

In [1], the remaining terms are considered constants including the gas volume fractions f, where we derive the semi-variational form of (1) and prove the existence and uniqueness of a solution to (1). Moreover, after rescaling (1) to the unit square, an Euler-implicit in time and a finite element space discretization is proposed which leads to a robust direct problem algorithm that is tested.

On the other hand, the inverse problem aims at recovering the diffusion coefficient $D_{CO2,air}(z)$ assuming that the concentration ρ_α^{o} of several gases is given at some time T_e. The gradient of objective function is computed using directional derivatives. Testings are performed on the efficiency of the computed gradient using MATLAB's optimization toolbox and the nonlinear conjugate gradient method.

Preliminary results are presented in the case where the gas volume fractions f is considered a function of z.

Acknowledgements This work was supported by the Alwaleed Center for American Studies and Research (CASAR) in the Faculty of Arts and Sciences at AUB; and by the AUB University Research Board grant number 104261 (Project 26742).

References

[1] S. Moufawad, N. Nassif, F. Triki, *Direct and inverse problem for gas diffusion in polar firn* Communications on Analysis and Computation **2(1)** (2024) 71-109

[2] E. Witrant, P. Martinerie, C. Hogan, J. C. Laube, K. Kawamura, E. Capron, S. A. Montzka, E. J. Dlugokencky, D. Etheridge, T. Blunier and W. T. Sturges, *A new multi-gas constrained model of trace gas non-homogeneous transport in Firn: Evaluation and behavior at eleven polar site*, Atmos. Chem. Phys.**12** 11465-11483.

Book of abstracts of the 9th International Conference on
Advanced Computational Methods in ENgineering and Applied Mathematics
September, 15–19, 2025.

Data-driven Construction of Reduced Size Models Using Computational Singular Perturbation Method.

Ismaila Muhammed[1], Dimitris M. Manias[1], Dimitris A. Goussis[2] and Haralampos Hatzikirou[1]

[1] *Department of Mathematics, Khalifa University of Science and Technology, Abu Dhabi 127788, UAE*

[2] *Department of Mechanical Engineering, Khalifa University of Science and Technology, Abu Dhabi 127788, UAE*

e-mails: 100061894@ku.ac.ae, dimitris.manias@ku.ac.ae, dimitris.goussis@ku.ac.ae, haralampos.hatzikirou@ku.ac.ae

Abstract

Biomedical systems often exhibit multi-scale dynamics, making accurate system identification challenging, especially when explicit governing equations are unavailable. Traditional approaches like Computational Singular Perturbation (CSP) rely on such equations, which limits their application in biomedical contexts where only observational data are available. To overcome this, we propose a data-driven CSP framework that combines Sparse Identification of Nonlinear Dynamics (SINDy) and neural networks (NNs) to identify fast and slow dynamics directly from data, enabling region-wise time-scale decomposition. The method is validated on the Michaelis-Menten model by identifying regions where valid quasi-steady-state approximations (sQSSA and rQSSA) can be analytically derived. In cases where SINDy fails due to noise, data sparsity, or model complexity, NNs are used to estimate the Jacobian matrix, allowing CSP to detect dominant dynamical structures. We examine cases spanning multiple dynamical regimes, where dataset partitioning allows SINDy to recover region-specific models. Results show that while SINDy alone is prone to failure in noisy, multi-scale contexts, its accuracy improves significantly when guided by CSP-based decomposition and region identification. This framework extends CSP to data-driven applications, offering a robust method for analyzing complex biological systems without requiring explicit equations.

Key words: Biomedical systems, Computational Singular Perturbation, Sparse Identification of Nonlinear dynamics (SINDy).
Mathematics Subject Classification: 37N25 (Dynamical Systems in Biology), 92C42 (Systems Biology), 68T07 (Artificial Neural Networks and Deep Learning)

1 Introduction

Biomedical systems often characterized by multi-timescale dynamics, present significant challenges for prediction and analysis[1]. Multi-scale analysis facilitates deeper insight into such systems. The computational Singular Perturbation (CSP) [2] method is a well-established method for reducing high-dimensional models while preserving time-scale separation and essential dynamic behaviors. By systematically eliminating fast transient dynamics, CSP makes

it possible to construct reduced-order models that preserve the key components of the original system, thereby offering a computationally tractable alternative for analysis and predictions. CSP has been successfully applied in fields such as reactive flows, biological systems, computer engineering, atmospheric science and pharmacokinetics.

Despite its effectiveness, CSP techniques rely solely on the explicit governing equations or models. This represents a significant limitation, especially in situations where experimental or observational data can offer valuable insights into systems' behavior. In order to utilize the capabilities of CSP, we propose a framework that combines it with data-driven methods, particularly Sparse Identification of Nonlinear Dynamics (SINDy)[3] for system Identification and Neural Networks (NNs) for Jacobian estimation.

Given a time series dataset, we first apply SINDy to identify the underlying dynamical systems, then CSP is applied accordingly to obtain reduced-order models. In a situation where SINDy fails, due to noise, data sparsity or low data volume, Neural ODEs (NODE) [4] is used to provide a uniform and dense vector field that is subsequently used in a NN [5] to estimate the Jacobian matrix. The resulting eigenvectors and eigenvalues of the estimated Jacobian serve as leading-order approximations of the system's corresponding fast/slow directions and time scales. Using the CSP theory and diagnostic tools , the dataset is then analyzed to identify regions where valid reduced models can be constructed. These regions enable the partitioning of the dataset into subsets, each corresponding to a different dynamical regime. Finally, SINDy is applied to each subset independently to derive region-specific reduced models that accurately capture the local dynamics within each regime.

References

[1] Akbari A, Haiman ZB, Palsson BO. A data-driven approach for timescale decomposition of biochemical reaction networks. mSystems. 2024;9(2):e01001–23. doi:10.1128/msystems.01001-23.

[2] Lam SH, Goussis DA. Understanding complex chemical kinetics with computational singular perturbation. In: Symposium (International) on Combustion. vol. 22. Elsevier; 1989. p. 931–941.

[3] Brunton SL, Proctor JL, Kutz JN. Discovering governing equations from data by sparse identification of nonlinear dynamical systems. Proceedings of the National Academy of Sciences. 2016;113(15):3932–3937. doi:10.1073/pnas.1517384113.

[4] Ricky T. Q. Chen, Yulia Rubanova, Jesse Bettencourt, and David K Duvenaud. Neural Ordinary Differential Equations. In Advances in Neural Information Processing Systems, volume 31. Curran Associates, Inc., 2018.

[5] Latremoliere F, Narayanappa S, Vojtechovsky P. Estimating the Jacobian matrix of an unknown multivariate function from sample values by means of a neural network. arXiv preprint arXiv:220400523. 2022;.

Book of abstracts of the 9th International Conference on
Advanced Computational Methods in ENgineering and Applied Mathematics
September, 15–19, 2025.

AI-based Detection of Small Dams in Kazakhstan Using Map Fragment Classification

Balgaisha Mukanova[1] and Tolkyn Mirgalikyzy[2]

[1] *Department of Computational and Data Science, Astana IT University, Astana, Kazakhstan*

[2] *Department of Computer and Software Engineering, Eurasian National University, Astana, Kazakhstan*

e-mails: mbsha01@gmail.com, m_t85@mail.ru

Abstract

In Kazakhstan, most small and medium-sized dams lack geographic coordinates in official records, hindering GIS-based monitoring. We developed a machine learning framework using neural networks trained on satellite maps to detect small dams (200 – 400 m). Applied to a 35,000 km^2 region, the model identified previously non-georeferenced structures. Results cover detection examples, model performance, and integration into monitoring systems.

Key words: Dam detection, GIS, Machine learning, Image analysis
MSC 2020: 68T07, 68T07, 68U10

1 Introduction

Geospatial data on dams is crucial for GIS development; however, in Kazakhstan, most official open sources do not provide coordinates for the majority of dams. Our team, developing a dam-monitoring GIS [1], faced this gap. Manual identification from maps was inefficient, and global datasets such as the Global Dam Tracker [2] cover only large and medium-sized dams.

In this study, we propose a deep neural network-based method for detecting small dams using satellite map fragments A labeled dataset from ESRI maps was used to train neural networks for binary classification. To our knowledge, this research is the first of its kind conducted in the Central Asian region

2 Results and Discussion

The dataset generation process for neural network training was carried out in several stages. For effective model training, a sufficient number of annotated dam images were required. At the first stage, dam locations were collected based on coordinates obtained from publicly available official databases using QGIS tools, as described in our earlier work [1]. Map images were generated in QGIS using predefined coordinates, scale, and size. As a result, over 15, 000 dam-containing images were generated for regions in Asia and Africa.

Subsequently, manual filtering was performed. Given the diverse shapes and typically simple geometries of dams (e.g., linear structures), negative examples, i.e. images without

dams, were included in the dataset. Image annotation and dataset preparation were performed using the Roboflow platform, where data augmentation was also applied. Initial annotations were created manually using various strategies and thoroughly verified to ensure high-quality labeling.

Applied to a 35, 000 km² region located in southern Kazakhstan, the most accurate models were able to detect several dams that had not been previously documented. The models' efficiency were evaluated using the mean Average Precision (mAP@50) and the FPS (frames per second) metrics. Optimal hyperparameters were determined for the selected models, and training was conducted on the prepared dataset. Nevertheless, training a model on this dataset initially yielded a moderate accuracy mAP@50 of 84 ± 3%. To improve performance, semi-automatic annotation was introduced using a model pre-trained on a small subset of the data. This increased the final accuracy by approximately 6 ± 3% (see Table 1). As a result, a refined dataset consisting of 22, 616 images was compiled for training the neural network, leveraging the pre-annotated base model.

The model training was conducted on an NVIDIA GeForce RTX 4080 Laptop GPU with 12, 282 MiB of VRAM. Table 1 shows the mAP@50 values and FPS for each tested model. The best overall performance was achieved by the YOLOv81 model, with mAP@50 reaching 93.9%. All models performed well on the test samples, delivering both high speed and accuracy.

Table 1: Test results for each model.

Model	Precition (%)	Recall(%)	mAP50(%)	Performance(FPS)
YOLOv8*m*	88.8	87.8	92.9	83
YOLOv81	91.3	87.6	93.9	56
YOLOv8*x*	90.6	86.2	93.5	43
YOLOv5*m*	86.8	88.8	92.9	125
YOLOv51	84.6	89.4	91.1	77
YOLOv5*x*	91.3	84.6	91.2	56

3 Conclusion

The proposed approach is scalable to larger regions. This work highlights the practical potential of data-driven modelling to enrich geospatial databases in low-data regions and supports initiatives in infrastructure safety, disaster preparedness, and sustainable water management.

Acknowledgements This work has been funded by the Committee of Science of the Ministry of Science and Higher Education of the Republic of Kazakhstan (Grant No. AP19675038)

References

[1] B. Mukanova et al., *Building of Geographic Information System for Monitoring of Dams in the Republic of Kazakhstan*, ICISCT2024, 7th-8th Nov., IEEE Conference ID: 64202, 2024.

[2] A. T. Zhang and V. X. Gu, *Global Dam Tracker: A Database of More than 35,000 Dams with Location, Catchment, and Attribute Information*, Scientific Data, **10(1)**(2023) 111.

Book of abstracts of the 9th International Conference on
Advanced Computational Methods in ENgineering and Applied Mathematics
September, 15–19, 2025.

Source identification in integro-differential pseudoparabolic models with memory

M. Mukhambetkaliyev[1]

[1] *Department of Mathematics, Al-Farabi Kazakh National University, Almaty, Kazakhstan*

e-mails: mukhambetkaliyevmurat@gmail.com

Abstract

In this paper, we investigate a time-dependent inverse source problem for a one-dimensional pseudoparabolic equation with a memory term. The problem is supplemented with an initial condition, homogeneous Dirichlet boundary conditions, and an additional integral overdetermination condition. We establish global-in-time existence and uniqueness of strong solutions to the inverse problem. The results contribute to the theory of inverse problems for pseudoparabolic equations with memory effects and may be applied in various physical models involving heat and mass transfer in materials with memory.

Key words: Inverse problem, Pseudo-parabolic equation with memory.

1 Introduction

In this work we study the following time dependent inverse source problem for the following one dimensional pseudoparabolic equation:

$$u_t - \alpha u_{xx} - \beta u_{xxt} - \int_0^t K(t-\tau)u_{xx}(x,\tau)d\tau = f(t)g(x,t) + h(x,t), \text{in } (0,l)\times(0,T), \quad (1)$$

supplemented by the initial condition

$$u(x,0) = u_0(x), \ \ x \in (0,l) \quad (2)$$

and boundary conditions

$$u(0,t) = u(l,t) = 0, \ \ t \in [0,T] \quad (3)$$

and the integral overdetermination condition

$$\int_0^l \left(u(x,t)\omega(x) + \beta u_x(x,t)\omega_x(x)\right) dx = \varphi(t), \ \ t \in [0,T], \quad (4)$$

where $0 < l, T < \infty$. The inverse problem consists of finding the the functions $u(x,t)$ and $f(t)$ from (1)-(4) by the given positive constants α, β, and the given functions $g(x,t)$, $h(x,t)$, $K(t)$, $u_0(x)$, $w(x)$, $\varphi(t)$.

In this work, we investigate the global in time existence and uniqueness of strong solution of the inverse problem (1)-(4).

Acknowledgements This work has been supported by the Grant no. AP19676624.

References

[1] Kh. Khompysh, *Inverse problem for 1D pseudo-parabolic equation*, Functional Analysis in Interdisciplinary Applications, 2017.

[2] A.I. Prilepko, D.G. Orlovsky, I.A. Vasin, *Methods for solving inverse problems in mathematical physics*, Marcel Dekker, 2000.

Book of abstracts of the 9th International Conference on
Advanced Computational Methods in ENgineering and Applied Mathematics
September, 15–19, 2025.

Applications of Constrained Curvature Flow in Plane

Maneesh Narayanan[1] **and Michal Beneš**[2]

[1] *Department of Mathematics, Faculty of Nuclear Sciences and Physical Engineering, Czech Technical University in Prague, Prague.*

e-mails: narayman@cvut.cz, michal.benes@fjfi.cvut.cz

Abstract

We investigate the area-preserving flow of a closed embedded curve under constrained motion with force terms. Specifically, we analyze the deformation of a circle under two force scenarios: a droplet under external force and a circular-shaped eukaryotic cell. Reformulating the motion law as a system of degenerate parabolic PDEs, we solve it numerically using the finite volume method. Our findings offer insights into constrained geometric flows with applications in physical and biological systems.

Key words: Curve evolution; Parametric method; Method of lines.
MSC 2020: 65M12, 65M20, 65N12, 65N40

1 Motion law

This article studies the planar non-local curvature flow for closed Jordan curves, relevant to natural sciences. The flow evolves by

$$V = -\kappa_\Gamma + I + \frac{\int_{\Gamma_t} (\kappa_\Gamma - I), d\Gamma}{\int_{\Gamma_t} d\Gamma}, \tag{1}$$

$$\Gamma_t\Big|_{t=0} = \Gamma_0, \tag{2}$$

where Γ_t is a smooth simple closed curve, V the normal velocity, $\mathbf{n}$ the outward unit normal, κ_Γ the curvature, and $F = F(t, x)$ the normal force. The motion law (1-2) and its applications are discussed in [2, 3, 4]. Motion law (1-2) is treated by the parametric method, and solved numerically by the Runge-Kutta-Merson method as in [3].

2 Examples

Droplet Shapes Falling Under Gravity. We examine the shape evolution of droplets falling under gravity, considering a planar vertical cross-section. The droplet boundary, a closed curve, evolves due to surface tension and air friction, governed by the evolution law (1). The external force, as given in [1], is

$$I(\theta) = 5 \cdot (1 - (8 \cdot \theta)^2) \cdot e^{-1.1 \cdot (4 \cdot \theta)^2},$$

where θ is the angle between normal vector and horizontal direction. Figure 1 (left) illustrates droplet motion under gravity.

Circular Eukaryotic Cell Under Force. Figure 1 (right) also shows a circular eukaryotic cell under external force. The constrained motion of its boundary is given by external force expression

$$I(t,\theta) = 3\left[1 + \delta_f \cos\left(\alpha(\theta - \Omega_0 \cos(2\pi t/t_{\text{rot}}))\right) + G\cos\left(\theta - \Omega_0 \cos(2\pi t/t_{\text{rot}})\right)\right]. \quad (3)$$

This formulation is essential for analyzing area-preserving flows in constrained motion.

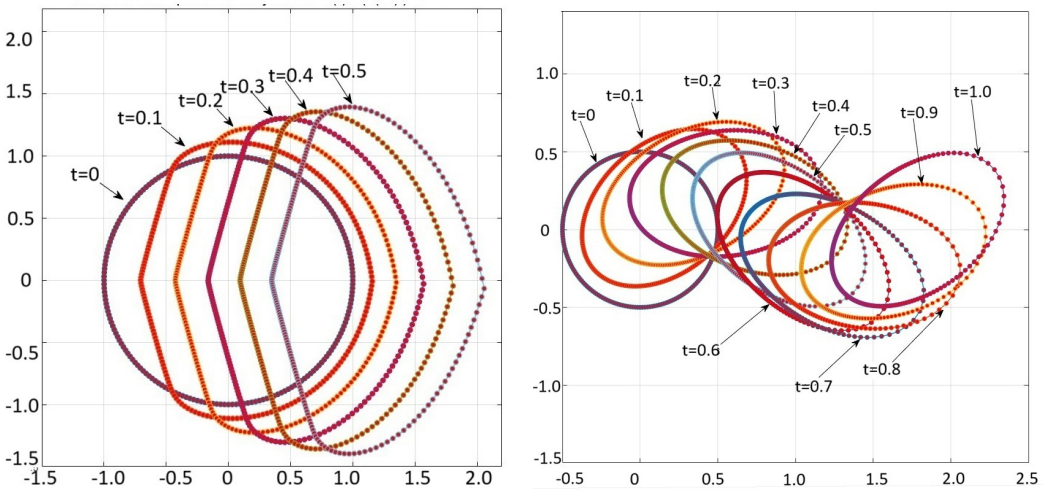

Figure 1: (Left) Simulation of droplet motion under force. (Right) Circular Eukaryotic Cell Under Force. ($\Omega_0 = 0.7853975$, $t_{\text{rot}} = 1.0$, $\delta_f = 0.55$, $\alpha = 2.0$, $G = -0.7$)

Acknowledgements The authors were partly supported by Czech Technical University of Prague, Czech Republic through the project SGS23/188/OHK4/3T/14.

References

[1] C. Magono, *On the shape of water drops falling in stagnant air*, Journal of Meteorology, vol. 11, pp. 77–79, 1954.

[2] M. Kolář, M. Beneš, and D. Ševčovič, *Computational analysis of the conserved curvature driven flow for open curves in the plane*, Math. Comput. Simul., vol. 126, pp. 1–13, 2016.

[3] M. Kolář, M. Beneš, and D. Ševčovič, *Computational studies of conserved mean-curvature flow*, Math. Bohem., vol. 139, no. 4, pp. 677–684, 2014.

[4] P. Pauš and M. Beneš, *Direct approach to mean-curvature flow with topological changes*, Kybernetika, vol. 45, pp. 591–604, 2009.

Book of abstracts of the 9th International Conference on
Advanced Computational Methods in ENgineering and Applied Mathematics
September, 15–19, 2025.

Error analysis for a finite element discretization of a radially symmetric harmonic map heat flow problem

Nam Anh Nguyen[1] **and Arnold Reusken**[1]

[1] *Institut für Geometrie und Praktische Mathematik, RWTH Aachen University, D-52056 Aachen, Germany*

e-mails: nguyen@igpm.rwth-aachen.de, reusken@igpm.rwth-aachen.de

Abstract

We consider the harmonic map heat flow problem for a radially symmetric case. For discretization of this problem we apply a H^1-conforming finite element method in space combined with a semi-implicit Euler time stepping. The semi-implicit Euler method results in a linear problem in each time step. We restrict to the regime of smooth solutions of the continuous problem and present an error analysis of this discretization method. This results in optimal order discretization error bounds. Key ingredients of the analysis are a discrete energy estimate, that mimics the energy dissipation of the continuous solution, and a convexity property that is essential for discrete stability and for control of the linearization error. We also present numerical results that validate the theoretical ones.

Key words: Harmonic map heat flow, finite element method, discrete energy estimates, discrete stability analysis, discretization error bounds

We study the harmonic map heat flow (HMHF) problem for a specific *radially symmetric* case. Given $0 < T < \infty$, $I := [0,1]$ and $u_0 \in C^2(I)$ with $u_0(0) = u_0(1) = 0$ and $\|u_0\|_{L^\infty(I)} < \pi$, determine $u = u(t,r)$ such that

$$\begin{aligned} \partial_t u &= \partial_{rr} u + \frac{1}{r}\partial_r u - \frac{\sin(2u)}{2r^2} \quad \text{for } r \in I, t \in (0,T], \\ u(0,r) &= u_0(r) \quad \text{for } r \in I, \\ u(t,0) &= u(t,1) = 0 \quad \text{for } t \in [0,T]. \end{aligned} \tag{1}$$

with the energy given by

$$\mathcal{E}(u) := \pi \int_0^1 \left((\partial_r u)^2 + \frac{\sin^2 u}{r^2} \right) r \mathrm{d}r. \tag{2}$$

(1) plays a fundamental role in the analysis of HMHF. In the seminal work [1], the authors prove the existence of finite time singularities for HMHF using (1). It has motivated further investigations of the blow-up behavior, e.g., the reverse bubbling phenomena [2] and the blow-up rate of solutions of (1) [3].

There are only very few papers in which numerical aspects of (1) are treated. The main contribution of this work is an error analysis for a finite element discretization of (1). We

restrict to the regime of smooth solutions of the continuous problem. We define the spaces

$$L^2_r := \left\{ v : [0,1] \to \mathbb{R} : \|v\|^2_{0,r} := (v,v)_{0,r} := \int_0^1 v(r)^2 r \mathrm{d}r < \infty \right\},$$
$$H^1_{r,0} := \left\{ v \in L^2_r : \|v\|_{H^1_r} := (\partial_r v, \partial_r v)_{0,r} + \left(\frac{v}{r}, \frac{v}{r}\right)_{0,r} < \infty, v(0) = v(1) = 0 \right\}.$$

We use grid points $r_i = ih, i = 0, \dots, N$, with $h = 1/N$ for some $N \in \mathbb{N}$ and a fixed time step τ, with $\tau J = T$ for some $J \in \mathbb{N}$. Let $S^k_{h,0}$ be the space of continuous and piecewise polynomial functions of degree k with homogeneous Dirichlet boundary condition. We propose the following discretization of (1): Given an initial value $u^0_h \in S^k_{h,0}$ that approximates u_0, for $j \geq 0$, determine $u^{j+1}_h \in S^k_{h,0}$ such that

$$\left(\frac{u^{j+1}_h - u^j_h}{\tau}, v_h\right)_{0,r} + \left(u^{j+1}_h, v_h\right)_{H^1_r} = \left(\frac{f(u^j_h)}{r^2}, v_h\right)_{0,r} \quad \text{for all } v_h \in S^k_{h,0}. \tag{3}$$

where $f(u) := u - \frac{1}{2}\sin(2u)$. We also define $F(u) := \frac{1}{2}(u^2 - \sin^2(u))$ with $f(u) = F'(u)$. Note the crucial identity $\mathcal{E}(u) = \frac{1}{2}\|u\| - \int_0^1 \frac{F(u(r))}{r}\mathrm{d}r$ and the convexity of $F(u)$ which are the main ingredients to show the following main results.

Theorem *For the solution $(u^j_h)_{1\leq j\leq J}$ of (3) the following holds:*

$$\mathcal{E}(u^{j+1}_h) \leq \mathcal{E}(u^j_h).$$

If $\mathcal{E}(u^0_h) \leq 2$, then $\|u^j_h\|_{L^\infty(I)} \leq \pi$ for all $0 \leq j \leq J$.

Theorem *Given $u_0 \in H^{k+1}(I)$ with $\mathcal{E}(u_0) \leq 2$, take $u^0_h \in S^k_{h,0}$ with $\mathcal{E}(u^0_h) \leq 2$. Assume $\|u_0 - u^0_h\|_{H^1_r} \leq ch^k$ and define the error $e^j_h := u^j_h - u(t_j)$, $1 \leq j \leq J$, for h and τ sufficiently small, we have*

$$\|e^j_h\|_{H^1_r} \leq C(\tau + h^k).$$

where the constant C is independent of h, τ but depend on T and on the regularity assumption of the exact solution u.

Acknowledgements The authors acknowledge funding by the Deutsche Forschungsgemeinschaft (DFG, German Research Foundation) – project number 442047500 – through the Collaborative Research Center "Sparsity and Singular Structures" (SFB 1481).

References

[1] Kung-Ching Chang, Wei Yue Ding, and Rugang Ye, Finite-time blow-up of the heat flow of harmonic maps from surfaces, *Journal of Differential Geometry*, **36**(2):507–515, 1992.

[2] Peter Topping, Reverse bubbling and nonuniqueness in the harmonic map flow, *International Mathematics Research Notices*, **2002**(10):505–520, 2002.

[3] Pierre Raphaël and Remi Schweyer, Stable blowup dynamics for the 1-corotational energy critical harmonic heat flow, *Communications on Pure and Applied Mathematics*, **66**(3):414–480, 2013.

Book of abstracts of the 9th International Conference on
Advanced Computational Methods in ENgineering and Applied Mathematics
September, 15–19, 2025.

Sixth-Order Compact Implicit Scheme for Time-Dependent Nonlinear Parabolic PDEs with Fisher-Kolmogorov and Reaction-Diffusion Applications

Niranjan[1], R. K. Mohanty[2] and Ankit Pandey[3]

[1,2,3] *Faculty of Mathematical Sciences, South Asian University, New Delhi*

e-mails: niranjanverma@students.sau.ac.in, rmohanty@sau.ac.in, pankit8386@gmail.com

Abstract

In this article, we present a novel three-level implicit numerical scheme, developed using the θ-method, which achieves $(2,6)$ order of accuracy for solving one-dimensional nonlinear parabolic equations. Using the Routh-Hurwitz stability criterion, we establish that the method is unconditionally stable for reaction-diffusion equations when $\theta > 1/4$. The scheme features a tridiagonal matrix structure, making it computationally efficient for advancing in time. We further extend the method to address fourth-order nonlinear parabolic equations. To facilitate practical implementation, a first-time-level approximation with $(2,6)$ accuracy is briefly described. Numerical experiments are conducted, and results are compared with those obtained using an available $(2,4)$ order method, confirming that the proposed approach achieves sixth-order spatial accuracy.

Key words: Sixth-order compact approximation, Nonlinear fourth-order parabolic PDEs, Nonlinear time-dependent reaction-diffusion equation, Unconditionally stable, Time-dependent Fisher-Kolmogorov equation, Fourth-order time-dependent reaction-diffusion equation.

1 Introduction

We consider the one-dimensional nonlinear parabolic partial differential equation of the form

$$u_{xx} = f(x,t,u,u_t), \quad 0 < x < a, \quad 0 < t < T, \tag{1}$$

subject to the initial condition

$$u(x,0) = g(x), \quad 0 \le x \le a, \tag{2}$$

and Dirichlet boundary conditions

$$u(0,t) = \phi_0(t), \quad u(a,t) = \phi_a(t), \quad 0 < t \le T. \tag{3}$$

2 Method and Stability Analysis

To solve equations (1)–(3) at each successive time level, the proposed method is given by

$$\frac{1}{h^2}\left(\bar{U}_{l+1}^j - 2\bar{U}_l^j + \bar{U}_{l-1}^j\right) = \frac{1}{60}\left(26\bar{F}_l^j + \bar{F}_{l+1}^j + \bar{F}_{l-1}^j + 16\left(\hat{F}_{l+\frac{1}{2}}^j + \hat{F}_{l-\frac{1}{2}}^j\right)\right) + \hat{T}_l^j. \tag{4}$$

The local truncation error (LTE) is given by

$$\hat{T}_l^j = O(k^2 + k^2h^2 + k^2h^4 + k^4h^2 + h^6).$$

Note that, for $k \propto h^3$, the LTE simplifies to $\hat{T}_l^j = O(h^6)$.

To analyze stability, we consider the reaction-diffusion equation (RDE):

$$\nu\frac{\partial^2 u}{\partial x^2} = \frac{\partial u}{\partial t} + \eta u + f(x,t), \quad 0 < x < 1,\ t > 0, \tag{5}$$

where $\nu > 0$ and $\eta \geq 0$ are constants, and $f(x,t)$ is a given forcing function. When $\eta > 0$, equation (5) represents a reaction-diffusion system; for $\eta = 0$, it reduces to a diffusion equation with a forcing term.

The scheme defined in equation (4) is unconditionally stable for all $\eta \geq 0$, $\nu > 0$, and for parameter values satisfying $\theta > 1/4$.

References

[1] R. S. Varga, *Matrix Iterative Analysis*, Springer, Berlin, 1999.

[2] R. K. Mohanty, S. McKee, and D. Kaur, *A class of two-level implicit unconditionally stable methods for a fourth order parabolic equation*, Appl. Math. Comput., 309 (2017), pp. 272–280.

[3] M. Heidari, M. Ghovatmand, M. N. Skandari, and D. Baleanu, *Numerical Solution of Reaction–Diffusion Equations with Convergence Analysis*, Nonlinear Math. Phys., 30 (2024), pp. 384–399.

Book of abstracts of the 9th International Conference on
Advanced Computational Methods in ENgineering and Applied Mathematics
September, 15–19, 2025.

Numerical Simulation of Flows at Open Channel Junctions with Various Confluence Angles

Nuray Öktem[1]

[1] *Department of Mathematics, Ankara Yıldırım Beyazıt University*

e-mails: nbozkaya@gmail.com

Abstract

This study presents a finite volume approach to numerically analyze the flow at open channel junctions. The flow is governed by the 2-Dimensional (2D) Shallow Water Equations (SWE). The numerical model uses a cell-centered Finite Volume Method (FVM) integrated with a Weighted Averaged Flux (WAF) method for the interface flux computations on unstructured triangular meshes. WAF is second order in its nature and improved by HLLC Riemann solver. For the time discretization the second order Runge-Kutta algorithm is employed. A detailed numerical assessment is performed to describe the effects of junction angle on the water depth and separation zone dimensions. Finally, it is represented that the distinctive 3-Dimensional (3D) characteristics of the flow at junctions are captured efficiently by the proposed 2D numerical model.

Key words: HLLC, junction flow, separation zone, unstructured mesh, WAF method
MSC 2020: 65M08, 76M12, 35L67, 76B07

1 Introduction

Developing mathematical models and appropriate numerical techniques is of growing interest to describe and explain flow structures in water confluences. But the majority of those studies are covered by experimental or field researches and still numerical models providing fast computations and reliable and practical output are lack.

The aim of the present work is to numerically simulate the junction flow and investigate the distinctive characteristics of confluent flow patterns. For the numerical solutions an efficient second order accurate FV algorithm developed by the author [1] is adopted to solve the 2D depth-integrated SWE [2] through channels with tributaries for varied confluence angles.

2 Mathematical Formulation and Results

The flood propagation through channels with lateral branch(s) may not satisfy the assumptions of shallow water flow theory (hyrostatic pressure and zero vertical acceleration), however SWE can still be used providing fast numerical solutions and useful output compensating marked flow features. The 2D time-dependent shallow water system can be derived [2] by integrating the Reynolds averaged Navier-Stokes equations over depth as follows,

$$\frac{\partial U}{\partial t} + \frac{\partial E(U)}{\partial x} + \frac{\partial G(U)}{\partial y} = S_b + S_f. \tag{1}$$

Here, the unknown is $U = (h, hu, hv)^T$ where h is the water depth, u and v are the velocity components. $E(U) = (hu, hu^2 + (gh^2)/2, huv)^T$ and $G(U) = (hv, huv, hv^2 + (gh^2)/2)^T$ are flux components and g is the gravity acceleration. $S_b = (0, -gh\partial z_b/\partial x, -gh\partial z_b/\partial y)^T$ is bed slope term with the bed elevation z_b. $S_f = (0, -ghS_{fx}, -ghS_{fy})^T$ is the bed friction term of which components are defined in terms of h, u, v and the Manning's roughness coefficient n.

Equation (1) is integrated spatially by the following finite volume discretization with rotational invariance property [2] where $\boldsymbol{T(\theta)}$ is the rotation matrix with rotation angle θ.

$$\frac{dU_i(t)}{dt} = -\frac{1}{A(\Omega_i)} \sum_{j=1}^{3} \boldsymbol{T(\theta)}_{ij}^{-1} E(\hat{U}_{ij}) \, |\Gamma_{ij}| + S_{bi} + S_{fi}. \tag{2}$$

Here, $A(\Omega_i)$ is the area of the triangle Ω_i with the boundary Γ_i where $|\Gamma_{ij}|$ denotes the length of j^{th} line element of i^{th} triangle. The rotation of U is $\hat{U} = (h, h\hat{u}, h\hat{v})^T$ with normal and tangential velocity components, $\hat{u} = un_x + vn_y$ and $\hat{v} = -un_y + vn_x$ where $\boldsymbol{n} = (n_x, n_y)$ is the outward normal vector along each line element of one control volume. Thus, it is cost-effective since only one component of the flux that is the rotated HLLC flux $E(\hat{U})$ will be computed. HLLC (Harten, Lax and van Leer , C refers contact waves) helps to describe the shock waves and give the opportunity to use flux limiters for interface flux computations.

Numerical computations are carried out for varied junction angles and the results are visualized by the Froude number (Fr) fields in addition to water depth profiles and velocity fields. The model is first validated for the simple right-angled junction [3]. A preliminary study of numerical calculations are presented in Figure 1 for the junction angle $\alpha = 90°$. The formation of the separation zone can be clearly observed at the downstream junction region.

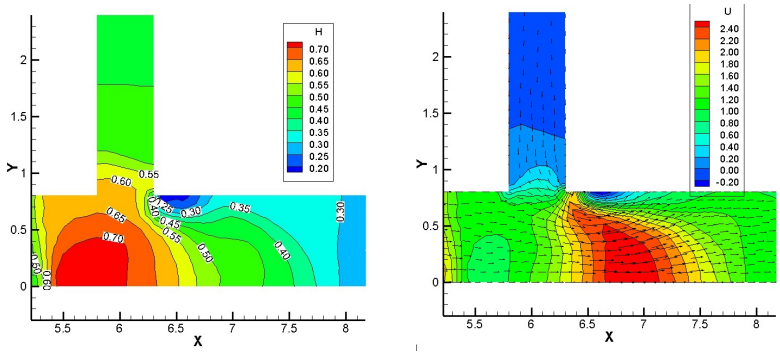

(a) Water depth profile, h.

(b) Velocity field and the component u.

Figure 1: Water depth and velocity field for $\alpha = 90°$.

References

[1] N. Öktem, *Computer Code Development for the Numerical Solution of Two Dimensional Shallow Flow Equations on Unstructured Grid*, Sakarya Uni. J. Sci. **22(2)** (2018) 364–382.

[2] E.F. Toro, *Shock-Capturing Methods for Free-Surface Shallow Flows*, John Wiley, 2001.

[3] L.J. Weber, E.D. Schumate and N. Mawer, *Experiments on Flow at a 90° Open-Channel Junction*, J. Hydraul. Eng. **127(5)** (2001) 340–350.

Book of abstracts of the 9th International Conference on
Advanced Computational Methods in ENgineering and Applied Mathematics
September, 15–19, 2025.

Stable field extrapolation for volumetric magnetizations

Juliette Leblond[1], Mubasharah Khalid Omer*[1] and Dmitry Ponomarev[1]

[1] *Inria, Center at Université Côte d'Azur*

e-mails: juliette.leblond@inria.fr, mubasharah.omer@inria.fr,
dmitry.ponomarev@inria.fr

Abstract

Scanning SQUID microscopes measure the vertical component of the magnetic field above a magnetized sample, but not its internal magnetization. Recovering the latter from noisy and limited field data requires solving an ill-posed inverse problem. To address this challenge, we develop a method for the simultaneous extrapolation and denoising of the measured data. The proposed approach is based on a stable regularization framework that exploits an explicit field–magnetization relation. While applicable to volumetric magnetization distributions, the method naturally extends to planar configurations.

Key words: Inverse magnetization problem, magnetic field extrapolation, paleomagnetism, regularization

1 Introduction

Deducing magnetization of geological samples holds significant importance in the field of paleomagnetism. However, recovering this quantity from measurements of a single magnetic field component, as in the SQUID microscope setup, constitutes an inherently ill-posed inverse problem [1].

Different methods of estimation of the magnetization distribution could be applied depending on sample-specific assumptions, such as unidirectionality, sparsity, or smoothness. However, across these techniques a significant challenge arises due to measurements' limited area and noise pollution. The consequent instability can be narrowed, for example, by extending the measured data through extrapolation techniques, as motivated in [2].

2 Methodology

We model the vertical magnetic field component B_3 in the upper half-space $\mathbb{H} := \{\vec{x} = (\mathbf{x}, x_3)^T \in \mathbb{R}^3 : x_3 > 0\}$, generated by a magnetization distribution $\vec{M} \in (L^2(S))^3$ with $S \subset \mathbb{R}^3 \setminus \mathbb{H}$, s.t. $\mathrm{supp}(\vec{M}) \subset S$ is compact. Using Maxwell's equations in the quasi-static regime, we express B_3 via the Poisson kernel $p_{\mathbb{H}}$ of the upper half-space and Riesz transforms, reducing the 3–D convolution problem to a 2–D framework, i.e. for $\vec{x} \in \mathbb{H}$, we derive the explicit formula:

$$B_3(\mathbf{x}, x_3) = -\frac{\mu_0}{2}\Big(\partial_{x_3} p_{\mathbb{H}}(\cdot, x_3) * f_M(\cdot)\Big)(\mathbf{x}), \tag{1}$$

where f_M is a scalar magnetization-dependent function.

Motivated by (1), we introduce the operator $\mathcal{B} : L^2(\mathbb{R}^2) \to L^2(Q)$, where $Q \subset \mathbb{R}^2$ denotes the measurement region. To proceed with the extrapolation procedure, we first formulate and solve a constrained least squares problem to approximate f_M, thereby solving the simplified inverse problem without reconstructing the full magnetization. Then, applying $\mathcal{B}$ to this reconstruction we obtain the extrapolated magnetic field B_3^{ext} over a larger domain U s.t. $Q \subset U \subset \mathbb{R}^2$. Formally, for given data $B_3^{meas} \in L^2(Q)$ and a constraint $C > 0$, we consider the following problem:

$$\min_{f \in L^2(\mathbb{R}^2)} \|B_3^{meas} - \mathcal{B}f\|_{L^2(Q)} \text{ subject to } \|f\|_{L^2(\mathbb{R}^2)} \leq C.$$

This problem admits a unique minimizer $f^\lambda \in L^2(\mathbb{R}^2)$ which satisfies:

$$\mathcal{B}^*\mathcal{B}f^\lambda + \lambda f^\lambda = \mathcal{B}^* B_3^{meas} \text{ in } \mathbb{R}^2, \tag{2}$$

where $\mathcal{B}^*$ is the adjoint operator of $\mathcal{B}$ and $\lambda > 0$ is s.t. $\|f^\lambda\|_{L^2(\mathbb{R}^2)} = C$.

We numerically implement the solution of (2) using a projection method. In this effort, we derive a basis on $\mathbb{R}^2$ from the spherical harmonics via the Kelvin transform. Furthermore, we exploit the structure of the Kelvin transform to relate the Poisson kernels of the upper half-space and the unit ball, enabling a reformulation of the forward operator that avoids nested convolutions.

3 Results

In Fig. 1, we illustrate the quality of extrapolating synthetically generated measured data B_3^{meas} on $Q = [-1, 1]^2$ to a larger region $U = [-10, 10]^2$, yielding the extrapolated field B_3^{ext}.

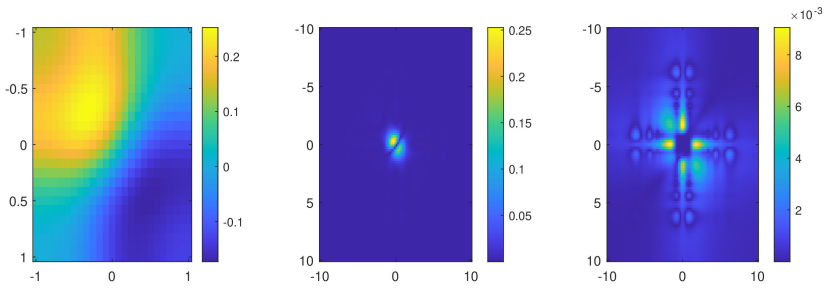

Figure 1: Measured data B_3^{meas} on Q (left), extrapolated field B_3^{ext} on U (center), and pointwise error on U between the true magnetic field B_3^{true} s.t. $B_3^{true}|_Q \simeq B_3^{meas}$ and B_3^{ext} (right).

References

[1] L. Baratchart, P. Bourdon, E. Lima, E. Saff, B. Weiss, *Characterizing kernels of operators related to thin-plate magnetizations via generalizations of Hodge decompositions*, IOP Publishing, Inverse Problems v29 (2012).

[2] D. Ponomarev, *A Method to Extrapolate the Data for the Inverse Magnetisation Problem with a Planar Sample*, IPMS Conf. 2024 (to appear), arXiv:2411.09331 (2024).

[3] S. Axler, P. Bourdon, W. Ramey, *Harmonic Function Theory*, Springer New York (2001).

Book of abstracts of the 9th International Conference on
Advanced Computational Methods in ENgineering and Applied Mathematics
September, 15–19, 2025.

A novel non-polynomial spline method and its convergence theory for nonlinear two-point derivative-dependent boundary value problems

Ankit Pandey[1] **and R.K. Mohanty**[1]

[1] *Faculty of Mathematical Sciences, South Asian University, New Delhi*

e-mails: pankit8386@students.sau.ac.in, rmohanty@sau.ac.in

Abstract

This paper introduces an innovative method for approximating generalized non-linear differential equations with derivative-dependent boundary conditions, employing three function evaluations per step with half-step discretization. The approach utilizes hyperbolic trigonometric functions to approximate the non-linear differential equation at three points and the boundary conditions at two points, leading to a compact finite difference scheme that forms a tridiagonal system. To demonstrate its effectiveness, the non-polynomial spline method is applied to various physical and engineering models, including heat source diffusion in the human head, the equilibrium of isothermal gas, and the Emden-Fowler equation. The obtained results are compared with existing solutions to confirm the accuracy and efficiency of the proposed method.

Key words: Convergence theory, Two-point boundary value problems, Singular boundary value problems,Spline-in-tension, Robin boundary value problems,

1 Introduction

This paper aims to investigate a numerical method for solving second-order boundary value problems (BVPs) that involve derivative-dependent boundary conditions. Such BVPs are typically represented as follows:

$$v_{xx} = \xi\left(x, y, y_x\right), \quad 0 < x < 1. \tag{1}$$

The derivative-dependent boundary conditions are described by:

$$\begin{aligned} v_x(0) &= 0, \\ \beta_1 v(1) + \beta_2 v_x(1) &= k_1, \end{aligned} \tag{2}$$

or

$$\begin{aligned} v_x(0) &= 0, \\ \beta_1 v(1) - \beta_2 v_x(1) &= k_1, \end{aligned} \tag{3}$$

Where β_0 and β_1 are greater than equal to zero; $\beta_1 + \beta_2 > 0; k_1$ are constants. The nonlinear ODEs (1), along with DDBVPs (2) or (3), are named as nonlinear derivative-dependent boundary value problems (NDDBVPs).

2 Methodology and Convergence

The fourth-order non-polynomial spline method for interior grids is derived as:

$$\frac{V_{i+1} - 2V_i + V_{i-1}}{h^2} = a\widehat{\xi}_{i+1/2} + (\rho_1 + \rho_2)\,\widehat{\xi}_i + c\widehat{\xi}_{i-1/2} + \widehat{T}_j. \tag{4}$$

where,

$$a = \frac{1}{2\theta^2}\left[\cosh\theta - \frac{\theta}{\sinh\theta}\right], \rho_1 = \frac{1}{\theta^2}[\theta\coth\theta - 1], \rho_2 = \frac{1}{\theta^2}[\theta\coth\theta - 1],$$
$$c = \frac{1}{2\theta^2}\left[\cosh\theta - \frac{\theta}{\sinh\theta}\right].$$

A convergence analysis uses a tridiagonal matrix analysis approach with the assistance of the paper [2] to prove that the proposed method achieves fourth-order accuracy at interior and boundary grid points.

$$\|E\| \leq O\left(h^4\right).$$

References

[1] H.B. Keller, *Numerical methods for two-point boundary-value problems*, Courier Dover Publications, 2018.

[2] R.S. Varga, *Matrix Iterative Analysis*, Springer, Berlin 1999.

[3] N. Sriwastav, A.K. Barnwal, H. Ramos, R.P. Agarwal, M. Singh, *Advanced numerical scheme and its convergence analysis for a class of two-point singular boundary value problems*, Math. and Comp. in Simul. **216** (2024) 30-48.

Book of abstracts of the 9th International Conference on
Advanced Computational Methods in ENgineering and Applied Mathematics
September, 15–19, 2025.

Addressing Solution Challenges in Bilevel Optimization through Set-Based Approaches

Daishi Kuroiwa[1], Narin Petrot[2] and Kazuki Seto[3]

[1] *Department of Mathematical Sciences, Shimane University*

[2] *Department of Mathematics, Naresuan University*

[2] *Education and Research Center of Mathematical and Data Science, Shimane University*

e-mails: kuroiwa@riko.shimane-u.ac.jp, narinp@nu.ac.th,
setok@riko.shimane-u.ac.jp

Abstract

Bilevel optimization models arise naturally in many real-world applications where decisions are made at two hierarchical levels, such as in engineering design, economics, and resource allocation. However, solving these problems is particularly challenging when the lower-level decision response is not unique, leading to ambiguity in the overall solution. This study introduces new concepts of optimistic and robust solutions, interpreted within a set optimization framework, to better capture such complexities. We highlight critical issues in ensuring the existence of robust solutions, especially when the lower-level problem is linear with box constraints, conditions often encountered in practice. To overcome these difficulties, we propose an approximate solution framework that guarantees existence and provides practical tools for decision-making when traditional solutions fail. This approach offers fresh insights and methodologies for tackling bilevel problems in uncertain or degenerate settings commonly found in applied contexts.

Key words: Vector-valued bilevel optimization, set optimization, optimistic bilevel solution, robust bilevel solution, robust bilevel approximate solution
MSC 2020: 90C70, 90C17, 49J53

1 Introduction

Bilevel optimization problems, originally studied in the work of von Stackelberg [1], represent a class of hierarchical models where two decision-makers interact sequentially. The upper-level (leader) makes a decision first, followed by the lower-level (follower), who optimizes their objective in response. Such problems are pervasive across domains like economics, transportation systems, and machine learning due to their natural modeling of hierarchical decision processes.

The standard bilevel formulation can be represented as follows:

$$\begin{array}{lll} \text{(UP)} & \text{Minimize} & F(x,y) \\ & \text{subject to} & x \in S_U \\ \text{(LP)} & \text{Minimize} & f(x,y) \\ & \text{subject to} & y \in S_L(x) \end{array}$$

Here, X and Y denote non-empty sets; the spaces $(Z_U, \preceq_U)$ and $(Z_L, \preceq_L)$ are partially ordered topological vector spaces; $F : X \times Y \to Z_U$ and $f : X \times Y \to Z_L$ are vector-valued objective functions; $S_U \subset X$ is the feasible region for the leader; and $S_L : X \rightrightarrows 2^Y$ is a set-valued mapping defining the follower's feasible set for each x. The ordering cones $K_U := \{p \in Z_U \mid 0 \preceq_U p\}$ and $K_L := \{p \in Z_L \mid 0 \preceq_L p\}$ are assumed to be pointed, closed, convex, and with non-empty interior. The strict partial orders $\prec_U$ and $\prec_L$ are defined by $p \prec_U p'$ if $p' - p \in \operatorname{int} K_U$, and similarly for $\prec_L$.

The lower-level solution set corresponding to a leader's decision $x \in S_U$ is given by

$$\mathrm{Sol}_{(\mathrm{LP})}(x) := w\text{-}\operatorname{argmin}\{f(x, y) \mid y \in S_L(x)\},$$

meaning that a point $y \in S_L(x)$ belongs to $\mathrm{Sol}_{(\mathrm{LP})}(x)$ if there exists no $y' \in S_L(x)$ such that $f(x, y') \prec_L f(x, y)$.

This study focuses on the fundamental challenge in bilevel optimization when the lower-level problem admits multiple optimal solutions, resulting in a set-valued solution mapping $\mathrm{Sol}_{(\mathrm{LP})}(\mathrm{x})$. Such ambiguity complicates both the theoretical analysis and practical resolution of bilevel problems. Within the framework of set optimization, we examine this issue by formalizing optimistic (l-type) and robust (u-type) solutions and establishing their existence under suitable conditions. Notably, we identify cases, such as linear lower-level problems with box constraints, where the solution mapping fails to be upper semicontinuous or becomes trivial, thus precluding robust solutions. To address this, we propose an approximate robust solution concept, for which we prove an existence theorem. This provides a flexible and well-posed alternative when exact robustness is not achievable, offering new theoretical insights and directions for developing algorithms and solution frameworks in more complex or uncertain bilevel settings.

Acknowledgements This work has been partially supported by National Research Council of Thailand (NRCT) and Naresuan University (Grant No. N42A660517).

References

[1] H. von Stackelberg *Marktform und Gleichgewicht. Die Handelsblatt-Bibliothek "Klassiker der Nationalökonomie*, J. Springer. (1934).

[2] D. Kuroiwa, N. Petrot, K. Seto, *Solution Concepts for Bilevel Optimization Problems via Frameworks of Set Optimization.*, (Submitted).

Book of abstracts of the 9th International Conference on
Advanced Computational Methods in ENgineering and Applied Mathematics
September, 15–19, 2025.

A Prüfer angle based shooting method for Sturm-Liouville problems with non-separated boundary conditions

Simon Reyntjens[1] **and Marnix Van Daele**[1]

[1] *Department of Mathematics, Computer Science and Statistics, Ghent University*

e-mails: Simon.Reyntjens@ugent.be, Marnix.Vandaele@ugent.be

Abstract

This talk will be devoted to the numerical solution of the Sturm-Liouville equation

$$(py')'(x) + (qy)(x) = \lambda(ry)(x), \quad x \in (0, \pi),$$

where p and r are positive functions and $\frac{1}{p}, q, r \in L_1(0, \pi)$.

For the case of separated boundary conditions

$$a_1 y(0) + a_2(py')(0) = 0 = b_1 y(\pi) + b_2(py')(\pi)$$

it is well-known that the eigenvalues are simple and can be ordered as an increasing sequence $\lambda_0 < \lambda_1 < \lambda_2 < \dots$ that tends to infinity. These eigenvalues can be computed numerically via a shooting procedure. However, as the index of the eigenvalue λ_i equals the number of zeroes of the associated eigenfunction y_i, such an eigenfunction becomes highly oscillatory as i increases. This in turn makes it very difficult, when an eigenvalue and corresponding eigenfunction have been found, to determine its index via the counting of the zeroes of the eigenfunction. This problem can however be avoided via Prüfer's transformation, a polar coordinate transformation in the phase plane which replaces the problem of counting zeroes by that of counting multiplies of π, a much easier task. This procedure has been used in the matlab packages Matslise [1] and Matslise 2.0 [2] and its C++ successor Matslise 3.0 [3].

In this paper we discuss an algorithm that extends the applicability of the Prüfer angle approach to the case of non-separated boundary conditions

$$[y(0) \quad y'(0)]^T = \mathbf{K}[y(\pi) \quad y'(\pi)]^T,$$

where $\mathbf{K}$ is a real 2×2 matrix with determinant 1. In particular, for $\mathbf{K} = \mathbf{I}$ periodic conditions are imposed, for $\mathbf{K} = -\mathbf{I}$ the anti-periodic case is obtained. Eigenvalues will no longer need to be simple in the case of non-separated boundary conditions. The algorithm we propose is a slightly adapted version of the one proposed in [4] and is based on a theory developed in [5] and [6].

References

[1] V. Ledoux, M. Van Daele, G. Vanden Berghe, *MATSLISE: A MATLAB package for the numerical solution of Sturm-Liouville and Schrödinger equations*,
ACM Trans. Math. Softw. **31** (4) (2005)
doi:10.1145/1114268.1114273.

[2] V. Ledoux, M. Van Daele, *Matslise 2.0: A Matlab Toolbox for Sturm-Liouville Computations*,
ACM Trans. Math. Softw. **42** (4) (2016), Article 29.

[3] T. Baeyens, M. Van Daele, *The fast and accurate computation of eigenvalues and eigenfunctions of time-independent one-dimensional Schrödinger equations*,
Comput. Phys. Comm. **258** (2021) 107568,
doi:10.1016/j.cpc.2020.107568.

[4] T. Baeyens, *Algorithms for time-indepenent Schrödinger equations*
Ghent University, Faculty of Sciences (2023),
ISBN: 9789082922264.

[5] P. Binding, H. Volkmer, *A Prüfer Angle Approach to the Periodic Sturm-Liouville Problem*,
The American Mathematical Monthly **119** (2012), 477-484
doi:10.4169/amer.math.monthly.119.06.477.

[6] P. Binding, H. Volkmer, *A Prüfer angle approach to semidefinite Sturm-Liouville problems with coupling boundary conditions*,
Journal of Differential Equations **255** (2013) 761-778,
doi: 10.1016/j.jde.2013.04.033.

Book of abstracts of the 9th International Conference on
Advanced Computational Methods in ENgineering and Applied Mathematics
September, 15–19, 2025.

Oil Propagation in a Substation Hydraulic System

Varvara Roubtsova[1], Mathieu Emond-Castonguay[2], Jean-Bernard Dastous1 [1] and Nathalie Thibeault[2]

[1] *Institut de recherche (CRHQ), Hydro-Québec*

[2] *Direction Expertise ingénierie et standardisation, Hydro-Québec*

e-mails: roubtsova.varvara@hydroquebec.com,
emond-castonguay.mathieu@hydroquebec.com,
dastous.jean-bernard@hydroquebec.com, thibeault.nathalie@hydroquebec.com

Abstract

This paper describes a methodology for assessing oil distribution in collection pits and in the conduit network connecting these pits to an oil-water separator, a substation hydraulic system designed to protect the environment from oil spills or leaks. The methodology is part of a comprehensive program for substation maintenance analysis developed by Hydro-Québec. The developed model is based on analytical solutions for viscous gravity flows and includes the flow on rigid horizontal and inclined planes as well as in and over porous media.

Key words: viscous gravity flows, oil collection pit, substation hydraulic system

1 Introduction

Oil leaks of varying intensity may occur when electrical equipment components are damaged. The leaking oil then flows into a collection pit, a reservoir of complex geometry with inclined surfaces and internal channels. Most pit channels are filled with gravel but some may have a perforated pipe to facilitate drainage to the outlet. In addition, pits can be connected to each other. At the lowest point of the pit bottom there is an outlet connected to a piping system that leads to the separator. Although collection pits are designed to recover all the oil contained in an electrical equipment component, some pits or trench drains do not have sufficient capacity and an overflow check must be performed. The separator must have the capacity to separate oil and water at a given discharge while minimizing oil leaks into the environment. The model described in this paper was developed to test existing substations with respect to these parameters and to provide guidance for the design of new substation oil collection pits. Since experimentation using real substations is complex, the proposed methodology was verified by checking the fundamental law of mass conservation.

2 Basic concept

The rate of oil volume flowing from the damaged component to the collection pit can be calculated with Torricelli's formula based on the geometric characteristics of the component.

Once in the pit, the oil is divided through the channels to the outlet under the influence of gravity. The propagation of oil in channels without gravel is a two-dimensional viscous gravity flow on a rigid inclined plane and the corresponding solution is given in [1]. The pit outlet can have different configurations, but the hydraulic flow in all cases can be described as a flow through a weir or an opening and a general formula can be used [3]. Combining all these solutions for a given geometry of a substation hydraulic system provides the complete oil flow process over time. The analytical solutions used in the cited references were validated by experiments, justifying their use in our methodology without additional tests.

3 Results

Fig. 1-4. shows an example of a calculation scenario with a hole in the bottom of a transformer leaking oil into a trench drain. This example demonstrates the ability to predict overflow timing and volume of spillage to optimize the work of the environmental intervention team. During the first few seconds, oil spreads through the channels (Fig.1). The oil level in the pit increases as the front advances, but the growth accelerates when the front reaches the pit outlet (Fig. 2) since the incoming flow is greater than the outgoing flow. After seven minutes, the oil completely fills the channels and begins to overflow the walls. Fig. 3. shows the volume balance. Fig. 4 shows inflow and outflow dynamics over time.

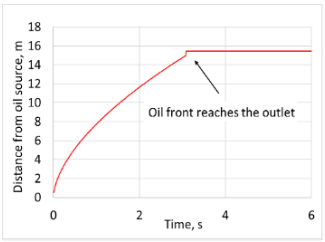

Figure 1. Spread of oil front in channels

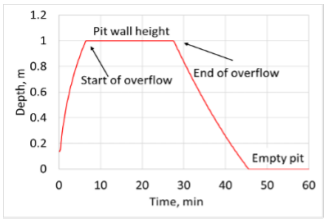

Figure 2. Oil height variation in channels

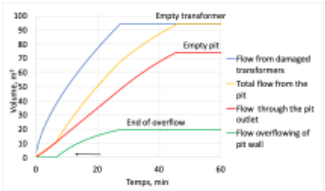

Figure 3. Volume balance

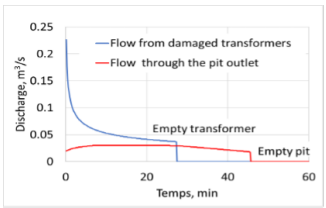

Figure 4. Incoming and outcoming discharges

References

[1] J. R. Lister, *Viscous flows down an inclined plane from point and line sources*, J. Fluid Mech. **242** (1992) 631–653.

[2] H. E. Huppert, A. W. Woods, *Gravity-driven flows in porous layers*, J. Fluid Mech. **292** (1995) 55–69.

[3] R. E. Horton, *Weir Experiments, Coefficients, and Formula*, Washington, 1907. Cited in: G. B. Ermentrout, D. H. Terman, *Mathematical Foundations of Neuroscience*, Springer, 2010.

Book of abstracts of the 9th International Conference on
Advanced Computational Methods in ENgineering and Applied Mathematics
September, 15–19, 2025.

Numerical Techniques for Distributed-Order Fractional Differential Equations Based on Spectral Methods

Zeynab Saki [1] **and Payam Mokhtary**[2]

[1] *Department of Basic Sciences, Sahand University of Technology*

e-mails: zeynabsakiii98@gmail.com, mokhtary.payam@gmail.com, mokhtary@sut.ac.ir

Abstract

I will present spectral methods for solving distributed-order fractional differential equations (DOFDEs), which are powerful tools for modeling complex systems with long-term memory and heterogeneous dynamics. I will start by outlining the motivation for using distributed-order (DO) models. Then, I will introduce the spectral approach, which uses global orthogonal basis functions to convert the problem into a numerical framework. I will show numerical results that confirm the high accuracy and efficiency of the method. This work aims to provide an effective and reliable tool for solving distributed-order fractional differential equations.

Key words: Distributed order, Fractional differential equations, Numerical solution, Spectral methods

1 Introduction

Fractional differential equations (FDEs) has emerged as a vital tool in various scientific and engineering disciplines over the past few decades due to its practical applications such aseconomics, biology, chemistry, and other sciences [1]. FDEs historically centered on constant-order operators. Yet, their fixed order proved insufficient for precisely modeling complex phenomena with evolving physics or multiple interacting orders. This limitation recently prompted the development of DO fractional calculus operators. DO derivatives are defined by integrating fractional derivatives over a specified range of differentiation orders. Consequently, distributed-order fractional differential equations (DOFDEs) naturally generalize both single-order and multi-term FDEs. These equations find application in various fields, including DO oscillators [2] and control systems [3]. Spectral methods, utilizing orthogonal functions, are highly regarded for solving dynamical systems. They offer significant accuracy and exponential convergence for smooth problems. Their main advantage lies in simplifying complex differential equations by transforming them into algebraic systems.

2 Problem Formulation

A general DOFDE is defined in the form:

$$\begin{cases} \int_{\mu_1}^{\mu_2} \varphi(\mu) {}_a^C D_x^\mu u(x) d\mu = f(x), \quad x \in \Omega = [a,b] \\ u^{(k)}(0) = c_k, \quad k = 0, 1, \ldots, \lceil \mu \rceil - 1, \end{cases} \tag{1}$$

where $\mu_1, \mu_1 \in \mathbb{R}^+$; ${}_a^C D_x^\mu$ is the Caputo type fractional derivative of order μ; $\lceil . \rceil$ denotes the ceiling function; $f(x) \in L^1[0,1]$; $u(x)$ is such that ${}_a^C D_x^\mu u(x) < M \; \forall t \in [0,\infty) \cap \forall \mu \in [\mu_1, \mu_2]$; $\varphi(\mu)$ is an absolutely integrable function on the interval $\mu \in [\mu_1, \mu_2]$ and satisfies $\int_{\mu_1}^{\mu_2} \varpi(\mu) s^\mu d\mu \neq 0$ for $\mathrm{Re}(s) > 0$. This

DO system has a unique solution given in [4]. Numerically approximating DO derivatives generally involves a two-step process. (i): Approximating the DO with Newton-Cotes or Gauss quadrature to convert DOFDEs into multi-term FDEs. (ii): Utilize an existing method to determine the solution to the multi-term FDEs. In step (ii) to solve (1) we apply a spectral method by approximating the solution $u(x)$ with a finite series

$$u_N(x) = \sum_{k=0}^{N} a_k \, \phi_k(x),$$

where $\{\phi_k\}$ are global basis functions chosen to satisfy the boundary conditions. The residual function is defined as

$$R_N(x) = \sum_{i=0}^{m} w_i \varphi(\mu_i) {}_a^C D_x^{\mu_i} u(x) \, d\mu - f(x),$$

which μ_i and w_i are the nodes and weights of the quadrature rules and $m \in \mathbb{N}$. To determine the unknown coefficients a_k, the residual is enforced to be orthogonal to a set of test functions $\{\psi_i\}$, leading to the condition

$$(R_N, \psi_i) = \int_\Omega R_N(x) \, \psi_i(x) \, dx = 0, \quad 0 \le i \le N.$$

This results in a system of $N + 1$ algebraic equations for the $N + 1$ unknowns $\{a_k\}$, which can be efficiently solved.

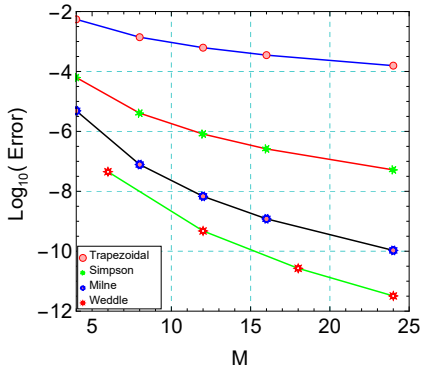

Figure 1: Semi-logarithmic plot of numerical errors in solving DOFDEs using spectral methods.

References

[1] R. Magin, *Fractional calculus in bioengineering, part 1*, Critical Reviews™ in Biomedical Engineering. **32** (2004).

[2] T. M. Atanackovic, M. Budincevic, *On a fractional distributed-order oscillator*, J. Phys. A: Math. Gen. **38** (2005) 6703.

[3] F. Zhou, Y. Zhao, *Design, implementation and application of distributed order PI control*, ISA Trans. **52** (2013) 429–437.

[4] W. Ding, S. Patnaik, S. Sidhardh, F. Semperlotti, *Applications of distributed-order fractional operators: A review*, Entropy **23** (2021) 110.

Book of abstracts of the 9th International Conference on
Advanced Computational Methods in ENgineering and Applied Mathematics
September, 15–19, 2025.

First-principles modeling of Li-ion cell dynamics and degradation in hybrid electric vehicles

Pavel Strachota[1], Michal Beneš[1] and Radek Fučík[1]

[1] *Department of Mathematics, Faculty of Nuclear Sciences and Physical Engineering, Czech Technical University in Prague*

e-mails: pavel.strachota@fjfi.cvut.cz, michal.benes@fjfi.cvut.cz, radek.fucik@fjfi.cvut.cz

Abstract

We propose a mathematical model and an efficient numerical solver for simulating the dynamic loading patterns and Li-ion cell degradation in battery packs of hybrid electric vehicles. We demonstrate the short-term and long-term battery behavior.

Key words: battery aging, first principles model, hybrid electric vehicles, Li-ion cell, numerical simulation
MSC 2020: 37M05, 80A19, 80A30, 78A57

1 Introduction

All Li-ion batteries undergo gradual degradation (aging) due to unwanted chemical and physical processes, mostly during charging. In hybrid electric vehicles (HEV's), the battery packs are rather small and thus special cells with a high power-to-energy (P/E) ratio have to be used. We developed a multiscale mathematical model of Li-ion battery pack dynamics based on first principles and implemented an efficient numerical solver for it. We demonstrate its use cases and results obtained specifically for high P/E ratio cells.

2 The ACOMEN2025 contribution

In [1], we proposed a novel and efficient numerical approach for solving the pseudo two-dimensional multiscale model of the Li-ion cell dynamics, describing the ion diffusion through the electrolyte and the porous electrodes, electric potential distribution, and Butler-Volmer kinetics. We start by a short summary of this model. Afterward, we explain its extension allowing to model the battery degradation phenomena by parasitic reactions and the formation of solid-electrolyte interface (SEI). Dependence of the parasitic reaction rate on temperature and heat transfer modeling will also be discussed.

Prediction of battery degradation requiring the simulation of a large number of charge-discharge cycles will be demonstrated (Fig. 1(a)). Next, simulations of the cell response to dynamic loading patterns will be shown. To this end, both constant-current and constant-voltage charging methods have been implemented. Parallel cell connections in a battery pack will be explained. Finally, simulations of realistic loading patterns during HEV operation

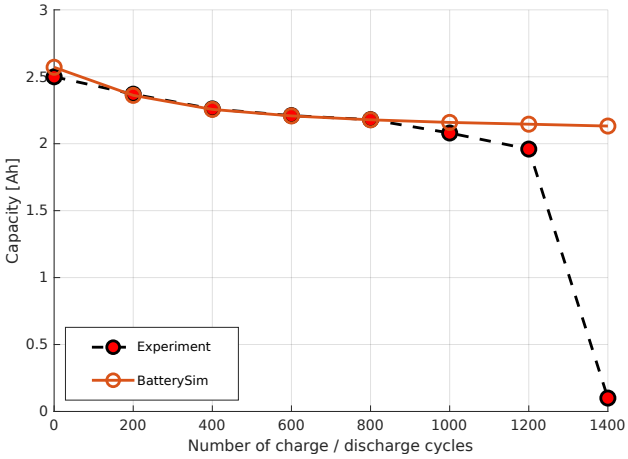

(a) Capacity degradation in the A123 Systems ANR26650 M1-B high P/E ratio cell: experiment vs. simulation.

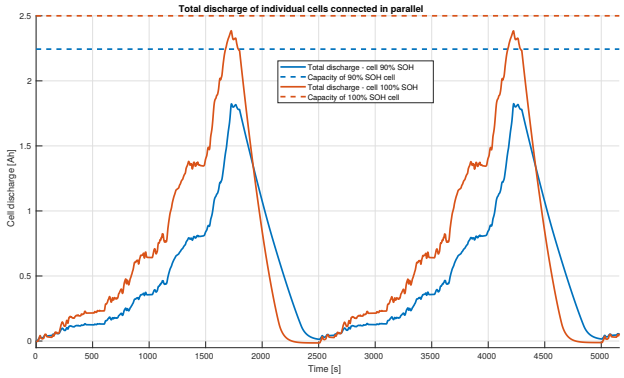

(b) Battery discharge distribution in a battery pack of two batteries with SOH=100% and SOH=90% subject to a real loading profile during HEV operation.

Figure 1: Simulations of long-term and short-term HEV-class Li-ion cell behavior performed by our BatterySim software.

will be presented. Battery packs containing cells with different states of health (SoH) will be considered (Fig. 1(b)).

Acknowledgements This work has been supported by the project No. TA04021244 of the Technology Agency of the Czech Republic: *Dynamic Lithium-Ion Battery Management for Hybrid Electric Vehicles.*

References

[1] M. Beneš, R. Fučík, V. Havlena, V. Klement, M. Kolář, O. Polívka, J. Solovský, P. Strachota, *An Efficient and Robust Numerical Solution of the Full-Order Multiscale Model of Lithium-Ion Battery*, Math. Probl. Eng. **vol. 2018** (2018) Article ID 3530975, 1–12.

Book of abstracts of the 9th International Conference on
Advanced Computational Methods in ENgineering and Applied Mathematics
September, 15–19, 2025.

Threshold-Driven Collapse and Recovery in a Simplified Wasp-Waist Ecosystem Model

Sam Subbey[1], Kamil V. Hlubek[2] and Anna S. Frank[3]

[1] *Institute of Marine Research, Bergen, Norway*

[2] *Department of Mathematics, Technical University of Munich, Germany*

[1] *The Norwegian Directorate of Fisheries, Bergen, Norway*

e-mails: samuels@imr.no, kamil.hlubek@tum.de, asfrank88@gmail.com

Abstract

We present a mechanistic model capturing collapse and recovery in a tri-trophic food web with producers (z), primary consumers (x), and apex predators (y). Using nonlinear ODEs with ratio-dependent responses, we examine dynamics starting from a producer-only state. The key control parameter is the initial predator-prey biomass ratio $R_0 = y(0)/x(0)$. We identify three distinct regimes—collapse, escape, and a sensitive "race condition"—governed by threshold values. These offer insight into resilience and suggest early-warning indicators for complex simulations.

Key words: collapse dynamics, marine ecosystems, multistability, predator-prey models, threshold effects
MSC 2020: 34C23, 92D25, 37N25, 92B05

1 Introduction

Wasp-waist ecosystems are structured around a few mid-trophic species linking producers and predators. Their collapse can trigger major trophic cascades, with resilience often tied to initial conditions.

We study a tri-trophic model to explore how introducing consumers to a producer-only state affects system dynamics, focusing on the role of the initial biomass ratio $R_0 = y(0)/x(0)$.

2 Model and Methodology

The system is:

$$\begin{aligned}
\frac{dz}{d\tau} &= z(1-z) - c_1\frac{xz}{x+z} - d_1 z^{\delta_1},\\
\frac{dx}{d\tau} &= b_{11}\frac{zx}{x+z} - c_2\frac{yx}{y+x} - d_2 x^{\delta_2},\\
\frac{dy}{d\tau} &= b_{21}\frac{xy}{y+x} - d_3 y^{\delta_3}.
\end{aligned}$$

We assume $\delta_1 = 0$, $\delta_2 = \delta_3 = 1$, and all rate constants positive. The system exhibits multistability and strong dependence on initial conditions.

We analyze the system's behavior near the producer-only equilibrium, treating $R_0 = y(0)/x(0)$ as a bifurcation-like parameter and identifying thresholds $R_{\text{crit},x}$ and $R_{\text{crit},R}$ governing system fate.

3 Analytical Results

Quasi-stationary Producers: When x, y are small, $z(\tau) \approx z_{\text{eq}}$, allowing a reduced analysis on (x, y).
Growth Thresholds: Two key functions determine consumer dynamics:

- $S_x^0(R) = (b_{11} - d_2) - c_2 \frac{R}{1+R}$: growth rate of x.
- $G(R) = \left(\frac{b_{21}}{1+R} - d_3\right) - S_x^0(R)$: rate of change of $R(\tau)$.

These define critical values $R_{\text{crit},x}$ and $R_{\text{crit},R}$, with $R_{\text{crit},x} < R_{\text{crit},R}$.
Three Regimes:

1. *Collapse* ($R_0 \geq R_{\text{crit},R}$): x declines, followed by y, returning to producer-only state.
2. *Escape* ($R_0 \leq R_{\text{crit},x}$): x grows, leading to coexistence.
3. *Race Condition* ($R_{\text{crit},x} < R_0 < R_{\text{crit},R}$): initial decline of x, but R may drop below $R_{\text{crit},x}$ fast enough to recover.

These regimes are derived via differential inequalities and validated with asymptotic and Grönwall-type arguments.

4 Ecological and Computational Implications

Our framework provides:

- Early-warning indicators via R_0 thresholds.
- A tractable reduced model for embedding into simulations or data analysis.
- A formal concept of *race condition*, emphasizing transient resilience.

Acknowledgements K.V.H. contributed via ERASMUS+ internship.

References

[1] A. Bakun, *Wasp-waist populations...*, Prog. Oceanogr., **68**(2–4), 2006.

[2] N. G. Hairston Jr. and Sr., *Cause-effect...*, Am. Nat., **142**(3), 1993.

[3] C. Boettiger et al., *Early warning signals...*, Theor. Ecol., **6**, 2013.

[4] M. A. Litzow and M. E. Hunsicker, *Early warning signals...*, Ecosphere, **7**(12), 2016.

[5] A. Frank et al., *Multistability and Bifurcation...*, in review, 2025.

Book of abstracts of the 9th International Conference on
Advanced Computational Methods in ENgineering and Applied Mathematics
September, 15–19, 2025.

Arrow-Hurwicz scheme for steady two-dimensional Grade-Two Fluid Equations

Aziz Takhirov[1], Basma Jaffal-Mourtada[2] and Driss Yakoubi[2]

[1] *Department of Mathematics, University of Sharjah, UAE*

[2] *Research Center, Léonard de Vinci Pôle Universitaire, 92 916 Paris La Défense, France*

e-mails: atakhirov@sharjah.ac.ae, basma.jaffal@devinci.fr, driss.yakoubi@devinci.fr

Abstract

This work develops an efficient Arrow-Hurwicz based finite-element scheme for solving steady second-grade flow equations in 2D, where the system is split into separate equations for each flow variable. Uniform boundedness and convergence results are established. Numerical tests show a significant convergence speed-up to a steady-state.

Key words: Arrow-Hurwicz, non-Newtonian incompressible fluids, second-grade fluid

1 Introduction

We consider approximating steady, incompressible grade-two fluids in a bounded domain $\Omega \subset \mathbb{R}^2$: Find $\mathbf{u} \in H_0^1(\Omega)$, $\mathbf{z} = (0, 0, z(x, y)) \in L^2(\Omega)$ and $p \in L_0^2(\Omega)$ solving

$$-\nu\Delta\mathbf{u} + \mathbf{z} \times \mathbf{u} + \nabla p = \mathbf{o} \text{ in } \Omega, \tag{1}$$

$$\nabla \cdot \mathbf{u} = 0 \text{ in } \Omega, \tag{2}$$

$$\nu z + \alpha\mathbf{u} \cdot \nabla z = \nu\nabla \times \mathbf{u} \text{ in } \Omega. \tag{3}$$

(1)-(3) is a simplified model of Rivlin–Ericksen fluids of complexity two [1]. It has been used to predict slow motions of slurry flows, food rheology, and flow of a water solution of polymers.

2 Numerical Approximation

Arrow-Hurwicz Algorithm. For some $\rho_1 > 0$, $\rho_2 > 0$, solve for $(\mathbf{u}_h^{n+1}, p_h^{n+1}, z_h^{n+1})$:

$$\frac{\left(\nabla(\mathbf{u}_h^{n+1} - \mathbf{u}_h^n), \nabla\mathbf{v}_h\right)}{\rho_1} + \nu(\nabla\mathbf{u}_h^{n+1}, \nabla\mathbf{v}_h) + (\nabla \cdot \mathbf{u}_h^{n+1}, \nabla \cdot \mathbf{v}_h) + \left(\mathbf{z}_h^n \times \mathbf{u}_h^{n+1}, \mathbf{v}_h\right) - (p_h^n, \nabla \cdot \mathbf{v}_h) = 0,$$

$$(p_h^{n+1} - p_h^n, q_h) + (q_h, \nabla \cdot \mathbf{u}_h^{n+1}) = 0,$$

$$\varepsilon\left(\nabla z_h^{n+1}, \nabla\phi_h\right) + \frac{(z_h^{n+1} - z_h^n, \phi_h)}{\rho_2} + \nu(z_h^{n+1}, \phi_h) + \alpha(\mathbf{u}_h^{n+1} \cdot \nabla z_h^{n+1}, \phi_h) = \nu(\nabla \times \mathbf{u}_h^{n+1}, \phi_h).$$

Theorem (Uniform boundedness and convergence) *For* $\Lambda_0 := C_4\|\nabla z_h\|_4 + \dfrac{\|z_h\|_\infty}{2} + C_4\|\mathbf{u}_h\|_4$, *if*

$$\Lambda_1 := \nu - \Lambda_0 > 0,\ \rho_1 < \frac{\Lambda_1}{\Lambda_0^2},\ \textit{and}\ \rho_2 < \frac{\Lambda_1}{C_4^2\|\mathbf{u}_h\|_4^2},$$

then $\{\mathbf{u}_h^n, p_h^n, z_h^n\}$ *is uniformly bounded and* $\mathbf{u}_h^n \xrightarrow{H^1} \mathbf{u}_h$, $p_h^n \xrightarrow{L^2} p_h$ *and* $z_h^n \xrightarrow{L^2} z_h$ *as* $n \to \infty$, *where* $\{\mathbf{u}_h^n, p_h^n, z_h^n\}$ *is the exact solution of the finite element approximation of* (1)-(3).

3 Lid driven cavity test

Re	α	Upwind of [4]	[2]	Upwind of [3]	AH with $\rho_1 = 100, \rho_2 = 100$
100	0.01	39	36	39	40
100	1	22	21	21	21
100	5	18	18	18	21
400	0.01	77	117	77	61
400	1	162	139	164	56
400	5	142	114	148	55

Table 1: Iterations needed for convergence with various schemes

Figure 1: Streamlines for $Re = 400$ and (left to right) $\alpha = 0$, $\alpha = 0.01$ and $\alpha = 5$.

References

[1] Rajagopal, K. R., *On the creeping flow of the second-order fluid*, J. Non-Newtonian Fluid Mech. **15(2)** (1984) 239–246.

[2] Jaffal-Mourtada, B., & Yakoubi, D., *Convergence analysis of an efficient scheme for the steady state second grade fluid model*, Comm. Nonl. Sci. Num. Sim. **138**(2024) 108254.

[3] Girault, V., & Scott, L. R., *Finite-element discretizations of a two-dimensional grade-two fluid model*, ESAIM: M2AN **35(6)** (2001) 1007–1053.

[4] Takhirov, A., & Jaffal-Mourtada, B., & Yakoubi, D., *Upwind iterative decoupling scheme for steady two-dimensional Grade-Two Fluid Equations*, submitted to Comm. Nonl. Sci. Num. Sim. (2025).

Book of abstracts of the 9th International Conference on
Advanced Computational Methods in ENgineering and Applied Mathematics
September, 15–19, 2025.

Modeling Somatic and Dendritic membrane potentials with a two-compartment Fractional Leaky Integrate and Fire model

Yash Vats[1], Mani Mehra[2] and Dietmar Oelz[3]

[1] *University of Queensland - IIT Delhi Research Academy (UQIDRA), Indian Institute of Technology Delhi, New Delhi, India*

[2] *Department of Mathematics, Indian Institute of Technology Delhi, New Delhi, India*

[3] *School of Mathematics and Physics, University of Queensland, Brisbane, Australia*

e-mails: yashvats425@gmail.com, mmehra@maths.iitd.ac.in, d.oelz@uq.edu.au

Abstract

How dendrite–soma coupling and membrane memory shape both subthreshold voltages and spiking patterns is a central question in neuronal modeling. We address this using a two-compartment leaky integrate-and-fire (LIF) neuron model and a fractional-order extension in which classical time derivatives are replaced by Caputo derivatives of order $\alpha \in (0, 1]$. In the subthreshold regime, we show analytically that axial coupling governs a static dendro-somatic transfer via a linear two-port, while the transient is controlled by the eigenstructure of the coupled system: exponentials in the classical model and Mittag–Leffler relaxations in the fractional model. Consequently, fractional dynamics preserve the same steady-state attenuation as the classical model but slow dendro-somatic equalization, prolonging attenuation and apparent delays—especially under strong coupling.

Key words: leaky integrate and fire model, two compartment neuron model, neuron, voltage membrane potential, fractional derivative

1 Introduction

Single-compartment LIF models compress dendritic processing and spatial input location into one lumped current, which can obscure mechanisms related to dendritic filtering and axial transfer. Two-compartment (soma–dendrite) LIF models restore these effects while retaining analytical tractability: the subthreshold dynamics are linear and exactly solvable, and the spike/reset makes the overall system hybrid [1, 2]. In this setting, the axial coupling conductance g_c controls how charge flows between compartments.

In this study, we show that how the coupling conductance between two compartments sculpts subthreshold voltage membrane potential dynamics in both classical and fractional two-compartment leaky integrate-and-fire model.

2 Fractional two-compartment LIF model

Let $V_s(t)$ and $V_d(t)$ be somatic and dendritic voltages; $C_s, C_d > 0$ capacitances; $g_{Ls}, g_{Ld} > 0$ leak conductances (reversal E_L); and $g_c \geq 0$ the axial coupling conductance. With current inputs $I_s(t), I_d(t)$

$$\begin{aligned} C_s\, {}^{C}D_t^{\alpha} V_s &= -\,g_{Ls}\,(V_s - E_L) \;-\; g_c\,(V_s - V_d) \;+\; I_s(t), \\ C_d\, {}^{C}D_t^{\alpha} V_d &= -\,g_{Ld}\,(V_d - E_L) \;-\; g_c\,(V_d - V_s) \;+\; I_d(t). \end{aligned} \tag{1}$$

with initial conditions $V_s(0) = V_d(0) = -65mV$. When $\alpha = 1$ the model reduces to classical two-compartment LIF model; when $0 < \alpha < 1$, the memory tail is $E_\alpha(-\lambda t^\alpha) \sim [\lambda\,\Gamma(1-\alpha)]^{-1} t^{-\alpha}$.

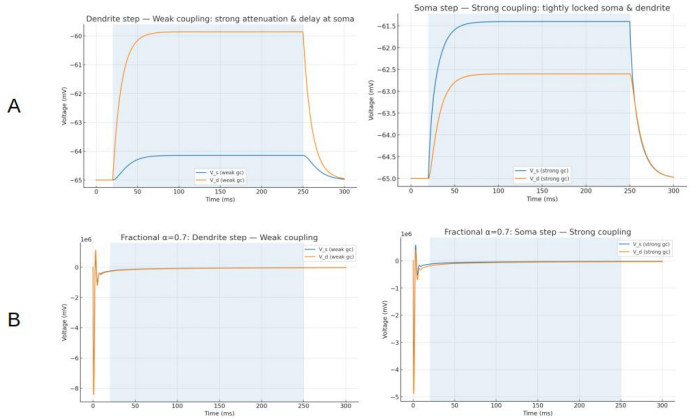

Figure 1: **Subthreshold coupling in a two-compartment neuron (soma & dendrite). A: Classical LIF model** ($\alpha = 1$). Left: dendrite-only step (60 pA, 20–250 ms) with weak coupling ($g_c = 2$ nS) produces strong attenuation at the soma and a clear lag. Right: soma-only step with strong coupling ($g_c = 20$ nS) yields a quasi-isopotential response ($V_s \approx V_d$) throughout the transient. **B: Fractional LIF model** ($\alpha = 0.7$) with identical parameters. The steady-state (DC) attenuation matches the classical case (same linear two-port), but the transient equalization is slower due to long-memory relaxation; all traces are subthreshold (no threshold/reset).

Acknowledgements This work has been supported by Prime Minister's Research fellowship grant provided by Prime Minister of India.

References

[1] G. Ermentrout, D. Terman, *Bistability in a Leaky Integrate-and-Fire Neuron with a Passive Dendrite*, SIAM Journal on Applied Dynamical Systems **11** (2012) 507–539.

[2] A. Saparov, M. A. Schwemmer, *Effects of passive dendritic tree properties on the firing dynamics of a leaky integrate-and-fire neuron*, Mathematical Biosciences **81** (1999) 161–167.

Book of abstracts of the 9th International Conference on
Advanced Computational Methods in ENgineering and Applied Mathematics
September, 15–19, 2025.

Mikusiński Operational Calculus for the Hadamard Fractional Derivative

Imtiaz Waheed[1,2]

[1] *Department of Mathematics, School of Natural Sciences, National University of Sciences and Technology, H-12, Islamabad, Pakistan*

[2] *Department of Mathematics: Analysis, Logic and Discrete Mathematics, University of Ghent, Belgium*

e-mails: imtiazwaheed96@gmail.com, Imtiaz.waheed@UGent.be

Abstract

Mikusiński's operational calculus provides a framework for finding the solution of differential equations. In this study, we extend Mikusiński's approach for the Hadamard fractional derivative. We demonstrate that, with minor adaptations, the operational calculus framework can be effectively applied to the Hadamard derivative. Additionally, we use the generalized Mellin convolution as an alternative to the Laplace convolution, enabling the derivation of exact solutions for fractional differential equations with constant coefficients. These solutions are expressed in terms of generalized Mittag-Leffler functions.

Keywords: Fractional differential equations, Hadmard fractional calculus, operational calculus, Mikusiński operational calculus

1 Background

Finding analytical solutions of fractional differential equations is challenging. Operational calculus provides a framework to treat calculus operators, such as differentiation and integration, algebraically, allowing differential equations to be handled as algebraic equations. This concept was significantly advanced by Jan Mikusiński in the 1950 [1], who redefined differentiation operators within an algebraic framework and represented differential equations symbolically. His approach treated convolution as multiplication within a ring of continuous functions, offering a more accessible and rigorous alternative to traditional methods like the Laplace transform [2].

2 Motivation

Classical methods for solving ordinary and partial differential equations, such as iteration, series, and transform techniques, are effective [3, 4, 5] but have limitations. For example, the Laplace transform struggles with forcing functions not of exponential order [6]. Mikusiński's operational calculus provides a powerful alternative, particularly for differential equations with non-integer order derivatives.

Since Mikusiński's foundational work, the fractional-order extension of his operational calculus has gained attention, with contributions from researchers like Luchko and others [7, 8, 9, 10]. Moreover key advancements include the development of operational calculus for Riemann–Liouville and Caputo operators and the exploration of Erdélyi–Kober operators [10, 9, 11], with applications in fractional integro-differential equations [12].

Motivated by recent research in this direction by several authors [7, 8, 9, 10, 11], we explore the following in this study:

(i) The development of Mikusiński's operational calculus for the Hadamard fractional derivative.

(ii) The use of the Generalized Mellin convolution instead of the classical Laplace convolution.

(iii) Applications of this method through the solution of fractional differential equations involving the Hadamard fractional derivative.

References

[1] Mikusiński, J. (1959) Operational Calculus. Pergamon Press, London.

[2] Flegg, H. G. (1974). Mikusinski's operational calculus. International Journal of Mathematical Education in Science and Technology, 5(2), 131-137.

[3] Samko, S. G., Kilbas, A. A. and Marichev, O.I. (1993) Fractional Integrals and Derivatives: Theory and Applications. Gordon and Breach, Yverdon.

[4] Oldham, K. B., Spanier, J., The Fractional Calculus, Academic Press, New York, 1974.

[5] Fernandez, A., Baleanu, D., & Fokas, A. S. (2018). Solving PDEs of fractional order using the unified transform method. Applied Mathematics and Computation, 339, 738-749.

[6] Podlubny, I. (1998). Fractional differential equations: an introduction to fractional derivatives, fractional differential equations, to methods of their solution and some of their applications. elsevier.

[7] Luchko, Y. (1999). Operational method in fractional calculus. Fract. Calc. Appl. Anal, 2(4), 463-488.

[8] Luchko, Y. F., & Yakubovich, S. B. (1994). An operational method for solving some classes of integro-differential equations. Differentsial'nye Uravneniya, 30(2), 269-280.

[9] Luchko, Y., & Gorenflo, R. (1999). An operational method for solving fractional differential equations with the Caputo derivatives. Acta Math. Vietnam, 24(2), 207-233.

[10] Hadid, S. B., & Luchko, Y. F. (1996). An operational method for solving fractional differential equations of an arbitrary real order. Panamer. Math. J, 6(1), 57-73.

[11] Luchko, Y. F., & Srivastava, H.M., The exact solution of certain differential equations of fractional order by using operational calculus. Comput. Math. Appl. 29 (1995), 73–85.

[12] Hanna, L. A., Al-Kandari, M., & Luchko, Y. (2020). Operational method for solving fractional differential equations with the left-and right-hand sided Erdélyi-Kober fractional derivatives. Fractional Calculus and Applied Analysis, 23(1), 103-125.

Book of abstracts of the 9th International Conference on
Advanced Computational Methods in ENgineering and Applied Mathematics
September, 15–19, 2025.

Very Weak Solutions to Parabolic Equations with Singular Coefficients and Boundary Data: Analysis and Computation

Alibek Yeskermessuly[1] and Arshyn Altybay[2]

[1] *Faculty of Natural Sciences and Informatization, Altynsarin University, Arkalyk, Kazakhstan*

[2] *Institute of Mathematics and Mathematical Modeling, Almaty, Kazakhstan*

e-mails: alibek.yeskermessuly@gmail.com, arshyn.altybay@gmail.com

Abstract

We investigate linear parabolic equations in divergence form with singular coefficients and non-smooth boundary data. When the diffusion, drift, or potential terms, as well as the initial or boundary conditions, are distributions rather than functions, classical and weak solution concepts become inadequate due to the ill-posedness of products involving distributions. To overcome this, we introduce a framework of very weak solutions based on regularization techniques and the theory of moderate nets. Existence of very weak solutions is established under minimal regularity assumptions. We further prove consistency with classical solutions when the data are smooth and demonstrate uniqueness via negligibility arguments. Finally, we present numerical computations that illustrate the robustness of the very weak solution framework in handling highly singular inputs, including delta-type potentials and distributional boundary traces.

Key words: divergence form, energy methods, Galerkin approximation, parabolic equation, regularisation, shift term, singular coefficients, very weak solution.
MSC 2020: 35K20, 35D30, 35K67

Poster Session

Book of abstracts of the 9th International Conference on
Advanced Computational Methods in ENgineering and Applied Mathematics
September, 15–19, 2025.

Continuum Modeling of the Interactions Between Noble Metals and Nanosheets

Mansoor H. Alshehri[1]

[1] *Mathematics Department, College of Science, King Saud University, P.O. Box 2455, Riyadh 11451, Saudi Arabia*

e-mails: mhalshehri@ksu.edu.sa

Abstract

Using classical applied mathematical modeling, we derive explicit analytical expressions to determine the binding energies of noble metals including copper, silver, gold, platinum and Iridium (Cu, Ag, Au, Pt and Ir) atoms on graphene and hexagonal boron nitride nano-sheets. We adopt the 6–12 Lennard-Jones potential function together with the continuous approach to determine the preferred minimum energy position of an offset metal atom above the surface of the graphene and hexagonal boron nitride nano-sheets. The main result of this study is an analytical expression for the interaction energies that we then utilize to report the mechanism of adsorption of the metal atoms on graphene and hexagonal boron nitride surfaces. Results observe that the minimum binding energy occurs when Cu, Ag, Au, Pt and Ir atoms are set at a perpendicular distances in the region from 3.302 Å to 3.683 Å above the nano-sheet surface which correspond to adsorption energies in the region from 0.842 to 2.978 (kcal/mol).

Key words: noble metalsl, graphene, h-BN, mathematical modeling, Lennard–Jones potential

1 Introduction

The interactions of graphene and graphene-like materials with metals, including the noble metals, have been used for many potential applications, such as improving the chemical, thermal, mechanical, electrical and optical properties, and as biodevices, sensors, catalysis, energy storage and nanomagnetic materials [1, 2, 3, 4]. Here, mathematical modeling is used to adopt continuous approximation, together with the Lennard–Jones potential function, to study the adsorption of noble metals on GRA and h-BN nanosheets.

2 Methodology

The binding energies between the metal atoms and nanosheets are determined using the 6–12 Lennard–Jones (LJ) potential function via a continuous approximation. The Lennard–Jones potential energy between a pair of atoms separated by a distance r is given by:

$$\Phi(r) = -\frac{A}{r^6} + \frac{B}{r^{12}},$$

where A and B are the attractive and repulsive constants, respectively. A hybrid discrete-continuous approach is used to determine the total interaction energy between a single metal atom and the sheet. The energy can be expressed as:

$$E = \sum_k h \int \Phi(r_k)\, dM, \tag{1}$$

where $\Phi(r_k)$ denotes the Lennard–Jones potential, r is the distance between the atom and a point on the nanosheet surface, and h is the surface atomic density and the term dM represents the differential mass element over the continuously modeled substrate. Assuming a Cartesian coordinate system, a typical point on the nanosheet lies at $(x, y, 0)$, while the metal atom is located at $(0, 0, \lambda)$, where λ is the perpendicular distance from the sheet. Therefore, the distance r between the atom and a point on the surface is:

$$r^2 = x^2 + y^2 + \lambda^2.$$

Thus, the total binding energy of a metal atom adsorbed on the graphene or h-BN nanosheet is derived analytically as:

$$E = h\left(\frac{-\pi A}{2\lambda^4} + \frac{\pi B}{5\lambda^{10}}\right). \tag{2}$$

3 Results and Discussion

Our findings show that the binding energies of the metal atoms on both GRA and h-BN nanosheets range from 0.842 to 2.978 kcal/mol, following the order Pt > Ir > Au > Ag > Cu. The calculated optimal equilibrium distances between the metal atoms and the nanosheets range from 3.302 Å to 3.683 Å. In general, h-BN exhibits slightly stronger binding affinities than GRA for most metal atoms, indicating substrate-dependent variation in interaction strength. These variations can be attributed to differences in electronic structure and polarizability of the metals, as well as the distinct nature of the nanosheet surfaces. Overall, the results provide key insights into the interaction energies between noble metal atoms and two-dimensional nanomaterials. Such information is valuable for guiding the design and optimization of nanosheet-based catalysts, sensors, and electronic devices.

References

[1] M. Amft, S. Lebègue, O. Eriksson, N. V. Skorodumova, *Adsorption of Cu, Ag, and Au atoms on graphene including van der Waals interactions*, J. Phys.: Condens. Matter **23** (2011), 395001.

[2] A. C. Neto, F. Guinea, N. M. Peres, K. S. Novoselov, A. K. Geim, *The electronic properties of graphene*, Rev. Mod. Phys. **81** (2009), 109.

[3] A. K. Geim, *Graphene: Status and prospects*, Science **324** (2009), 1530–1534.

[4] S. Basu, S. K. Hazra, *Graphene–Noble Metal Nano-Composites and Applications for Hydrogen Sensors*, C **3** (2017), 2311–5629.

Book of abstracts of the 9th International Conference on
Advanced Computational Methods in ENgineering and Applied Mathematics
September, 15–19, 2025.

Alignment-Free Bioinformatics Methods

Dorota Bielińska-Wąż[1] and Piotr Wąż[2]

[1] *Department of Radiological Informatics and Statistics, Medical University of Gdańsk, 80-210 Gdańsk, Poland*

[2] *Department of Nuclear Medicine, Medical University of Gdańsk, 80-210 Gdańsk, Poland*

e-mails: djwaz@gumed.edu.pl, phwaz@gumed.edu.pl

Abstract

Alignment-free bioinformatics methods developed by our team are reviewed, with applications demonstrated for genome sequence similarity analysis. The resulting similarity maps are presented, where the axes correspond to numerical characteristics derived from graph-based representations of the sequences.

Key words: alignment-free methods, bioinformatics, machine learning

1 Introduction

The rapid growth of biomedical data has driven the development of novel mathematical frameworks to analyze large-scale biological datasets [1, 2]. Among these, alignment-free bioinformatics methods stand out - efficient computational techniques for comparing DNA, RNA, and protein sequences without traditional alignment (reviewed in [3]). Combining principles from mathematics, computer science, and biology, these approaches achieve high computational efficiency and scalability [4]. Here, we present our contributions to the field, including innovative alignment-free methods [5–13].

2 Results

We have developed a series of novel alignment-free bioinformatics methods, including:

- *2D-Dynamic Representation of DNA Sequences* [5],
- *Four-Component Spectral Representation of DNA Sequences* [6],
- *3D-Dynamic Representation of DNA Sequences* [7],
- *Spectral-Dynamic Representation of DNA Sequences* [8],
- 20D-Dynamic Representation of Protein Sequences [9],
- *4D-Dynamic Representation of DNA/RNA Sequences* [10].

These methods have been successfully applied in various studies, some of which are highlighted in this presentation [11–13]. Notably, our 3D-Dynamic Representation of DNA/RNA Sequences, paired with a random forest algorithm, successfully classifies subtypes of influenza A virus strains [12]. In our recent work, integration of the 20D-Dynamic Representation of Protein Sequences with *K*-means clustering proved effective for protein sequence analysis [13].

References

[1] X. Du, R. Zhu, Y. Li, A. Anjum, *Language model-based auto- matic prefix abbreviation expansion method for biomedical big data analysis*, Future Gener. Comput. Syst. **98** (2019) 238–251.

[2] J. Lötsch, S. Malkusch, A. Ultsch, *Optimal distribution- preserving downsampling of large biomedical data sets (opdis- Downsampling)*, PLoS One **16** (2021) e0255838.

[3] N. Ramanathan, J. Ramamurthy, G. Natarajan, *Numerical characterization of DNA sequences for alignment-free sequence comparison - A review*, Comb. Chem. High T. Scr. **25** (2022) 365–380.

[4] T. Wang, Z.G. Yu, J. Li, *CGRWDL: Alignment-free phylogeny reconstruction method for viruses based on chaos game representation weighted by dynamical language model*, Front. Microbiol. **15** (2024) 1339156.

[5] D. Bielińska-Wąż, T. Clark, P. Wąż, W. Nowak, A. Nandy, *2D-dynamic representation of DNA sequences*, Chem. Phys. Lett. **442** (2007) 140–144.

[6] D. Bielińska-Wąż, *Four-component spectral representation of DNA sequences* J. Math. Chem. **47** (2010) 41–51.

[7] P. Wąż, D. Bielińska-Wąż, *3D-dynamic representation of DNA sequences*, J. Mol. Model. **20** (2014) 2141.

[8] D. Bielińska-Wąż, P. Wąż, *Spectral-dynamic representation of DNA sequences*, J. Biomed. Inform. **72** (2017) 1–7.

[9] A. Czerniecka, D. Bielińska-Wąż, P. Wąż, T. Clark, *20D-dynamic representation of protein sequences*, Genomics **107** (2016) 16–23.

[10] D. Bielińska-Wąż, P. Wąż, *Non-standard bioinformatics characterization of SARS-CoV-2*, Comput. Biol. Med. **131** (2021) 104247.

[11] D. Bielińska-Wąż, P. Wąż, A. Lass, J. Karamon, *4D-Dynamic Representation of DNA/RNA Sequences: Studies on Genetic Diversity of Echinococcus Multilocularis in Red Foxes in Poland*, Life **12** (2022) 877.

[12] D. Bielińska-Wąż, P. Wąż, D. Panas, *Applications of 2D and 3D-Dynamic Representations of DNA/RNA Sequences for a Description of Genome Sequences of Viruses*, Comb. Chem. High T. Scr. **25** (2022) 429–438.

[13] D. Bielińska-Wąż, P. Wąż, A. Błaczkowska, *20D-Dynamic Representation of Protein Sequences Combined with K-means Clustering*, Comb. Chem. High T. Scr. In print (2025) DOI: 10.2174/0113862073359729250220131623

Book of abstracts of the 9th International Conference on
Advanced Computational Methods in ENgineering and Applied Mathematics
September, 15–19, 2025.

The MFS reconstruction of an interior inverse generalized impedance problem for the Modified Helmholtz Equation

Bandar Bin-Mohsin[1]

[1] *Mathematics Department, College of Science, King Saud University, P.O. Box 2455, Riyadh 11451, Saudi Arabia*

e-mails: balmohsen@ksu.edu.sa

Abstract

Accurate reconstruction of hidden and irregularly shaped targets from limited surface measurements is a critical problem in tomographic imaging, with important applications such as detecting breast tumors or locating buried landmines. This study presents a novel numerical method for identifying internal defects within a surrounding medium, using only five pairs of non-invasive Cauchy boundary data. The unknown defects are assumed to satisfy impedance or generalized impedance boundary conditions. The reconstruction is carried out using the Method of Fundamental Solutions (MFS), a mesh-free technique well-suited for handling complex geometries. The physical model is based on the modified Helmholtz equation, which describes steady-state processes in heat transfer and bio-heat diffusion. To tackle the inverse problem, we construct a regularized least-squares functional that measures the discrepancy between measured and simulated data. The functional is minimized using MATLAB's lsqnonlin solver. The approach demonstrates both robustness and potential for practical imaging applications.

Key words: : Modified Helmholtz's Equation, Inverse Problem, Method of Fundamental Solutions, Nonlinear Optimization.

1 Introduction

Reconstruction of interior defects, e.g. inclusions, cavities and cracks, subjected to more realistic boundary conditions is very important in mathematical modelling of inverse instrumental techniques such as tomography, scanning and imaging. We consider a simply-connected bounded planar domain $\Omega \subset \mathbb{R}^2$ containing an unknown obstacle $D \subset \Omega$ such as that the domain $\Omega \setminus D$ is doubly-connected having two disjoint closed boundary portions, namely, $\partial\Omega$ the exterior boundary and ∂D the interior boundary, which are assumed sufficiently smooth, e.g. of class C^2.

We consider the steady-state bio-heat equation for the temperature u given by the modified Helmholtz equation

$$\nabla^2 u - \kappa^2 u = 0 \qquad \text{in } \Omega\backslash\overline{D}, \tag{1}$$

where $\kappa = 0$ is a physical quantity related to the heat transfer coefficient or the blood perfusion. On the boundary ∂D of the unknown defect D we prescribe the generalized impedance boundary condition[1],

$$\frac{\partial u}{\partial n} + \lambda u - \frac{d}{ds}(\mu \frac{du}{ds}) = 0 \quad \text{on } \partial D$$

where $\partial u/\partial n = \partial_n u := \nabla u \cdot \underline{n}$ represents the normal derivative with respect to n, the outward unit normal to the boundary $\partial(\Omega\backslash\overline{D})$, s is the arc-length on ∂D, and

$$0 \leq \lambda \in C^1(\partial\backslash\overline{D}), \lambda \not\equiv 0,\ 0 < \mu \in C^1(\partial D)$$

2 The method of fundamental solutions (MFS)

The solution of the modified Helmholtz equation (1) in the doubly-connected domain $\overline{\Omega}\backslash D$ is approximated as

$$u(\underline{X}) = \sum_{j=1}^{2M} a_j G(\underline{X}, \underline{\xi}^j), \qquad \underline{X} \in \overline{\Omega} \setminus D \tag{2}$$

where the $2M$ points $(\underline{\xi}^j)_{j=\overline{1,2M}}$ are distinct source points located outside domain $\overline{\Omega}$ and inside domain D, and

$$G(\underline{X}, \underline{\xi}^j) = K_0(\kappa\|\underline{X} - \underline{\xi}^j\|)$$

is the fundamental solution of the modified Helmholtz equation in two-dimensions and K_0 is the modified Bessel function of second kind of order zero. Density results justifying the expansion (2) have been recently proved in [2].

3 Results and Discussion

In this work, the numerical reconstruction of inner boundaries subjected to generalized impedance boundary conditions from five Cauchy data pairs of boundary measurements has been accomplished using the meshless MFS, which is a versatile method for solving inverse geometric and coefficient identification problems, [3],[4]. Accurate numerical results have been obtained for noiseless data. Furthermore, the need of employing regularization for stabilizing the solution of the nonlinear inverse and ill-posed problem when noisy data are inverted, has been stressed.

References

[1] F. Cakoni, R. Kress, *Integral equation methods for the inverse obstacle problem with generalized impedance boundary condition*, Inverse Problems, **V.29**, **N.1**, (2013), 015005.

[2] C.J.S Alves, N.F.M Martins, S.S. Valtchev, *Domain decomposition methods with fundamental solutions for Helmholtz problems with discontinuous source terms*, Computers and Mathematics with Applications, **88** (2021), 16-32.

[3] B. Bin-Mohsin, D. Lesnic, *Determination of inner boundaries in modified Helmholtz inverse geometric problems using the method of fundamental solutions*, Mathematics and Computers in Simulation **V.82 N.8**(2012), 1445–1458.

[4] A. Karageorghis, B. Bin-Mohsin, D. Lesnic, L. Marin, *Simultaneous numerical determination of a corroded boundary and its admittance*, Inverse Problems in Science and Engineering, **V.23, N.7** (2015), 1120–1137.

Book of abstracts of the 9th International Conference on
Advanced Computational Methods in ENgineering and Applied Mathematics
September, 15–19, 2025.

In Silico Investigation of the Role of Local and Global Inflammation-Driven Feedback in Myelopoiesis and Clonal Cell Expansion

Yusuf Jamilu Umar[1], Symeon Savvopoulos[2] and Haralampos Hatzikirou [1]

[1] *Department of Mathematics, Khalifa University Abu Dhabi*

[2] *Department of Mathematics, Khalifa University Abu Dhabi*

e-mails: 100060967@ku.ac.ae, symeon.savvopoulos@ku.ac.ae, haralampos.hatzikirou@ku.ac.ae

Abstract

Chronic inflammation perturbs hematopoietic homeostasis, promoting aberrant myelopoiesis and clonal expansion of mutated stem cells. Here, we develop a mathematical model that integrates both local (bone marrow-intrinsic) and global (systemic/peripheral) inflammation-driven feedback mechanisms to investigate their roles in hematopoietic regulation and disease progression. Our model captures the nonlinear interplay between self-renewal, progenitor proliferation, and inflam- matory cues, enabling classification of healthy, myelodysplastic, and leukemic states based on stem cell population dynamics. We show that global inflammatory feedback enhances the resilience of hematopoiesis, while excessive feedback on progenitor cells under chronic inflammation drives instability and clonal dominance. Using sensitivity analysis and parameter space mapping, we identify critical feedback thresholds governing transitions between hematopoietic states and reveal how mutated clones exploit inflammation to outcompete wild-type cells. This systems-level framework offers mechanistic insights into the emergence of myeloid malignancies and provides a computational platform for exploring potential anti-inflammatory therapeutic strategies.

Key words: Acute Myeloid Leukemia (AML),Chronic Inflammation,Hematopoiesis, Myelodysplastic Syndromes (MDS),Systems Biology Modeling.

1 Introduction

Inflammation is a conserved mechanism that ensures the restoration of homeostasis in response to infection and injury. An important aspect of this mechanism is the response of the hematopoietic system to inflammatory mediators that ensures the demand-adapted replenishment of immune cells. Hematopoietic stem cells (HSC) in bone marrow (BM) can respond to inflammatory stimuli, including pathogen-derived products and inflammatory mediators, resulting in enhanced proliferation and myeloid differentiation [1]. Chronic inflammation, however, leads to loss of HSC fitness, resulting in their depletion ([2, 3, 4]). Aging is considered a chronic inflammatory condition associated with defects in the self-renewal capacity of HSCs, myeloid-priming and increased prevalence of clonal hematopoiesis and myeloid malignancies [5]. Indeed, aging is characterized by a deregulation of the immune system, with

enhanced production of inflammatory cytokines that results in a chronic low-dose inflammatory status, which further supports the development and progression of aging-associated disorders, such as cardiovascular disorders and cancer [6].

Emergency granulopoiesis, i.e. the generation of neutrophils in response to inflammation, is a hallmark of acute inflammation [1]. HSC are equipped with a variety of receptors that sense inflammatory stimuli, including Toll-like receptors, cytokine receptors [1, 3] and receptors for myeloid lineage growth factors which enables their rapid adaptation to inflammation with enhanced proliferation and myeloid differentiation. However, beyond these direct effects, global feedback mechanisms emerge from systemic inflammatory responses, in which circulating inflammatory signals influence hematopoiesis both in the bone marrow and at peripheral tissues. In the case of chronic inflammation, the exit from dormancy in response to chronic cytokine stimulation, including interferons and interleukin (IL)-1, —forces HSCs into continuous activation, resulting in loss of self-renewal potential, HSC injury, and eventual attrition [3].

Acknowledgements We would like to aknowledge the support of Volkswagenstiftung for its support of the "Life?" program (96732). We also acknowledge the support of the RIG-2023-051 grant from Khalifa University. Finally, we would like to thank for the support of the UAE-NIH Collaborative Research grant AJF-NIH-25-KU.

References

[1] T. Chavakis, I. Mitroulis, G. Hajishengallis, *Hematopoietic progenitor cells as integrative hubs for adaptation to and fine-tuning of inflammation*, Nature Immunology, 20 (2019), 802–811.

[2] K. A. Mattatall, M. Jeong, S. Chen, D. Sun, F. Chen, Q. Mo, M. Kimmel, K. Y. King, *Chronic Infection Depletes Hematopoietic Stem Cells through Stress-Induced Terminal Differentiation*, Cell Reports, 17 (2016), 2584–2595.

[3] E. M. Pietras, C. Mirantes-Barbeito, S. Fong, D. Loeffler, L. V. Kovtonyuk, S. Zhang, R. Lakshminarasimhan, C. P. Chin, J.-M. Techner, B. Will, et al., *Chronic interleukin-1 exposure drives haematopoietic stem cells towards precocious myeloid differentiation at the expense of self-renewal*, Nature Cell Biology, 18 (2016), 607–618.

[4] T. Sato, N. Onai, H. Yoshihara, F. Arai, T. Suda, T. Ohteki, *Interferon regulatory factor-2 protects quiescent hematopoietic stem cells from type I interferon-dependent exhaustion*, Nature Medicine, 15 (2009), 696–700.

[5] F. Caiado, E. M. Pietras, M. G. Manz, *Inflammation as a regulator of hematopoietic stem cell function in disease, aging, and clonal selection*, Journal of Experimental Medicine, 218 (2021).

[6] C. Franceschi, P. Garagnani, P. Parini, C. Giuliani, A. Santoro, *Inflammaging: a new immune-metabolic viewpoint for age-related diseases*, Nature Reviews Endocrinology, 14 (2018), 576–590.

Book of abstracts of the 9th International Conference on
Advanced Computational Methods in ENgineering and Applied Mathematics
September, 15–19, 2025.

Fractional Order Dynamics of a Prey-Predator Mathematical Model with Holling Type IV Functional Response, Intraspecific Competition, and Harvesting Effect

Eucharia Nwachukwu[1] and Francis Nzerem[2]

[1] *Department of Mathematics and Statistics, University of Port Harcourt, Nigeria*

[2] *Department of Mathematics and Statistics, University of Port Harcourt, Nigeria*

e-mails: eucharia.nwachukwu@uniport.edu.ng, francis.nzerem@uniport.edu.ng

Abstract

This study investigates the complex dynamics of a three-species fractional order prey-predator model that incorporates a Holling Type IV functional response, intraspecific competition, and harvesting effects. The model consists of two prey species (x and y) and a predator species (z), where the prey populations grow logistically, compete among themselves, and are subject to predation with a Holling Type IV response. In addition, one of the prey species (y) is influenced by an external harvesting term. The growth of predators is regulated by a ratio-dependent carrying capacity linked to the densities of prey. We analyze the existence and stability of equilibrium points, perform bifurcation analysis to explore dynamical transitions, and perform numerical simulations to illustrate chaotic and stable behaviors. The results highlight the impact of harvesting, competition, and predation on species coexistence and extinction. The fractional-order derivative introduces memory effects, providing a more realistic representation of ecological interactions. Our results shall be presented and discussed.

Key words: Fractional-order model, Prey-predator dynamics, Holling Type IV, Intraspecific competition, Harvesting effect, Stability analysis, Bifurcation.
MSC 2020: Mathematics Subject Classification.

References

[1] Matignon, D. *Stability results for fractional differential equations with applications to control processing. Computational Engineering in Systems Applications, 2, 963–968. 1996.*

[2] Diethelm, K, *The Analysis of Fractional Differential Equations: An application-oriented exposition using differential operators of Caputo type.*, Springer, 2010.

[3] Holling, C. S. *The functional response of predators to prey density and its role in mimicry and population regulation.*

[4] Munkaila Dasumani et al *A nonlinear fractional fishery resource system model with Crowley–Martin functional response under Mittag-Leffler kernel Results in Control and Optimization , 16, Elsevier*

[5] Chakraborty, K., Das, S., *&* Kar, T. K. Harvesting induced stability and instability in a predator-prey system. Journal of Theoretical Biology, 339, 26–34.

Book of abstracts of the 9th International Conference on
Advanced Computational Methods in ENgineering and Applied Mathematics
September, 15–19, 2025.

Stochastic Comparisons of Extreme Order Statistics Under Archimedean Dependence

Mansour Shrahili[1]

[1] *Department of Statistics and Operations Research, College of Science, King Saud University, P.O. Box 2455, Riyadh 11451, Saudi Arabia*

e-mails: msharahili@ksu.edu.sa

Abstract

Order statistics play a crucial role in reliability and survival analysis, particularly in modeling systems with components that may fail independently or dependently. Traditional studies focused largely on independent and identically distributed (i.i.d.) settings. However, many real-world systems exhibit dependence structures, especially in engineering, actuarial science, and operational risk modeling. One effective way to capture such dependence is through Archimedean copulas, which offer analytical tractability and flexibility. Despite this, there remains a significant gap in establishing stochastic ordering results for extreme order statistics (e.g., series and parallel systems) under dependent, heterogeneous conditions. This proposal aims to fill this gap by developing a theory for stochastic comparisons of such systems, particularly focusing on dispersive and usual stochastic orders..

Key words: stochastic, dispersive order, extreme order statistics, archimedean copula generators

1 Objectives

- To derive conditions under which the dispersive order holds between parallel systems with dependent exponential lifetimes.
- To establish usual stochastic ordering between systems with general one-parameter lifetime distributions.
- To analyze how different Archimedean copula generators influence stochastic behavior in extreme order statistics.
- To apply majorization theory to compare system reliabilities.
- To illustrate the theoretical findings with practical examples using common copulas like Clayton and Gumbel.

2 Methodology

- **Mathematical Framework:** Define series and parallel systems via the smallest and largest order statistics from dependent exponential variables.
- **Copula Modeling:** Employ Archimedean copulas to model dependency structures. Use properties of their generators (e.g., monotonicity, convexity).
- **Stochastic Orders:**
  - Develop sufficient conditions for dispersive ordering (e.g., via Chebyshev's inequality and function convexity).
  - Establish usual stochastic order results by proving Schur-convexity/concavity of survival functions under parameter majorization.
- **Examples:** Use distributions such as Lomax, exponential, and custom lifetime models; apply Clayton and Gumbel copulas to demonstrate applicability.
- **Counterexamples:** Provide cases where assumptions fail to underscore the necessity of conditions.

3 Expected Outcomes

- Novel ordering results for systems with dependent, heterogeneous components.
- Identification of key conditions (e.g., log-concavity of lifetime distributions, convexity of copula generator derivatives).
- Extension of classical stochastic comparison results to broader, more realistic models.
- Insights useful for decision-makers in system design, quality control, and reliability engineering.

References

[1] M. Shaked, J. G. Shanthikumar, *Stochastic Orders*, Springer, 2007.

[2] A. Müller, D. Stoyan, *Comparison Methods for Stochastic Models and Risks*, Wiley, 2002.

[3] A. W. Marshall, I. Olkin, B. C. Arnold, *Inequalities: Theory of Majorization and Its Applications*, Springer, 2011.

[4] R. Dykstra, S. C. Kochar, J. Rojo, *Stochastic comparisons of parallel systems of heterogeneous exponential components*, J. Stat. Plan. Inference **65** (1997), no. 2, 203–211.

Book of abstracts of the 9th International Conference on
Advanced Computational Methods in ENgineering and Applied Mathematics
September, 15–19, 2025.

Exploring the S-Curvature Tensor on Semi-Riemannian Manifolds with Applications in Relativity

Abdallah Abdelhameed Syied[1], Uday Chand De[2], Mohamed F. Ismail[3] and Nasser Bin Turki[4]

[1] *Department of Mathematics, Faculty of Science, Zagazig University, P.O. Box 44519, Zagazig, Egypt*

[2] *Department of Pure Mathematics, University of Calcutta, 35, Ballygaunge Circular Road, Kolkata 700019, West Bengal, India*

[3] *Faculty of Computers and Information System, Egyptian Chinese University, Cairo, Egypt*

[4] *Department of Mathematics, College of Science, King Saud University, P.O. Box 2455, Riyadh 11451, Saudi Arabia*

e-mails: a.a_syied@yahoo.com, uc_de@yahoo.com, m.fekry2015@yahoo.com, nassert@ksu.edu.sa

Abstract

This article introduces a new curvature tensor, the S-curvature tensor, which is seen as a comprehensive extension of various curvature tensors. It is demonstrated that a semi-Riemannian manifold with traceless S-curvature tensor is Einstein. It is proved that a S-curvature flat semi-Riemannian manifold is of constant sectional curvature. Moreover, we show that a perfect fluid S-curvature flat space-time represents dark matter era. It is shown that a perfect fluid space-time with $\nabla_h S_{hjkl} = 0$ is expansion-free and shear-free and its flow is geodesic, but not necessarily vorticity-free. We show that a pseudo S-symmetric manifold is reduced to pseudo symmetric manifold if and only if the scalar curvature is constant. Finally, a concrete example of pseudo S-symmetric manifolds is introduced.

Key words: S-curvature tensor, semi-Riemannian, S-symmetric manifolds, space-time, differential geometry

1 Introduction

Curvature invariants are fundamental in differential geometry and general relativity, offering key insights into spacetime curvature, manifold structure, and gravitational phenomena, independent of coordinates.

In semi-Riemannian geometry, these invariants are scalar values created from a variety of curvature tensors, with the most well-known ones being the Riemann, Ricci, and Weyl tensors (for example see [1]). Inspired by the significance of the curvature tensors in differential geometry and general relativity, we propose a novel curvature tensor known as the *S-curvature tensor*, which is defined as follows:

$$S_{ijkl} = b_0 R_{ijkl} + b_1 g_{ij} R_{kl} + b_2 g_{ik} R_{jl} + b_3 g_{il} R_{jk} + b_4 g_{jk} R_{il} + b_5 g_{jl} R_{ik} + b_6 g_{kl} R_{ij} + b_7 R(g_{il} g_{jk} - g_{jl} g_{ik}),$$

where b_i are constants, R_{ijkl}, R_{ij}, and R represent the Riemann curvature tensor, Ricci tensor, and scalar curvature, respectively.

This tensor generalizes many known curvature tensors under specific choices of the constants b_i. The study explores its implications in both mathematical and physical contexts, especially within relativistic spacetimes.

2 Example

In this section, an example of pseudo S-symmetric semi-Riemannian manifolds is introduced. Let us now make the assumption that the manifold M is of dimension 4 and equipped with a metric g, which can be expressed in the following manner:

$$ds^2 = g_{hk}dx^h dx^k = \left(\frac{dx^1}{x_1^2} + \frac{dx^2}{x_2^2} + \frac{dx^3}{x_2^2} - (dx^4)^2\right), \quad \text{for } h,k = 1,2,3,4.$$

Christoffel symbols Γ^i_{jk} have the following non-zero components:

$$\Gamma^3_{23} = \frac{1}{x_2}, \quad \Gamma^2_{12} = \frac{1}{x_1}, \quad \Gamma^2_{33} = -\frac{x_2}{x_1^2}, \quad \Gamma^1_{22} = -x_1.$$

Consequently, it arises

$$R_{12} = -\frac{1}{x_1 x_2}, \quad R_{1332} = -\frac{x_2}{x_1}.$$

It is observed that $R = 0$. The non-zero component of the S-tensor is

$$S_{1332} = -\frac{(b_0 + b_4)x_2}{x_1},$$

and its covariant derivatives are expressed as

$$\nabla_1 S_{1332} = \frac{(b_0 + b_4)x_2}{x_1^2}, \quad \nabla_2 S_{1332} = -\frac{(b_0 + b_4)}{x_1}.$$

Choosing the associated covector ϕ_i as given in the subsequent form:

$$\phi_i(x) = \begin{cases} \frac{1}{3x_1} & i = 1, \\ \frac{1}{3x_2} & i = 2, \\ 0 & \text{otherwise.} \end{cases}$$

$$\nabla_1 S_{1332} = 3\phi_1 S_{1332} = \frac{(b_0 + b_4)x_2}{x_1^2},$$

$$\nabla_2 S_{1332} = 3\phi_2 S_{1332} = -\frac{(b_0 + b_4)}{x_1}.$$

Thus, the considered manifold is a 4-dimensional $(PSS)_4$ semi-Riemannian manifold.

References

[1] B.-Y. Chen, *Pseudo-Riemannian Geometry, δ-Invariants and Applications*, World Scientific, Hackensack, 2011.

Book of abstracts of the 9th International Conference on
Advanced Computational Methods in ENgineering and Applied Mathematics
September, 15–19, 2025.

Nonstandard Analysis of Questionnaire Data: AI Application and Classification in Quality of Life Studies

Piotr Wąż[1], Dorota Bielińska-Wąż[2] and Agnieszka Bielińska-Kaczmarek[3]

[1] *Department of Nuclear Medicine, Medical University of Gdańsk, 80-210 Gdańsk, Poland*

[2] *Department of Radiological Informatics and Statistics, Medical University of Gdańsk, 80-210 Gdańsk, Poland*

[3] *Faculty of Health Sciences and Physical Education, Kazimierz Wielki University, 85-064 Bydgoszcz, Poland*

e-mails: phwaz@gumed.edu.pl, djwaz@gumed.edu.pl, bielinska@ukw.edu.pl

Abstract

This study presents a novel analysis of questionnaire data using advanced computational methods, combining traditional analytical approaches with Artificial Intelligence (AI) techniques. Focusing on quality-of-life survey responses, we employ similarity/dissimilarity classification to uncover relationships between different respondent groups. Our interdisciplinary methodology extends prior work on biological and spectral data analysis to the domain of social research. As a key application, we examine the retirement threshold problem, demonstrating how our approach provides new insights into this well-known socioeconomic phenomenon. The results highlight the potential of AI-enhanced questionnaire analysis for extracting meaningful patterns from complex survey data.

Key words: artificial intelligence, correspondence analysis, quality of life, retirement threshold

1 Introduction

This presentation reviews our work on the analysis of questionnaire data [1–6]. We also introduce new, unpublished results demonstrating the application of Artificial Intelligence (AI) to questionnaire-based datasets.

Our study focuses on groups of individuals and their responses to quality of life questionnaires. We classify the results according to specific properties, framing the problem as a similarity/dissimilarity analysis. This interdisciplinary approach reveals relationships between different types of objects, extending methodologies we previously developed for biological sequences [7], stellar spectra [8], and molecular spectra [9].

A key application discussed here is the retirement threshold problem, a well studied topic in the literature [10].

2 Results

The study cohort comprised 480 individuals selected from Bydgoszcz, Poland. Participants were first categorized as either retirees or employees, with retirees additionally providing information about their attendance at lectures offered by the University of the Third Age. After applying an age threshold of 50 years, the final analysis included 449 subjects: 160 employed individuals (100 women and 60 men) and 289 retirees (186 women and 103 men). All participants completed three assessment tools: the WHOQOL-BREF questionnaire, a standardized instrument for quality-of-life evaluation, and two purpose-designed questionnaires developed by our research team.

For data visualization and interpretation, we implemented correspondence analysis, a multivariate statistical technique particularly suited for exploring relationships within categorical datasets. This approach generated spatial representations where analyzed entities formed distinct clusters, with their relative positions and groupings providing meaningful insights into underlying patterns.

Additionally, we present preliminary findings from ongoing work applying artificial intelligence methodologies to questionnaire-based data analysis, representing a novel extension of our research framework.

References

[1] A. Bielińska, M. Majkowicz, D. Bielińska-Wąż, P. Wąż, *Classification Studies in Various Areas of Science*, Lecture Notes in Computer Science **11189** (2019) 326–333, Springer, 2019.

[2] A. Bielińska, M. Majkowicz, P. Wąż, D. Bielińska-Wąż, *Mathematical Modeling: Interdisciplinary Similarity Studies*, Lecture Notes in Computer Science **11189** (2019) 334–341, Springer, 2019.

[3] A. Bielińska, M. Majkowicz, D. Bielińska-Wąż, P. Wąż, *A New Method in Bioinformatics—Interdisciplinary Similarity Studies*, AIP Conf. Proc. **2116** (2019) 450013.

[4] A. Bielińska, M. Majkowicz, P. Wąż, D. Bielińska-Wąż, *A New Computational Method: Interdisciplinary Classification Analysis*, AIP Conf. Proc. **2116** (2019) 450014.

[5] A. Bielińska, D. Bielińska-Wąż, P. Wąż, *Classification Maps in Studies on the Retirement Threshold*, Appl. Sci. **10** (2020) 1282.

[6] A. Bielińska, P. Wąż, D. Bielińska-Wąż, *A Computational Model of Similarity Analysis in Quality of Life Research: An Example of Studies in Poland*, Life **12** (2022) 56.

[7] D. Bielińska-Wąż, P. Wąż, *Non-standard bioinformatics characterization of SARS-CoV-2*, Comput. Biol. Med. **131** (2021) 104247.

[8] P. Wąż, D. Bielińska-Wąż, A. Strobel, A. Pleskacz, *Statistical indicators of astrophysical parameters*, Acta Astron. **60** (2010) 283–293.

[9] D. Bielińska-Wąż, P. Wąż, K. Jagiełło, T. Puzyn, *Spectral Density Distribution Moments as Novel Descriptors for QSAR/QSPR*, Struct. Chem. **25** (2014) 29–35.

[10] M. Bär, N. Gatzert, J. Russ, *Optimal asset allocation in retirement planning: threshold-based utility maximization*, J. Risk Finance **22** (2021) 345–362.